

https://dspace.org/

Electrochemical reactors for PGM recovery

Ferreira, Bronwynne Kim

2006-02-14
http://hdl.handle.net/10539/186

Downloaded from a DSpace repository. https://dspace.org/

E L E C T R O C H E M I C A L R E A C T O R S
F O R P G M R E C O V E R Y

Bronwynne Kim Ferreira

A dissertation submitted to the Faculty of Engineering, University of the Witwatersrand, in fulfilment of the requirements for the degree of Master of Science in Engineering.

Johannesburg, 2004

DECLARATION

I declare that this dissertation is my own work. It is being submitted for the Degree of Master of Science in Engineering in the University of the Witwatersrand, Johannesburg. It has not been submitted before for any degree or examination in any other University.

I obtained the information used in this dissertation while employed by Anglo Platinum.

_____
B. K. Ferreira

_____ day of _____ (year) _____

ABSTRACT

The employment of an electrochemical process is an attractive alternative for the treatment of effluents. When dealing with solutions of low metal ion concentrations mass transport limitations are significant and large electrode surfaces are required. The use of a reactor containing a three-dimensional electrode is preferable as the surface area per unit volume is orders of magnitude greater than that of the familiar plate type reactor.

A benchscale electrochemical reactor was designed and constructed to incorporate a cylindrical packed bed cathode. The flow of electrolyte is perpendicular to the direction of the flow of the current and the system is operated galvanostatically in a batch recirculation mode. The industrial stream selected for examination contains palladium and copper ions and a small concentration of platinum in a chloride medium containing ammines. The evolution of chlorine gas at the anode by the oxidation of the chloride ions is prevented by the inclusion of a cation exchange membrane and a separate anolyte, namely sulphuric acid, is introduced to the outer anodic chamber.

Tests were conducted on both synthetic and industrial solutions and a simplified model which was derived was used to estimate the mass transfer coefficients. The concentrations of the palladium, copper and platinum in the plant effluent were approximately 150, 200 and 10 ppm respectively. The results show that the metal ions can be rapidly reduced to well below 1 ppm in each case.

The separation of the palladium and copper ions is shown to occur to a limited degree during electrodeposition, with the extent of separation increasing for lower current densities. Enhanced separation may be possible during the removal of the deposited metals from the cathode either by anodic stripping or chemical treatment. A further method for the recovery of the metals is the combustion of the graphite particles.

The high value of palladium, coupled with the significant recoveries shown to be achievable, suggest economic viability in addition to the environmental benefits.

Dedicated to my husband, Trevor,
for all his support and patience.
Kookai

ACKNOWLEDGEMENTS

I would like to acknowledge and thank the following persons for their assistance:

- Anton van Aswegen for the volume of information supplied pertaining to the electrochemistry of the solutions used. Anton will be publishing his work in the form of his dissertation.

- Prof D. Hildebrandt, Prof A. Bryson and Prof I. Cukrowski (University of the Witwatersrand) for their combined supervision of the work.

- Prof E. Cukrowska and Rufat Morena (Analytical Laboratory, University of the Witwatersrand) for the numerous sample analyses.

- The staff of the Physics Workshop and the Process and Materials Engineering Workshop (University of the Witwatersrand) for the construction of many of the components used in the reactor.

- Dianne and Stewart Williams, for their parental support and for their individual contributions in the manufacturing of several of the prototype parts leading to the final design of the equipment.

- P. Charlesworth, H. Müller and S. Woollam (Anglo Platinum) for the generous funding of the project, the supply of the PGM solutions and for providing me the opportunity to complete my MSc.

CONTENTS

DECLARATION II
ABSTRACT III
ACKNOWLEDGEMENTS V
CONTENTS VI
LIST OF FIGURES IX
LIST OF TABLES XI
LIST OF SYMBOLS XII
NOMENCLATURE XIV

1 INTRODUCTION 1

1.1 BACKGROUND 1
1.2 STATEMENT OF THE PROBLEM 2
1.3 OBJECTIVES 3

2 LITERATURE SURVEY 5

2.1 PGM ELECTROCHEMISTRY 5
2.1.1 Deposition Reactions 6
2.1.2 Dissolution and Passivation Reactions 11
2.1.3 Side Reactions 21
2.1.4 Surface Effects 24

2.2 VARIANTS OF THREE-DIMENSIONAL ELECTRODES 26
2.2.1 Porous Substrates 26
2.2.2 Screens or Grids 27
2.2.3 Fluidised Bed Electrodes (FBE) 28
2.2.4 Packed Bed Electrodes (PBE) 30
2.2.5 Circulating Bed Electrodes 31
2.2.6 Three-phase Systems 33

2.3 DESIGN CONSIDERATIONS 35
2.3.1 Flow Arrangement 35
2.3.2 Cell Geometry 36
2.3.3 Modes of Operation 38
2.3.4 Anode Material and Design 39
2.3.5 Cathode Material and Current Feeders 40
2.3.6 Diaphragms and Membranes 41

2.4 SCALED-UP AND INDUSTRIAL REACTORS 42
2.4.1 Rotating Electrodes 43
2.4.2 Extended Surface Electrodes 43
2.4.3 Parallel Electrodes with Fluidised Electrolytes 44
2.4.4 Packed Bed Electrodes 44
2.4.5 Fluidised Bed Electrodes 44

2.5 ECONOMICS 46

2.6 MODELLING 48

2.7 SURVEY CONCLUSIONS 49
2.7.1 PGM Electrochemistry 49
2.7.2 Reactor Configuration 50

3 THEORY 52

3.1 ELECTROCHEMICAL REACTION RATES 53

3.2 CONTROLLING RATE 54
3.2.1 Electron Transfer Controlled 54
3.2.2 Mass Transport Controlled 57
3.2.3 Mixed Control 59

4 EXPERIMENTAL 62

4.1 EXPERIMENTAL APPARATUS 62
4.1.1 Electrochemical Reactor 62
4.1.2 Flow Circuit 66
4.1.3 Power Supply and Control 67

4.2 REAGENTS 68

4.3 EXPERIMENTAL PROCEDURE 70

4.4 ANALYTICAL PROCEDURE 71

5 MODEL DERIVATION 72

5.1 SINGLE PASS PLUG FLOW REACTOR 72

5.2 BATCH RECIRCULATION PLUG FLOW REACTOR 75

5.3 MASS TRANSPORT CONTROLLED CONDITIONS 78

5.4 CURRENT CONTROLLED CONDITIONS 81

5.5 VALIDITY OF ASSUMPTIONS 83
5.5.1 Reservoir 84
5.5.2 Reactor 84
5.5.3 Reaction Rate 85
5.5.4 Particles 86
5.5.5 Side Reaction 86

6 RESULTS 87

6.1 PLANT SOLUTION 87
6.1.1 Degree of Removal 89
6.1.2 Reaction Kinetics 90
6.1.3 Potential Profile 93
6.1.4 Corrosion of Current Collector 94

6.2 PALLADIUM IONS IN SYNTHETIC INDUSTRIAL EFFLUENT 95
6.2.1 Reaction Mechanisms 96
6.2.2 Reaction Kinetics 98
6.2.3 Potential Profile 100

6.3 COPPER IONS IN SYNTHETIC INDUSTRIAL EFFLUENT 102
6.3.1 Reaction Mechanisms 103
6.3.2 Reaction Kinetics 106
6.3.3 Potential Profile 108

6.4 COPPER AND PALLADIUM IONS IN SYNTHETIC INDUSTRIAL EFFLUENT 111
6.4.1 Degree of Separation 112
6.4.2 Reaction Kinetics 113
6.4.3 Potential profile 116

6.5 GENERAL RESULTS 117
6.5.1 Membrane Permeability 117
6.5.2 Hydrogen Evolution 117
6.5.3 Temperatures 119
6.5.4 Cathodic Protection and Corrosion 119
6.5.5 Accuracy and Reproducibility 121

7 CONCLUSIONS AND RECOMMENDATIONS.....122

7.1 METAL DEPOSITION..... 122

7.2 DEGREE OF SEPARATION..... 123

7.3 METAL RECOVERY..... 123

7.4 RECOMMENDATIONS FOR FUTURE WORK..... 124

8 REFERENCES.....126

APPENDICES

APPENDIX A Reactor components

APPENDIX B Results for Run 1 – Plant solution testwork

APPENDIX C Results for Run 2 – Pd SMISIE testwork

APPENDIX D Results for Run 3 – Cu SMISIE testwork

APPENDIX E Results for Run 4 – Cu / Pd SIE testwork

LIST OF FIGURES

Figure 2.1	Schematic diagrams of circulating bed electrodes	32
Figure 2.2	Diagram illustrating flow-through and flow-by configurations	35
Figure 2.3	Schematic representations of various design concepts of three-dimensional flow-by electrodes with cylindrical arrangement	37
Figure 3.1	Concentration profile assumed by Nernst diffusion layer model versus actual concentration profile	58
Figure 3.2	Concentration profiles in the Nernst diffusion layer	59
Figure 4.1	Schematic diagram of the electrochemical reactor	64
Figure 4.2	Cross section through mid height of the reactor	65
Figure 4.3	Modified salt bridge containing reference electrode	65
Figure 4.4	A schematic diagram showing the set-up of the apparatus, flow circuit and electrical circuit	66
Figure 4.5	Photograph of the control system hardware	67
Figure 5.1	Single pass plug flow reactor	72
Figure 5.2	Batch recirculation plug flow reactor	75
Figure 5.3	Performance of batch recirculation plug flow reactor for the condition $I_{app} \geq I_L(t=0)$	79
Figure 5.4	Current-potential curves for the primary and side reactions for the condition $I_{app} \geq I_L(t=0)$	80
Figure 5.5	Performance of batch recirculation plug flow reactor for the condition $I_{app} < I_L(t=0)$	82
Figure 5.6	Current-potential curves for the primary and side reactions for the condition $I_{app} < I_L(t=0)$	83
Figure 6.1	Concentration profile for Cu and Pd removal from plant solution catholytes for an applied current of 1.4 A	88
Figure 6.2	Concentration profile for Cu and Pd removal from plant solution catholytes for an applied current of 1.4 A and 2.0 A	89
Figure 6.3	Plot of the natural logarithm of the concentration as a function of time for plant solution catholytes	91
Figure 6.4	Cathode potential profiles for plant solution catholytes	93
Figure 6.5	Concentration profile for Pd removal from Pd SMISIE catholytes for various applied currents	95
Figure 6.6	Concentration profile for Pd removal from Pd SMISIE catholytes for an applied current of 1.4 A to show reproducibility and surface effects	96
Figure 6.7	Cyclic voltammogram of Pd SMISIE solution	98

Figure 6.8	Plot of the natural logarithm of the concentration as a function of time for Pd SMISIE catholytes	99
Figure 6.9	Cathode potential profiles for Pd SMISIE catholytes	101
Figure 6.10	Concentration profile for Cu removal from Cu SMISIE catholytes for various applied currents	102
Figure 6.11	Cyclic voltammogram of Cu SMISIE solution	104
Figure 6.12	Plot of the natural logarithm of the concentration as a function of time for Cu SMISIE catholytes	107
Figure 6.13	Cathode potential and concentration profiles for Cu reduction from Cu SMISIE catholyte with applied current of 1.4 A	109
Figure 6.14	Cathode potential profiles for Cu SMISIE catholytes	110
Figure 6.15	Concentration profile for Cu removal from Cu / Pd SIE catholytes for various applied currents	111
Figure 6.16	Concentration profile for Pd removal from Cu / Pd SIE catholytes for various applied currents	112
Figure 6.17	Plot of the natural logarithm of the Cu concentration as a function of time for Cu / Pd SIE catholytes	115
Figure 6.18	Plot of the natural logarithm of the Pd concentration as a function of time for Cu / Pd SIE catholytes	115
Figure 6.19	Cathode potential profiles for Cu / Pd SIE catholytes	116
Figure 6.20	Cell voltages measured for Cu SMISIE catholytes	118

LIST OF TABLES

Table 2.1	Comparison of standard potentials and calculated reversible potentials for reduction of chloro-palladium species	9
Table 2.2	Comparison of dissolution potentials to standard potentials	15
Table 4.1	Details of the components in the reactor	63
Table 4.2	Computer recorded data and accuracy of measurements	68
Table 4.3	Suppliers and grades of the reagents used	69
Table 4.4	Compositions of the catholyte solutions used	69
Table 6.1	Concentrations of metal ions in the plant solution	87
Table 6.2	Parameter estimation for the copper reactions under mass transport controlled conditions for plant solution catholytes	91
Table 6.3	Parameter estimation for the palladium reactions under mass transport controlled conditions for plant solution catholytes	92
Table 6.4	Parameter estimation for the metal deposition reaction during current controlled conditions for Pd SMISIE catholytes	98
Table 6.5	Parameter estimation for the metal deposition reaction under mass transport controlled conditions for Pd SMISIE catholytes	99
Table 6.6	Parameter estimation for the metal deposition reaction during current controlled conditions for Cu SMISIE catholytes	106
Table 6.7	Parameter estimation for the metal deposition reaction under mass transport controlled conditions for Cu SMISIE catholytes	107
Table 6.8	Process efficiencies for reducing the copper concentration from 400 ppm of Cu^{2+} to 10 ppm Cu^{+} from Cu SMISIE catholytes	108
Table 6.9	Concentration of copper when palladium deposition commences for various applied currents	112
Table 6.10	Parameter estimation for the copper metal deposition reaction under mass transport controlled conditions for Cu / Pd SIE catholytes	114
Table 6.11	Parameter estimation for the palladium metal deposition reaction under mass transport controlled conditions for Cu / Pd SIE catholytes	114

LIST OF SYMBOLS

a	Specific active surface area of particles	m^2m^{-3}
a_O	Activity of the oxidised species	
a_R	Activity of the reduced species	
A	Cross sectional area of bed	m^2
A_p	Active surface area of the particles	m^2
c	Concentration in the bulk solution	gm^{-3}
c_{in}	Concentration in the inlet stream to the reactor	gm^{-3}
c_{out}	Concentration in the outlet stream from the reactor	gm^{-3}
c_{in}^{0}	Initial concentration in the inlet stream to the reactor	gm^{-3}
D	Diffusion coefficient	m^2s^{-1}
E	Potential versus reference electrode	V
E_e	Equilibrium (reversible) potential versus reference electrode	V
E_e^A	Potential of anodic reaction versus reference electrode	V
E_e^C	Potential of cathodic reaction versus reference electrode	V
E^o	Standard electrode potential versus reference electrode	V
F	Faraday constant	$Cmol^{-1}$
ΔG	Gibbs free energy change	$Jmol^{-1}$
I	Current	A
I_{app}	Constant current applied	A
I_L	Limiting current for reaction under mass transport control	A
I_{rxn}	Current used in primary reaction	A
j	Current density (Equation 3.7)	Am^{-2}
$\vec{j}$	Partial cathodic current density	Am^{-2}
$\overleftarrow{j}$	Partial anodic current density	Am^{-2}
j_0	Exchange current density (Equation 3.18)	Am^{-2}
j_{app}	Current density applied	Am^{-2}
j_{ET}	Current density for electron transfer controlled reaction	Am^{-2}
j_L	Limiting current density for mass transport controlled reaction	Am^{-2}
j_{rxn}	Current density used in primary reaction	Am^{-2}
k	First order rate constant	ms^{-1}
$\vec{k}$	Electron transfer rate constant for the cathodic reaction	ms^{-1}
$\overleftarrow{k}$	Electron transfer rate constant for the anodic reaction	ms^{-1}
$\vec{k}_o$	Electron transfer rate constant for the cathodic reaction when E = 0 V vs. reference potential	ms^{-1}
$\overleftarrow{k}_o$	Electron transfer rate constant for the anodic reaction when E = 0 V vs. reference potential	ms^{-1}
k_m	Mass transport coefficient	ms^{-1}
ℓ	Vertical co-ordinate from bottom of bed	m
L	Length of the reactor	m

m	Mass	g
$\dot{m}$	Mass flowrate	gs^{-1}
M	Species M	
M_w	Molecular mass of species	$gmol^{-1}$
n	Number of electrons transferred in reaction	
N	Material flux	$gm^{-2}s^{-1}$
Q	Charge	C
Q_{rxn}	Charge consumed in primary reaction	C
Q_{app}	Charge supplied	C
$\dot{Q}$	Volumetric flowrate	m^3s^{-1}
r	Rate of reaction	gs^{-1}
$\dot{r}$	Rate of reaction per unit surface area	$gm^{-2}s^{-1}$
R	Gas constant	$Jmol^{-1}K^{-1}$
t	Time	s
t_m	Time at which limiting current is equal to applied current	s
t_{Pd}	Time at which palladium deposition begins	s
T	Temperature	K
V	Volume of solution in reactor	m^3
V_{res}	Volume of solution in the reservoir	m^3
x	Distance from the electrode surface	m
X_{SP}	Fractional conversion of material entering the reactor in a single pass	
X_{BR}	Overall conversion of initial material in a batch recirculating reactor	
α_A	Transfer coefficient for anodic reaction	
α_C	Transfer coefficient for cathodic reaction	
δ	Thickness of diffusion layer	m
ε	Bed voidage	
ϕ	Current efficiency (Equation 3.11)	
ϕ_p	Charge yield (Equation 3.10)	
γ	Activity coefficient	
η	Overpotential (Equation 3.16)	V
τ_{res}	Residence time of solution in reservoir	s

Subscripts

i	Component i
in	Inlet stream to the reactor (outlet stream from reservoir)
out	Outlet stream from reactor (inlet stream to reservoir)
O	Oxidised species
R	Reduced species
sor	Sorbed species
x=0	Surface of electrode

NOMENCLATURE

BMR	Base Metal Refinery
CPE	Carbon Paste Electrode
CSTR	Constantly Stirred Tank Reactor
CV	Cyclic Voltammogram
DCCU	Direct Current Control Unit
DSA	Dimensionally Stable Anode
ECP	Electro Conductive Partition
EQCM	Electrochemical Quartz Crystal Microbalance
FBE	Fluidised Bed Electrode
HMDE	Hanging Mercury Drop Electrode
HOPG	Highly Orientated Pyrolytic Graphite
ICPOES	Inductively Coupled Plasma Optical Emission Spectroscopy
MBE	Moving Bed Electrode
MCI	Measurement and Control Interface
MSE	Mercurous Sulphate Electrode
MSRS	Modulated Specular-Reflection Spectroscopy
NHE	Normal Hydrogen Electrode
NMR	Nuclear Magnetic Resonance
PBE	Packed Bed Electrode
PFR	Plug Flow Reactor
PGM	Platinum Group Metal
PMR	Precious Metal Refinery
PS	Power Supply
PSS	Platinum Salt Sensitivity
pzc	Potential of Zero Charge
RDE	Rotating Disc Electrode
RHE	Reversible Hydrogen Electrode
RRDE	Rotating Ring Disc Electrode
SBE	Spouted Bed Electrode
SCE	Saturated Calomel Electrode
SERS	Surface Enhanced Raman Spectroscopy
SHE	Standard Hydrogen Electrode
SIE	Synthetic Industrial Effluent
SMISIE	Single Metal Ion in Synthetic Industrial Effluent
SWPS	Square Wave Potential Sweep
UPD	Underpotential Deposition
VBE	Vortex Bed Electrode
XPES	X-ray Photoelectron Spectroscopy

1 INTRODUCTION

1.1 BACKGROUND

The platinum group metals (PGMs) comprise platinum (Pt), palladium (Pd), rhodium (Rh), ruthenium (Ru), iridium (Ir) and osmium (Os). These transition metals exhibit catalytic properties and are extensively used in the exhaust systems of automobiles and fuel cell technologies. The PGMs and some of their alloys also serve a protective function due to their inert character and strength. The appearance and nobility of platinum metal further renders it a useful material in the manufacture of jewellery. For any of the catalytic, protective or decorative purposes, these precious metals are often coated onto less expensive substrates due to the high cost of these materials.

The PGMs are rare metals but form part of South Africa's vast mineral resources and the country is home to the world leader in platinum production, namely Anglo Platinum. The production process incorporates mining, concentrating, smelting and refining operations. A considerable cost is associated with each of these operations and thus it is necessary to continually strive to improve current technology or develop superior methods for the extraction of the metals. A substantial amount of resources are dedicated to all areas of research but of particular importance is the recovery of the PGMs from the waste streams before discarding them to the effluent dams. Due to the high value and rarity of these metals it can be economically viable to reduce the concentration to only a few parts per million before disposal of the barren streams.

In addition to the economic rewards from increasing the degree of removal of the precious metals there are also environmental benefits. The significance of sustainable development has been acknowledged worldwide and regulations regarding the metal concentrations in effluents have and will continue to become more stringent. It is therefore imperative that technology be advanced to meet these demands.

Several different methods for removal of heavy metals from wastewaters exist, each with their individual advantages and disadvantages. Conventional techniques, such as chemical precipitation and cementation, are limited when the PGMs are strongly complexed in solution. Although the cementation and chemical precipitation methods enable the recovery of the precious metals, they result in further chemical contamination of the waste stream which, therefore, requires further treatment before disposal. Ion exchange has recently been shown to be a powerful tool for the selective recovery of the PGMs from industrial effluents[1], however, difficulties in the elution of these metals from the chelating ion exchangers have been experienced. Other non-conventional recovery methods include the adsorption of the PGMs onto spherical particles of a high polymer product contained in a packed column[2] or selective sorption onto polyurethane foams [3, 4]. Electrochemical methods for PGM removal from dilute streams have also been discussed in proprietary and patented literature and include electrochemical deposition[5-10] and electrochemical sorption[11,12] techniques.

1.2 STATEMENT OF THE PROBLEM

A chemical reduction process is currently employed by industry for the recovery of the platinum group metals from waste streams. Various negative aspects of this method are identified. These include:

- The generation of a substantial amount of effluent due to the large dilution effects of the multiple chemical additions required. The volume output from the process is sometimes twice as high as the volume input.
- The possible spontaneous formation of an unwanted gaseous by-product.
- The process efficiency being heavily reliant on the performance of the operators with many batches having to be reprocessed.
- The low turn around times for the numerous sample analyses that need to be performed between the stages of the process.

Furthermore the process in general is fairly time consuming, labour intensive and large equipment is required. Multiple waste streams are currently being combined and treated simultaneously resulting in a large variation in the composition of each batch to be treated and causing chemical complication, whereas small modules treating individual waste streams at source would be preferred for optimum efficiency.

Alternatives to the process are sought and the possibility of an electrochemical reduction process is considered. The main advantage of an electrochemical process is that, generally speaking, no chemical additions are required. The waste stream is passed directly through the reactor and the electrons for reducing the metal ions are supplied from an external power supply. There is therefore no increase in the volume of effluent and the risk associated with the handling of chemicals is reduced. Furthermore, as no chemicals are added there is a significant saving in reagent costs and there is no further contamination of the waste stream. The by-products of the electrochemical process include oxygen, an environmentally friendly gas and an industrially useful gas, hydrogen. Other potential benefits include the continuous on-line monitoring and control of the process and the possibility of separation of the platinum group metals from the base metals, thus the recovered precious material could be recycled within the refineries and not returned to the smelting process. Another important prospective benefit regarding safety is that, unlike the current recovery method where the PGMs are recovered as precipitated salts, the electrochemical method reduces the ions to the metal state. It is known that the platinum salts are allergenic and Platinum Salt Sensitivity (PSS) poses a health risk to employees. The PGMs are safe to handle if in the metal state.

However, the performance of conventional electrochemical cells is limited at low metal ion concentrations. To achieve the high degree of removal at a sufficient rate, very large surface areas are required such that a reasonable current may be applied but a low current density established at the surface. In addition, some means of enhancing the rate of mass transfer is necessary. The use of a parallel plate-type cell in such applications would result in a large volume reactor.

1.3 OBJECTIVES

The aim of the testwork is to investigate the possibility of an electrochemical process as a method for PGM recovery from dilute waste streams. This entails the identification of a suitable technique for reducing the PGM content to a total concentration of less than 10 ppm. Taking into consideration that the process must be suitable for a refining environment, the method should be rapid, reliable and controllable. The recovered material should also be in a recyclable form.

A single waste stream is selected for examination. The stream contains mainly palladium and copper ions and a small concentration of platinum in a chloride medium containing ammines. The extent to which the palladium ions can be removed from the actual plant effluent is to be determined and a qualitative understanding of the individual reaction mechanisms and rates obtained. Although the co-deposition of the PGM and base metal would be acceptable, a method whereby the palladium is selectively deposited or the purity of the product enhanced would be far more appealing. The recovered material would then not have to be rerouted back to the smelting process and the PGM could be recycled within the precious metal refinery (PMR) and the copper sent to the base metal refinery (BMR).

It is not the intention of this work to optimise the process parameters or to determine what would affect the scale-up of the equipment. The scope of this dissertation is limited to establishing the feasibility of further, more comprehensive research which would encompass these areas.

2 LITERATURE SURVEY

Two separate areas of research were reviewed. Firstly, a survey of the literature pertaining to the electrochemistry of PGMs was undertaken. Particular attention was paid to the reactions of palladium, and to a lesser degree platinum, as these were the major PGM species in the plant effluent under investigation. The information obtained is discussed in Section 2.1.

The second literature survey related to electrochemical reactors for the removal of metal ions from dilute streams. When dealing with dilute streams, mass transport effects are significant and it was evident that the conventional plate electrochemical reactor would not be suitable. The use of a three-dimensional electrode seemed far more appealing due to the surface area per unit volume being orders of magnitude greater than the planar electrodes and that the rate of mass transfer would be significantly enhanced. Although the successful removal of PGMs using three-dimensional electrodes has been reported in literature[13] and patents[5-7] the fundamental principles and the influence of the design parameters were still lacking. Numerous articles relating to three-dimensional electrodes were therefore analysed and are discussed in some detail in Sections 2.2 to 2.6. Although not dealing with the recovery of PGMs in particular, they offered insight to the effects of the process parameters and reactor configurations concerned. The initial design of the bench-scale electrochemical reactor that was constructed for this testwork was based on the conclusions, given in Section 2.7, that were drawn from this review.

2.1 PGM ELECTROCHEMISTRY

The platinum group metals are commonly used as electrodes due to their catalytic properties. They also serve a protective function due to their superior resistance to corrosion or oxidation and are even used for decorative purposes. However as the cost of these metals is substantial, they are most often coated onto a particular substrate. Electrochemical plating from a PGM containing bath is a widely used technique. Therefore numerous studies have been conducted to determine the reaction rates and mechanisms of the electrodeposition, dissolution and passivation of the PGMs in a variety of electrolytes onto various substrates.

2.1.1 Deposition Reactions

2.1.1.1 Ammine Complexes of Platinum

Voltammetric studies[14] were conducted on a solution consisting of platinum tetrammine ($Pt(NH_3)_4^{2+}$) where it was found that the reduction of the Pt(II) species from this electrolyte was never diffusion controlled over the range 0 V to -1.0 V (SCE). No reduction peaks were obtained for experiments at room temperature but well formed peaks were formed at 95 ^oC. The strong dependence of the cathodic peak current density on temperature indicated that one or more chemical steps preceded the electron transfer step. It was concluded that the $Pt(NH_3)_4^{2+}$ species was not itself electroactive but that ligand substitution was more likely to occur. This chemical step was rate determining for platinum deposition and high temperatures were required to drive the slow reaction. Hydrogen adsorption was also stated to inhibit the platinum deposition.

In a later study to determine the extent of ligand replacement needed for the Pt(II) species to accept electrons at a reasonable rate, the electrochemistry of solutions of $Pt(NH_3)_{4-x}(H_2O)_x^{2+}$ (x = 0-2) complexes in an aqueous phosphate buffer were investigated[15]. It was shown that the greater the number of ammonia ligands attached, the smaller the current density and the slightly more negative the peak potential.

Platinum deposition was always noted when potentials were held more negative than –0.7 V (Ag/AgCl). At increased temperatures the peak current densities were significantly increased but no marked shift in the peak potentials was observed. Using NMR, it was confirmed that no change in the major species in solution occurred for all solutions at higher temperatures. From the similarities in the reduction peak potentials for all three of the Pt(II) species investigated it was stated that a common reducible intermediate was formed. The replacement of the NH_3 ligands with H_2O was said to precede the electron transfer reaction and unstable $Pt(H_2O)_4^{2+}$ was the species that was reduced at the surface via Reaction 2.1.

$$Pt(H_2O)_4^{2+} + 2e^- \rightarrow Pt + 4H_2O \qquad [2.1]$$

2.1.1.2 Chloro complexes of Platinum

Both $Pt(H_2O)_4^{2+}$ and $PtCl_4^{2-}$ were shown to be reduced by direct electron transfer reactions in acidic media via Reactions 2.1 and 2.2 respectively.

$$PtCl_4^{2-} + 2e^- \rightarrow Pt + 4Cl^- \qquad [2.2]$$

The $PtCl_4^{2-}$ species are reduced at more negative potentials than $Pt(H_2O)_4^{2+}$, as is expected for more stable or stronger complexes. The other chloro species, $PtCl(H_2O)_3^+$, $PtCl_2(H_2O)_2$ and $PtCl_3(H_2O)^-$, although assumed to also be reducible at intermediate potentials, are susceptible to ligand substitution even at room temperature and Gregory et al.[15] concluded that the major pathway for these complexes involved the displacement of the Cl^- by H_2O and the reduction of the $Pt(H_2O)_4^{2+}$ species as shown by Reaction 2.1.

The rapid ligand substitution mechanism explained the very similar voltammetric responses of the solutions containing $Pt(H_2O)_4^{2+}$, $PtCl(H_2O)_3^+$ and $PtCl_2(H_2O)_2$ consisting of a single, well-formed reduction waves, thus indicating a common Pt(II) species undergoing mass transport controlled reduction. Acidic solution containing $PtCl_4^{2-}$ in the presence of 1.5 M excess Cl^- ions showed a single peak just before hydrogen evolution indicating the suppression of the hydrolysis reaction and the direct reduction of the platinum species. Solutions containing a mixture of $PtCl_3(H_2O)^-$ and $PtCl_4^{2-}$ in the absence of free Cl^- ions produced more complicated voltammograms consisting of two waves and one peak. The first wave corresponded to the reduction wave observed for the hydrolysed species and the peak coincided with the direct reduction of the $PtCl_4^{2-}$. A second wave noted at potentials between the first wave and the peak was attributed to the reduction of $PtCl_3(H_2O)^-$.

Gregory et al. found that a substantial overpotential was necessary to drive the formation of Pt nuclei on a carbon surface[15]. Platinum deposition onto a carbon substrate from a 0.1 M H_2SO_4 solution containing 2 mM K_2PtCl_6 was performed by Gloaguen et al.[16] by holding the potential constant at –0.5 V (MSE). It was stated that at this potential hydrogen evolution is negligible and as the partial reduction of $PtCl_6^{2-}$ to Pt^{2+} species would occur at potentials more positive than –0.3 V (MSE) that high current efficiencies could be expected.

2.1.1.3 Ammine Complexes of Palladium

Tsventarnyi and Kravtsov[17] discuss the controversial work done by previous authors on the reduction mechanism of ammonia complexes of palladium. While some authors claimed that the slow electrochemical stage is preceded by a chemical stage which involves the abstraction of some ammonia molecules from the initial complex, other authors concluded that no chemical stage was evident but rather the hydrogen atoms participated in the reduction process. Therefore the said authors conducted detailed studies of the electroreduction of ammonia complexes of palladium(II) at various pH and ammonia concentrations. To minimise the concurrent hydrogen adsorption and absorption during electroreduction, the pH of the solutions were increased and at pH 12.8 the effects of hydrogen were found to be negligible. However, for pH 7.9 the results indicate that the palladium surface is covered with adsorbed hydrogen and that these atoms hamper the reduction of the ammonia complexes as apposed to the previously proposed participation in the reaction. Furthermore, no evidence of a preceding chemical stage was elucidated, but rather the reduction was found to be an irreversible reaction which was limited by the transfer of the first electron. This testwork was conducted in ammonium sulphate solutions, however for solutions containing ammonium chloride the chemical reaction involving ligand detachment was found to occur. For solutions containing high concentrations of chloride ions relative to ammonia concentrations mixed chloride-ammonia complexes form and undergo reduction at more positive potentials than for solutions containing ammonium sulphate.

Voltammetric studies at a HMDE by Munichandraiah et al.[18] showed that the reduction of Pd(II) in its complex with ammonia takes place irreversibly in water as well as in the other solvent mixtures tested, namely acetonitrile, methanol, dimethyl sulfoxide, dimethylformamide and dioxane. Different kinetics were established for the various solvents and it was found that the standard rate constant increases with the increase of the dielectric constant of the medium.

2.1.1.4 Chloro complexes of Palladium

The composition of a solution containing palladium species will depend on the concentration of chloride ions in solution and the ionic equilibria that are established.

For high chloride concentrations the formation of species with large chloride/palladium atom ratio (e.g. $PdCl_4^{2-}$, $PdCl_3^-$) is favoured. The reactions involving the various chloro species are shown in Reactions 2.3 to 2.7 below.

$$Pd^{2+} + 2e^- \Leftrightarrow Pd \quad [2.3]$$

$$PdCl^+ + 2e^- \Leftrightarrow Pd + Cl^- \quad [2.4]$$

$$PdCl_2 + 2e^- \Leftrightarrow Pd + 2Cl^- \quad [2.5]$$

$$PdCl_3^- + 2e^- \Leftrightarrow Pd + 3Cl^- \quad [2.6]$$

$$PdCl_4^{2-} + 2e^- \Leftrightarrow Pd + 4Cl^- \quad [2.7]$$

The standard potentials for each of the reactions above are listed in Table 2.1, but the reversible potentials are dependent on the concentrations present at equilibrium and hence dependent on the chloride concentration as shown by comparing the reversible potentials of the reactions in solutions of different Cl^- concentrations as determined by Gimeno et al.[19].

Table 2.1 Comparison of standard potentials (E^o) and calculated reversible potentials (E_e) for reduction of chloro-palladium species[19].

	Pd^{2+}	**$PdCl^+$**	**$PdCl_2$**	**$PdCl_3^-$**	**$PdCl_4^{2-}$**
E^o vs. SCE	0.709	0.529	0.396	0.325	0.349
E_e vs. SCE $[Cl^-]$ = 0.41 mM	0.526	0.528	0.491	0.493	0.640
E_e vs. SCE $[Cl^-]$ = 5.52 mM	0.508	0.460	0.423	0.425	0.487

In a solution with a chloride concentration greater than 0.5 M the palladium species is predominantly tetrachloropalladate[21]. The deposition of palladium from such a solution was found to occur at potentials negative to 0.2 V vs. Ag/AgCl[22, 23]. It was shown from cyclic voltammetry experiments[22] that palladium electrodeposition from a tetrachloropalladate solution occurs via Reaction 2.7. The shift of the cathodic peak potential toward more positive values with each scan was attributed to Reaction 2.7 occurring on the deposited palladium (instead of the carbon surface) thus causing the decrease of the Pd deposition overpotential. The deposition of palladium onto a highly oriented pyrolytic graphite (HOPG) substrate occurs by a nucleation and

growth process. Gimeno et al.[19] investigated the formation and topology of the palladium islands and proposed two mechanisms which depended on whether the cathodic potential was above or below the potential of zero charge (pzc) of bulk palladium. If above the pzc, the chloride ions are first adsorbed onto the surface defects on the HOPG substrate. These adsorbed ions interact with the dissolved palladium species to form $PdCl_2$, which is an adsorbed precursor for the formation of nuclei. It is on these centres containing the precursor that the palladium deposition reaction occurs via the transfer of electrons. Due to the lower work function of HOPG as compared to palladium the electrodeposition on the palladium islands is favoured. However, at greater cathodic overpotentials, such that the potential is below the pzc of bulk palladium, the palladium species will be electrodeposited onto the carbon directly without the formation of the critical nuclei.

Kibler et al.[24] deposited palladium onto a gold substrate from a solution of less than 1 mM H_2PdCl_4 in 0.1 M H_2SO_4 and found that Pd starts to deposit onto gold just below 0.6 V (SCE). The equilibrium potential for such an electrolyte, with the major species being $PdCl_2(H_2O)_2$ and $PdCl(H_2O)_3^+$, was stated to be 0.5 V and thus underpotential deposition (UPD) was said to occur. Moreover, two UPD peaks were observed and two anodic peaks on the reverse scan. These two peaks are discussed further in Section 2.1.4. Although $PdCl_4^{2-}$ was not the predominant species in solution, it was assumed that the palladium deposition reaction occurred via the reduction of adsorbed tetrachloropalladate. The surface was found to be covered by palladium anions in a wide range of potentials positive of the pzc of gold (0.23 V vs. SCE) where adsorption of the negatively charged complex would be energetically favoured. Bulk deposition of palladium commenced at 0.49 V (SCE).

2.1.1.5 Forced deposition of Palladium

The so-called "forced deposition" of palladium was carried out by Al-Akl and Attard[25] to form an electrode with a well-defined coverage of palladium supported on platinum. This was achieved by placing a droplet of aqueous palladium nitrate solution onto the surface of a freshly flamed Pt electrode and then passing hydrogen gas over the droplet for a period of time. The resulting redox reaction was as follows:

$$Pd^{2+}(aq) + H_2(g) \rightarrow Pd(adsorbed) + 2H^+(aq) \qquad [2.8]$$

2.1.2 Dissolution and Passivation Reactions

Although testwork for removal of the deposited metal falls beyond the scope of this dissertation, literature pertaining to the anodic dissolution of the PGMs was reviewed to evaluate the possibility of such a recovery method and to identify the most suitable electrolyte.

Unfortunately, due to the passivation of the noble metals this process is generally difficult[26]. The formation of oxides on noble metal electrodes in sulphuric acid solutions has been investigated and proposed mechanisms have been reported for platinum[27-30], palladium[30-35] and rhodium[36] substrates. Mechanisms for the oxidation and dissolution processes in chloride containing media have also been put forward for platinum[37] and palladium [22, 23, 26]. These mechanisms are discussed in the following sections.

2.1.2.1 Platinum dissolution and passivation in sulphuric media

Cyclic voltammetry, using a Pt wire electrode, was used to investigate the oxide formation in sulphuric acid media by Tilak et al.[27], Folquer et al.[28] and Chialvo et al.[29]. The above authors all postulate the formation of an oxygen containing monolayer via an intermediate Pt(OH) species. The reactions relating to this oxide layer are shown in Reactions 2.9 to 2.11 below, where Reaction 2.9 was found to be a fast reversible electrochemical process.

$$Pt + H_2O \Leftrightarrow Pt(OH) + H^+ + e^- \quad [2.9]$$

$$Pt(OH) \Leftrightarrow Pt^*(O) + H^+ + e^- \quad [2.10]$$

$$Pt^*(O) \Leftrightarrow PtO \quad [2.11]$$

Pt*(O) is related to a non-equilibrium oxygen containing species which forms a more stable PtO aged species. Folquer et al.[28] demonstrated this aging effect by comparing CV of conventional triangular potential sweeps with the CV after open circuit aging. During the cathodic scan of the triangular potential sweeps Reactions 2.12 to 2.15 were all noted. After open circuit aging reactions only Reactions 2.13 and 2.15 were found to occur on the return cathodic scan.

$$PtO \Leftrightarrow Pt^{*}(O) \quad [2.12]$$

$$PtO + H^{+} + e^{-} \Leftrightarrow Pt(OH) \quad [2.13]$$

$$Pt^{*}(O) + H^{+} + e^{-} \Leftrightarrow Pt(OH) \quad [2.14]$$

$$Pt(OH) + H^{+} + e^{-} \Leftrightarrow Pt + H_2O \quad [2.15]$$

The processes occurring when the positive potential limit assigned to the monolayer formation, 1.1 V (RHE)[27], is exceeded during CV are significantly more complicated and involve the formation of more stable rearranged oxide species, higher platinum oxides PtO_2/PtO_3 and film growth. Therefore, the switching potential and the time at which the potential is held constant has a significant effect on the CV that is generated, with the cathodic sweep potential depending on the degree of oxidation.

Although Folquer et al.[28] did not consider Pt dissolution in the analysis of their results and Chialvo et al.[29] found no evidence of dissolved species during SWPS (square wave potential sweeps), the authors do acknowledge the existence of such reactions. Indeed, Pt dissolution was found to occur during anodic treatment of Pt electrodes in sulphuric acid media by Rand and Woods[30]. Multiple CV cycles were performed and the charge for each cycle was integrated. It was found that the overall anodic charge was greater than the overall cathodic charge and that the difference was in good agreement with the amount of metal in solution. It was therefore concluded that Pt metal undergoes anodic dissolution in acid media when the anodic potential of the sweep reversal is greater than 1.07 V (RHE). Furthermore the formation of oxides was stated to inhibit the dissolution reaction.

2.1.2.2 Platinum dissolution and passivation in chloride media

An investigation of the dissolution and passivation of platinum in acid solutions was conducted by Finkelstein et al.[37]. The following conclusions were drawn from CV, Modulated Specular-Reflection Spectroscopy (MSRS) and steady state potentiostatic experiments on a platinum surface in concentrated HCl.

At potentials more positive to 1.10 V (NHE) both platinum dissolution and chlorine evolution occur simultaneously. The dissolution was shown to be a first order reaction with respect to chloride concentration and is potential dependent. The dissolution mechanism involves an initial reaction shown in Reaction 2.16 below,

which is the rate determining step, followed by a series of fast electron-transfer steps to the first stable species, namely $PtCl_4^{2-}$. The rate of dissolution is therefore faster in more concentrated chloride solutions. Increased temperatures were also shown to enhance the rate of dissolution.

$$Pt + Cl^- \rightarrow PtCl^- + e^- \qquad [2.16]$$

Evidence that Pt-chloro complexes were adsorbed onto the surface was given. Oxidation of adsorbed $PtCl_4^{2-}$ was observed at approximately 1.0 V (NHE) in 2 M HCl solutions and at 0.75 V (NHE) in 12 M HCl. The products of this oxidation process are dependent on the chloride concentration and in 12 M HCl solutions only the reduction of $PtCl_6^{2-}$ was noted at 0.47 V (NHE) but in 2 M HCl and a second reduction reaction for the $PtCl_5(H_2O)^-$ adsorbed species was seen as well at 0.61 V (NHE). The platinum chlorocomplexes were shown to be strongly adsorbed and the rate of desorption very slow. The formation of these adsorbed species were shown to result in a partial inhibition of the of the dissolution process. These species may be removed however by cathodic treatment.

Passivation was also found to occur and was determined to be due to the formation of oxides at potentials greater than 1.15 V (NHE). The rate of oxide formation is very low in chloride solutions compared to sulphate solutions due to the slow desorption process of the adsorbed chlorocomplexes formed at potentials lower than those for oxide formation. The oxide formation on platinum is complex and multiple species are formed but unfortunately as the reaction occurs so slowly the oxide formation is only detectable at very slow sweep rates using CV and the use of MSRS was unable to detect the oxide let alone identify the species.

The removal of the oxide species by the chloride ions is also very slow and occurs in two stages. The first stage is rapid while the remainder required longer periods of exposure, thus confirming that different forms of oxides species are present.

2.1.2.3 Palladium dissolution and passivation in sulphuric media

Bolzan et al. studied the anodic behaviour of palladium metal in sulphate solutions, using a Pd wire electrode[33] and a ring-disc rotating electrode[34] and found that

palladium metal dissolved from the electrode in both the forward and reverse scan. This effect was however remarkably dependent on the electrode history and it was stated that oxygen adsorption inhibits the electrochemical dissolution of the noble metals.[30, 32, 34]

The anodic dissolution and oxidation reactions were deemed to be competing processes[34] for an initial intermediate, Pd(OH), formed via Reaction 2.17 which is a fast process[33]:

$$Pd + H_2O \Leftrightarrow Pd(OH) + H^+ + e^- \qquad [2.17]$$

The dissolution reaction occurs from the Pd(OH) in the following two steps:

$$Pd(OH) \Leftrightarrow Pd(OH)^+ + e^- \qquad [2.18a]$$

$$Pd(OH)^+ \Leftrightarrow Pd^{2+}(aq) + OH^- \qquad [2.18b]$$

Thus the overall reaction for the dissolution, given by the sum of Reactions 2.17, 2.18a and 2.18b was

$$Pd \Leftrightarrow Pd^{2+} + 2e^- \qquad [2.18]$$

The oxidation reaction also occurs from the Pd(OH) but in the following manner:

$$Pd(OH) \Leftrightarrow Pd(O) + H^+ + e^- \qquad [2.19a]$$

$$Pd(O) \rightarrow \text{oxygen} - \text{containing layer} \qquad [2.19b]$$

The overall oxidation reaction shown as

$$Pd + H_2O \Leftrightarrow PdO + 2H^+ + 2e^- \qquad [2.19]$$

The thermodynamic threshold potentials for Reactions 2.18 and 2.19 are 0.987 V and 0.917 V (SHE) thus the simultaneous occurrence was not surprising.

The anodic dissolution of the Pd metal in 1 M H_2SO_4 was confirmed by Rand and Woods[30] using CV. The total cathodic and anodic charges were integrated for each cycle. The anodic charge was found to be greater and although other authors have confirmed this, they attributed this to the oxidation of organics present or to the incomplete reduction of the oxide layer. Rand and Woods[30] dispute these claims as

the net difference in charge after numerous cycles remained anodic and thus could not be due to organics unless present in large amounts. Furthermore the said authors state that the surface was shown to return to its original state after reduction thus indicating the complete reduction of the oxide layer. Evidence in support of an anodic mechanism was the agreement between the net charge difference calculated after multiple cycles and the amount of palladium found in solution. Furthermore the anodic potential of the sweep reversal above which metal dissolution occurred was found to be in reasonable when compared to the standard potential of the metal / metal ion couple. These potentials are listed in Table 2.2 below. The dissolution potentials should theoretically approximate the reversible potentials of the metal / metal ion couples, but as the metal ion concentrations at the surface of the electrode and the stability constant for the soluble species in solution are not known, the reversible potentials for the reactions could not be obtained.

Table 2.2 Comparison of dissolution potentials[30] to standard potentials

Metal / Metal ion couple	**Dissolution Potential (V vs. RHE)**	**Standard Potential (V vs. RHE)**
Rh / Rh^{3+}	0.67	0.80
Pd / Pd^{2+}	0.98	0.99
Pt / Pt^{2+}	1.07	1.19
Au / Au^{3+}	1.41	1.50

Bolzan et al.[33] also found that the anodic to cathodic charge ratio during potential cycling was greater than one but after prolonged cycling the Pd dissolution was suppressed and the charge ratio was then equal to one. This once again indicates the inhibition of the dissolution by the formation of the oxide layer and the influence of the electrode history on the reaction mechanisms.

The charge associated with the dissolution reaction was too small in comparison to the total anodic charge to observe an identifying peak relating to the dissolution reaction. However, increasing the temperature was found to increase the rate of Pd dissolution to a greater extent than the increase in the rate of oxygen adsorption, and

a peak was identifiable at 0.96 V (RHE)[30]. The amount of dissolved metal was dependent on the nature and pre-treatment of the electrode and the experimental conditions. The anodic dissolution was attributed to the direct dissolution of the metal (Reaction 2.18) as well as the chemical dissolution, shown by Reaction 2.20,[30, 32-34] of an anodically formed intermediate species, such as the PdO formed in Reaction 2.19.

$$PdO + 2H^{+} \rightarrow Pd^{2+} + H_2O \qquad [2.20]$$

Cathodic reactions for the metal dissolution, such as that shown in Reaction 2.21, were disputed by Rand and Woods as it could not account for the shape of the voltammograms obtained. The dissolution current on the cathodic scan became negligible when the potential was swept to high values thus indicating the inhibition of the corrosion by the oxide species.

$$PdO_2 + 4H^{+} + 2e^{-} \Leftrightarrow Pt^{2+} + 2H_2O \qquad [2.21]$$

The oxide species formed depends on the potential range that is covered during experimentation with the oxides formed at lower potentials being easily reduced[32].
The X-ray Photoelectron Spectroscopy technique was employed by Kim et al.[31] to characterise the various palladium-oxygen species on the surface of electrochemically oxidised palladium electrodes in sulphuric acid and the presence of hydrated PdO or PdO_2, or the corresponding $Pd(OH)_2$ or $Pd(OH)_4$ species were clearly indicated.

Palladium behaves in many ways like platinum but shows greater susceptibility to oxide formation and dissolution[35]. Palladium is significantly more prone to dissolution than platinum, especially under potential cycling conditions.

2.1.2.4 Palladium dissolution and passivation in chloride containing media

The anodic dissolution of palladium, that had been deposited by potentiostatic treatment, was studied by Lubert, Guttmann and Beyer[23] using cyclic voltammetry at carbon paste electrodes. In the case of low amounts of deposited palladium only one oxidation peak was observed. When larger amounts of palladium were deposited, two oxidation peaks were observed and it was concluded that the peak at the less

positive potential (+0.1 V vs. SCE) represented the dissolution of the monolayer (Pd deposited onto the carbon surface) and that the peak at more positive potential (+0.45 V vs. SCE) indicated the dissolution of the palladium multilayer (Pd deposited onto Pd islands). The possibility of a stepwise anodic dissolution process with an intermediate, such as Pd(I), forming was considered by the said authors, but deemed less probable than the formation of multilayers and monolayers. It was shown previously by Lubert et al.[38] that the amount of sorbed hydrogen increases with the amount of deposited palladium and hence the authors could not attribute the oxidation peaks to hydrogen due to the disappearance of the peak at +0.1 V vs. SCE after deposition of larger amounts of palladium.

It was further concluded that the dissolution of Pd^0 from the multilayer is not complete[22] and that palladium remains partly on the electrode surface. The oxidation peak relating to the dissolution of the multilayer, was not observed in testwork with solutions containing sulphates or perchlorates, and led to the assumption that the chlorides were involved in the dissolution of the Pd^0.

The proposed mechanism was the oxidation of the multilayer forming chloropalladate(II) species which were absorbed or chemisorbed on the remaining palladium (Reactions 2.22). When the surface concentration of the chloropalladate increases it diffuses into the solution or to the uncovered carbon (Reaction 2.23). The subscripts Pd and C in the reactions below indicate the corresponding species localised at palladium islands or at the uncovered carbon respectively.

$$\left[Pd^{0}\right]_{Pd} + nCl^{-} \rightarrow \left\{\left[Pd^{II}Cl_{n}\right]^{-n+2}\right\}_{Pd} + 2e^{-} \qquad [2.22]$$

$$\left\{\left[Pd^{II}Cl_{n}\right]^{-n+2}\right\}_{Pd} \rightarrow \left\{\left[Pd^{II}Cl_{n}\right]^{-n+2}\right\}_{C} \qquad [2.23]$$

Chloride ions were found to be chemically bonded to glassy carbon surfaces when treated anodically (E>1.2 V vs. RHE), and could not be removed by cathodic treatment or rinsing[39, 40]. The adsorption or chemisorption of the $[PdCl_4]^{2-}$ anion was not only proposed by Lubert et al.[22] but also discussed by Kibler et al.[24] and Naohara et al.[41], and was suggested to play a decisive role in the deposition and dissolution processes of palladium in the presence of chlorides. Palladium deposition onto a gold substrate from chloride-free solutions was stated as being highly

irreversible, thus making the removal of the deposit by electro-oxidation by a simple potential cycle impossible[24].

It was reported that halides inhibit the onset of oxide formation on transition metal electrodes and surface roughening via oxide formation is therefore prevented in such electrolytes[25]. Indeed, during an anodic scan two anodic peaks were detected at 0.89 V and 0.96 V (RHE) when applied to a freshly deposited palladium surface on a gold substrate in a sulphuric electrolyte containing chlorides[41]. Using EQCM, a mass decrease was observed as soon as the anodic current began to flow. It was concluded that the observed anodic current was only due to the dissolution of palladium as the mass would have increased if the (hydro-)oxide was formed. Furthermore the mass decrease indicated that all of the deposited layer was dissolved. The absence of the formation of oxides in this testwork may also be attributed to the electrode history, whereby the dissolution process is predominant on a freshly deposited surface. Styrkas and Styrkas[26], however, state that a passivating layer is formed in chloride containing media and propose an efficient method for the electrochemical dissolution of Pd and other PGM metals. The technique involves the application of an alternating current to the metal immersed in highly concentrated chloride media. Thus any oxides formed are removed during the cathodic phase. Dissolution rates were reported to be orders of magnitude greater than the rates obtained when applying a constant anodic current. The alternating current also produces electromechanical effects that may contribute to the break-down of the passivating layer. Furthermore, increased rates of electrochemical dissolution were noted at higher temperatures.

2.1.2.5 Palladium dissolution and passivation in perchlorate media

The testwork done by Chierchie et al.[42] using a Pd electrode in perchlorate solutions produced the very familiar CV trend for the oxidation of a noble metal, with the sharp cathodic peak corresponding to the reduction of the oxides formed. When the scan rate was significantly slower, three cathodic peaks were noted, the presence or position of which were dependent on the positive inversion potential of the CV scan. The oxide layers were therefore assumed to form in a stepwise fashion with increasing potentials. The palladium species assumed to form were PdOH and PdO and the mechanisms proposed were similar to those mentioned in Section 2.1.2.3.

Although no direct measurement of the dissolution of the Pd was made, the workers did comment that this process was assumed to be superimposed on the process of the oxide formation. Using in-situ surface enhanced Raman spectroscopy and performing a potential sweep from 0 V to 1.0 V and back to 0 V (SCE) on a Pd surface showed the formation of oxide above 0.8 V and the removal below 0.4 V in a 0.1 M $HClO_4$ solution[43]. The palladium species assumed during the water electroreduction was also PdO although the mechanism was not discussed.

2.1.2.6 Palladium dissolution and passivation in alkaline media

Bolzan[44] conducted studies using a rotating ring-disc electrode (RRDE) with a Pd disc in alkaline solutions. The electroformation of a Pd oxide film was found to begin at approximately 0.6 V (SCE). The following four steps were concluded to occur during an anodic scan.

Step 1:

$$[Pd]_x + OH^- \Leftrightarrow [Pd]_x(OH) + e^- \qquad [2.24a]$$

or

$$[Pd]_x + H_2O \Leftrightarrow [Pd]_x(OH) + H^+ + e^- \qquad [2.24b]$$

The species, $[Pd]_x(OH)$, represents a chemisorbed state of OH on an x site of the Pd lattice. This reaction was stated to be fast and reversible.

Step 2:

$$[Pd]_x(OH) \Leftrightarrow [Pd]_x(O)^* + H^+ + e^- \qquad [2.25]$$

This reversible deprotonation of the Pd(OH) species forms an unstable state of the O atom. This PdO* species appeared to be the precursor of the O monolayer formation.

Step 3:

$$[Pd]_x(O)^* \rightarrow [Pd]_x(O) \qquad [2.26]$$

This irreversible reaction represents the formation of the PdO or $Pd(OH)_2$ monolayer.

Step 4:

$$Pd(O) + 2OH^- \rightarrow PdO_2 + 2e^- + H_2O \qquad [2.27]$$

For E > 1.25 V (SCE) a second oxide layer namely, PdO_2 or $Pd(OH)_4$ begins to grow.

On the cathodic scan, two peaks are noted for the oxide reduction. The peak corresponding to the reduction of the second oxide layer is represented by the reverse reaction of 2.27. The reduction of this layer is not complete and hence the electroadsorption of hydrogen is inhibited. The second reduction peak was found to consist of two components, one reversible and one irreversible. The reduction reactions were given by 2.28 and 2.29

$$Pd(O) + H_2O + e^- \rightarrow Pd(OH) + OH^- \qquad [2.28]$$

$$Pd(OH) + e^- \rightarrow Pd + OH^- \qquad [2.29]$$

The reduction of the stable PdO species is not reversible, but the Pd(OH) species was found to behave reversibly. This reversible stage was not observed if the potential at which the CV was reversed, or the sweep rate was increased.

The ring-disc electrode showed that soluble palladium species formed during the oxide film growth and during the electroreduction of these species. However, the dissolution reactions were hindered in alkaline solutions due to the high concentration of OH, which stabilises the hydroxide layer on the surface. This can be seen from Reactions 2.18a and 2.18b which describe the mechanism for dissolution. Thus, the reaction mechanisms proposed by Bolzan in alkaline solutions are virtually identical to those proposed by the said author and co-authors in sulphuric acid electrolytes, discussed in Section 2.1.2.3. Although the formation of soluble Pd species was noted, the electrodissolution of Pd in basic solutions was found to be much smaller than in acidic media. The electroformation of the Pd oxide was found to begin at approximately 0.6 V (RHE) in alkaline solutions[44] but only at roughly 0.8 V (RHE) in acidic media[34, 35]. Burke and Roche[35] reported a decrease in the potential for the onset of surface oxidation of approximately 13 mV per unit increase in solution pH and state that previous authors have also reported the decrease in the potential with increasing pH.

2.1.3 Side Reactions

2.1.3.1 Hydrogen Reactions

Different mechanisms for the reduction of hydrogen on a carbon paste electrode in the presence of tetrachloropalladate at were identified[38]. The hydrogen ions are reduced via Reaction 2.30 either simultaneously with the Pd^{2+} reduction or immediately after some metal deposition.

$$H^+ + e^- \xrightarrow{Pd^0} H^0_{sor} \qquad [2.30]$$

Reaction 2.30 was said to occur on the deposited Pd surface and the hydrogen species is either absorbed or adsorbed onto this surface.

An additional mechanism for the reduction of the hydrogen was identified from a cathodic peak at a more negative potential than for Reaction 2.30. This reaction, assumed to be the reduction of the protonated chloropalladate species on the carbon surface, occurred according to Reaction 2.31.

$$\left[HPdCl_4\right]^- + 3e^- \rightarrow Pd^0 + H^0_{sor} + 4Cl^- \qquad [2.31]$$

It is known that the chloropalladate species exist in protonated forms depending on the solution pH. The concentration of the protonated species is greater in solutions of lower pH and thus Reaction 2.31 was predominant in tests performed at pH 3 and minor for tests at greater pH. However, when the electrode was subjected to potentiostatic pretreatment, allowing the species to accumulate at the electrode surface, Reaction 2.31 was found to occur in solutions of pH 5 and pH 7.

The oxidation current observed at negative potentials vs. SCE was attributed to the oxidation of sorbed hydrogen. The potential at which the sorbed hydrogen was oxidised was more positive for solutions with lower pH. For solutions with higher pH two oxidation peaks were observed in the CV experiments performed at higher palladium concentrations. This double oxidation peak was also noted after multiple cycles were performed, and was attributed to the energetically different oxidation

steps caused by the sorption of hydrogen at the different surfaces namely, the deposited palladium surface and the carbon surface[38].

The mechanisms relating to the hydrogen reactions on a palladium substrate were also investigated by Bolzan[44] using modulated voltammetry in alkaline media. This technique distinguishes between the adsorbed and absorbed hydrogen. It was shown that in the cathodic sweep below 0.4 V (RHE) hydrogen is electroadsorbed onto a palladium surface in a reversible process shown by

$$Pd_x(e^-) + H_2O \Leftrightarrow Pd_x(H) + OH^- \qquad [2.32a]$$

or

$$Pd_x(e^-) + H^+ \Leftrightarrow Pd_x(H) \qquad [2.32b]$$

Thus electroadsorption on a Pd_x site is the first step before absorption or hydrogen evolution can occur. Reaction 2.32b is identical to 2.30. These H adatoms then diffuse into the bulk Pd from the surface. This diffusion process is the absorption of hydrogen and is denoted by Reaction 2.33, where (H) stands for an adsorbed H atom on Pd_x and $[(H)Pd_x]$ represents an absorbed H atom.

$$Pd_x(H) \rightarrow [(H)Pd_x] \qquad [2.33]$$

As the concentration of the hydrogen in the bulk increases the α and eventually the β phase of PdH are formed. The electroadsorption process is impeded on a H-loaded Pd electrode and subsequently hydrogen evolution becomes more difficult. During a cathodic sweep the absorbed hydrogen was said to be oxidised via adsorbed H atoms and hence this electrodesorption process results in the conversion of the H-loaded Pd electrode to Pd.

Well-defined peaks associated with the electroadsorption of hydrogen are noted on ultra-thin Pd electrodes, but not observed on bulk palladium electrodes. This was attributed to the lower overpotential for hydrogen absorption process on bulk Pd whereby masking the presence of the electroadsorbed species[44]. As the absorption of hydrogen is kinetically hindered on very thin palladium films this enables the adsorption process to be studied[24]. The reaction rate of electroadsorption is dependent on the electrolyte composition and anions were indicated to interact

strongly with the H adatom, with sharper, higher peaks observed in sulphuric acid than alkaline solutions[44].

The characteristic hydrogen adsorption-desorption peak pair on the PGM surface was observed by numerous researchers[14, 15, 28-30, 44, 45].
As was mentioned previously, the adsorbed hydrogen atoms inhibit the deposition of the PGMs[14, 15, 17] and as the absorbed atoms were found to be difficult to remove and said to be the cause of surface roughening many researches preferred to work in potential regions where hydrogen reactions were excluded[30, 42].

2.1.3.2 Carbon Surface Oxide Reactions

The redox reactions of the carbon surface groups were discussed by Lubert et al.[46]. At positive potentials the carbon surface groups are oxidised and, depending on the potential, possibly undergo simultaneous reduction with the Pd^{2+} species. A further mechanism at more negative potentials was proposed whereby the surface groups, designated as carbonyl groups, are reduced with the participation of protons according to the Reaction 2.34.

$$\begin{array}{c} | \\ C{=}O \\ | \end{array} + H^+ + e^- \rightarrow \begin{array}{c} | \\ -C- OH \\ | \end{array} \qquad [2.34]$$

Cyclic voltammograms recorded on a carbon powder electrode in 0.1 M H_2SO_4 solution by Gloaguen et al.[16] exhibited a wide anodic peak at -0.1 V (MSE) and a wide cathodic peak at -0.2 V (MSE). These peaks were also attributed to the oxidation and reduction of the carbon surface oxide groups. The surface oxides created from the chemical or electrochemical oxidation of the carbon powder were said to consist mainly of carboxylic and phenol groups. The potential cycling of a carbon electrode is a well known pre-treatment technique for activating the electrode surface by the formation of many oxygen functional groups[45].

2.1.3.3 Chemical oxidants

The formation and removal of PGM oxides from solutions of 0.1 M $HClO_4$ containing chemical oxidants was studied using in situ electrochemical surface enhanced Raman Spectroscopy (SERS) experiments[43]. It was found that in the presence of

NO a very stable and distinctive oxide species was formed on the Ir surface compared to oxide formed during water electro-oxidation. This stable oxide was identified as a crystalline IrO_2 film. The formation of oxide during water electro-oxidation is given by Reaction 2.35:

$$IrO_2 + 4H^+ + 4e^- \rightarrow Ir + 2H_2O \qquad [2.35]$$

Unlike Reaction 2.35 above, the formation of IrO_2 from NO involves no net consumption or release of electrons and was written formally as:

$$Ir + 2NO \rightarrow IrO_2 + N_2 \qquad [2.36]$$

Thus NO was shown to have the ability to act as an efficient oxygen-atom source upon dissociative chemisorption, and which, unlike water, does not require electro-oxidation to form metal oxide. Dissolved oxygen was also found to be an effective source of oxide from aqueous solution although less effective than NO.

2.1.4 Surface Effects

It is well known that the material of the electrode surface has a significant effect on the potential and rate of the reactions occurring, such as the low overpotential for hydrogen evolution on palladium but carbon surfaces have been characterised by relatively low electrocatalytic activity for the hydrogen reaction[47]. However, other surface properties also influence the reaction rates and mechanisms. The pre-treatment of the electrode, the ligands available at the surface, the structure and presence of surface defects as well as the formation of nuclei or alloys during deposition are briefly mentioned below.

The stability and the reactivity of the Pd surface oxides are highly dependent on the electrode history[32]. Under oxidizing conditions it was found that the dissolution of palladium will occur preferentially on a fresh electrode[33], but this reaction becomes inhibited by the formation of Pd-oxide or Pd-hydroxide species[26, 30, 33]. Thus the rate of dissolution is dependent on the extent of oxidation of the electrode and the coverage of this oxide layer. Anodic-cathodic potential treatments are known to result in an increase in electrocatalytic activity of platinum. This surface activation

was attributed the removal of surface impurities and to alterations of the surface structure[30].

Testwork in chloride media containing palladium using a CPE modified with derivatives of N-benzoylthiourea the CV generated was vastly different from those using the unmodified CPE and ligand exchange with the modified electrode surface was assumed to occur resulting in different reaction mechanisms[20]. Furthermore the anodic peak corresponding to the oxidation of sorbed hydrogen at palladium was not noted using the modified CPE. This was attributed to the modified surface, since the addition of thiourea to the electrolyte has been shown to impede this sorption process[48].

The two UPD peaks and the two anodic peaks mentioned in Section 2.1.1.4, were attributed to the deposition and dissolution of palladium on the surface steps and terraces of the gold substrate. It was shown that palladium nucleates on the flat terraces at more negative potentials than at the steps. Similarly dissolution of the palladium monolayer is seen to occur at the steps (or defect sites) prior to the terraces[24]. Naohara et al.[41] also studied the deposition of palladium onto a gold substrate and also found that nucleation of palladium occurred at the surface defects. It was also suggested that $PdCl_4^{2-}$ adsorbs onto both the substrate and the palladium islands, and plays a significant role in the growth mechanism of the deposit. This adlayer was said to inhibit the vertical, but favour the lateral growth, thus palladium deposition proceeds in a layer by layer growth mode. Even on HOPG surfaces the formation of Pd islands on surface defect sites was favoured over the HOPG terraces[19], but as discussed in Section 2.1.1.4 the species involved in the deposition process depended on the applied potential. Zou and Weaver[49] recommended using a constant current method for producing uniform PGM films on substrates rather than the previously used constant potential methods. The problems associated with the latter were that rapid deposition rates were initially produced resulting in the formation of metal clusters or islands. The constant current technique provides uniform deposition rates and produces thin pin-hole free films.

A Cu-Pd alloy formed when copper deposited onto palladium substrate[25]. No alloy formation was observed between the deposited palladium and the gold substrate used by Naohara et al.[41] or Kibler et al.[24].

2.2 VARIANTS OF THREE-DIMENSIONAL ELECTRODES

Three-dimensional electrodes have been considered for a variety of applications. These include:

- Fuel cells and batteries[50-52]
- Hydrogen peroxide synthesis[53]
- Organic electrosynthesis[54-56]
- Chlor-alkali reactors[57]
- Recovery of silver from photographic process liquors[58,59]
- Chromium recovery from effluents[60]
- Electrochemical dissolution of copper from scrap steel[61]
- Trace metal analysis[62]
- Extraction metallurgy[63]

In particular, particulate electrodes were considered advantageous for use in electrometallurgical processes that could only be carried out economically at low current densities. This constraint applied to removal of heavy metals from very dilute solutions. Due to their significantly larger surface area compared to conventional cells of the same volume, it is possible to operate at low current densities but still maintain the high cell throughput required. Planar electrodes, Akzo[64] says, usually can operate efficiently down to heavy metals feedstream concentrations of 30 ppm, while fluidised-bed electrolysis can work as low as 1 ppm. For the recovery of Hg(II) from aqueous chloride solutions final concentrations of 2 ppb have been reported with typical current efficiencies of 99% utilising fluidised bed electrodes[65].

Previous reviews of electrochemical reactors have been reported by Houghton and Kuhn[66], Coeuret[67] and Weininger[68]. A large variety of three-dimensional electrodes exist, each with their associated advantages and disadvantages. These are discussed individually in Sections 2.2.1 to 2.2.6 below.

2.2.1 Porous Substrates

The one dimensional model proposed by Newman and Tobias[69] for porous electrodes is widely referred to in literature and often adapted to other three-

dimensional forms of electrodes. Theoretical studies have also been conducted by Tobias and Grens[70, 71] and an extensive review of flooded porous electrodes was reported by Newman and Tiedemann[50], with particular reference to battery applications. Porous electrodes include materials such as conducting foams or fibres[72]. Forms of fibres available are papers, veils, chopped or milled fibres, non woven mats and felts. These fixed beds may however trap gas bubbles that are likely to form simultaneously in a side reaction in dilute streams and consequently increase the cell resistance and electrical energy consumption[73]. Furthermore, these materials result in a considerable pressure drop across the bed.

2.2.2 Screens or Grids

The use of screens and expanded metals in building three-dimensional electrodes offer many advantages such as high specific area, high turbulence promoting ability, high porosity and relatively low pressure drop, ease of coating with a catalyst and ready availability at modest cost[74]. In addition they present a rigid structure and are relatively easy to construct. A variety of testwork utilising metallic nets, grids or screens has been reported[74-82].

Leroux and Coeuret[75] as well as Letord-Quémére et al.[76] reported increased mass transfer values using an alternative superposition arrangement than with the exact superposition arrangement. A study by Zaki et al.[77] showed that vibrating screens increase the rate of mass transfer at horizontal screens by a factor ranging from 3.5 to 12 depending on the frequency and amplitude of vibration, physical properties of the solution and the geometry of the vibrating screen.

Higher rates of mass transfer were obtained at horizontal screens for a given set of conditions and may be attributed to the local increase in solution velocity (jetting effect) as the solution passes through the openings of the horizontal screens. This effect was absent in the case of vertical screens which were parallel to the flow. However, for electrochemical reactors, the vertical orientation was recommended by Mobarak et al.[74] and Storck et al.[78] as this geometry was considered better for scale-up as the current and potential distributions were more uniform.

2.2.3 Fluidised Bed Electrodes (FBE)

High mass transfer rates are obtained in fluidised bed electrodes due to turbulence of the moving particles. During electrodeposition, the bed particles grow as discrete entities and hence there is no clogging of the bed by particle agglomeration[83, 84]. The process can be operated continuously by adding small particles in the top and removing large particles from the bottom and is not hindered by any solid impurities which may be present in the feed stream.

However, the fluidised bed electrode does exhibit a number of inherent limitations. The most significant drawback of the FBE is the range of overpotentials spatially distributed within the bed. The condition that the fluidised bed electrode operates under pure mass transport control is often inaccessible[85]. Modelling of the overpotential distribution requires the spatial variations of both the particle and electrolyte potentials. These potential profiles will depend on the resistivities of the phases and the mechanism for charge transfer.

A variety of mechanisms have been proposed for the transfer of charge in the solid phase of a FBE. These include:

- Convective / Collision Mechanism – Charged particles move in the bed and complete or partial charge sharing occurs during elastic collisions with other single particles[86-88]. Beenackers et al.[89] later disputed this mechanism based on ideal fluidisation and proposed a model for charge transfer based on the occurrence of particle aggregates in the bed.
- Conductive Mechanism – Charge is conducted electronically through a chain of particles connected to the current feeder[90, 91].
- Parallel Effective Resistance Model – Kusakabe et al.[92] proposed a model which incorporated both the collision and conductive mechanisms. They stated that charge transfer in the solid phase is dominated by the conductive mechanism at low bed expansions and by the collision mechanism at high bed expansions.
- Bipolar Mechanism – The mechanisms postulated above imply that the particles are all of the same polarity as the current feeder, i.e. monopolar. However, Plimley and Wright[93] put forth the concept that particle aggregates that are isolated from the current feeder exhibit bipolar characteristics. This

mechanism was verified by Lee et al.[94, 95] and accounted for the observed formation of zones of positive overpotential in cathodic beds resulting in the oxidation of deposited metals. This redissolution of the metals[67, 96] resulted in decreased current efficiencies especially at low current densities[97]. Zones of negative overpotential were also noted during anodic stripping of metals[98].

Thus a variety of mechanisms have been proposed and the operational conditions will determine which mechanism is dominant.

The cathodic potential is the highest at the surface of the membrane and near the current feeder for the flow-by arrangement[84, 99]. Hence the deposit formation and preferential growth rate is greatest in this area which can result in the tearing of the diaphragm or membrane. Deposition on the current feeder to the bed seems inevitable and may initiate the agglomeration of the bed for processing of solutions with concentrations of over 1 g/l. It is possible that such agglomeration may still take place in the case of dilute feed solutions (near 100 ppm) but after a much longer period of time. Furthermore agglomeration of particles occurs in those parts of the bed which cease to be mobile. These agglomerates can lead to defluidisation of the bed. The method of fluidisation is therefore crucial to the effective operation of the FBE. Two methods of supplying the fluidising agent are available namely, uniform and jet fluidisation.

Uniform fluidisation was used widely in the design of the first cells employing FBEs. All the designs used a flow predistributor in the form of a stack of grids or porous plate placed at the bottom of rectangular working chamber. Kazdobin et al.[100] stated that the inequalities of the flow velocities of the electrolyte in the bulk of the chamber and at the walls, near to the diaphragm and the current collector, resulted in the dilution of the bed in the bulk and its sedimentation near the walls. Therefore uniform fluidisation could cause the undesirable polarisation distribution in FBEs, the emergence of zones of anodic polarisation under total cathodic polarisation, and adherence and deposition of particles on the surface of diaphragm and current collector. An electrolyser design was proposed[101-103] in which the electrolyte was supplied through a system of slots or jets in the bottom of the cell, with inclined periphery walls. These designs were improved upon by Kazdobin et al.[100] by placing the current collector on the peripheral wall of the cell and the flow

predistributor on the plane of the diaphragm. Thus, polarisation of the FBE near to the diaphragm and current collectors was practically excluded, which protected them from metal deposition, and the zones of anodic polarisation were also eliminated.

2.2.4 Packed Bed Electrodes (PBE)

Packed bed electrodes, like the FBE, have the advantage of a large surface area per unit volume and high mass transfer rates due to turbulence generated as the stream passes through the bed[104]. They surpass the FBE in that they are not penalised by the formation of anodic zones in cathodic beds[67], have higher bed conductivities[90] and offer no abrasive wear on the diaphragm and current feeder. Flowrate control is crucial when operating the FBE to maintain the required bed expansion, thus the process operation is simplified using the PBE as the electrolyte flowrate is not critical to the successful performance and either high flowrates (increased mass transfer) or low flowrates (greater conversion per pass) may be utilised.

The major drawback of a fixed bed is that since the particles are in permanent contact, deposition of the metal occurs within the matrix and gradually blocks the interstices. This causes agglomeration of the bed and impairs mass transfer performance. The pressure drop across the cell increases and after prolonged metal deposition satisfactory operation becomes impossible[105].

Periodic fluidisation or pulsation of a fixed bed is one means of avoiding particle agglomeration, thus allowing continuous metal recovery on the particles. A further practical advantage is that the intervallic fluidisation of the bed would classify the particles within the bed. The fine particles would be situated at the top and the larger particles at the bottom. As the cathodic potential is greater at the top of the bed (for a flow-through configuration) the finer particles would mainly recover the metal and increase in size. Then the introduction of fine particles to the top and the extraction of larger particles at the bottom is a possibility. Although the pulsation time interval is very low, the pulsed situation has a predominant influence on the electrochemical behaviour of the bed. The problems associated with the flow of current during the pulsed state of the bed (those relating to the FBE) may be avoided if the current feed to the cell is switched off during the fluidisation of the bed. Then the pulsed/fixed bed only recovers the metal during the fixed bed situation. As the only aim of the

pulsation is to avoid agglomeration, this time interval should be as short as possible[106].

In the work done by Le Bolay et al.[56] a sinusoidal pulse was superimposed on the base flow of the fluid by means of a piston. When the fluid velocity is greater than minimum fluidising velocity of the particles, the bed is dislocated provoking the circulation of the particles. When the instantaneous velocity is lower than this minimum the bed is a fixed one. The velocity of the liquid may even be negative during a fraction of the period.

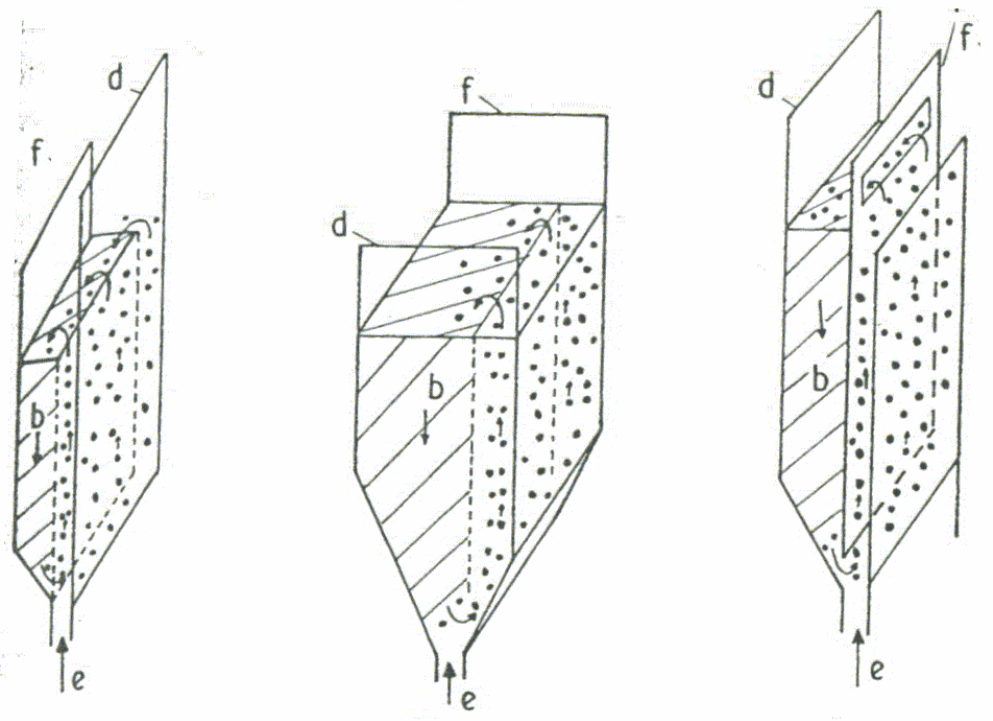
The concept of the ultrasonically stimulated cell was also introduced such that a particulate cell could be operated at very low velocities, and thus achieve higher conversions per pass, but the particles would retain their individual identity due to the low amplitude vibration transmitted. The cell is thus 'fluidised' independently of the liquid flowrate and the velocity is no longer a constraint. An increase in the mass transfer rate with stimulation was observed and consequently higher percentage extractions.[105] (The current efficiencies were assumed and not verified). It was visually observed that during ultrasonic stimulation the particles circulate slowly in the bed and that bed expansion is very small. However, cavitation was observed at the probe surface.

A further method identified for continuous operation using a packed bed but eliminating blockage was the periodic removal of the deposited material by anodic stripping[62, 107, 108]. This can be achieved by reversing the current (or switching the bed potentials) such that the cathode on which the metal was deposited becomes the anode. This technique has the advantages that the electrode need not be removed from the reactor and circulation of a small volume of anolyte results in a high concentration solution.

2.2.5 Circulating Bed Electrodes

The circulating bed electrode falls between the extremes of the packed bed electrode and the fluidised bed electrode. Three circulating beds which have evolved and utilise a common type of circulating particle motion, namely the spouted bed electrode (SBE) the moving bed electrode (MBE) and the vortex bed electrode (VBE) were discussed by Scott[109]. The circulating motion tends to produce two regions of

solid/liquid flow; a hydraulic conveying region where particulates are transported as a relatively dilute phase and a falling almost packed bed region where the solid and liquid flows are countercurrent. The position of the feeder and the diaphragm determine the type of bed obtained and are shown schematically in Figure 2.1 below.



(a) (b) (c)

Figure 2.1 Schematic diagrams of circulating bed electrodes[109].
(a) Spouting bed, (b) Vortex bed, (c) Moving bed
d – diaphragm, f – feeder, e – electrolyte flow

Pressure losses measured for circulating beds (in the hydraulic conveying region) were found to be similar for all three types of circulating beds. These pressure losses are greater than for fluidised beds, but not radically so. Therefore the circulating beds are only slightly disadvantages in respect to the pressure losses incurred. The three electrodes will exhibit different potential distributions and regions of anodic activity have been identified for the SBE. Relatively high liquid velocities are required to induce bed circulation, but only a fairly small fraction of the total flow passes through the 'packed bed' region. Therefore the electrodes would have to operate with a recycle or be arranged in a series of banks due to the small degree of reactant

conversion per pass. Only the SBE can operate without a diaphragm or separator to isolate the conductive bed from the counter electrode. A further problem associated with moving beds is that if the rate of gas evolution is relatively high then, due to the downward motion of the bed, slugging may occur. This has been observed to some extent in the MBE at high current densities, and to a lesser extent in the SBE. A particular problem arises with slugging in that the bed may become stationary. Should the bed become stationary adjacent to the diaphragm the consequences could be catastrophic, in that this would allow metal deposition to occur on the diaphragm. Deposition onto the diaphragm was indeed reported by Scott and Lui[110] during the electrowinning of cobalt using a MBE at high applied currents. As the SBE arrangement, has the conveying taking place next to the diaphragm, this would be the preferred arrangement in regard to this problem.

In flow-by electrodes an increase in scale can only be effectively achieved in the two dimensions associated with the feeder or diaphragm cross-sectional areas. Thus both the SBE and the MBE would be amenable to scale-up in this way, but the VBE appears to have a limited size on scale-up. This is due to regions in the VBE becoming stationary, and thus susceptible to agglomeration, during deposition on scale-up perpendicular to the electrolyte flow. As the three circulating beds have similar performance characteristics in terms of efficiency, all are potential candidates for metal recoveries from dilute solutions, but due to the consideration of scale-up, the SBE has a wider appeal for metal recovery applications[109].

A spouted bed electrode with a draft tube was employed in an investigation by Salas-Morales et al.[111, 112] for zinc electrowinning. The draft tube confines the spread of the central jet of fluid; in this way, spouted beds of large height-to-width ratio can be operated. The tube employed in the cylindrical cell was made from aluminium and also served as the current feeder. Although the particles in the draft tube are not cathodically protected, minimal zinc dissolution will occur as the residence time in this tube is very low.

2.2.6 Three-phase Systems

A variety of testwork has been conducted in which a third phase, namely a gas, is present in the system. Such setups include systems where the solution is stagnant and air is sparged through[113] or oxygen is generated in a second electrochemical

cell[114-116]. In others there is a two-phase flow where both the gas and the liquid are flowing. The gas is either externally introduced[73, 74, 92, 117] or generated at the working cathode itself[118].

It was shown that the presence of a gas, in any of the setups, improves mass transfer, but that the degree to which the mass transfer is enhanced is dependent on the flowrate of the electrolyte[74]. The high rate of mass transfer at low solution velocities was said to be caused by the ability of a rising bubble to generate turbulence in its wake and induce radial momentum. In addition the bubbles will collide with the solid particles. By increasing the solution velocity, the rise velocity of the bubbles will increase resulting in a decrease in gas hold-up. As the concentration of these turbulent promoting bubbles decreases, their effect on the rate of mass transfer will be less influential and the turbulence due to the liquid flow will become responsible for enhancing the rate of mass transfer.

For a given superficial gas velocity, electrolytically generated gas bubbles were more effective in enhancing the rate of mass transfer than external gases introduced to the cell through porous or perforated spargers. The difference in behaviour was explained in terms of the much smaller size of the electrolytically generated gas bubbles, which lead to a higher gas hold-up and a higher concentration of the turbulence promoting bubbles. Furthermore for a given discharge rate of O_2 gas, the rate of mass transfer is much higher in acidic solutions since oxygen bubbles generated from acidic solutions were stated to be smaller than those generated from alkaline solutions[116].

Two-phase flow (gas and liquid) has the advantage that it can allow the reactor to operate with low solution flowrates and thus achieve higher residence times without detrimental effects to the rate of mass transfer. This results in higher conversion per pass. The use of an inert gas may also provide the function of purging an unwanted gas from the system[117]. However, there are penalties associated with the presence of the gaseous phase in the reactor. The increase in the resistivity of the electrolyte leads to an increase in specific energy consumption. The presence of an electrogenerated bubble phase in the fixed bed causes an obstruction to electrolyte flow and an enhanced pressure drop. However the pressure drop in the fluidised state is less with the presence of a bubble phase than for the identical conditions without gas evolution due to the gas hold-up[118].

2.3 DESIGN CONSIDERATIONS

Many configurations for three-dimensional electrodes exist. These differ in the shape of the cell, direction of flow of current and electrolyte and position of the counter electrode. Furthermore the correct selection of the anode and cathode materials can prove crucial to the design and successful operation of the reactor.

2.3.1 Flow Arrangement

Two configurations are possible regarding the direction of current flow with respect to the direction of electrolyte flow. These are illustrated in Figure 2.2 below.

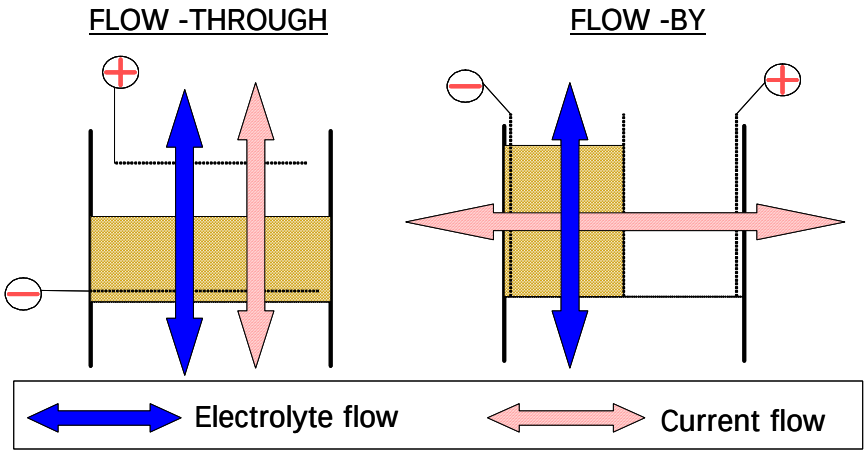


Figure 2.2 Diagram illustrating flow-through and flow-by configurations

In the flow-through configuration the flow of electrolyte and current are parallel. This is also sometimes referred to as axial field flow. The flow-by configuration also known as radial field flow exhibits a perpendicular flow arrangement.

The behaviour and applications of a variety of flow-through porous electrodes have been studied. It has been shown that the height of a bed in an axial field electrode is limited by local potential distributions[119, 120]. On account of that, a part of the bed may be inactive if it is too thick or the reaction selectivity may be poor. However, if the bed height is minimised, locally non-uniform flow or channelling could occur which would diminish the residence time of the electrolyte and also adversely affect the desired high mass transfer rate.

In order to decrease the length of inactive region of the particulate electrode but maintain a suitable residence time of the electrolyte and to have a good selectivity, the electrode can be made narrow in the direction of current flow, and long in the direction of fluid flow. This configuration, called radial field flow, has a potential distribution more complex than in the case of axial field flow[79, 119, 121].

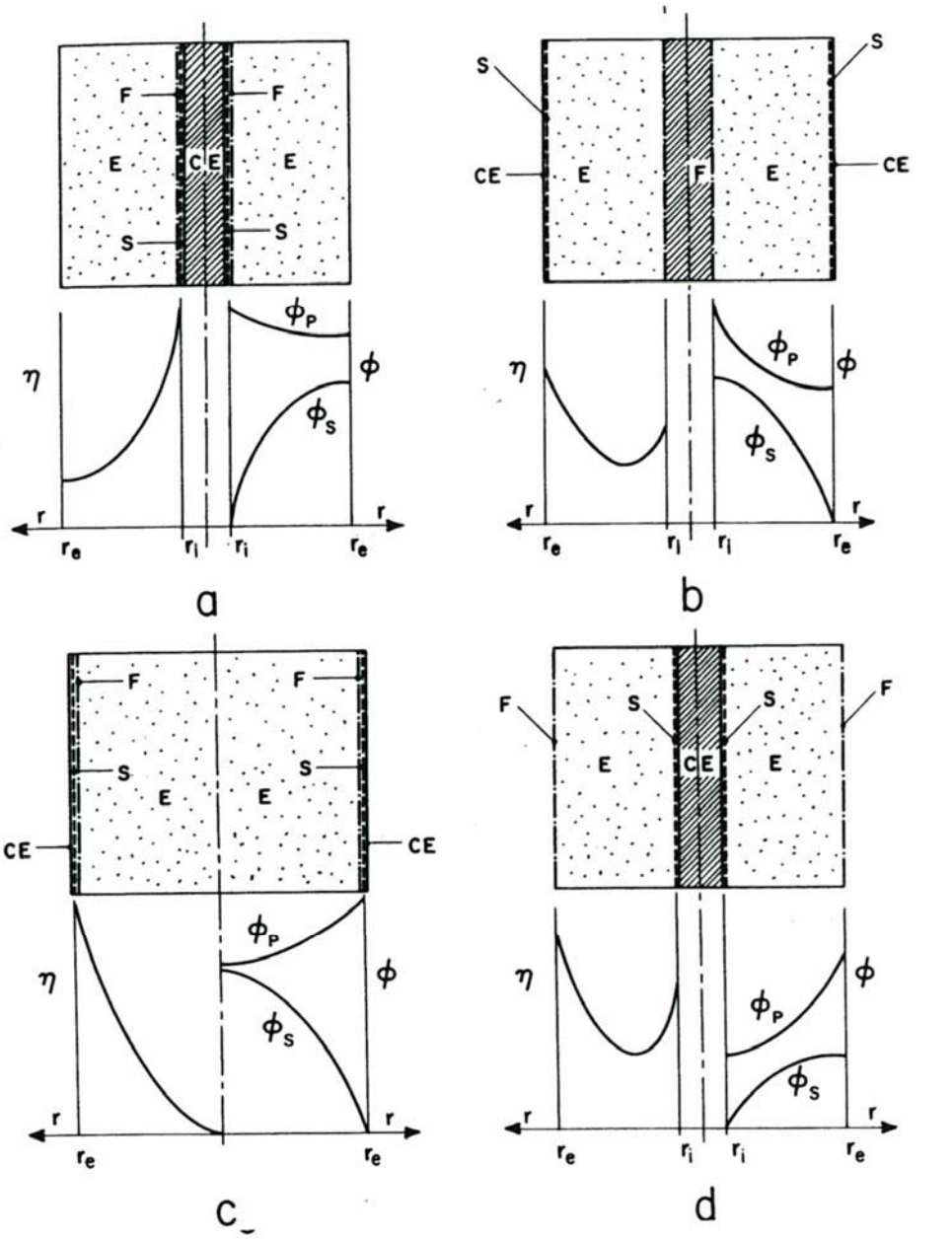
As the flow-through configuration simplifies modelling it is often used on laboratory scale and has been detailed by several authors[122-132]. However, in view of the limitations to scale-up it is unlikely to be employed on a commercial scale[96, 131].

2.3.2 Cell Geometry

The cell geometry may be cylindrical or rectangular and a variety of possibilities for the position of the counter electrode exist. To test each arrangement individually to determine the most effective would be far too costly and time consuming. Fortunately Kreysa et al.[99] conducted a theoretical analysis of the different design concepts through the development of a model for flow-by reactors. Many simplifying assumptions were made in the derivations and hence the analysis was only rough approximation. The various positions of the counter electrode for the cylindrical arrangement as well as the modelled potential distributions are shown in Figure 2.3.

It was concluded that the counter electrode and current feeder should not be adjacent due to the high overpotential distribution that results as shown in Figures 2.3a and 2.3c. It was also concluded that for a given value of the effective solution resistivity, the cylindrical configuration with an outer counter electrode was better than the rectangular geometry because the cylindrical arrangement allowed larger values of bed depth with smaller values of effective resistivity of the particulate phase and also of the ohmic drop across the bed. The cylindrical arrangement did however, present a more complex situation for modelling. As the materials required for stable anodes are usually expensive, the anode is sometimes placed inside of the cathode chamber to reduce the surface area requirements and hence reduce costs[83].

The theoretical effects of the electrode placements for systems with parallel current and fluid flow were discussed by Trainham and Newman[133] where a downstream placement of the counterelectrode was shown to be inferior.



CE	Counter electrode	ϕ	Electrode potential	r	Radial co-ordinate
E	3-D electrode	ϕ_p	Particle potential	r_e	External radius
F	Current feeder	ϕ_s	Solution potential	r_i	Internal radius
S	Separator	η	Overpotential		

Figure 2.3 Schematic representations of various design concepts of three-dimensional flow-by electrodes with cylindrical arrangement[99].

a Inner counter electrode, Inner current feeder

b Outer counter electrode, Inner current feeder

c Outer counter electrode, Outer current feeder

d Inner counter electrode, Outer current feeder

2.3.3 Modes of Operation

2.3.3.1 Electrolyte flow

The simple batch mode of operation is particularly useful for laboratory studies, developments or troubleshooting work and small-scale operations. However for commercial use two alternative modes of operation are preferred, namely batch recirculation and once-through flow. In the former method product from the cell is mixed with the feed and the liquor concentration gradually decreases in value during operation until the required terminal concentration is achieved. In the latter the inlet and outlet cell concentrations remain constant with time and the process is ended when all the liquor is passed through the cell.

From an analysis by Sioda[134] it was suggested that the once-through flow mode was the most economical. However, in order to achieve very low exit concentrations with once through flow it is necessary to operate with high cell residence times, i.e. low flow rates. The true single stage, single pass operation is rare; in practice, most cells have too low fractional conversion or are too difficult to control when operated in such a fashion. Batch recirculation is by far the most common mode of operation in practical installations[58].

2.3.3.2 Current Flow

Different methods for the electrical connections to the cell are possible. For cells containing multiple electrodes, these may be connected in series or in parallel. Furthermore the bed may be operated in a monopolar or bipolar fashion. The drawback of bipolar connections is that the electrode must act as both the anode and cathode and it is often difficult to find suitable materials[135].

Bipolar packed beds[117, 136] and fluidised beds[137, 138] have proven very useful for synthesising reactions. The advantages include the simplicity of the design, the possibility of scale up in the direction of current flow and the self cleaning action of the electrode surface. However by-passing of the current and high energy consumptions were reported[139]. As each individual particle exhibits a cathodic and anodic side they are not suitable for metal recovery processes due to the redissolution of the deposited metals.

2.3.4 Anode Material and Design

The conventional anode materials used for copper electrowinning are Pb or Pb-Sb alloys[140]. However these anodes have been shown to suffer from several disadvantages such as a relatively high potential for oxygen evolution due to the formation of a lead dioxide film, contamination of the electrolyte by corrosion and physical distortions due to the high ductility of the material[141]. These problems can generally be averted by the use of dimensionally stable anodes (DSA). These anodes generally consist of titanium but because of the formation of a thin, nonporous, non conducting TiO_2 film an electrocatalytic coating is mandatory. The oxides of the PGMs serve as excellent coatings.

Many previous investigations for metal electrowinning using a FBE have reported high cell voltages (i.e. high electrical energy consumptions) compared to conventional electrowinning. This is likely to be due to the conventional anodes used in their cells, rather than to the fluidised cathode[110, 142, 143]. The voltage distribution for the cell used in the work of Sabacky and Evans[91, 144] for copper electrowinning, was determined by Ziegler et al.[145]. It was found that the conventional anode chamber accounted for a significant part of the cell voltage (64.7%), and hence an investigation was undertaken to discover superior anodes. A variety of anodes and anodic reactions were evaluated with some offering improved energy consumptions compared to that of the conventional electrowinning plants. Although the investigation was not sufficiently detailed to identify which was the best, it did highlight that although the anode chamber has little effect on the current efficiency of the cathodic reactions the choice of anode material and reactions greatly affects the cell voltage and therefore power consumptions.

Difficulties with the use of conventional anodes in fluidised bed electrowinning exist. Masterson and Evans[96] have reported on the complications of adequately supporting the diaphragm of a large cell and of avoiding a bypass phenomenon where catholyte flows through the diaphragm into the anode chamber due to the differing bulk densities, resulting in different hydrostatic pressure gradients, on either side of the diaphragm. A possible solution is to provide an anode chamber where the pressure gradient matches (or is slightly higher than) that in the cathode chamber, such as particulate bed anodes. It should be noted that for cells without this matching

pressure gradient the force on the diaphragm would increase, on scale up, as the cube of the cell dimensions[145].

2.3.5 Cathode Material and Current Feeders

The particles used in bed electrodes are generally of the same metal as that to be recovered[83], except for mercury and precious metals, in which event such materials as copper or iron are used, with subsequent separation by conventional means[64]. Various types of cathode particles were investigated for the deposition of silver[146] including graphite particles. The concept was that these particles could be easily removed, without contamination of the product, during silver melting subsequent to electrolysis. Furthermore, the particles are "worthless", and their use would minimise security problems. While silver could deposit on the graphite particles, the deposit was dendritic, rather than smooth, and after some deposition of silver, the particles became difficult to fluidise. Silver particles and copper-coated silver particles were found to be more adequate. The current efficiencies were a little higher for the silver particles than for the silver coated copper particles, although this could be attributed to the higher electrolyte flow rates required to maintained a 25% bed expansion (and therefore improved mass transfer) around the larger and denser silver particles.

It is advantageous if the overpotential of hydrogen on the material is high, as this will provide a large working potential range within the bed electrode. Lead is an example of such a material[65], although it does pose health risks. Carbon materials have also been characterised by relatively low electrocatalytic activity for the reaction of hydrogen evolution[47]. The rates of electrochemical reactions occurring on carbon substrates are strongly influenced by the type of carbon used. The differences can be due to the level of oxygen functionalities and / or impurities present[147]. These impurities can inhibit or accelerate the electrode processes.

The conductivity of the graphite electrode matrix depends not only on the type of the material used, but also on the contact resistance between the particles in the bed and can be of the same order of magnitude as the conductivity of the electrolyte. Oloman et al.[72] increased the conductivity of a fixed bed consisting of graphite fibres by mechanically compressing the bed. As could be expected, bed conductivities decrease with increasing bed expansion[148,149].

Electrodes with poor conductivity, especially FBE, require a current feeder producing a good distribution of the current over the whole electrode and not one limited to a single point or zone. This can be achieved by the use of three-dimensional current feeders such as grids, spirals or fins.

Feeder efficiency depends on the number of collisions between the particles and feeder, as well as on the local density of particles close to the feeder. Thus, for grids, Vatistas and Bartolozzi[150] state that the arrangement of alternate superposition should be more efficient. The said authors also conducted experiments utilising copper spirals as the current feeder. Although spirals are not the optimal three-dimensional feeder, they were easy to construct and adequate for the purposes of the experiments and the current densities achieved during potentiostatic operation were five times greater using the three-dimensional feeder as compared to the two-dimensional feeder with the same applied overpotential. The effect of the velocity on the current density was found to be opposite for the two-dimensional and three-dimensional feeders. For the three-dimensional feeder the current density decreases as the velocity rises. This was attributed to the high degree of the expansion of the bed, which reduces the area in contact with the feeder. Yen and Yao[84] confirmed this relationship between velocity and current density for short-fin current feeders, but on the contrary, when using the long-fin current feeder, the current density was enhanced with increasing bed expansions, and the performance of metal recovery was improved.

2.3.6 Diaphragms and Membranes

Many complications relating to the employment of a diaphragm in both the laboratory and industrial scale reactors have been reported. Masterson and Evans[96] encountered problems such as leaks, fractures, deformations and bypassing of electrolyte through diaphragms that were too porous. A further experimental difficulty which was also reported by other authors[110, 142-144] was the metal deposition occurring on the diaphragm. Sabacky and Evans[144] found that copper deposits formed dendritic growths that extended through the diaphragm into the anode chamber eventually touching the anode and short circuiting the cell. This was reported to be more of a problem at low particle sizes and at low bed expansions and often accompanied non-uniform fluidisation (channelling and stagnation). Dubrovsky

and Evans[143] prevented this deposition problem by keeping a high degree of fluidisation (25-30%) and slightly tilting the bed the cell by 2 – 4 degrees.

Akzo Zout Chemie[83] claim to have developed a diaphragm that solves many of the usual problems. The mechanical strength is high, thus the diaphragm is able to withstand the pressure of the fluidised bed and is resistant to the erosion of the moving particles. In addition, the high mechanical strength makes it possible to subject the anode compartment to overpressure in order to prevent contamination of the anolyte by the catholyte. It is made of materials with a high chemical resistance and is therefore not attacked by aggressive media, such as chlorine gas and concentrated acids. The hydrodynamic permeability is very low, approximately 0.01 m^3 water per hour per m^2 of diaphragm at a pressure difference of 1 atm. The low hydrodynamic permeability is required in order to prevent a substantial loss of catholyte to the anode compartment due to pressure differences over the diaphragm of up to 0.5 atm. The low permeability of this diaphragm allows operation with a high bed height so that a high depletion per pass can be achieved. Moreover, the anolyte can be chosen irrespective of the catholyte. The structure of the diaphragm is such that the electrical resistance factor is low, and in consequence the contribution of the diaphragm to the cell voltage is low. Furthermore, the smooth diaphragm surface prevents adhesion of particles.

Goodridge et al.[151] showed that it is possible to operate without a diaphragm separating the particles from the anode. Although diaphragmless operation does reduce the current efficiency, the saving in energy consumption related to the lower cell voltage is significant. Furthermore, the cell design is simplified and less maintenance is required. However, in systems where the electrolyte may possibly produce an unwanted reaction at the anode, such as the evolution of chlorine gas, an ion selective membrane is required to prevent the chloride ions in the electrolyte from reaching the anode.

2.4 SCALED-UP AND INDUSTRIAL REACTORS

As will be shown below, a large spectrum of cell designs have been reported, particularly in the propriety and patent literature. It is difficult to know which of these designs have progressed beyond the prototype stage; but relatively few have

advanced into the commercial arena[58]. The cell designs are often an un-optimised empirical process due to lack of appreciation of the critical design factors.

2.4.1 Rotating Electrodes

Eco-Cell[2] features a rotating cathode surrounded by an outer stationary anode. The two chambers are separated by an ion-exchange membrane. The wastewater passes through the cathodic cavity and the dendritic metal crystals that grow on the cathode are swept away by the turbulent flow. Separation equipment then divides the slurry into a metals-depleted water stream and a concentrated powder/water mixture that goes on for metal recovery. The electrolytic device treats wastewater with metal concentrations ranging from 100 to 100 000 ppm, typically decreasing the contamination to between 2 and 10 ppm. The 20.4 ton/yr, 2 000 Amp, skid-mounted demonstration unit was field proven over a number of years before aiming at commercial clean up jobs in 1975.

2.4.2 Extended Surface Electrodes

Du Pont developed a porous, high-surface area spiral device to remove metals by electroplating them onto the unit as water flows through it. A 100 gal/min, 1 ft^3 demonstration unit cut copper levels in wastewater by 75-90 %, at concentrations from 5 - 100 ppm[152]. Besides copper, the unit has successfully handled gold, silver, mercury and lead in laboratory tests. Intermittent leaching removes the metals from the cathodes which are then recovered by flat plate electrolysis[2].

The Zandra cell is commonly used to electrowin silver from aqueous cyanide solutions[146]. This cell employed an extended surface area cathode consisting of steel wool. The cell was operated in a semi-batch mode with periodic shutdown for removal of the silver and replacement of the steel wool. The cell suffered from the disadvantage that the cathode degraded as it underwent a cementation reaction with the silver in solution. Consequently, the silver obtained from the cell was in the form of particles admixed with fragments of steel wool and required further processing to yield bullion.

EA Technology[10] has developed the Porocell, which is a cylindrical casing containing carbon felt cathode, for the electrochemical removal of heavy metals from waste streams. The solution is passed through the cell until the deposited material causes a significant pressure drop at which time the carbon cartridge is removed and replaced. The metals are recovered by chemical treatment or incineration. Metal concentrations are reduced to below 1 ppm and the process is said to be well suited for the removal of PGMs from dilute effluents.

2.4.3 Parallel Electrodes with Fluidised Electrolytes

The Chemelec cell[153, 154a] is a rectangular cell that employs alternating metal (or mesh) anodes and cathodes with electrolyte fluidisation of inert particles such as glass beads. The cell can be operated both with and without separators between the electrodes. The cathodes generally have a roughened surface (i.e. contain protrusions or peaks etc.) as this improves electrolyte mixing close to the cathode surface. The cathodes are slightly wider and longer than the anodes, such that deposition at the edges is not enhanced.

2.4.4 Packed Bed Electrodes

The EnViro-Cell described by Frank Walsh[154a] consisted of a packed bed of carbon granules and was used in the flow-by configuration. The modular arrangement allowed the reactor units to be stacked to accommodate various duties, whilst a high cathode area per unit volume resulted in a high fractional conversion in a single pass. Recovered metal may be removed from the reactor at intervals by vacuuming out the packed bed or by dissolving the deposited metal in a small electrolyte volume to produce a concentrate. Concentric versions of this model have also been developed. A further rectangular stationary particulate bed electrode was patented[155] in which metals were deposited onto carbonaceous particulate beds. A cylindrical bed with an inner working electrode has also been patented for the production of hypochlorite[156].

2.4.5 Fluidised Bed Electrodes

Three papers describing pilot plant sized FBEs are those by Wilkinson and Haines[142], Goodridge and Vance[157] and Boon et al.[83]. Wilkinson and Haines, who

patented their FBE[101-103], used a rectangular geometry with a diaphragm area of about 0.12 m^2 for reducing copper concentrations from 3000 ppm to 1 ppm, current densities ranging from 1000-5000 A/m^2 of diaphragm surface. Goodridge and Vance[157] also employed a rectangular cell with diaphragm area of about 0.2 m^2 for the electrodeposition of copper from sulphate solutions. From the pilot plant trials it was shown that provided the characteristic dimension in the direction of current flow is kept constant, similar potential and current distributions as those for the smaller cell are obtained. Boon et al.[83] used a cylindrical geometry with a multiplicity of rod-shaped current feeders and anodes. Each of the anodes was surrounded by a diaphragm. Testwork studies included the deposition and simultaneous separation of copper and cadmium from a concentrated zinc stream and the removal of mercury from brine. The largest cell used a bed height of 1.2 m and seven diaphragms were contained in a diameter of 0.35 m. This FBE, developed by Akzo Zout Chemie is by far the most commonly known scaled up version and was referred to in numerous articles[64, 67, 93, 157, 158]. Unfortunately owing to the non-optimum hydrodynamic conditions, the process was reported to not have progressed from pilot plant tests[100].

Other articles offering more interesting modifications of the FBE are discussed below.

The limitations of bed expansion and bed thickness are clear obstacles to increasing the feed rate of electrolyte. For the treatment of large quantities of industrial wastes within a short time, it is necessary to increase the effective bed thickness. Yasuda et al.[159] found that one method of scaling up the effective bed depth was to insert electro-conductive partition plates (ECPs) into the fluidised bed. The rectangular cell was divided into three fluidised beds by the insertion of two ECPs and three sheets of diaphragms. The particles are activated as the electrode by utilising the bipolar action of the ECP and by the collision of particles with the ECP. The method using the ECPs was found to be effective for scaling up the FBE since the power consumption hardly increased with an increase in the electrolytic capacity (kg Cu/C).

The publication of Verma et al.[112] is a continuation of the investigation of SBE described previously[111] in Section 2.2.5, where the bed employed was only 10-20 cm high and 6-10 cm across. When using a draft tube, beds of 1.7 m high were successfully spouted under all conditions tested. This height was limited only by the

height of the apparatus that could be accommodated in the laboratory. There appeared to be no reason why yet taller beds with draft tubes could not be spouted. However, without a draft tube, beds of greater than 0.26 m height could not be spouted. It seemed that a full-length draft tube was a necessary and desirable feature of a tall thin spouting bed. Electrodeposition of metal in regions of a SBE where the particles are stationary ("dead zones") is to be avoided, because such a dead zone will grow with time as metal is deposited onto it. It was found that a draft tube would bring about downward motion in the annular region to only a limited horizontal distance from the tube.

In a patented design of a fluidised bed electrochemical reactor, Zaromb[160] incorporated a system of horizontal jets. This enabled the use of high electrolyte velocities, thus enhancing mass transfer without the negative aspects associated with large bed expansions.

A number of other FBE designs have also been patented for metal recoveries [161-168]

2.5 ECONOMICS

Most investigations concerning three-dimensional electrodes were made from an academic point of view describing the parameter effects on the potential and current distributions, the current efficiencies and cell voltages, but little economic comparisons of three-dimensional electrodes compared to other processes for metal recovery have been reported.

Stankovic and Janes[169] therefore began work to examine the economic aspects of three-dimensional electrodes and to obtain areas of viability and areas of nonviability for metal winning. They claimed that the four main cost contributions are capital investment, cost of energy, cost of raw material and labour costs. The effects of parameters such as flowrate and concentration were investigated for a three-dimensional bed, a bed of inert particles and a cell with an empty channel.

It was found that a change in fluid flowrate did not significantly affect the capital cost over the given range of velocity that was used (2-10 cm/s). However, of great importance was the fact that the capital costs were determined to be two orders of

magnitude lower in the case of the three-dimensional electrode cell as compared to the cases of an empty channel cell and a cell with fluidised inert particles. The total costs per unit of metal produced decrease with increasing electrolyte velocity in the case of the empty cell. For the other two cells they remain practically constant over the given range of velocity.

The inlet concentration of the reacting ions had a greater influence on the production costs. A strong increase of capital costs was associated with a decrease of concentration while the energy costs passed through a minimum which was more marked for a three-dimensional electrode cell. The lowest total costs were provided by the three-dimensional electrode cell for concentrations less than 1 g/dm^3. Optimal costs are obtained for a feed concentration range of about 0.06 to 1 g/dm^3.

Akzo Zout Chemie Nederland B.V. (Akzo) introduced a commercial-scale application of the FBE to a firm in West Germany to replace the ion exchange process for copper recovery from a waste acid stream. The ion exchange process required neutralisation of the stream with ammonia thus rendering the recycle of the sulphuric acid impossible. Since the use of a FBE allows the acid to recycle, the reduced consumption of that material and the ammonia resulted in an annual operating saving of around $200 000 per FBE unit[64]. Akzo maintained that the capital costs of FBE and ion exchange are comparable.

The removal of copper and cadmium from a zinc solution is usually accomplished by cementation. With the cementation method, a typical stream containing 150 g/l Zn, 800 ppm Cu and 800 ppm Cd, can be treated with 3 g/l Zn powder to produce a purified stream of 152 g/l Zn, 1 ppm Cu and 10 ppm Cd. For the same application, a two-step FBE technique can reduce copper content to less than 0.1 ppm and Cd to 1 ppm. And unlike the cementation step, which yields a byproduct copper/cadmium "cement", FBE can produce 90 % pure Cd and 99$^+$ % pure copper. Comparing cementation with FBE, Akzo Zout Chemie calculated that the investment in a cementation plant of a 150 000 mt/yr zinc refinery would amount to $8 million, with operating costs of $800 000 /yr. An FBE plant for the same task would cost $6 million, with operating costs totalling $1.3 million /yr. The higher operating costs are offset by credits, however. Somewhat greater zinc output (because Zn for cementation is eliminated), plus higher-grade recovered copper and cadmium, result

in credits of $3.2 million /yr. Hence it was claimed that investment is $2 million lower, while gross operating profits are $2.7 million higher[64, 83, 158].

The economics of the Eco-cell described in Section 2.4.1 looked attractive, according to Ecological Engineering's estimates[2]. For example, a unit handling about 3 200 gal/h of an effluent containing 368 ppm copper should win 37.4 tons/yr of the metal. The value of the recovered copper at the prices in 1975 was about $38 000 easily outpacing the annual operating costs of the Eco-Cell installation of about $15 000.

Rough estimates of the capital and running costs of a packed bed electrochemical reactor were shown by Bennion and Newman[62] to be economically viable for the reduction of copper ions.

2.6 MODELLING

Due to the complexity of the electrochemical system with a three-dimensional electrode, a large number of assumptions are usually made to simplify the computations. Some of these assumptions seriously limit the utility of the solution. In the articles concerned with modelling, the cathode material was generally the same as the metal to be deposited and therefore the changes in the properties of the electrode during reaction were not considered. If however, the cathode material is dramatically altered during reaction, the modelling of such effects could prove to be impossible.

Numerous parameters are required for detailed modelling. These values can be found from independent experiments, but such experiments are expensive and time consuming. Also, parameters determined from isolated experiments may not apply to the interacting phenomena of a real process[170].

As a result of the vast amount of research done concerning different types of three-dimensional electrodes and the variety of configurations available for each, a melange of models have been proposed, thus making it impractical to recount on all of them. Of particular interest was the model derived from the overall mass and charge balances across the reactor without concern for the distributions within the three-dimensional electrode. This model allows the determination of the spatially

averaged mass transfer coefficient and the current efficiency of the primary reaction. Models of this type were used by Matic[171], Walker and Wragg[172-174], Welse et al.[175] and Stankovic and Wragg[176]. A similar derivation is given in Section 5 and used for analysis in the present investigation. For engineering requirements, the model provides a convenient way of predicting the concentration-time behaviour.

2.7 SURVEY CONCLUSIONS

2.7.1 PGM Electrochemistry

Cyclic voltammetry was shown to be a powerful tool for investigating reaction mechanisms and the influence of various parameters, especially when used in conjunction with other techniques such as

- Nuclear Magnetic Resonance (NMR)[15]
- Modulated Specular-Reflection Spectroscopy (MSRS)[37]
- Surface Enhanced Raman Spectroscopy (SERS)[43, 49]
- Scanning Tunnelling Microscopy (STM)[19, 24, 41, 45]
- Transmission Electron Microscopy (TEM)[16]
- Electrochemical Quartz Crystal Microbalance (EQCM)[41]
- X-ray photoelectron spectroscopy (XPES) [31, 45]
- X-ray diffraction (XRD)[41]

Both platinum and palladium were shown to be easily electrodeposited. Palladium was found to be less resistant to corrosion[44], with higher rates of electrodissolution being reported in acidic media[30] and cyanide baths[177] compared to platinum. Palladium exhibits the unusual capability for hydrogen absorption[44] thus resulting in complicated electrochemistry. The literature survey highlighted potential problems regarding the deposition and anodic dissolution of the PGM material due to hydrogen adsorption and oxide formation respectively. However, possible methods to overcome such obstacles were also mentioned such as the use of an alternating current during anodic stripping to remove the oxides formed or the additive of a compound to the electrolyte or adjustment of the pH to hinder the hydrogen adsorption.

The reaction rates and mechanisms occurring during electrochemical treatment are dependent on many factors such as the substrate material and state, the concentration and speciation of the electroactive species, pH, temperature and composition of the supporting electrolyte to mention but a few. The anions in solution affect the surface state of the electrode and thereby influence the properties of the substrate and the reactions occurring. Furthermore, as different complexes are formed in various electrolytes, different mechanisms are involved in the reduction/oxidation processes.

Thus, although literature pertaining to similar systems may offer insight into possible, or at best likely, reactions it is not sufficient to draw direct conclusions from previous testwork. A detailed investigation was therefore undertaken, in parallel with this testwork, to examine the electrochemical reactions occurring in a solution of similar composition to the plant solution to be treated[178]. Techniques such as cyclic voltammetry and microscopy were utilised and the reactions were conducted on various surfaces including the graphite material employed in the benchscale electrochemical reactor. This work provided a great deal of insight and reference to the material is made.

2.7.2 Reactor Configuration

Numerous researches have shown that it is possible to reduce metal concentration in a solution down to as little as 1 ppm using various three-dimensional cathodes[10, 62, 64, 142, 146, 174, 179]. The recovery of metals, such as copper, has been publicised to be highly cost effective. As the market value of precious metals is substantially greater than these metals, it can be assumed that this process would prove even more economically viable.

Three-dimensional electrodes are definitely the answer to waste stream treatment. For the intended application, a particulate bed was selected over a rigid electrode such as the porous or screen electrodes in that the reactor may be charged or discharged as necessary without the employment of manual labour. This has key advantages such as the minimisation of the health risks associated with PGM containing solutions and security benefits. Also the pressure drop across the particulate bed is significantly lower than that associated with a porous electrode and

the surface area per unit volume of a packed bed of small particles is greater than that of a screen.

Fluidised bed electrodes seemed very attractive for metal recovery from the viewpoint that these electrodes offer high surface area and avoid agglomeration of particles, thus allowing continuous operation. However, the existence of a definite dissolution zone in which overpotentials are positive in a nominally cathodic bed is a major drawback. Fixed beds were therefore deemed preferential as such zones are not present. Furthermore, the specific agitation effect of the particles decrease as the bed expands therefore the efficiency of a bed electrode is greater at the state of the packed bed than at the state of the fluidised bed. The primary disadvantage of the packed bed is the agglomeration of particles but methods have been established for continuous operation. Furthermore, operation of a packed bed is simpler in that the control and distribution of the flow of electrolyte is not crucial to the performance of the reactor as it is for the FBE and moving beds.

Although the modelling of the processes occurring is simplified using the flow-through configuration, this arrangement is not practical for industrial scale applications and thus it was deemed more appropriate to conduct the testwork using the flow-by configuration. It has been suggested that a cylindrical arrangement with an outer counter electrode on the opposite side of the bed of the current feeder would be more beneficial in terms of the potential distribution generated. A cation exchange membrane is necessary to avoid the production of chlorine gas at the anode. The preferred anode material for oxygen evolution would be titanium with a propriety coating as this is resistant to corrosion in the acidic medium to be used. It has been shown that the anode chamber has little effect on the current efficiencies but greatly affects the cell voltage. The distance between the anode and the membrane should therefore be minimised.

Electrochemical deposition of platinum and palladium from dilute effluent streams has been shown to be possible using a carbon cathode, although the co-deposition of base metals such as nickel and copper and other contaminants has been noted[9]. Carbon is relatively inexpensive and the metals are easily recovered. The use of a different cathode material could however, lead to a more selective process.

3 THEORY

Metal ions can be removed from solution by reducing them to the metallic state with the addition of electrons. These electrons can be supplied either by homogeneous electrochemical reaction, that is to say from a simultaneous redox reaction, or heterogeneous electrochemical process whereby the electrons are provided from an external power supply. However, both methods require an oxidation reaction to occur either to supply the electrons directly or to complete the circuit to the power supply.

For the heterogeneous electrochemical reduction of palladium in aqueous acid chloride solutions the following electrode reaction occurs at the cathode:

$$PdCl_4^{2-} + 2e^- \rightarrow Pd + 4Cl^- \qquad [3.1]$$

Hydrogen is also produced at the cathode by the reaction:

$$H^+ + e^- \rightarrow \tfrac{1}{2}H_2 \qquad [3.2]$$

For electrolytes containing chloride ions, the evolution of chlorine gas will occur at the anode according to Reaction 3.3.

$$2Cl^- \rightarrow Cl_2 + 2e^- \qquad [3.3]$$

The insertion of a cation exchange membrane to form separate anode and cathode chambers allows for a chloride free solution to be used as the anolyte and hence prevents the formation of chlorine gas. With sulphuric acid as the anolyte, the anodic reaction is the oxidation of water and is shown by:

$$2H_2O \rightarrow O_2 + 4H^+ + 4e^- \qquad [3.4]$$

The hydrogen ions formed in Reaction 3.4 pass through the membrane to maintain electroneutrality of the electrolytes.

3.1 ELECTROCHEMICAL REACTION RATES

For the electrochemical reaction

$$M^{n+} + ne^- \rightarrow M \qquad [3.5]$$

the reaction rate (r) is given by Faraday's Law[154b] as

$$r = \frac{M_w I}{nF} \qquad [3.6]$$

The current density (j) on the electrode surface is defined as

$$j = \frac{I}{A_p} \qquad [3.7]$$

As the reactions occur on the electrode surface, it is more suitable to define the reaction rate per surface area of the electrode ($\dot{r}$), given by

$$\dot{r} = \frac{M_w j}{nF} \qquad [3.8]$$

If the rate of reaction is assumed to be first order, then the rate is proportional to the concentration of the reacting species.

$$\dot{r} = kc \qquad [3.9]$$

As side reactions may also occur, we define the charge yield (ϕ_P) as the fraction of the applied charge used in the reaction of interest.

$$\phi_P = \frac{Q_{rxn}}{Q_{app}} \qquad [3.10]$$

The fraction of the applied current or current density used in the primary reaction is termed the current efficiency (ϕ) and defined in Equation 3.11. If a constant current is applied and the reaction rate remains constant with time, the current efficiency will be equal to the charge yield.

$$\phi = \frac{I_{rxn}}{I_{app}} = \frac{j_{rxn}}{j_{app}} \qquad [3.11]$$

Thus the overall reaction rate expressed in terms of the applied current density is given by

$$\dot{r} = \frac{M_w \phi \, j_{app}}{nF} = kc \qquad [3.12]$$

3.2 CONTROLLING RATE

For the reaction to take place a series of processes must occur, namely the reactants must diffuse from the bulk solution to the surface, electrons must be transferred at the surface and the products transported back to the bulk solution. The reaction may be controlled by the rate of electron transfer or by the rate of mass transfer or both, referred to as mixed control.

3.2.1 Electron Transfer Controlled

The equilibrium potential E_e for the reaction

$$O + ne^- \Leftrightarrow R \qquad [3.13]$$

can be calculated using the Nernst equation[154c] below

$$E_e = E^\circ - \frac{RT}{nF} \ln \frac{a_R}{a_O} \qquad [3.14]$$

For solutions with low ionic strength, the activity coefficients are approximately unity and the standard potential (E^o) and concentrations of the species may then be used to calculate the reversible potential. For solutions with high ionic strength the activity coefficients are necessary for accurate determination. Estimations of these activity coefficients are complex especially for multicomponent systems. As the reduced state is a solid, the reductive activity is unity (a_R = 1) and therefore this leads to:

$$E_e = E^\circ - \frac{RT}{nF} \ln \frac{1}{\gamma_o c_O} \qquad [3.15]$$

The overpotential (η) is defined as the potential shift from the equilibrium potential and therefore the overpotential at equilibrium is zero (η = 0).

$$\eta = E - E_e \qquad [3.16]$$

The observed current density is the algebraic sum of the partial cathodic and anodic current densities at a particular electrode (cathode or anode):

$$j = \vec{j} + \overleftarrow{j} \qquad [3.17]$$

At equilibrium the observed current density is zero (j = 0) as the partial current densities are equal in magnitude but opposite in sign. The partial current density at equilibrium is known as the exchange current density (j_0).

$$j_0 = -\vec{j} = \overleftarrow{j} \qquad [3.18]$$

The partial current densities of the anodic and cathodic reactions may be expressed by equating the rate expressions given by Equations 3.8 and 3.9 as follows:

$$\text{Rate of cathodic reaction} = -\vec{k}(c_O)_{x=0} = \frac{M_w \vec{j}}{nF} \quad \Rightarrow \quad \vec{j} = -\frac{nF\vec{k}(c_O)_{x=0}}{M_w} \qquad [3.19]$$

$$\text{Rate of anodic reaction} = \overleftarrow{k}(c_R)_{x=0} = \frac{M_w \overleftarrow{j}}{nF} \quad \Rightarrow \quad \overleftarrow{j} = \frac{nF\overleftarrow{k}(c_R)_{x=0}}{M_w} \qquad [3.20]$$

The reactions occur at the electrode-electrolyte interface and therefore the rate is proportional to the concentration of the reacting species at the electrode surface which is denoted by $(c_O)_{x=0}$ and $(c_R)_{x=0}$ for the oxidised and reduced species respectively. The electron transfer rate constants ($\vec{k}, \overleftarrow{k}$) are highly dependent on the electrode potential (E) and empirical expressions for these rate constants are reported by Walsh[154d] to be:

$$\vec{k} = \vec{k}_0 \exp\left[\frac{-\alpha_C nF}{RT}E\right] \qquad [3.21]$$

$$\overleftarrow{k} = \overleftarrow{k}_0 \exp\left[\frac{\alpha_A nF}{RT}E\right] \qquad [3.22]$$

The constants $\vec{k}_0$ and $\overleftarrow{k}_0$ are the rate constants for electron transfer of the cathodic and anodic reactions respectively when the electrode potential is zero versus the reference potential. These constants have no fundamental significance because of their arbitrary nature.

Substituting Equations 3.19 to 3.22 into Equation 3.17 and Equation 3.18 results in the current density and exchange current density being represented by the following two equations respectively:

$$j = \frac{nF\overleftarrow{k}_0(c_R)_{x=0}}{M_w}\exp\left[\frac{\alpha_A nF}{RT}E\right] - \frac{nF\vec{k}_0(c_O)_{x=0}}{M_w}\exp\left[\frac{-\alpha_C nF}{RT}E\right] \qquad [3.23]$$

$$j_0 = \frac{nF\overleftarrow{k}_0(c_R)_{x=0}}{M_w}\exp\left[\frac{\alpha_A nF}{RT}E_e\right] = \frac{nF\vec{k}_0(c_O)_{x=0}}{M_w}\exp\left[\frac{-\alpha_C nF}{RT}E_e\right] \qquad [3.24]$$

Using the above expression, we can substitute the exchange current density into Equation 3.23 to give

$$j = j_0\frac{\exp\left[\frac{\alpha_A nF}{RT}E\right]}{\exp\left[\frac{\alpha_A nF}{RT}E_e\right]} - j_0\frac{\exp\left[\frac{-\alpha_C nF}{RT}E\right]}{\exp\left[\frac{-\alpha_C nF}{RT}E_e\right]} \qquad [3.25]$$

From the definition of overpotential given in Equation 3.16, the above gives rise to the well known Butler-Volmer equation shown below. This equation is only applicable to electron transfer controlled reactions.

$$j = j_0\left\{\exp\left[\frac{\alpha_A nF}{RT}\eta\right] - \exp\left[\frac{-\alpha_C nF}{RT}\eta\right]\right\} \qquad [3.26]$$

The overall reaction rate at the electrode is described by:

$$\dot{r} = \frac{M_w j}{nF} = \overleftarrow{k}(c_R)_{x=0} - \vec{k}(c_O)_{x=0} \qquad [3.27]$$

As the rate of the oxidation reaction may be assumed negligible for very negative overpotentials [$|\eta|$>118/n mV], this simplifies the rate for cathodic reactions to

$$\dot{r} = \frac{M_w j}{nF} = -\vec{k}(c_O)_{x=0} \qquad [3.28]$$

The surface reaction occurs at such a low rate the concentration of the species at the surface can be assumed to be equal to the bulk concentration. Under such circumstances the current density is referred to as the electron transfer controlled current density (j_{ET}).

$$\dot{r} = \frac{M_w j_{ET}}{nF} = -\vec{k}c \qquad [3.29]$$

3.2.2 Mass Transport Controlled

Diffusion, convection and migration are the three general forms of mass transport. Migration of the reacting species can be neglected as the migration current is mainly carried by the ions of a chemically inert conductive electrolyte that is present in high concentration in solution. Thus convective-diffusion will be considered as the main form of mass transport.

Complex velocity and concentration profiles arise near the electrode surface when convection and diffusion co-exist. The Nernst diffusion layer model was used to simplify the description of these profiles. The model assumes a stagnant layer of thickness δ near the electrode surface. The only form of mass transport in this layer is diffusion. Beyond this stationary layer, i.e. ($x > \delta$), is the convection zone where the concentration is assumed to be uniform.

Fick's First Law[154e], as given in the equation below, can be used to relate the flux resulting from diffusion to the reactant concentration gradient:

$$N = -D\frac{dc}{dx} \qquad [3.30]$$

Strictly speaking, this expression is only valid for linear diffusion to a planar electrode. This implies that the active electrode surface is flat and the concentration varies perpendicular to the electrode surface.

As mass is conserved at the electrode surface the flux of the reacting species to surface can be set equal to both the rate of reaction and the flux of the reduced species (if any) away from the surface. Using the reaction rate (given by Equation 3.8) and the above expression for the flux of a species, the mass balance is shown by:

$$-D_O\left(\frac{dc_O}{dx}\right)_{x=0} = \frac{M_w j}{nF} = D_R\left(\frac{dc_R}{dx}\right)_{x=0} \qquad [3.31]$$

Due to the assumption that only diffusion occurs in the boundary layer the concentration profiles at steady state are linear and the concentration gradient takes the form:

$$\left(\frac{dc_O}{dx}\right)_{x=0} = \frac{c_O - (c_O)_{x=0}}{\delta} \qquad [3.32]$$

In reality there is no exact boundary separating the regions between pure diffusion and convection at x = δ, but rather a gradual transition occurs between the two forms of mass transfer. The realistic concentration profile and that predicted by the Nernst model are shown in Figure 3.1.

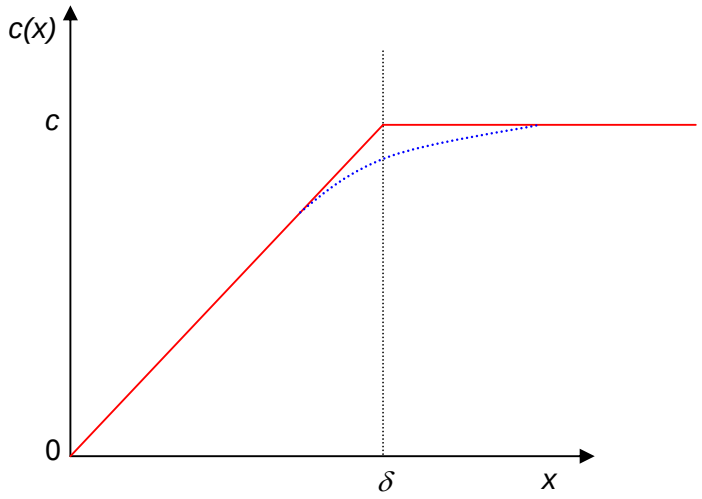


Figure 3.1 Concentration profile assumed by Nernst diffusion layer model versus actual concentration profile shown by a dotted line

Substituting Equation 3.32 into Equation 3.31 and rearranging for *j*:

$$j = \frac{-nFD_O[c_O - (c_O)_{x=0}]}{M_w \delta} \qquad [3.33]$$

The mass transport coefficient (k_m) is defined as

$$k_m = \frac{D}{\delta} \qquad [3.34]$$

The current density expressed in terms of the mass transport coefficient is then

$$j = \frac{-nFk_m[c_O - (c_O)_{x=0}]}{M_w} \qquad [3.35]$$

and thus the rate of reaction is given by

$$\dot{r} = \frac{M_w j}{nF} = -k_m [c_O - (c_O)_{x=0}] \qquad [3.36]$$

Under complete mass transport control the concentration of the reacting species at the electrode-solution interface is zero i.e. $(c_O)_{x=0} = 0$. The limiting current density (j_L) is reached and the rate of reaction for these conditions is:

$$\dot{r} = \frac{M_w j_L}{nF} = -k_m c_O \qquad [3.37]$$

3.2.3 Mixed Control

Mixed control occurs when the reaction rate is governed by both the supply of the reactant and the electron transfer to and from the electrode surface. When the rate constants for electron transfer ($\vec{k}$) and mass transport (k_m) become comparable, the surface concentration of reactant lies between the concentration of that species in the bulk solution and zero. The concentration profile for mixed control is shown as curve (b) in Figure 3.2 with a surface concentration of $(c_O)_{x=0}$.

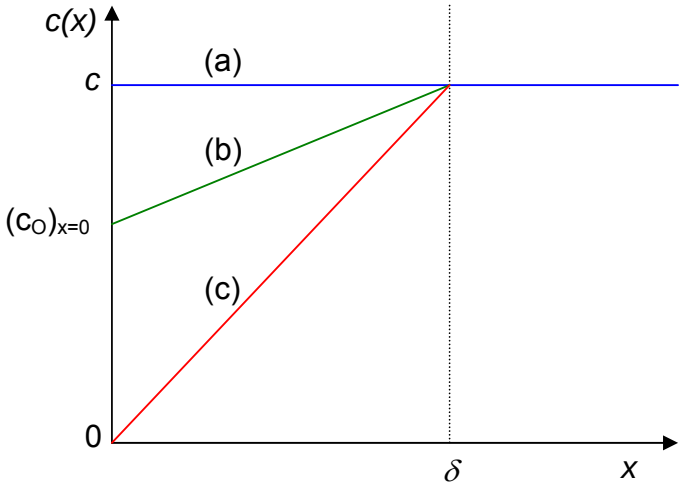


Figure 3.2 Concentration profiles in the Nernst diffusion layer

(a) Electron transfer controlled reaction

(b) Mixed controlled reaction

(c) Mass transport controlled reaction

In this study it is assumed that the system under investigation is at a pseudo-steady state, even though the reaction rate varies with time, allowing one to set the rate of electron transfer (Equation 3.28) equal to that of mass transport (Equation 3.36) and rearranging to solve for $(c_O)_{x=0}$

$$\dot{r} = \frac{M_w j}{nF} = -k_m\left[c_O - (c_O)_{x=0}\right] = -\vec{k}(c_O)_{x=0} \qquad [3.38]$$

$$(c_O)_{x=0}\left[\vec{k} + k_m\right] = k_m c_O \qquad [3.39]$$

$$(c_O)_{x=0} = \frac{k_m c_O}{\vec{k} + k_m} \qquad [3.40]$$

Substituting Equation 3.40 above into either equation for reaction rate gives rise to an expression for the reaction rate under mixed control in terms of the bulk concentration:

$$\dot{r} = \frac{M_w j}{nF} = -\frac{1}{\frac{1}{k_m} + \frac{1}{\vec{k}}} c_O \qquad [3.41]$$

The observed current density (j) during mixed control can be expressed in terms of the limiting current density (j_L) and the current density due to electron transfer (j_{ET}) by manipulating Equation 3.41 and substituting Equations 3.29 and 3.37 as follows:

$$j = -\frac{1}{\frac{1}{k_m} + \frac{1}{\vec{k}}} \frac{nFc_O}{M_w} \qquad [3.42]$$

$$\frac{1}{j} = -\frac{k_m + \vec{k}}{k_m \vec{k}} \frac{M_w}{nFc_O} \qquad [3.43]$$

$$\frac{1}{j} = \left(-\frac{k_m}{k_m \vec{k}} \frac{M_w}{nFc_O}\right) + \left(-\frac{\vec{k}}{k_m \vec{k}} \frac{M_w}{nFc_O}\right) \qquad [3.44]$$

$$\frac{1}{j} = \frac{1}{j_{ET}} + \frac{1}{j_L} \qquad [3.45]$$

Under mixed control the rate of reaction will, to some extent depending on the ratio of j_L to j_{ET}, be a function of the electrode potential. The relationship is shown by

substituting the electron transfer rate constant in Equation 3.42 with Equation 3.21 as shown below.

$$j = \frac{-\frac{nFc_O}{M_w}}{\frac{1}{\vec{k}_0 \exp\left[\frac{-\alpha_C nF}{RT}E\right]} + \frac{1}{k_m}} \qquad [3.46]$$

The onset of mixed control was stated to occur when the current density reached a mere 5% of the limiting current[(154f)].

4 EXPERIMENTAL

4.1 EXPERIMENTAL APPARATUS

As was shown in the literature survey an assortment of reactor designs are possible. Time limitations did not permit the study of each configuration. The chosen design of the reactor and the experimental set-up was deemed the most appropriate based on the conclusions drawn from the literature review discussed in Section 2.7.2.

4.1.1 Electrochemical Reactor

The bench scale electrochemical reactor is shown schematically in Figure 4.1, and a cross section through the bed is shown in Figure 4.2. The reactor was of cylindrical geometry with an inner cathodic chamber surrounded by the anodic compartment. A membrane was used to support the particulate bed and separate the electrolytes. As the catholyte to be treated contained chloride ions, a cation exchange membrane was essential to avoid the evolution of chlorine gas at the anode. In addition to this, the membrane also prevented the oxidation of the metal ions to higher oxidation states which would then reduce the current efficiency of the process.

The catholyte entered the reactor via a calming chamber which was constructed of titanium. It was pumped upward through the packed bed cathode which was made up of graphite particles. The particles were of a size fraction between 600 μm and 1000 μm. A polypropylene mesh with an opening of 500 μm was used to contain the bed. A titanium rod with a proprietary coating, described in Table 4.1, functioned as the current collector and passed through the centre of the bed. The rod was supported by a PVC stand placed in the calming chamber and was insulated using heat shrinking PVC, exposing only the length through the bed and the tip for the electrical connection to the external circuit. The catholyte exited the reactor via an overflow from the side of the perspex hood. The hydrogen gas evolved from the secondary reduction reaction was vented from the outlet positioned at the top of the hood.

The anolyte entered the annulus formed between the membrane and the outer anode through the inlet at the base of the anode. The solution was pumped upward through the chamber and exited from the outlet near the top of the compartment located at the opposite side of the inlet. The anode compartment contained a plastic mesh. This mesh provided support for the membrane as well as allowed for the gas generated to channel up to the outlet and exit with the anolyte stream.

A plastic capillary was connected to a specially modified salt bridge, shown in Figure 4.3, which contained the Ag/AgCl reference electrode. The open end of the capillary was placed at the base of the exposed current collector. The salt bridge and capillary were filled with 3 M KCl and a syringe connected to the salt bridge allowed for the injection of fresh solution as well as the removal of any bubbles from the capillary. The reference electrode allowed for the monitoring of the cathode potential at the specific location.

Table 4.1 Details of the components in the reactor

Component	**Material**	**Dimensions**
Membrane	Membranes International CMI-7000/CR Cation Exchange	Diameter: 36 mm Height: 100 mm Surface area: 113 cm^2
Particles	Isostatically pressed graphite	Size range: 0.6 - 1.0 mm Surface area: 0.5 m^2
Current Collector	Iridium oxide (IrO_2) / tantalum oxide (Ta_2O_5) coated titanium rod	Diameter: 6 mm Length: 100 mm Surface area: 19 cm^2
Anode	Iridium oxide / tantalum oxide coated titanium supplied by Titanium International Fabricators (Pty) Ltd	Inner diameter: 45 mm Height: 100 mm Surface area: 140 cm^2

The technical specifications of the membrane and the graphite particles used in the testwork are given in Appendices A1 and A2 respectively. The total surface area of the particles referred to in Table 4.1 is based on the approximate geometrical surface area calculated from the mean particle diameter.

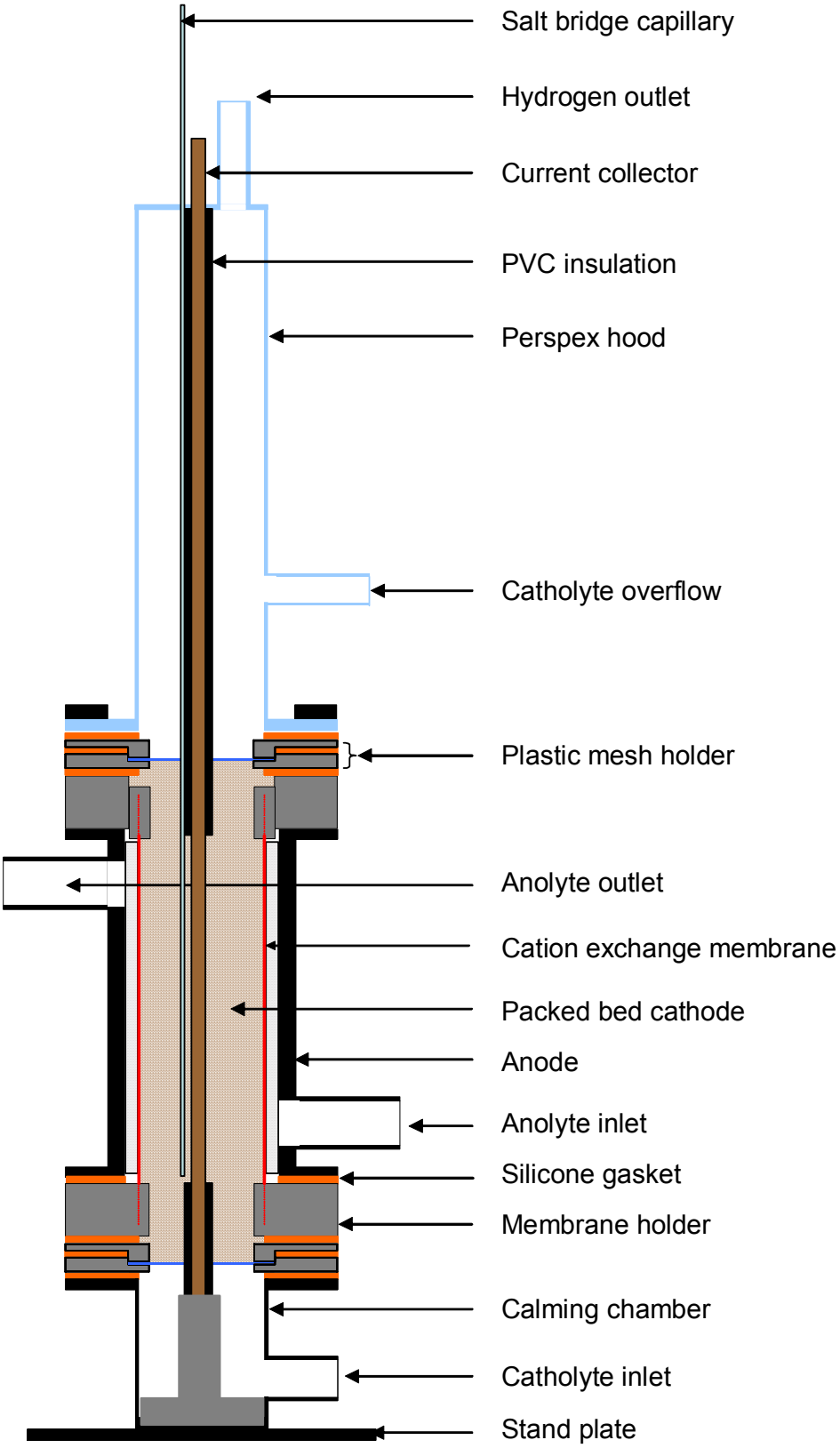


Figure 4.1 Schematic diagram of the electrochemical reactor

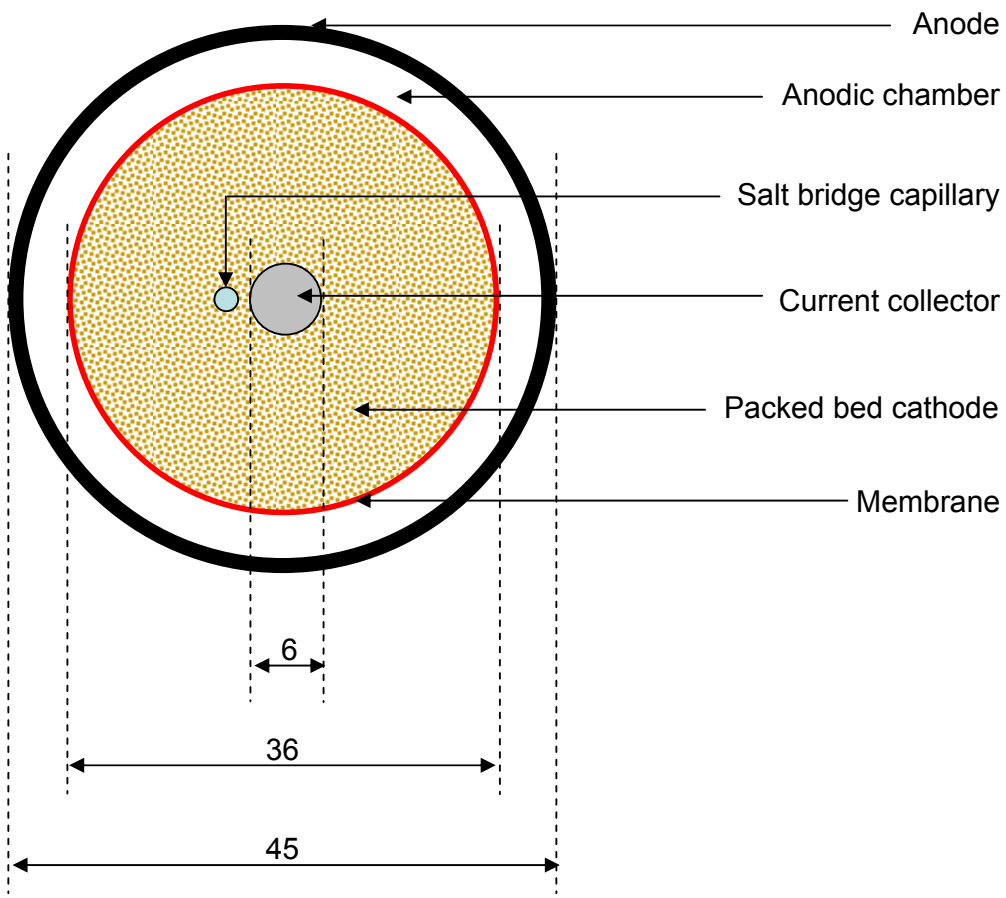


Figure 4.2 Cross section through mid height of the reactor. (All dimensions shown are in millimetres)



Figure 4.3 Modified salt bridge containing reference electrode

4.1.2 Flow Circuit

A batch recirculation system was used for both the electrolytes. A Masterflex® peristaltic pump was used with two Easy-Load II® pump heads mounted onto the standard digital drive. Tygon® silicone tubing (L/S® 18) was used through the pump channels with the remainder of the system using standard silicone tubing of various sizes. A schematic diagram showing the layout of the apparatus and the flow circuit is given in Figure 4.4.

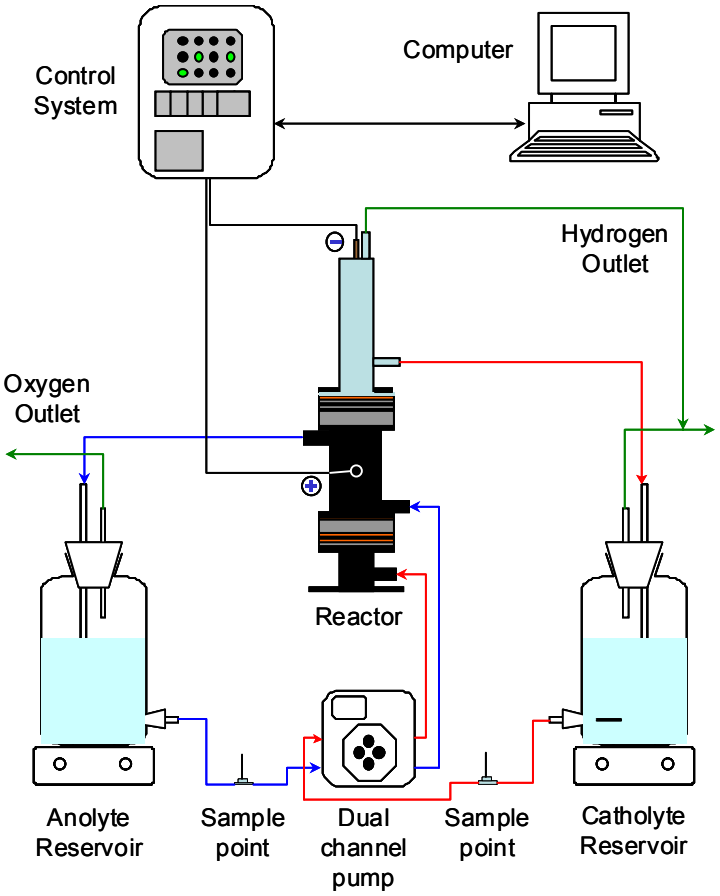


Figure 4.4 A schematic diagram showing the set-up of the apparatus, flow circuit and electrical circuit.

The catholyte and anolyte were circulated from their respective five litre glass reservoirs through tee fittings that each contained a septum. Using a syringe, the solutions leaving each reservoir could be sampled via the septum. These containers were constantly stirred with magnetic stirrers. A measuring tape, marked in millimetres and placed along the length of each container, allowed for the monitoring

of the solution levels and hence the volumes of the electrolytes, with the graduations indicating 24 millilitre intervals.

The necks of the reservoirs were each sealed with a perspex fitting containing multiple tapered slots into which glass tubes were fitted. Seven slots were available for each reservoir and provided for the temperature probes, gas outlets, recycled solutions and electrolyte additions, with spare ports available for possible future modifications such as level probes.

4.1.3 Power Supply and Control

A sophisticated experiment control system, developed by Danntech Process Instrumentation, was used. The system consisted of a 4 Amp power supply (PS), a direct current control unit (DCCU) and a measurement and control interface (MCI) shown in Figure 4.5.

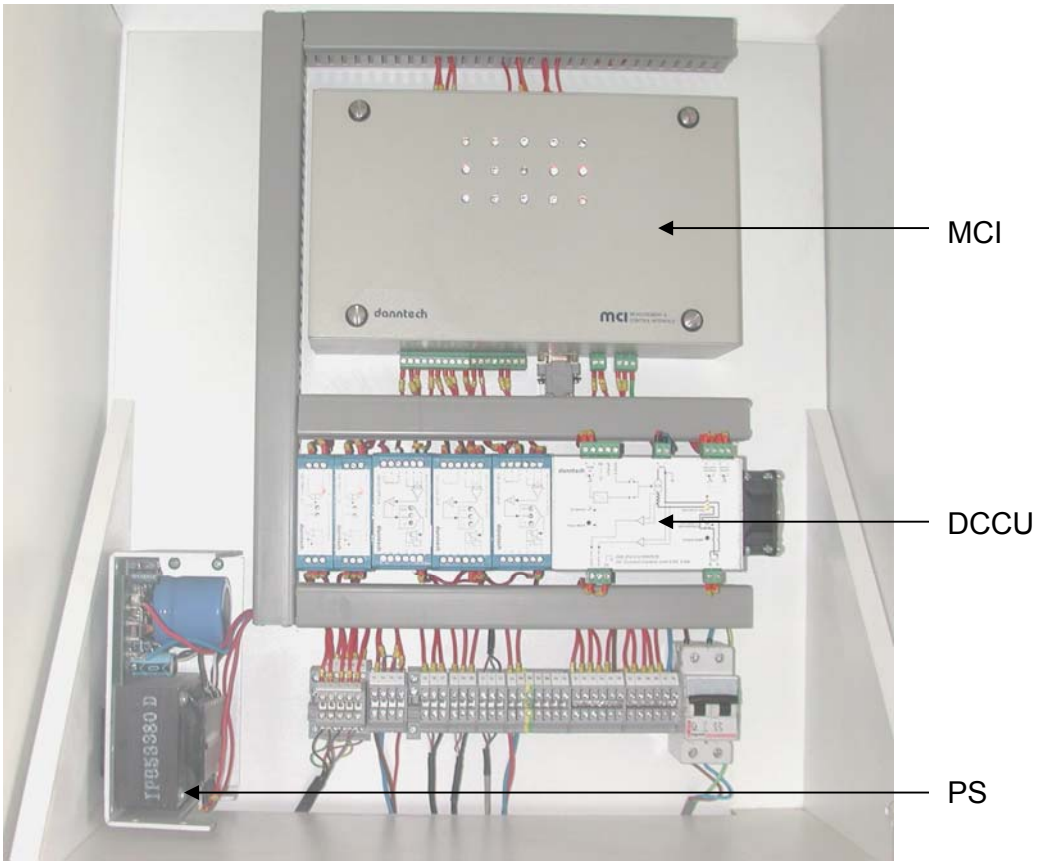


Figure 4.5 Photograph of the control system hardware

The system was computer controlled and allowed the user to input the desired electrolyte flowrates and applied current. Numerous measurements were also logged and recorded at regular intervals specified by the user. The information recorded is listed in Table 4.2. Graphical and numerical values were also displayed on the screen for monitoring purposes during the experiment. Electrical connections were made to the cathode via the tip of the current collector that extended out of the hood. A protruding bar from mid height of the anode provided for its connection. The system was operated in a constant current mode.

Table 4.2 Computer recorded data and accuracy of measurements

Data Recorded	**Measurement Accuracy**
Current: Set Point	0.01 A
Current: Measured	0.1 A
Pump Speed: Set Point	0.1 %
Pump Speed: Measured	0.1 %
Temperature: Anolyte	0.1 ^{o}C
Temperature: Catholyte	0.1 ^{o}C
Potential difference between anode and cathode	0.01 V
Potential difference between cathode and reference	0.001 V

4.2 REAGENTS

The suppliers and grades of all the reagents used are given in Table 4.3. The potassium chloride (3 M) was used as the salt bridge solution. Sulphuric acid was used for the anolyte and as the cation exchange membrane employed could only be used above pH 1 a solution of 0.005 M sulphuric acid (pH 2) was utilised. The remaining chemicals in the table were used for producing the synthetic catholytes.

Several different catholyte solutions were utilised and are listed in Table 4.4, denoting the compositions of each. The actual plant effluent was used without the addition of any reagents. To study the individual removal kinetics of each of the key metal ions in solution, namely palladium and copper, it was necessary to mimic the background composition of the plant solution but add only one of the metal ions.

These solutions were named 'Single Metal Ion in Synthetic Industrial Effluent' and were abbreviated to SMISIE. Both of the metal ions were then added to the synthetic industrial effluent background (Cu / Pd SIE) to determine the cumulative effect and for comparison to the actual industrial effluent.

Table 4.3 Suppliers and grades of the reagents used

Chemical	Formula	Supplier	Grade
Potassium Chloride	KCl	Saarchem	UNIV AR
Sulphuric Acid	H_2SO_4	BDH Chemicals	AnalaR
Sodium Chloride	NaCl	Saarchem	UNI LAB
Ammonium Acetate	CH_3COONH_4	Saarchem	UNIV AR
Acetic Acid	CH_3COOH	Saarchem	UNI LAB
Copper Chloride	$CuCl_2.2H_2O$	Saarchem	UNIV AR
Palladium Chloride	H_2PdCl_4	Anglo Platinum	_____

Table 4.4 Compositions of the catholyte solutions used

	Cu SMISIE	Pd SMISIE	Cu / Pd SIE	Plant solution
NaCl	1 mol/l	1 mol/l	1 mol/l	As received
CH_3COONH_4	1 mol/l	1 mol/l	1 mol/l	
CH_3COOH	1 mol/l	1 mol/l	1 mol/l	
Pd^{2+}	0	200 ppm	200 ppm	
Cu^{2+}	400 ppm	0	200 ppm	
pH	4.5	4.5	4.5	4.3

The exact composition of the industrial solution was unknown, but was estimated to contain sodium chloride, ammonium acetate and acetic acid all of a one molar concentration. These components were used to buffer the SMISIE solution to a pH of 4.5 which was approximately the same as the pH of the plant solution of 4.3.

The palladium ions are known to exhibit slow kinetics to reach equilibrium species. Therefore, when making up catholytes containing these ions the solutions were heated to 70^{o}C for approximately 1 ½ hours then cooled and left overnight. If higher concentrations of Pd ions were added to the catholyte solutions, a yellow precipitate

was seen to form after an extended period of time. The Cu SMISIE solution displayed rapid equilibrium kinetics with distinct colour changes with the addition of each of the chemicals used in the make up.

4.3 EXPERIMENTAL PROCEDURE

Multiple runs were executed, with each run comprising several experiments. The reactor was assembled and fresh particles were used at the start of each run. Distilled water was circulated through the system to confirm the absence of any leaks and to soak the dry graphite particles. The water was removed from both of the tanks and each of the reservoirs was refilled with four litres of electrolyte. The reactor was under no circumstances allowed to stand dry (the distilled water or solution from a previous experiment was never drained from the reactor) to prevent the membrane from drying out and cracking. As the fluid in the cathode chamber and related tubing constituted only a small volume compared to the volume of solution in the reservoir only a minor dilution effect was anticipated.

The control system was activated and the solutions were pumped through the reactor prior to the start of electrolysis. After approximately four to ten minutes of recirculation, to ensure complete displacement of the former solution in the reactor and tubing, a sample was taken of each electrolyte to allow determination of the exact starting composition. The current was then applied stepwise using 0.2 A increments every 20 seconds until the required applied current was reached. Samples of approximately 3 ml were taken at one or two minute intervals. When the solution appeared colourless, the measured cathode potential remained fairly constant and significant amounts of hydrogen bubbles were present in the hood, the experiment was deemed to have reached completion and a few more samples were taken at extended intervals to ensure that the end concentration was amply low. A final sample was taken of both electrolytes prior to decreasing the applied current. The pH of the electrolytes at the start and completion of each experiment was measured.

From preliminary testwork (runs prior to Run 2) it was found that cathodic protection was necessary between the experiments due to the slow redissolution of the deposited metals. Thus at the end of an experiment the current was decreased to

between 0.05 and 0.15 A, and the flowrate reduced. The system was left cathodically protected until the start of the next experiment of that run. The flowrates of the electrolytes were initially only calibrated at the start of a run. However, it was found that due to the lengthy period of a run, extending up to a few weeks, the wear of the tubing in the pump channel became significant and adversely affected the flowrates. Thus for all runs subsequent to Run 2 the flowrate was calibrated at the start of each individual experiment and the tubing replaced when necessary.

4.4 ANALYTICAL PROCEDURE

All samples were sent to the Analytical Laboratory at Wits, School of Chemistry, for ICP OES analysis. The samples were all diluted with demineralised water prior to chemical analysis. As the concentration of the supporting electrolyte of the solutions was high, the minimum dilution factor possible was 10, and as the palladium calibration standards ranged from 1 ppm to 0.1 ppm, the maximum dilution factor was 400. For the higher dilutions a double dilution technique was used to minimise the error. The samples were analysed starting from the solutions with the lowest concentrations to reduce contamination effects although the system was thoroughly rinsed between samples. With each batch of samples submitted, three identical solutions of approximately known concentration were included to confirm reproducibility.

5 MODEL DERIVATION

For simple two-dimensional electrodes the reaction is restricted to a well defined interface between the solid and electrolyte. This interface is usually a plane surface and the electrode is equipotential. When dealing with three-dimensional electrodes there is a large range of reaction rates throughout the electrode and their distribution depends on the physical structure and conductivity of the matrix and of the electrolyte. Detailed modelling of the processes occurring would require knowledge of numerous parameters which are often unknown and difficult to measure. Determination of these parameters may be necessary for optimisation purposes however a simplified macroscopic model, derived only from mass and charge balances across the reactor, produces a useful tool for predicting the concentration-time behaviour of the system and the influence of operating conditions such as applied current and flowrate.

Although the laboratory equipment was configured for operation with recirculation of the electrolyte, models are developed in the proceeding sections for both single pass and batch recirculation modes. The conditions under which the reaction rate is controlled by either the applied current or mass transport are also discussed.

5.1 SINGLE PASS PLUG FLOW REACTOR

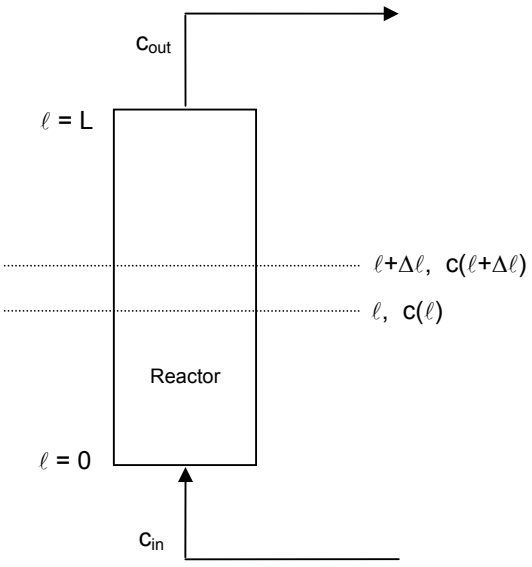


Figure 5.1 Single pass plug flow reactor

As the term suggests, for a single pass plug flow reactor, the electrolyte passes through the reactor only once. The inlet and outlet concentrations are therefore independent of time once steady state has been established. If the electrochemical reactor is modelled as a plug flow reactor (PFR) and axial dispersion is neglected, the mass balance across a segment of the reactor, depicted in Figure 5.1, can be written as follows:

$$\dot{m}\big|_{\ell+\Delta\ell} = \dot{m}\big|_{\ell} + \dot{r}\Delta A_p \qquad [5.1]$$

We can express the mass flowrate ($\dot{m}$) and the active surface area of the particles in the segment (ΔA_p) using the relationships given by Equations 5.2 and 5.3 respectively.

$$\dot{m} = c\dot{Q} \qquad [5.2]$$

$$\Delta A_p = aA\Delta\ell \qquad [5.3]$$

Using the rate of reaction given by Equations 3.9 and substituting the above two equations into Equation 5.1 we obtain

$$\left(c\big|_{\ell+\Delta\ell} - c_{\ell}\right)\dot{Q} = -kcaA\Delta\ell \qquad [5.4]$$

Equation 5.4 can be written in terms of a differential equation as

$$\frac{dc}{d\ell} = \frac{-kcaA}{\dot{Q}} \qquad [5.5]$$

To integrate Equation 5.5 an expression for the reaction rate constant as a function of reactor length is required. If we assume that all points on the electrode support a reaction which is fully mass transport controlled, we can integrate Equation 5.5 by substituting k_m, the spatially-averaged mass transport coefficient which is independent on the length of the reactor, for the reaction rate coefficient, k.

$$\int_{c_{in}}^{c_{out}} \frac{dc}{c} = \frac{-k_m aA}{\dot{Q}} \int_0^L d\ell \qquad [5.6]$$

Integrating the above across the entire length of the reactor (L) using the limits shown we obtain:

$$\ln\left(\frac{c_{out}}{c_{in}}\right) = \frac{-k_m aAL}{\dot{Q}} \qquad [5.7]$$

Rewriting Equation 5.7 in terms of the concentration of the stream exiting the reactor (c_{out}) and noting that the product of aAL is merely the total active surface area of the particles in the reactor (A_p) we find

$$c_{out} = c_{in} \exp\left(-\frac{k_m A_p}{\dot{Q}}\right) \qquad [5.8]$$

Defining the fractional conversion in a single pass plug flow reactor (X_{SP}) as

$$X_{SP} = \frac{c_{in} - c_{out}}{c_{in}} = 1 - \frac{c_{out}}{c_{in}} \qquad [5.9]$$

and substituting Equation 5.8 we obtain an expression for X_{SP} in terms of the operational parameters.

$$X_{SP} = 1 - \exp\left(-\frac{k_m A_p}{\dot{Q}}\right) \qquad [5.10]$$

The rate of removal (r) in a single pass reactor is constant (for a constant applied current) and is calculated by the product of the flowrate and change in concentration:

$$r = \dot{Q}(c_{in} - c_{out}) \qquad [5.11]$$

As mass transport was assumed to control, the rate of reaction is given by the limiting current (I_L). Using Faraday's Law as given by Equation 3.6, and substituting Equation 5.11 above, the expression for the limiting current (I_L) in terms of the inlet concentration is given by

$$\dot{Q}(c_{in} - c_{out}) = \frac{M_w I_L}{nF} \qquad [5.12]$$

Rearranging and substituting Equation 5.9 for the change in concentration across the reactor, the limiting current can be expressed in terms of the fractional conversion by:

$$I_L = \frac{nF\dot{Q}c_{in}X_{SP}}{M_w} \qquad [5.13]$$

5.2 BATCH RECIRCULATION PLUG FLOW REACTOR

Batch recirculation is a particularly versatile mode of operation especially for laboratory scale apparatus as the electrolyte inventory is substantially increased. The use of a well mixed reservoir also provides advantages for process control. The pH, temperature and composition of the supporting electrolyte can be monitored and easily adjusted if necessary. The tank also serves to disengage the gas generated in the reactor.

The modelling of the batch recirculation plug flow reactor is more complex than that of the single pass plug flow reactor as both the reactor and reservoir have time-dependent concentrations associated with them. However, it is possible to simplify the model by manipulating the setup such that pseudo-steady state, isothermal conditions are achieved.

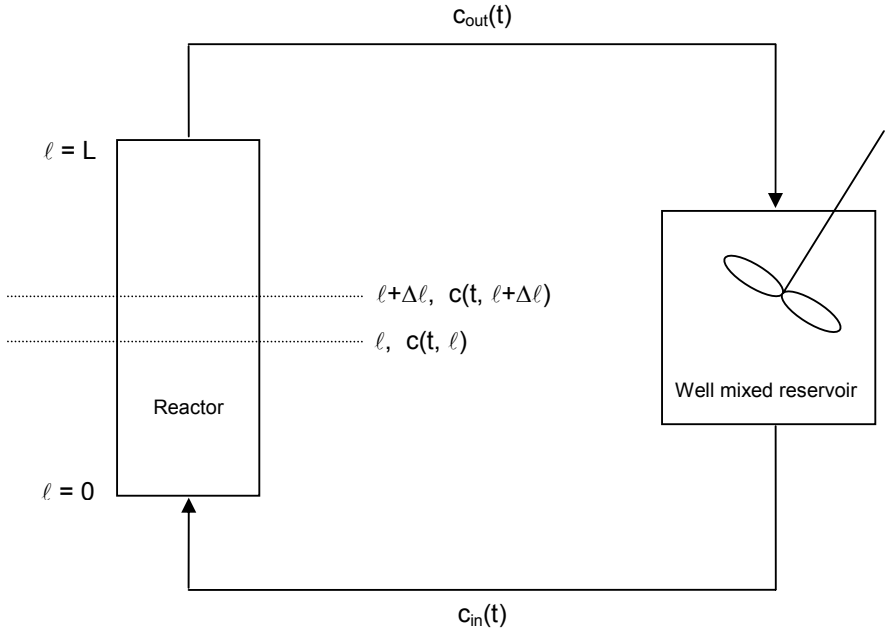


Figure 5.2 Batch recirculation plug flow reactor.

The mass balance over the reservoir, modelled as a continuously stirred tank reactor, (CSTR) is given by

$$m\big|_{t+\Delta t} = m\big|_{t} + \dot{m}_{out}\Delta t - \dot{m}_{in}\Delta t \qquad [5.14]$$

Substituting for the mass flowrates using Equation 5.2 and noting that for a CSTR the concentration in the reservoir is assumed to be equal to the concentration of the stream leaving the tank, Equation 5.14 can be written in differential form as:

$$\frac{d(c_{in}V_{res})}{dt} = c_{out}\dot{Q}_{out} - c_{in}\dot{Q}_{in} \qquad [5.15]$$

If we then assume that the volumetric flowrate of solution entering and leaving the tank are equal hence, the volume in the reservoir remains constant with time, we can express Equation 5.15 as follows

$$\frac{dc_{in}}{dt} = (c_{out} - c_{in})\frac{\dot{Q}}{V_{res}} = \frac{(c_{out} - c_{in})}{\tau_{res}} \qquad [5.16]$$

where τ_{res} is the residence time of the solution in the reservoir.

The segmental mass balance across the plug flow reactor is given by

$$m\big|_t + \dot{m}\big|_\ell \Delta t + \dot{r}\Delta A_p \Delta t = m\big|_{t+\Delta t} + \dot{m}\big|_{\ell+\Delta\ell}\Delta t \qquad [5.17]$$

where m is the mass of species in solution in the chosen segment of the reactor. This mass is given by the product of the concentration with the volume of solution in that segment (ΔV). The voidage of the particulate bed (ε) has to therefore be taken into consideration.

$$m = c\Delta V = c\varepsilon A\Delta\ell \qquad [5.18]$$

Substituting Equations 3.9, 5.2, 5.3 and 5.18 into Equation 5.17 we obtain Equation 5.19 which can be written in terms of partial derivatives as shown in Equation 5.20.

$$(c\big|_{t+\Delta t} - c\big|_t)\varepsilon A\Delta\ell + (c\big|_{\ell+\Delta\ell} - c\big|_\ell)\dot{Q}\Delta t = -kcaA\Delta\ell\Delta t \qquad [5.19]$$

$$\varepsilon A\frac{\partial c}{\partial t} + \dot{Q}\frac{\partial c}{\partial \ell} = -kcaA \qquad [5.20]$$

A pseudo-steady state system is approached by the use of a reservoir with a far greater volume than that of the reactor, such that the change in concentration with time at any given point in the reactor is insignificant in comparison to the change in concentration with distance through the reactor.

Using this assumption of pseudo-steady state the $\partial c / \partial t$ term can be neglected and the equation is identical to that of Equation 5.5. As in Section 5.1, assuming that all points on the electrode support a reaction which is fully mass transport controlled we can substitute k_m, the spatially-averaged mass transport coefficient which is independent on the length of the reactor, for the reaction rate coefficient, k. The integrated form was given by Equation 5.8 and was shown to be

$$c_{out} = c_{in} \exp\left(- \frac{k_m A_p}{\dot{Q}} \right) \qquad [5.21]$$

Combining the expression for c_{out} derived above into the mass balance equation for the reservoir (Equation 5.16) we obtain the differential equation for the concentration change with time.

$$\frac{dc_{in}}{dt} = \frac{1}{\tau_{res}} \left[c_{in} \exp\left(\frac{- k_m A_p}{\dot{Q}} \right) - c_{in} \right] \qquad [5.22]$$

The above equation is integrated between the limits shown in Equation 5.23 below to give the concentration in the reservoir as a function of time shown by Equation 5.24.

$$\int_{c_{in}^0}^{c_{in}(t)} \frac{dc_{in}}{c_{in}} = -\frac{1}{\tau_{res}} \left[1 - \exp\left(- \frac{k_m A_p}{\dot{Q}} \right) \right] \int_0^t dt \qquad [5.23]$$

$$\ln\left(\frac{c_{in}(t)}{c_{in}^0} \right) = -\frac{1}{\tau_{res}} \left[1 - \exp\left(- \frac{k_m A_p}{\dot{Q}} \right) \right] t \qquad [5.24]$$

Noting that the expression in the square brackets was shown, by Equation 5.10, to be the fractional conversion in a single pass through a plug flow reactor, this equation can be written as

$$\ln\left(\frac{c_{in}(t)}{c_{in}^0} \right) = -\frac{X_{SP}}{\tau_{res}} t \qquad [5.25]$$

Rearranging the above, the concentration in the reservoir as a function of time is given by

$$c_{in}(t) = c_{in}^0 \exp\left(- \frac{X_{SP}}{\tau_{res}} t \right) \qquad [5.26]$$

The overall conversion with time of a batch recirculation plug flow reactor (X_{BR}), based on the initial concentration, is defined by

$$X_{BR} = \frac{c_{in}^{0} - c_{in}(t)}{c_{in}^{0}} = 1 - \frac{c_{in}(t)}{c_{in}^{0}} \qquad [5.27]$$

and is given in terms of the fractional conversion per pass from Equation 5.26 as

$$X_{BR} = 1 - \exp\left(- \frac{X_{SP}}{\tau_{res}} t \right) \qquad [5.28]$$

5.3 MASS TRANSPORT CONTROLLED CONDITIONS

In the derivations of the models described in Sections 5.1 and 5.2 it was assumed that the entire electrode surface operated under complete mass transport controlled conditions. Indeed, from Figure 5.3(a) it can be seen that if the current applied is equal to or greater than the limiting current at the initial conditions i.e. $I_{app} \geq I_L(t=0)$, the rate of metal deposition will be mass transport controlled and the concentration profile of the solution in the reservoir will decrease exponentially with time (shown in Figure 5.3(b)) as described by Equation 5.26 for a batch recirculation system. A plot of $\ln c_{in}(t)$ versus time will therefore produce a straight line graph with a slope of $-X_{SP}/\tau_{res}$ as shown in Figure 5.3(c).

The limiting current was shown to be directly proportional to the concentration of the inlet stream to the reactor by Equation 5.13 which was derived for single pass reactors where the concentration of the inlet stream remained constant. For batch recirculation of the electrolyte the inlet concentration decreases with time and hence the limiting current will also be a function of time.

$$I_L(t) = \frac{nF\dot{Q}X_{SP}c_{in}(t)}{M_w} \qquad [5.29]$$

The current efficiency was previously defined in Equation 3.11 as the fraction of the applied current used in the primary reaction. Under mass transport controlled conditions the current used in this reaction is the limiting current and hence the

current efficiency as a function of time is given by Equation 5.30 and depicted graphically in Figure 5.3(d) according to the equation

$$\phi(t) = \frac{I_L(t)}{I_{app}} = \frac{nF\dot{Q}X_{SP}c_{in}(t)}{I_{app}} \qquad [5.30]$$

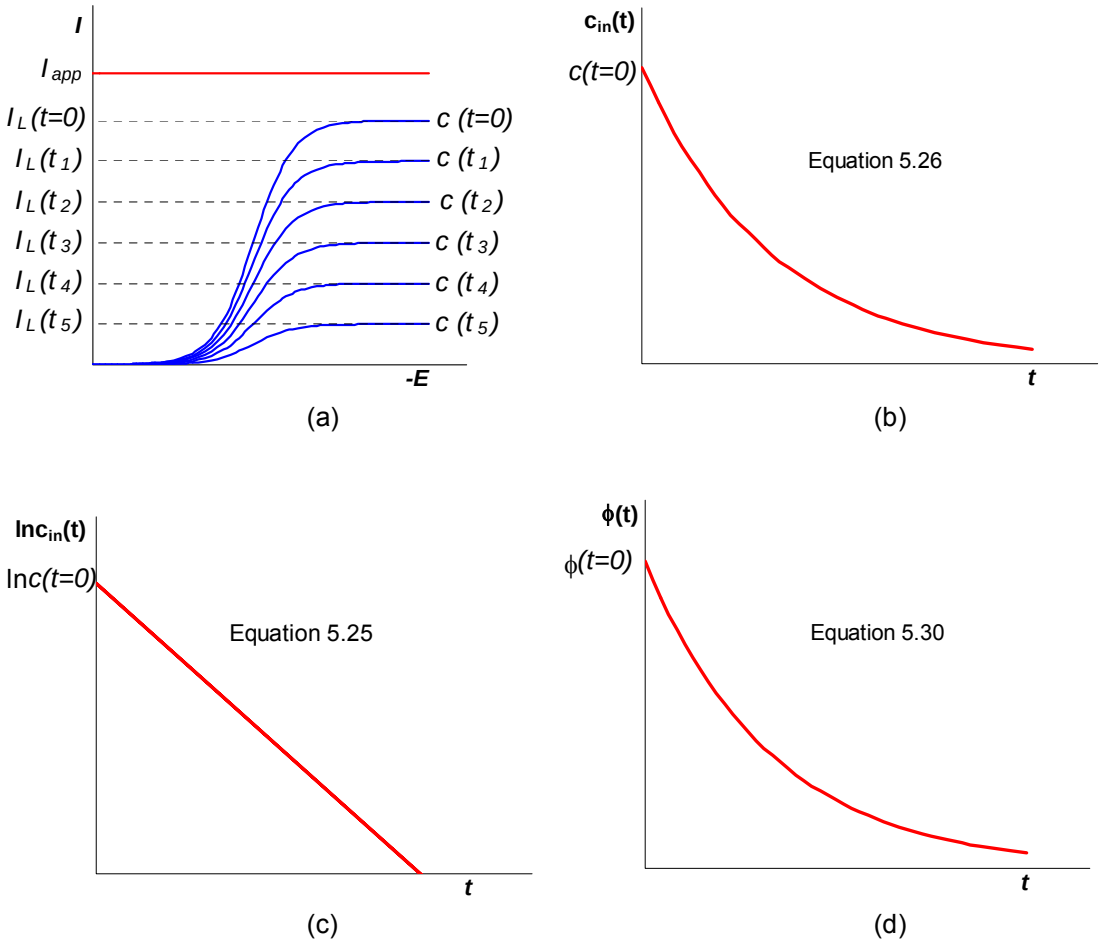


Figure 5.3 Performance of batch recirculation plug flow reactor for the condition $I_{app} \geq I_L(t=0)$

(a) Typical current potential curves for the concentrations of electroactive species at various times

(b) Concentration profile in the reservoir as a function of time

(c) Logarithmic plot of the concentration in the reservoir with time

(d) Current efficiency as a function of time

As the applied current will always be greater than the current used in the primary reaction a simultaneous secondary reaction, typically hydrogen evolution, must occur. Under galvanostatic operation, the rate of this side reaction must increase as the rate of the metal deposition decreases. The cathode potential should then gradually shift to more negative potentials with time, until virtually all the applied current is utilised by the side reaction. The cathode potential will remain constant once the concentration of the metal ions has been reduced to the possible minimum for that given applied current. The shift in potential with time is illustrated in Figure 5.4.

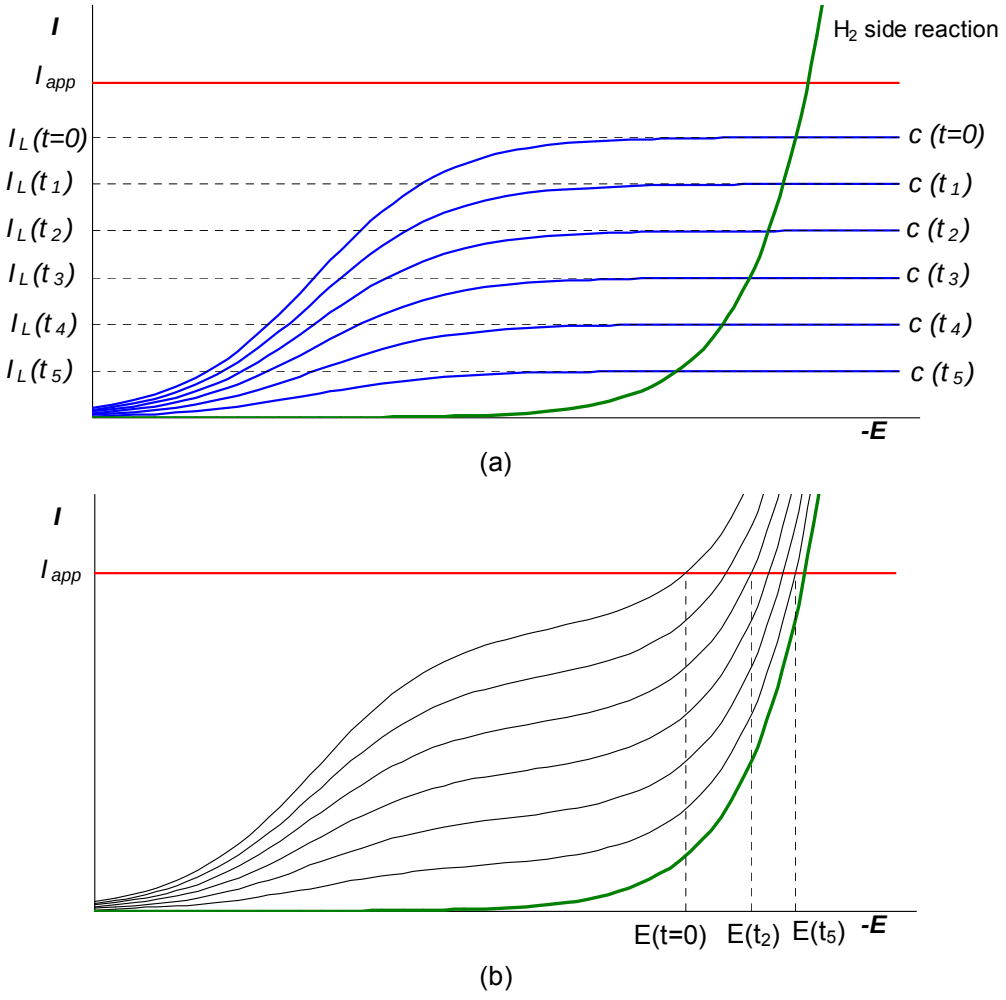


Figure 5.4 Current-potential curves for the primary and side reactions for the condition $I_{app} \geq I_L(t=0)$

(a) Individual curves of the primary reaction at various times and the side reaction

(b) The combined current-potential curves at various times

5.4 CURRENT CONTROLLED CONDITIONS

Due to the turbulence generated by the flow of the electrolyte through the packed bed, the rate of mass transport is significantly enhanced and the limiting current densities are increased. Furthermore as a large surface area is available in a packed bed reasonably low current densities are produced at the electrode surface. Thus in the early stages of electrolysis (with higher concentrations entering the reactor) the applied current may be such that the current density formed at the electrode surface is well below the limiting current density. The concentration will then decrease linearly with time with the reaction rate being controlled by the applied current. As the concentration decreases, so too does the limiting current and at the time $t = t_m$ the concentration is such that the limiting current is equal to the applied current (assuming no side reactions occur at that potential) and mass transport ensues. This current controlled zone, when $t < t_m$, is demonstrated graphically in Figure 5.5.

The linear decrease in concentration when $t < t_m$ is given by

$$c_{in}(t) = c_{in}^{0} - \frac{I_{rxn} M_w}{nFV_{res}} t \qquad [5.31]$$

When shown on the logarithmic scale the equation is given by

$$\ln c_{in}(t) = \ln\left(c_{in}^{0} - \frac{I_{rxn} M_w}{nFV_{res}} t \right) \qquad [5.32]$$

The current efficiency is constant during the current controlled stage and equal to one if no side reactions occur. This efficiency is calculated as

$$\phi(t) = \frac{I_{rxn}}{I_{app}} = \frac{nFV_{res}(c_{in}^{0} - c_{in}(t))}{I_{app} M_w t} \qquad [5.33]$$

Should the side reaction require a significantly higher overpotential than that of the primary reaction as shown in Figure 5.6(a), during current control the cathode potential will slowly shift toward more negative values and then rapidly decrease as mass transport begins to control the rate of the reaction. The potential will then again gradually decrease and approach that of the side reaction for the given applied current and the concentration will reach the possible minimum. This shift in the cathode potential is illustrated in Figure 5.6(b).

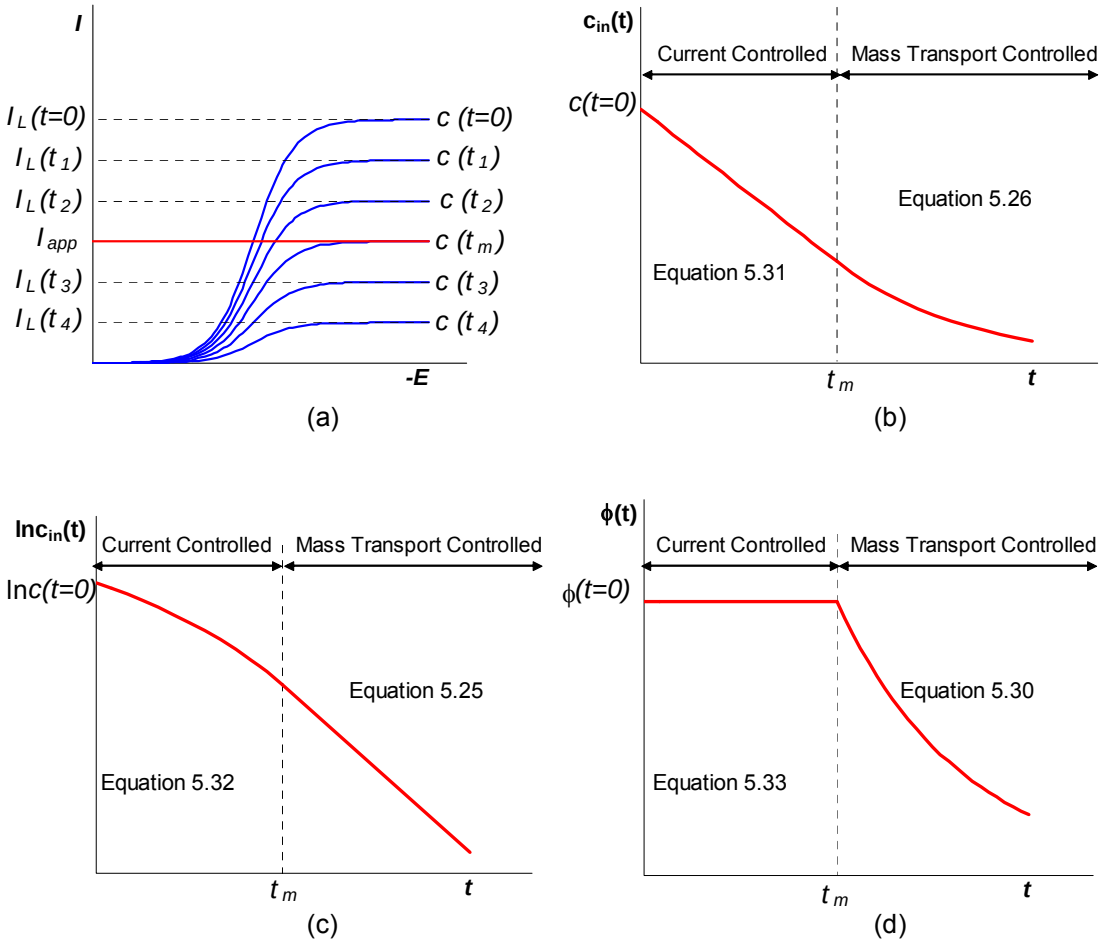


Figure 5.5 Performance of batch recirculation plug flow reactor for the condition $I_{app} < I_L(t=0)$

(a) Typical current potential curves for the concentrations of electroactive species at various times

(b) Concentration profile in the reservoir as a function of time

(c) Logarithmic plot of the concentration in the reservoir with time

(d) Current efficiency as a function of time

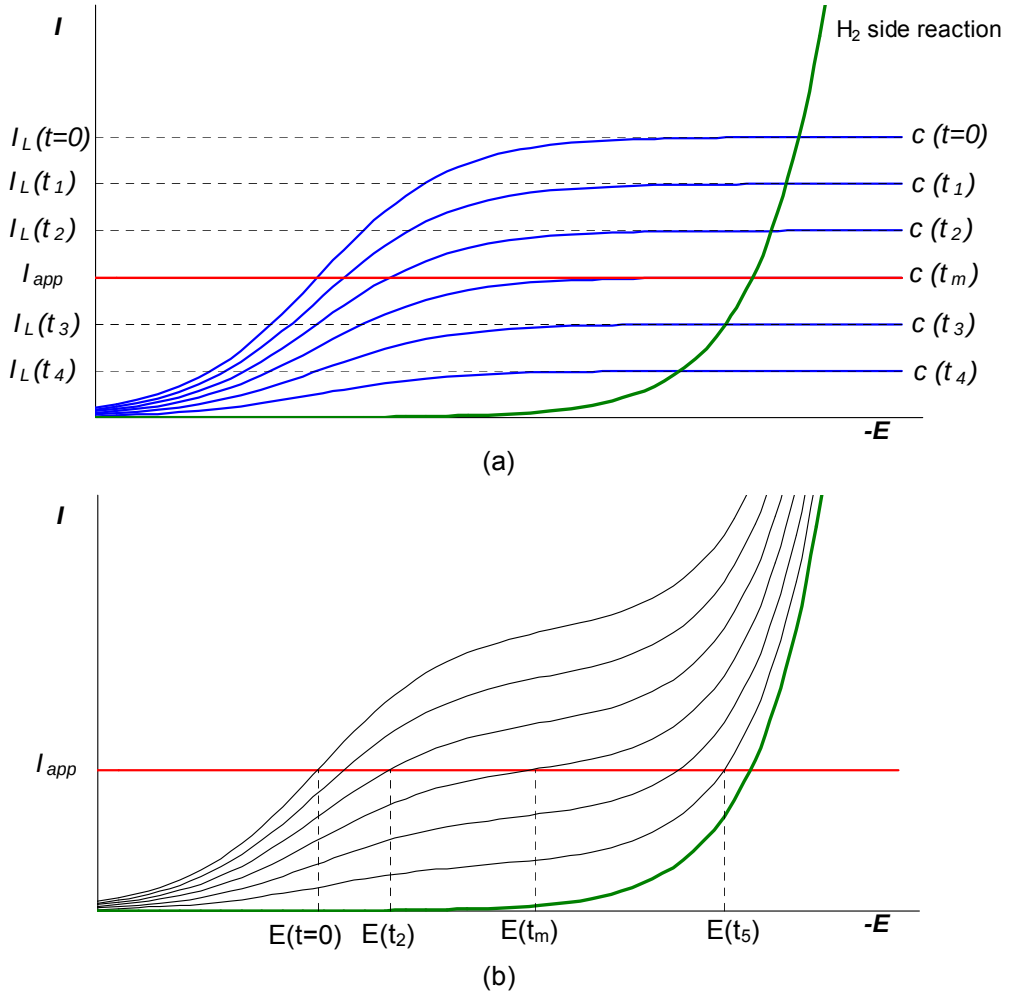


Figure 5.6 Current-potential curves for the primary and side reactions for the condition $I_{app} < I_L(t = 0)$

(a) Individual curves of the primary reaction at various times and the side reaction

(b) The combined current-potential curves at various times

5.5 VALIDITY OF ASSUMPTIONS

When deriving this model certain assumptions were made. These were either stated or implied and are summarised below. Although some of the assumptions were justifiable others were merely for simplification purposes.

5.5.1 Reservoir

- The reservoir was modelled as a perfectly mixed system and therefore solution properties in the tank, such as temperature and concentration, were uniform and equivalent to those entering the reactor.
- The time lag between the reservoir outlet and reactor inlet was assumed negligible.
- The flow of solution through the membrane was also assumed negligible and thus the flowrates in and out of the reactor were identical and the volume in the reservoir remained constant.

The speed of the magnetic stirrer was set reasonably high and thus good mixing was achieved in the reservoir. The tubing between the reactors was kept to a minimum and thin tubing was used therefore small residence times were expected. The average volume change in the reservoir was 20 ml/h, hence only a fairly small volume of solution passed through the membrane.

5.5.2 Reactor

- The reactor was modelled as a plug flow reactor and therefore there was no radial variance in the solution properties or velocity profile.
- No axial dispersion was assumed to occur.
- The volume of the reactor was insignificant in comparison to the volume of the reservoir such that the change in concentration with time was insignificant in comparison to the change with distance through the reactor. The system therefore approached a pseudo-steady state, whereby the partial differential term $\partial c / \partial t$ could be neglected.

As the height to diameter ratio of the reactor was greater than 3:1 the assumption of plug flow was valid. Mustoe and Wragg[180] showed that the error introduced by neglecting dispersion effects was in the order of only 1%. Walker and Wragg[172] compared the results of both the rigorous analysis of Equation 5.20 and the approximation given by Equation 5.21 and showed that after 150 minutes the error introduced was only 3 percent for a system with a reactor to reservoir volume ratio of 1:400. The error was reported to increase at larger times but after the 150 minutes

98 percent of the copper had already been removed. Repeating the calculations using the same operating parameters, but with a reactor to reservoir volume ratio of 1:40, it was shown that the error sets in far more rapidly with a difference of 2.5 percent reported after 13 minutes, however by this time 96 percent of the copper had been removed. Employing this assumption drastically simplified the mathematics of the modelling and as the system under present investigation had a ratio of approximately 1:80 the error introduced was deemed tolerable.

5.5.3 Reaction Rate

- The reaction rate was first order and the mass transport coefficient was assumed to remain constant with time and direction in the reactor.
- The Nernst diffusion layer model was deemed to be applicable.
- The overpotential was such that the reverse reaction was considered negligible.
- The concentration of the electroactive species was dilute and the solution properties, such as viscosity or conductivity, remained unaltered by the reaction.
- A high concentration of the supporting electrolyte ensured negligible migration effects of the reacting species.

The mass transport coefficient is dependent on the hydrodynamics of the system and thus entrance effects may have caused slight differences in the reaction rates at the inlet and outlet, but the entrance effects should only affect a small portion of the bed. It was possible for surface roughening to occur with time and hence alter the mass transport coefficient but to allow for such effects would have been too arduous. Although strictly speaking the Nernst diffusion layer model is only valid for linear diffusion to a planar electrode, i.e. the active electrode surface is flat and the concentration varies perpendicular to the electrode surface, this model was deemed applicable for simplification purposes. The high field approximation was stated in Section 3.2.1 to be valid for overpotentials greater than 118/n mV and hence the reverse reactions were negligible for a reasonable applied current. As the concentration of the reacting species were in the ppm range and the spectator ions were in mol/l, it was justified to assume negligible variation in the solution properties or migration effects of the electroactive species.

5.5.4 Particles

- The particulate bed was isotropic and wall effects or channelling were insignificant.
- The surface area of the particles was approximated by the geometrical surface area. The particles were assumed to be perfectly spherical and the average diameter was calculated from the square root of the product of the minimum and maximum of the sieved range.
- The porosity was considered to be negligible
- The particle size remained constant with time.
- The electrode properties did not change when material was deposited.

The ratio of the particle size to bed diameter was greater than 30:1 and therefore channelling should be minimal. As exact active electrode surface area was unknown, the values calculated for k_m were only approximates and therefore could not be accurately compared to values determined on other systems. Low porosity graphite particles were used thereby decreasing the error in calculating the surface area. The concentration of the reacting species was low and the cathode was not loaded for extended periods, thus no noticeable change in the particle size was envisioned. It was considered practically impossible to allow for the change in the electrode properties due to deposition.

5.5.5 Side Reaction

- The gas evolved did not influence electrolyte flow distribution
- The physical properties of the catholyte were not altered by the gas reaction
- The gas did not affect the available surface area.

Hydrogen evolution occurred as the side reaction but its influence on the operations could not be allowed for in any practical manner and thus were neglected for simplification purposes.

6 RESULTS

The construction and commissioning of the bench scale reactor was a protracted process with numerous problems associated with the sealing of the reactor, assembly of the membrane and current leakages. When satisfactory operation was achieved four sets of tests using different catholyte solutions were conducted as follows:

Run 1	Plant Solution Testwork
Run 2	Pd SMISIE Testwork
Run 3	Cu SMISIE Testwork
Run 4	Cu / Pd SIE Testwork

6.1 PLANT SOLUTION

Approximately 20 litres of the industrial effluent (Palladium Diammine Mother Liquor) was delivered from PMR for the necessary testwork. An analysis of the head sample showed the major metal constituents to be copper, palladium and platinum, the concentrations of which are shown in Table 6.1 below. Other metal ions such as iron, chromium and nickel were all below 1 ppm.

Table 6.1 Concentrations of metal ions in the head sample of the plant solution

Metal ion	Concentration (ppm)
Copper	211
Palladium	146
Platinum	6.8

Subsequent to the commissioning of the reactor, during which time some of the plant solution was utilised, the remaining liquor was only sufficient for three experiments. Run 1 therefore consisted of the following three tests under galvanostatic control with the currents applied in each as follows:

Run 1.1	Current applied = 1.4 A
Run 1.2	Current applied = 1.4 A
Run 1.3	Current applied = 2.0 A

Run 1.1 was conducted on a clean bed of particles and therefore Run 1.2 was a repeat of the first test to determine the effects, if any, of the metals deposited during Run 1.1. The anolyte solution was not replaced between the runs and no cathodic protection was applied. The pump was stopped and the wires all disconnected at the end of each test.

The plant solution was recirculated through the reactor for approximately one hour prior to the application of a current. Samples were taken at regular intervals to monitor the concentration to determine whether physical adsorption of the metal ions occurred on the particular grade of graphite particles used.

The measured concentrations of the copper and palladium ions in the reservoir with time are shown in Figure 6.1 below for Run 1.1 and 1.2. The time t = 0 represents the time at which the full current (1.4 A) had been applied.

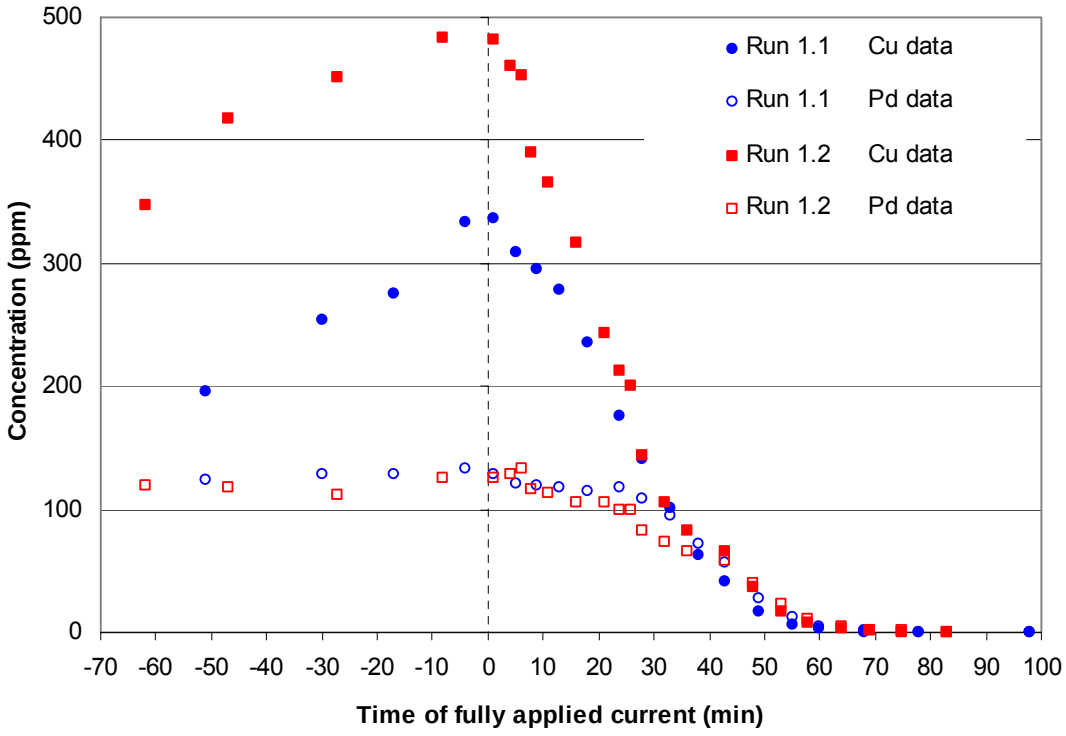


Figure 6.1 Concentration profile for Cu and Pd removal from plant solution catholytes for an applied current of 1.4 A

The final test using plant solution was conducted with a greater applied current. The results for Run 1.3 are shown in Figure 6.2 with Run 1.2 shown for comparison.

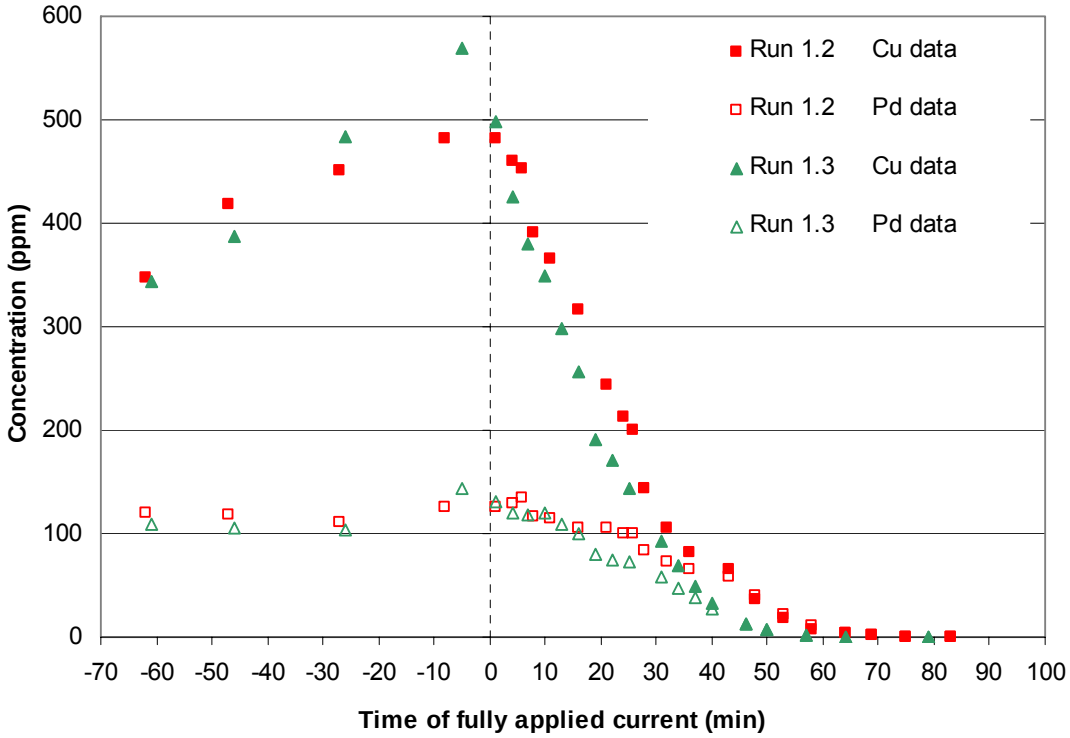


Figure 6.2 Concentration profile for Cu and Pd removal from plant solution catholytes for an applied current of 1.4 A (Run 1.2) and 2.0 A (Run 1.3)

6.1.1 Degree of Removal

From Figure 6.1 it is clear that Pd ions are not adsorbed onto the graphite particles as the concentration remains virtually constant for the time period prior to the application of current. During this time however, a considerable increase in the copper concentration can be seen. For Run 1.1 the only source of copper is the current collector rod through the centre of the bed and the increase in concentration was attributed to the dissolution of the copper rod due to the presence of ammonium ions in solution which are known to cause vigorous corrosion of copper[181a]. The more pronounced rise in Cu concentration for Run 1.2 could be due to the extended period of recirculation (Run 1.2 recirculation time was 23 minutes longer than for Run 1.1) or due to the additional surface area of copper available for dissolution from the copper deposited in Run 1.1. Once current is applied to the reactor the concentration

of Cu decreases rapidly and for roughly 30 minutes only a minimal change in the Pd concentration is observed.

Similar trends were noted for the test conducted with a greater applied current. The palladium showed no indication of adsorption onto the graphite during recirculation and the concentration of copper again increased during this period. With the exception of the data point at -5 minutes for Run 1.3, the rise in copper concentration is similar to that of Run 1.2. The circulation times for both experiments were comparable with Run 1.2 only 6 minutes longer than Run 1.3 and both experiments were conducted on beds where copper had previously been deposited.

The primary objective of the plant solution testwork was to determine to what extent the palladium, platinum and copper ions are removed from solution. As was indicated, for galvanostatic operation, the copper is the first to deposit and the time at which the palladium begins to deposit is dependent on the applied current. As was expected, the time required to reduce the metal concentrations was less for the greater applied current. The palladium concentration begins to fall after only 10 minutes. All the stated metals were recovered to the limit of detection for the analytical procedure, namely 0.1 ppm, which is well below the targeted concentrations. The starting concentration for platinum ions in solution was very low and although monitored to confirm removal and it was not deemed meaningful to evaluate the associated reaction rate.

6.1.2 Reaction Kinetics

Figure 6.3 shows the results plotted on a natural logarithmic scale. The linear regions shown by the fitted trendlines indicate the mass transport controlled regions. Significant amounts of hydrogen were seen to evolve approximately 50 minutes after applying a current of 1.4 A and about 30 minutes after applying a current of 2.0 A, which is in fair agreement with the times of the onset of mass transport control indicated in the graph.

Using Equations 5.24 and 5.25 and the slope of the trend plotted in Figure 6.3 the fractional conversion per pass through the reactor and the mass transport coefficients

for the metal ion reductions can be calculated for each experiment as shown in Tables 6.2 and 6.3 for copper and palladium respectively.

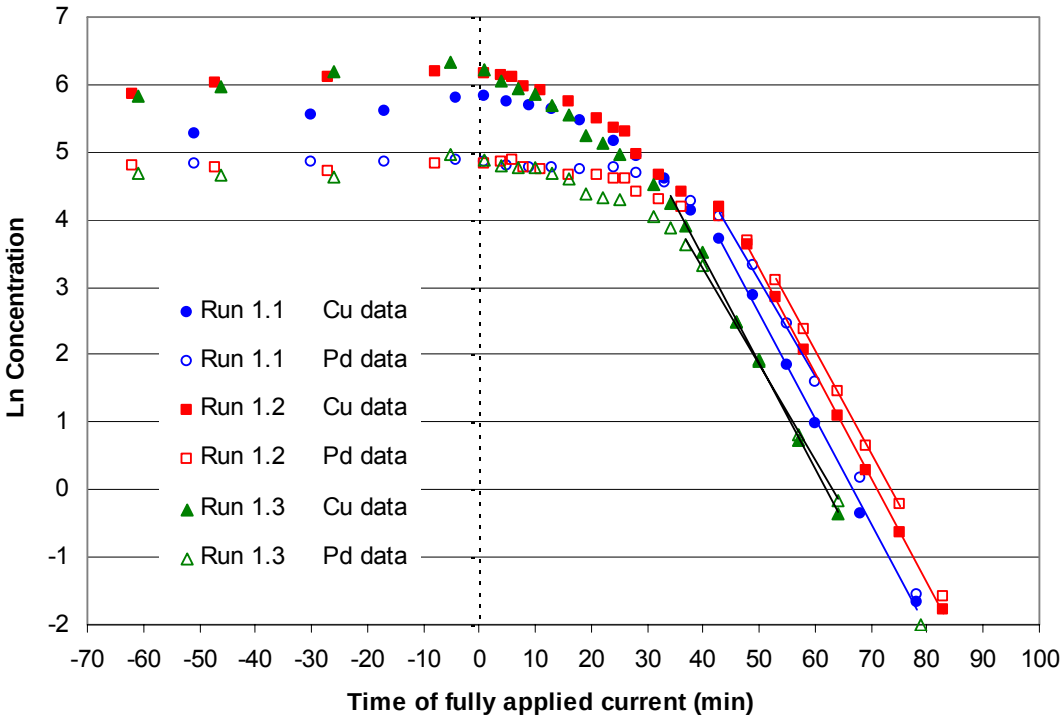


Figure 6.3 Plot of the natural logarithm of the concentration as a function of time for plant solution catholytes. Applied current = 1.4 A (Run 1.1 and 1.2). Applied current = 2.0 A (Run 1.3)

Table 6.2 Parameter estimation for the copper reactions under mass transport controlled conditions for plant solution catholytes

Test	*Slope (1/min)*	$\dot{Q}$ *(ml/min)*	V_{res} *(l)*	X_{SP}	k_m *(10^{-5} m/s)*
Run 1.1	-0.157	620	3.72	0.94	5.9
Run 1.2	-0.156	620	3.60	0.90	4.8
Run 1.3	-0.156	620	3.72	0.94	5.7

Table 6.3 Parameter estimation for the palladium reactions under mass transport controlled conditions for plant solution catholytes

Test	*Slope* (1/min)	$\dot{Q}$ (ml/min)	V_{res} (l)	X_{SP}	k_m (10^{-5} m/s)
Run 1.1	-0.143	620	3.72	0.86	4.0
Run 1.2	-0.153	620	3.60	0.89	4.5
Run 1.3	-0.143	620	3.72	0.86	4.0

During the initial period when current was applied but the palladium concentration remains virtually constant, almost all the current must be used for the Cu reduction. When attempting to perform a charge balance over this time period certain problems were encountered. For Run 1.3 palladium begins to deposit after only 10 minutes so the window of data is rather small for accurate analysis. For Run 1.1 and Run 1.2 the rate of the copper reaction is not constant and seems to increase after 13 minutes and 6 minutes respectively. The fitted linear trends are shown in Appendix B and from the slope, assuming a two electron transfer reaction, current efficiencies in excess of 100% were calculated and assuming a single electron transfer reaction, current efficiencies below 100 % were calculated for the copper reduction reaction. Furthermore, the copper concentration at t = 0 for Run 1.2 was significantly greater than for Run 1.1 and although the applied current was identical, after 30 minutes the concentrations for both tests were the same. These seemingly peculiar results were explained following testwork on the synthetic effluent containing only copper ions discussed in Section 6.3.

The current efficiencies for the palladium reactions were not determined as the deposition occurred simultaneously with the copper and thus were affected by changes in copper rates (see Run 1.2 and Run 1.3). Furthermore, as mass transport control begins shortly after the concentration begins to decrease insufficient data points are available for trend fitting (see Run 1.1).

The mechanisms and kinetics of the individual reactions were investigated in detail using synthetic effluents containing only the metal ion of interest. These results are given in Sections 6.2 and 6.3 for palladium and copper respectively.

6.1.3 Potential Profile

The cathode potential was monitored at the base of the bed adjacent to the current collector. The recorded profiles for the tests of Run 1 are shown in Figure 6.4.

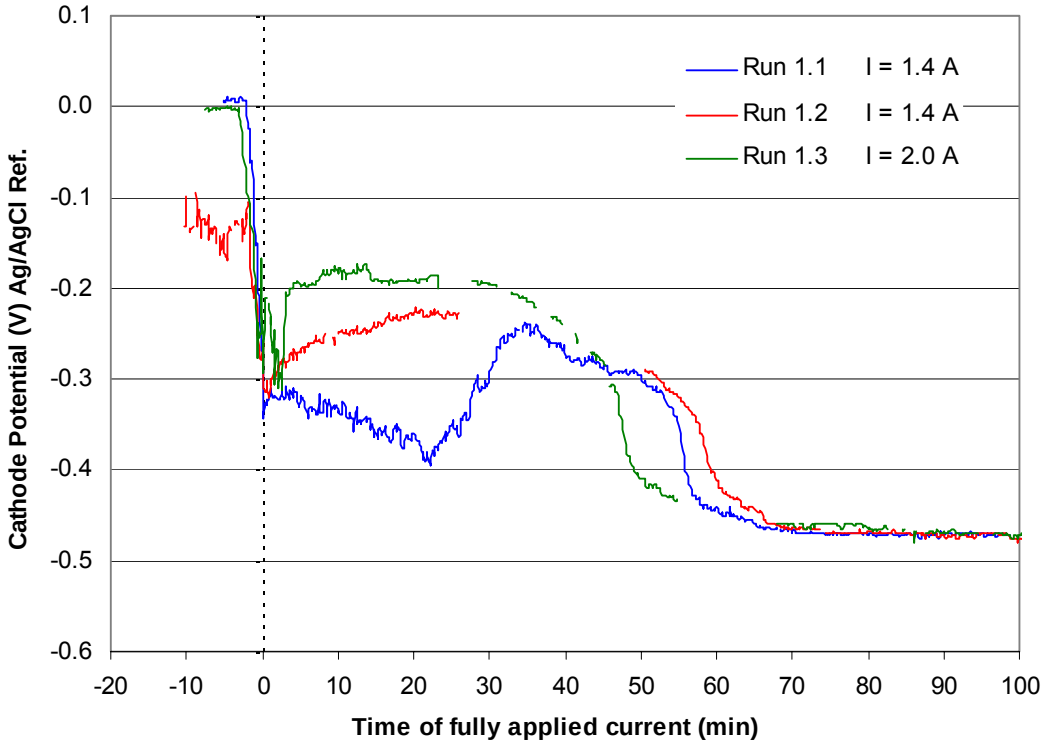


Figure 6.4 Cathode potential profiles for plant solution catholytes

The potential measured while the solution was recirculating without the application of any current can be seen to be approximately 0 V for Run 1.1 and Run 1.3. The potential measured for Run 1.2 is more negative but was rather unstable.

The current was applied in small increments of 0.2 A every 20 seconds in an attempt to avoid the charging effects of the double layer capacitance at the solution / electrode interface. This rate may however still have been too rapid as the potentials in Figure 6.4 are seen to initially reach very negative potentials which then decay to less negative values. A possible explanation for the "unusual" trend in the cathode potential recorded during the first 20 minutes for Run 1.1 is that a large overpotential is required for copper nucleation on the graphite surface. This nucleation overpotential is referred to in literature[182a] and was further confirmed in the experimental work of van Aswegen[178], conducted on the same graphite material.

Once sufficient nuclei are formed the deposition reaction occurs at lower overpotentials. For Run 1.2 the potential begins to decay as soon as the full current had been applied as sufficient nuclei are present from the previous experiment. As Run 1.3 was conducted with higher applied currents and this could have necessitated the formation of additional nuclei and hence the potential decay was delayed by a few minutes.

The potentials measured for Runs 1.1 and 1.2 are comparable after 50 minutes and the drop in potential, indicating mass transport control and the start of hydrogen evolution agree well with the results discussed in Section 6.1.1. The earlier onset of mass transport control for a higher applied is also evident. The potentials can be seen to stabilize at approximately 80 minutes at which time no further metal recovery is achieved and all the current is used up by the evolution of hydrogen. No noticeable difference in the potential for hydrogen evolution for the different currents can be identified.

The straight glass capillary used for Run 1 had the open end pointing downward and thus was susceptible to blockages from the particles and hydrogen. This necessitated intermittent injecting of the KCl solution to unblock the tip. Unfortunately as a result of the blockages periods of recorded data were lost. The use of a glass capillary also resulted in difficulties in the assembly of the reactor, as the delicate glass tube was often broken. This design for the capillary was therefore altered for subsequent runs and is described in Section 6.2.3.

6.1.4 Corrosion of Current Collector

When the cell was dismantled and the copper current collector removed from the reactor, significant corrosion was evident. This is shown in Figure A2 of Appendix A. The copper was therefore replaced by a rod with the same dimensions but possessing a corrosion resistant coating consisting of iridium oxide (IrO_2) / tantalum oxide (Ta_2O_5) for further testwork.

6.2 PALLADIUM IONS IN SYNTHETIC INDUSTRIAL EFFLUENT

Run 2 consisted of four consecutive tests on the same bed of particles. The composition of the Pd SMISIE catholyte was given previously in Table 4.4. The experiments were all conducted under galvanostatic control with the currents applied in each shown below. To assess the reproducibility of the Pd removal and the effect of Cu metal on the electrode surface, a repeat experiment of Run 2.1 was later conducted following the Cu SMISIE trials discussed in Section 6.3. The results of this test, Run 2.5, are shown and discussed in this section.

Run 2.1	Current applied = 1.4 A
Run 2.2	Current applied = 2.0 A
Run 2.3	Current applied = 0.8 A
Run 2.4	Current applied = 2.6 A
Run 2.5	Current applied = 1.4 A

The measured concentrations of palladium ions in the reservoir with time are shown in Figure 6.5 below for Run 2.1 to Run 2.4. The concentration profiles for Run 2.1 and Run 2.5 are shown for comparison in Figure 6.6.

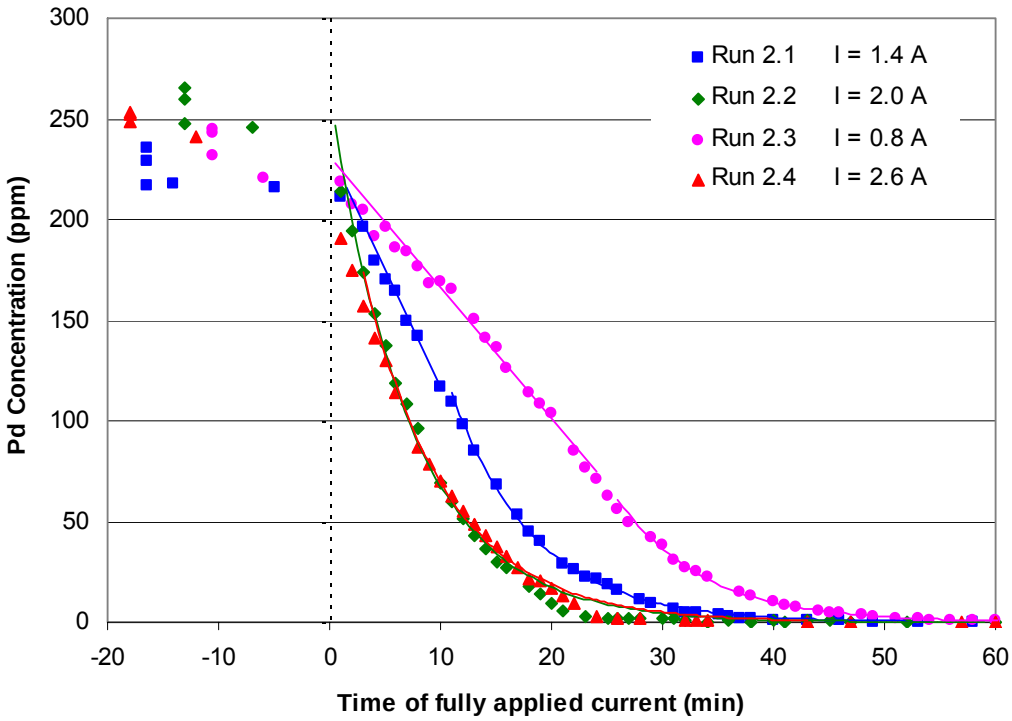


Figure 6.5 Concentration profile for Pd removal from Pd SMISIE catholytes for various applied currents

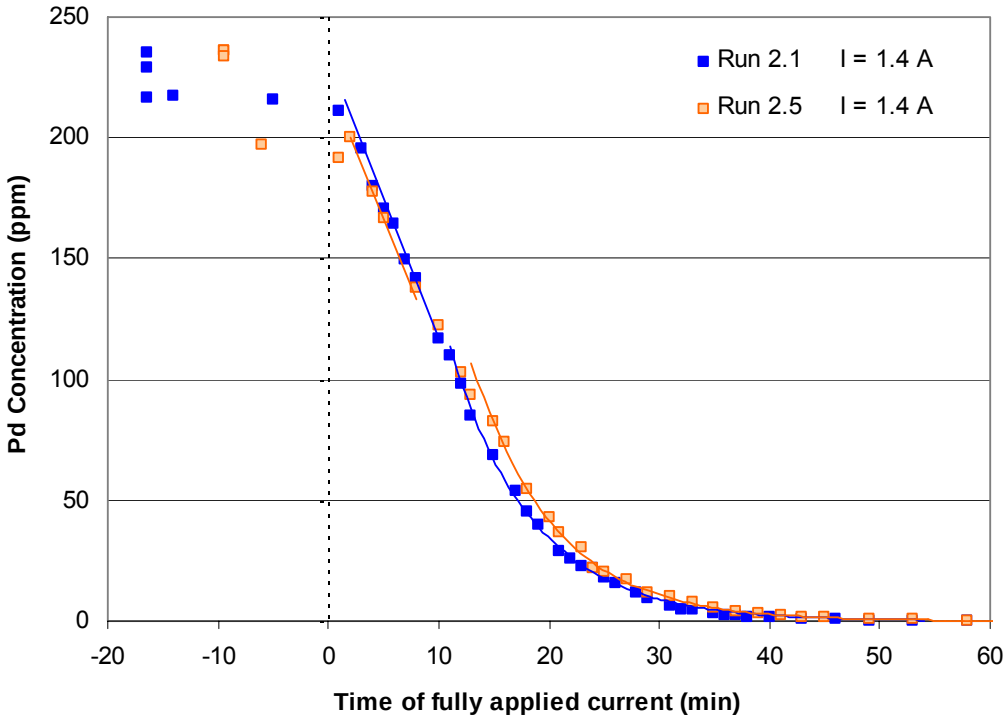


Figure 6.6 Concentration profile for Pd removal from Pd SMISIE catholytes for an applied current of 1.4 A to show reproducibility and surface effects

In Figure 6.6 the results of Run 2.1 and Run 2.5 are seen to be almost identical although the electrode surface was different for each experiment. Run 2.1 was conducted on a bed of fresh graphite particles and Run 2.5 was conducted on a different batch of particles on which several experiments were performed during which copper was deposited onto the bed. The results confirm reproducibility and no serious surface effects are evident.

6.2.1 Reaction Mechanisms

Three samples of the made-up catholyte solution were sent for analysis to determine the concentrations of Pd in the head samples shown in Figure 6.5. The reported concentrations were in excess of the expected 200 ppm and ranged between 220 and 260 ppm.

A linear decrease in the concentration with time is initially observed for the lower applied currents indicating a current controlled reaction rate. The reaction mechanism was determined to be that of a two electron transfer and hence the expected deposition of Pd^{2+} ions to Pd metal.

As the concentration is decreased, mass transport control commences, as shown in Figure 6.5 by the exponential decay in the profile. For applied currents of 0.8 A and 1.4 A mass transport control is observed when the concentration reaches approximately 50 ppm and 100 ppm respectively. As predicted by theory the concentration at which mass transport begins to control is smaller for lower applied currents. For Runs 2.2 and 2.4 the applied currents were such that mass transport controlled the electrochemical process from the start of the experiment and as this is the maximum rate at which the palladium ions are reduced, the concentration profiles are practically identical.

The time required to recover palladium from solution is shorter for larger applied currents. However applying a current far above the limiting current for the initial concentration does not enhance the recovery rate as the excess current is merely be consumed by the hydrogen side reaction.

The cyclic voltammograms (CV) conducted by van Aswegen[178] on the Pd SMISIE catholyte solution are shown in Figure 6.7. The voltammograms show the three sweeps in the potential range between 0.6 V and -1.0 V, relative to a Ag/AgCl (3 M KCl) reference electrode, at a scan rate of 250 mV/s and a step potential of 0.0049 V. The working electrode used consisted of the same graphite particles as those used in the reactor. The solution was not purged with nitrogen to remove the oxygen in solution such that comparison with testwork using the benchscale reactor could be made. Hydrogen is rapidly evolved below a potential of roughly -0.8 V. From the Pd SMISIE scans, the Pd is seen to deposit below potentials of -0.3 V (Peak 1) and the deposited Pd metal catalyses the hydrogen reaction with the measured potential shifting to between -0.5 and -0.6 V. The deposition reaction is also catalysed by the palladium deposit with the reduction potential shifting with each scan. Peak 2 was attributed to the oxidation of the sorbed hydrogen on the palladium surface discussed in Section 2.1.3.1. The palladium is oxidised at potentials positive to 0.4 V and from the broad shape of the peak both dissolution and oxide formation are likely to occur.

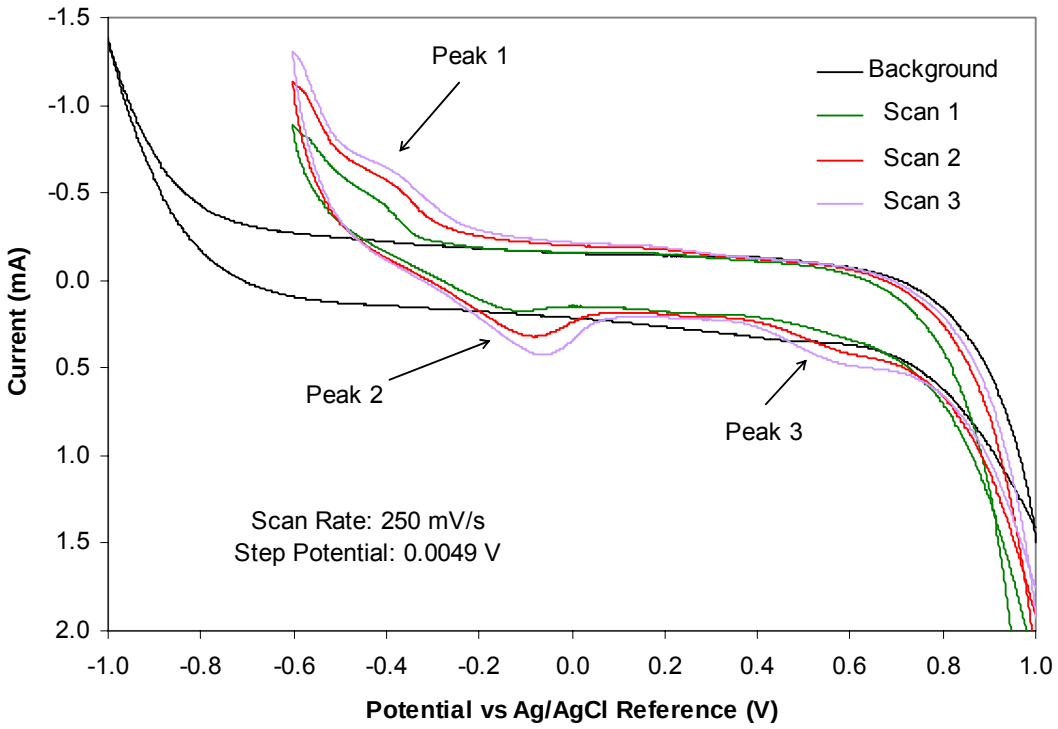


Figure 6.7 Cyclic voltammogram of Pd SMISIE solution

6.2.2 Reaction Kinetics

The region of a current controlled reaction rate was identified and indicated by the plotted linear trends in Figure 6.5 for Runs 2.1 and 2.3 and in Figure 6.6 for Run 2.5. As shown in Table 6.4, using the relationship given by Equation 5.33, the slopes of these trendlines indicate a two electron transfer reaction with approximately 100% current efficiency.

Table 6.4 Parameter estimation for the metal deposition reaction during current controlled conditions for Pd SMISIE catholytes

Test	*Slope* (ppm/min)	*n*	I_{rxn} (A)	I_{app} (A)	ϕ
Run 2.1	-11.594	2	1.40	1.40	1.00
Run 2.3	-6.538	2	0.79	0.80	0.99
Run 2.5	-11.129	2	1.34	1.40	0.95

Under mass transport controlled conditions, using the expression given by Equation 5.24, it was possible to estimate the mass transport coefficient and the conversion per pass from the linear slope of the plot of the natural logarithm of the concentration as a function of time as given in Figure 6.8. These approximated parameters are reported in Table 6.5.

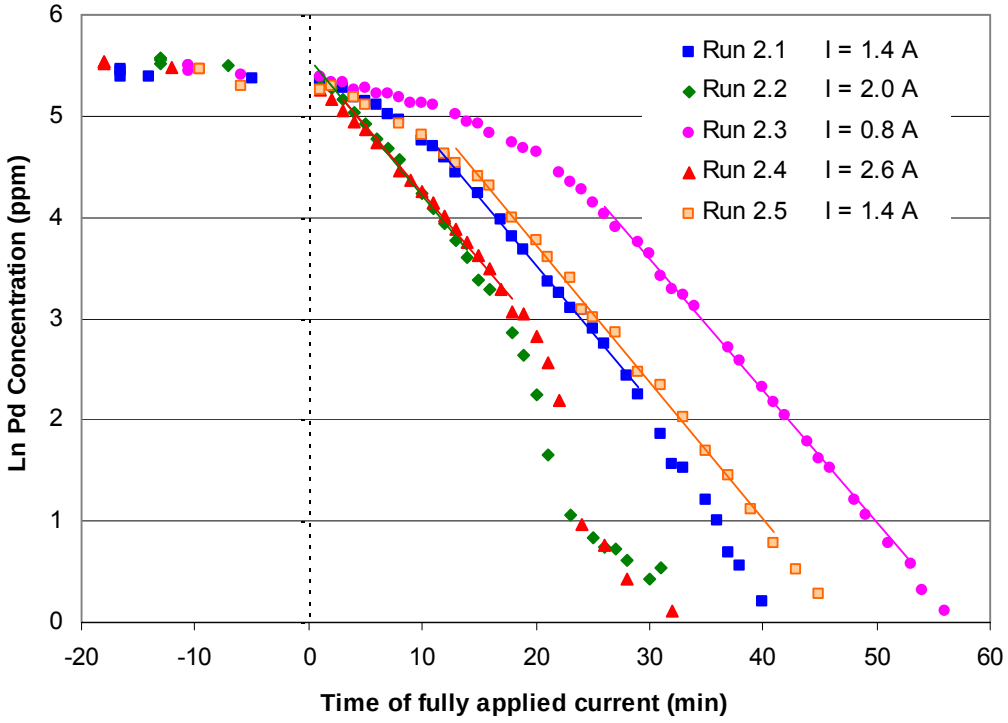


Figure 6.8 Plot of the natural logarithm of the concentration as a function of time for Pd SMISIE catholytes

Table 6.5 Parameter estimation for the metal deposition reaction under mass transport controlled conditions for Pd SMISIE catholytes

Test	*Slope* (1/min)	$\dot{Q}$ (ml/min)	V_{res} (l)	X_{SP}	k_m (10^{-5} m/s)
Run 2.1	-0.134	620	3.84	0.83	3.6
Run 2.2	-0.136	620	3.77	0.83	3.6
Run 2.3	-0.131	620	3.82	0.80	3.4
Run 2.4	-0.131	620	3.87	0.82	3.5
Run 2.5	-0.135	555	3.90	0.95	5.5

The tabulated results above show similar slopes were determined for the mass controlled reaction rate. However, the flowrate is an important parameter in determining the conversion per pass and the mass transport coefficient. The flowrate was calibrated during the commissioning of the experimental setup and the same setting was used on the pump for all of the tests performed. However, it was realized that due to wear on the pump tubing, the flowrate was slowly diminishing with time. Unfortunately this was only noted after Run 2.4. Thus for the Runs 2.1 to 2.4 the actual flowrate was not measured and the calibrated flow of 620 ml/min was assumed. This was certainly not the correct flowrate as numerous experiments had been performed following the calibration. The values reported for these runs in Table 6.5 for the conversion per pass and the mass transport coefficient are therefore too low.

More accurate determination of the kinetic parameters is reflected by the results of Run 2.5 which was conducted at a later stage of the testwork. The flowrate for this run was determined just before the test using a measuring cylinder and stopwatch and although not precise, it is a fair estimate.

For the experiments conducted with higher applied currents (Run 2.2 and Run 2.4) the profiles shown in Figure 6.8 deviate from the linear trend toward the end of the run. This could possibly be due to the vast amounts of hydrogen produced.

6.2.3 Potential Profile

The cathode potential was monitored at the centre base of the bed. A plastic capillary was used for this run and was attached to the modified glass salt bridge by means of heat shrinking PVC. The capillary was inverted to form a U-shape at the end and filter paper was used to plug the opening. This overcame the problems associated with the tube blockages by graphite particles and hydrogen bubbles. The recorded profiles for Run 2 are shown in Figure 6.9.

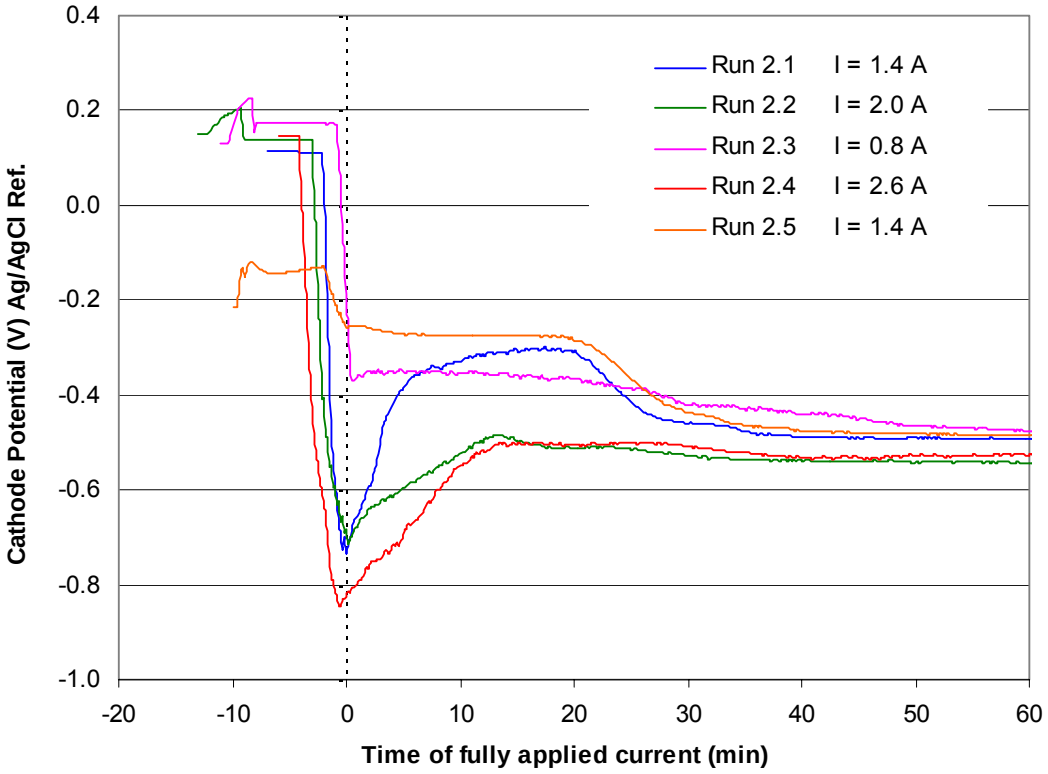


Figure 6.9 Cathode potential profiles for Pd SMISIE catholytes

As mentioned previously the charging effect of the double layer capacitance could account for the very negative potentials measured at the start of the Runs 2.1, 2.2 and 2.4 which then decay to less negative values. This effect is negligible for Run 2.3 which was conducted with a low applied current. An interesting observation is that when comparing the trends for Run 2.5 and Run 2.1, which had the same applied current, the potential profiles are very similar after 20 minutes but the initial potential for Run 2.5 does not exhibit the charging effect of the electrode / electrolyte capacitor. The open circuit potential for Run 2.5 was considerably more negative than that of the other runs and this is attributed to the copper deposit present on the electrode surface for this experiment. Thus when the current was applied the change in the potential was less abrupt and hence the charging of the capacitor was minimal.

6.3 COPPER IONS IN SYNTHETIC INDUSTRIAL EFFLUENT

Run 3 consisted of four consecutive tests on the same bed of particles. The composition of the Cu SMISIE catholyte was given previously in Table 4.4. The experiments were all conducted under galvanostatic control with the currents applied in each as follows:

Run 3.1	Current applied = 1.4 A
Run 3.2	Current applied = 2.6 A
Run 3.3	Current applied = 2.0 A
Run 3.4	Current applied = 1.4 A

Run 3.4 was a repeat of Run 3.1 to assess the reproducibility of the experiments. The results for each test are given in Appendix D. The measured concentrations of copper ions in the reservoir with time are shown in Figure 6.10 below, where time t = 0 represents the time at which the full current required had been applied.

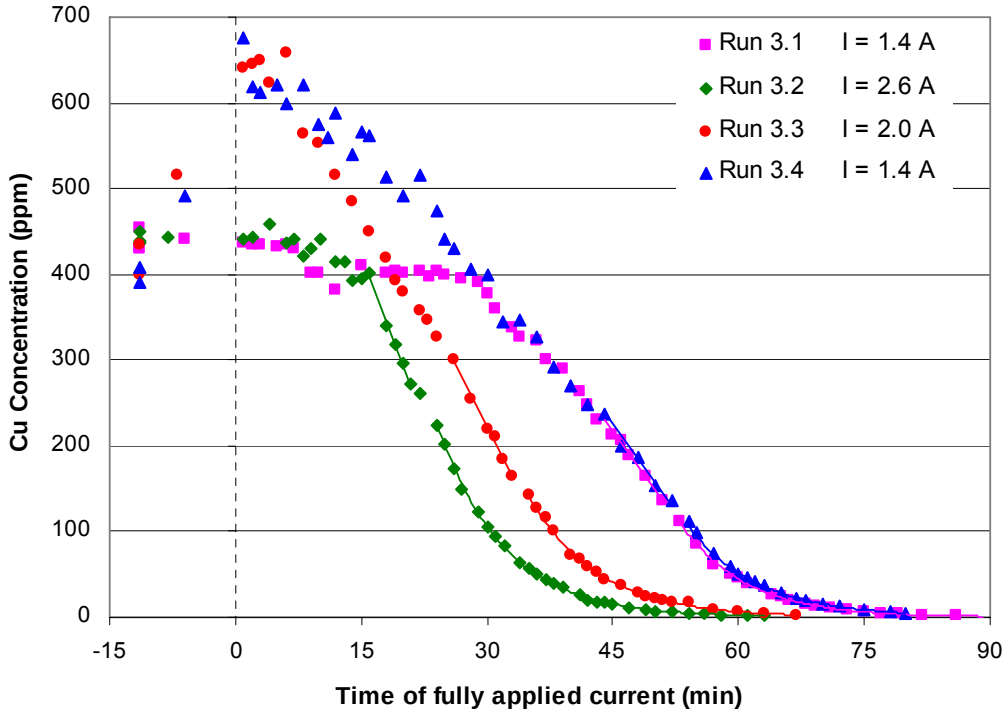


Figure 6.10 Concentration profile for Cu removal from Cu SMISIE catholytes for various applied currents

All the tests were performed on synthetic solutions initially containing 400 ppm of Cu^{2+} ions. Three samples of each starting solution were submitted for analysis. The reported concentrations (shown in Figure 6.10 at time t = -12 min) ranged from 390 to 450 ppm. These discrepancies were attributed to the large dilutions that were required for the ICP to operate within the calibrated range, thereby enhancing any errors. The imprecision due to dilution is further evident by noting the large scatter of data for the more concentrated samples.

6.3.1 Reaction Mechanisms

For Run 3.1, little or no change in the concentration was noted for the first 30 minutes of applied current. A similar observation was made for Run 3.2, but the time period was only 16 minutes. Thus a reaction other than the deposition of copper metal or the evolution of hydrogen, as no gas bubbles were noted during this time period, must have occurred. The concentrations then decreased at a rate that, from a charge balance, indicated a single electron transfer mechanism.

These trends can be accounted for if the Cu^{2+} ions are initially reduced to Cu^{+} ions and as the ICP analysis measures the total concentration of copper no change is recorded. As the solution is depleted of Cu^{2+} ions the Cu^{+} ions are then reduced to Cu metal and the measured concentration of ions in the solution decreases. The reduction of Cu^{+} to metal requires only a single electron transfer, as was observed. Using Faraday's Law, a charge balance was conducted over the initial concentration plateau. For a constant current of 1.4 A and 2.6 A the times required to reduce 400 ppm of Cu^{2+} to Cu^{+} from a batch of 4 litres are 28.9 minutes and 15.6 minutes respectively. These times compare well with those at which the concentrations began to rapidly decrease in the tests, indicating that the majority of the Cu^{2+} ions are reduced before the metal deposition reaction commences. Thus the copper is reduced in two single electron transfer reactions given by Reactions 6.1 and 6.2.

$$Cu^{2+} + e^{-} \rightarrow Cu^{+} \qquad [6.1]$$

$$Cu^{+} + e^{-} \rightarrow Cu^{0} \qquad [6.2]$$

Conclusive evidence of the copper reduction via Reactions 6.1 and 6.2 was given by the cyclic voltammograms, shown in Figure 6.11, recorded by Aswegen[178] on the same catholyte solution. The voltammograms show three sweeps in the potential range between 0.6 V and -1.0 V, relative to a Ag/AgCl (3M KCl) reference electrode, at a scan rate of 20 mV/s and a step potential of 0.0049 V. The working electrode used consisted of the same graphite particles as those used in the reactor. The CV shows reduction peaks at approximately 0.08 V and -0.3V, and oxidation peaks at approximately -0.1 V and 0.2V. As interpreted by van Aswegen, Peak 3 was characteristic of a typical anodic stripping peak and represented the oxidation of Cu metal to Cu^{+} ions. Peaks 1 and 4 are the respective reduction and oxidation peaks for the Cu^{2+}/Cu^{+} redox couple. Peak 2 was believed to be the result of the reduction of Cu^{+} to Cu metal.

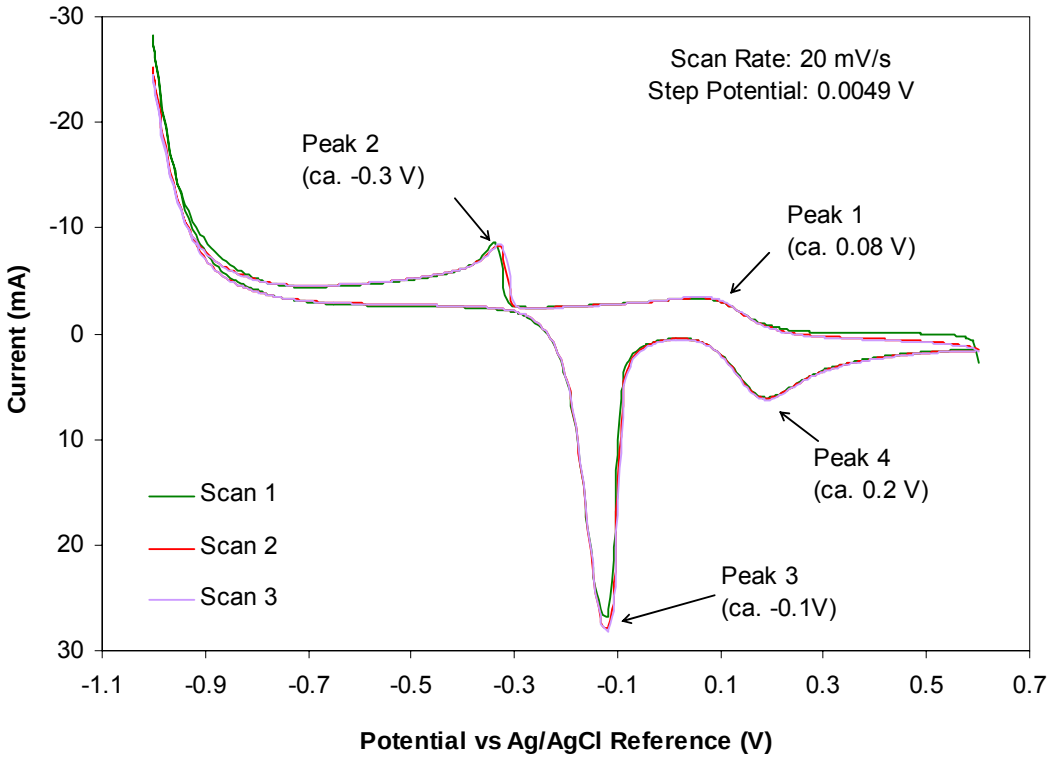


Figure 6.11 Cyclic voltammogram of Cu SMISIE solution

For Run 3.3 and Run 3.4, the exceptionally high results for the initial concentrations of copper ions, as shown in Figure 6.10, were unexpected considering that the starting catholyte for all tests were of the same composition. Even though it was thought unlikely to be an analytical error as distinctive trends were noted, the samples were re-analysed and the reported values confirmed. The increase in

concentration was attributed to the dissolution of the copper metal, deposited in previous experiments, during the approximately 10 minutes of start-up when no current was applied. Deposited copper was found to readily dissolve back into solution if inadequate cathodic protection was applied between tests. Prior to Run 3.2, a sample of the solution in the reservoir that was left circulating overnight with an applied current of 0.05 A revealed that almost all the copper had been removed from the electrode. As Run 3.1 was conducted on a fresh bed of particles both Run 3.1 and Run 3.2 were conducted on copper-free particles and hence no increases in the concentrations were noted at commencement of these tests. However, following Run 3.2 higher cathodic protection (0.1 A) was applied to the bed between experiments and virtually no copper was removed from the particles in the bed.

Although Run 3.4 showed a concentration of above 600 ppm, the trend lines toward the end of the experiment were virtually identical to those for Run 3.1, conducted at the same applied current, but with an initial concentration of only 400 ppm. This can be explained by the equilibrium potentials of the Cu^{2+}/Cu^{+} and Cu^{+}/Cu^{0} couples shown in the cyclic voltammograms. It can be seen that,

$$E_e(Cu^{+}/Cu^{0}) \approx -0.2\,V \qquad [6.3]$$

$$E_e(Cu^{2+}/Cu^{+}) \approx 0.15\,V \qquad [6.4]$$

Thus the reduction of Cu^{2+} in solution (Reaction 6.5) and the oxidation of the Cu metal deposit (Reaction 6.6) will form a redox reaction given by Reaction 6.7.

$$Cu^{2+} + e^{-} \rightarrow Cu^{+} \qquad E_e^C = 0.15\,V \qquad [6.5]$$

$$Cu^{0} \rightarrow Cu^{+} + e^{-} \qquad E_e^A = -0.2\,V \qquad [6.6]$$

$$Cu^{2+} + Cu^{0} \rightarrow 2Cu^{+} \qquad \Delta E_e = E_e^C - E_e^A \qquad [6.7]$$

This reaction will occur spontaneously as the resulting Gibbs free energy change (ΔG), shown below, is negative[(154g)].

$$\Delta G = -nF\Delta E_e \qquad [6.8]$$

The additional copper ions for Runs 3.3 and 3.4 were therefore due to the oxidation of copper metal on the particles, and the simultaneous reduction of the Cu^{2+} ions initially in solution. The concentrations of copper reported at the start of Run 3.3 and Run 3.4 are the combination of the Cu^{2+} and Cu^{+} ions. Therefore, although an overall increase in concentration was noted, the time required to reduce the copper ions would be the same as that to reduce the 400 ppm of Cu^{2+} as the moles of positive charge remain the same.

6.3.2 Reaction Kinetics

No quantitative information was obtained for the kinetic parameters for the reduction of Cu^{2+} to Cu^{+} as accurate trendlines could not be fitted to data pertaining to this reaction. For the metal deposition reaction, Cu^{+} to Cu^{0}, the region of a current controlled reaction rate was identified and is indicated in Figure 6.10 by the plotted linear trends. As shown in Table 6.6, using the relationship given by Equation 5.33, the slopes of these trendlines indicate a single electron transfer reaction with approximately 100% current efficiency.

Table 6.6 Parameter estimation for the metal deposition reaction during current controlled conditions for Cu SMISIE catholytes

Test	***Slope*** **(ppm/min)**	***n***	I_{rxn} **(A)**	I_{app} **(A)**	ϕ
Run 3.1	-13.533	1	1.37	1.40	0.98
Run 3.2	-25.808	1	2.61	2.60	1.00
Run 3.3	-19.330	1	1.96	2.00	0.98
Run 3.4	-13.643	1	1.38	1.40	0.99

Under mass transport controlled conditions, using the expression given by Equation 5.24, it was possible to estimate the mass transport coefficient and the conversion per pass from the linear slope of the plot of shown in Figure 6.12. These approximated parameters are reported in Table 6.7.

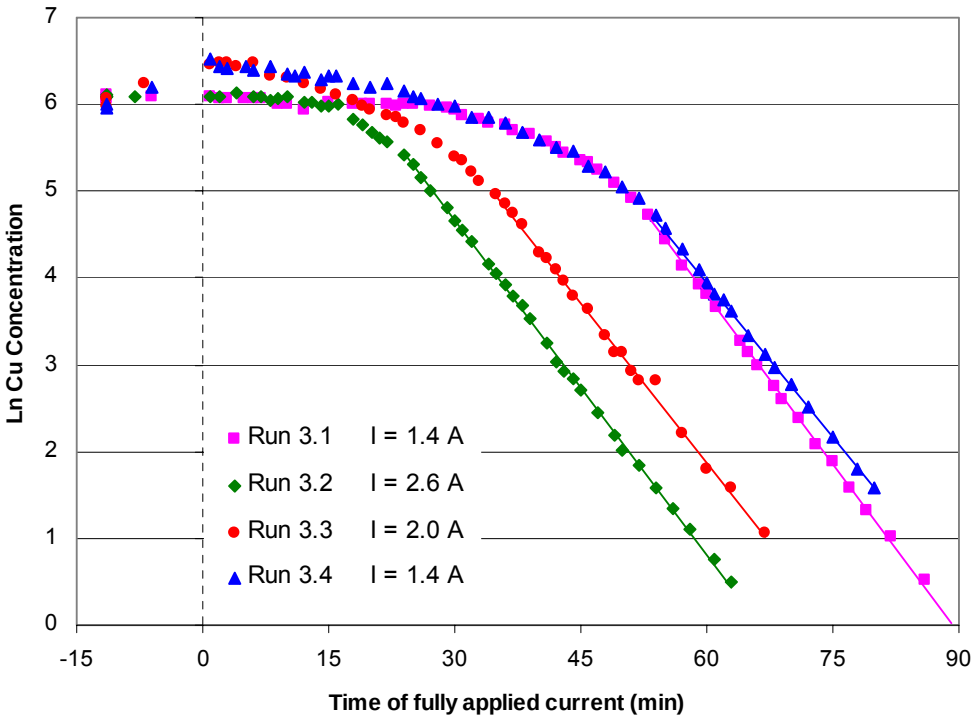


Figure 6.12 Plot of the natural logarithm of the concentration as a function of time for Cu SMISIE catholytes

Table 6.7 Parameter estimation for the metal deposition reaction under mass transport controlled conditions for Cu SMISIE catholytes

Test	*Slope* (1/min)	$\dot{Q}$ (ml/min)	V_{res} (l)	X_{SP}	k_m (10^{-5} m/s)
Run 3.1	-0.130	530	3.9	0.96	5.5
Run 3.2	-0.128	515	3.9	0.97	6.0
Run 3.3	-0.123	495	3.9	0.97	5.8
Run 3.4	-0.119	475	3.9	0.97	5.8

From a charge balance it can be shown that for the time period prior to the start of mass transport control of the metal deposition reaction, virtually all the current applied was utilised in the copper ion reductions. The process efficiency begins to decrease when hydrogen gas is evolved. The calculated overall process efficiencies to reduce the concentration to 10 ppm are tabulated in Table 6.8.

Table 6.8 Process efficiencies for reducing the copper concentration from 400 ppm of Cu^{2+} to 10 ppm Cu^{+} from Cu SMISIE catholytes

I_{rxn} (A)	t (min)	Q_{app} (C)	Q_{rxn} (C)	ϕ_p (%)
1.4	73	6132	4799	78
2.0	56	6720	4799	71
2.6	48	7488	4799	64

As the applied current is increased, the time to reach a concentration of 10 ppm is reduced but as expected, the overall efficiency of the process decreases. Thus a compromise must be drawn from an economic analysis following the study of the effects of the various process parameters and their optimisation.

6.3.3 Potential Profile

The cathode potential was monitored at the centre base of the bed. The recorded profile for Run 3.4 is shown in Figure 6.13 along with the measured concentrations in the reservoir.

The potential profile offers insight into the reactions occurring. From Figure 6.13, it can be seen that initially the reaction was completely controlled by the rate of electron transfer as the potential remained constant and the proposed reduction of Cu^{2+} to Cu^{+} was confirmed from the negligible change in the copper concentration prior to marker A, indicated on the graph. As the concentration of Cu^{2+} ions decreased this reaction became limited by mass transport and the current efficiency was reduced. The potential therefore began to shift toward more negative values with the onset of the following reaction, namely the reduction of Cu^{+} to metal shown by the decrease in the concentration profile subsequent to marker A. Between markers B and C the majority of the applied current was used in the metal deposition reaction as only a small change in potential with time was noted. The current efficiency of this reaction, determined from the slope of the concentration profile, slowly increased reaching 100% when the rate of Cu^{2+} to Cu^{+} reaction became negligible. The potential once again showed a sharp decline in the trend at marker C signifying the commencement of a further reaction, namely hydrogen evolution, as

the deposition reaction became mass transport controlled. These trends agree well with the visual observation of the first gas bubble rising from the bed at approximately 54 minutes after the application of current.

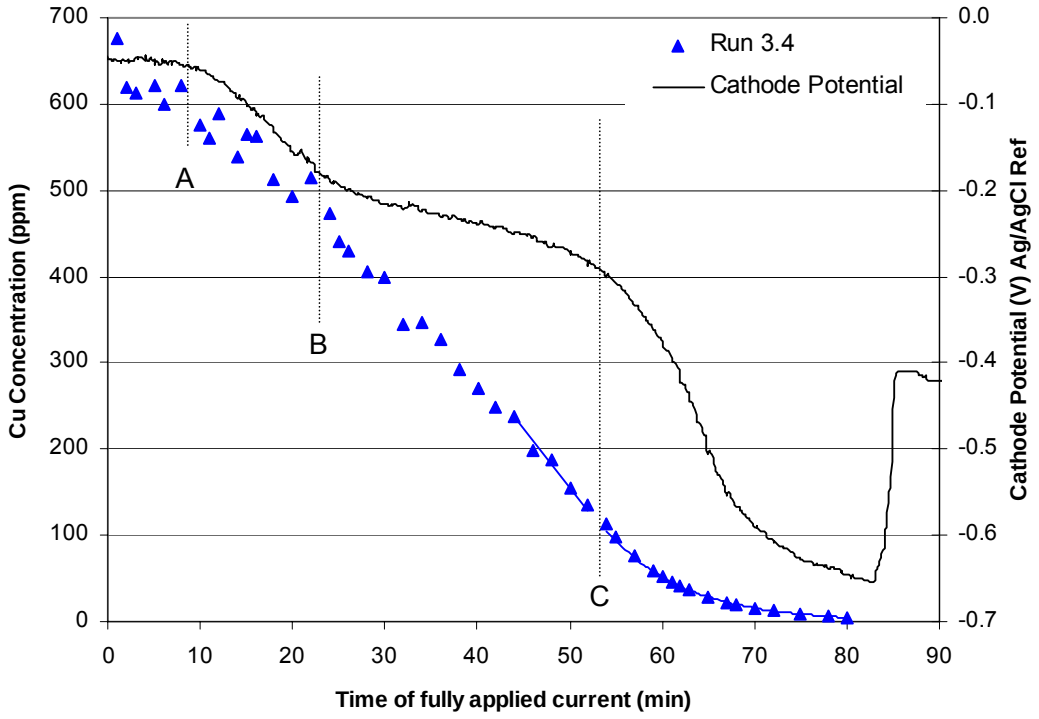


Figure 6.13 Cathode potential and concentration profiles for Cu reduction from Cu SMISIE catholyte with applied current of 1.4 A

The potential profiles of all the experiments performed on Cu SMISIE catholytes are shown in Figure 6.14 below for comparison. Run 3.1 and Run 3.2 were performed on copper-free beds and hence their open circuit potentials are more positive than those performed on beds containing copper deposits where, as shown in Figure 6.11, a redox couple is between the reaction Cu^0 to Cu^+ and the reaction Cu^{2+} to Cu^+ is formed at more negative potentials.

The charging effect of the double layer capacitance and the overpotential required for copper nucleation on graphite are evident in Run 3.2 where a high current was applied to a copper-free bed. Although Run 3.1 was also conducted on a copper-free bed, the initial reaction was not that of metal deposition but rather the reduction of Cu^{2+} to Cu^+ and hence no nuclei were formed initially. The initial difference in the

potential profiles for Run 3.1 and Run 3.4, which were conducted at the same applied current, is due to the decreased concentration of Cu^{2+} for Run 3.4 thus requiring a higher overpotential for the reduction reaction.

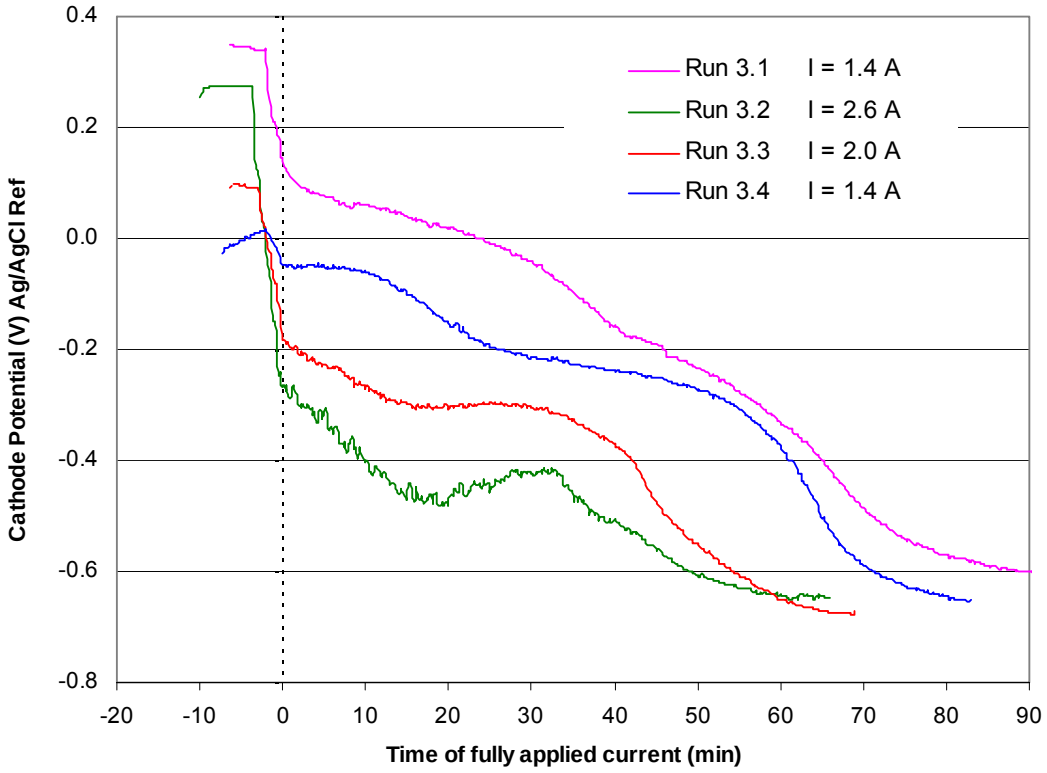


Figure 6.14 Cathode potential profiles for Cu SMISIE catholytes

6.4 COPPER AND PALLADIUM IONS IN SYNTHETIC INDUSTRIAL EFFLUENT

Run 4 consisted of four consecutive tests on the same bed of particles as that already used for Run 3 and for Run 2.5 as the reactor was not dismantled after these experiments. The composition of the Cu / Pd SIE catholyte was given previously in Table 4.4 and it should be noted that unlike Run 3 the concentration of copper ions was approximately 200 ppm. The experiments were all conducted under galvanostatic control with the currents applied in each shown below.

Run 4.1	Current applied = 1.4 A
Run 4.2	Current applied = 2.6 A
Run 4.3	Current applied = 0.8 A
Run 4.4	Current applied = 2.0 A

The measured concentrations of copper ions and palladium ions in the reservoir with time are shown in Figures 6.15 and 6.16 respectively. The time t = 0 represents the time at which the full current required had been applied.

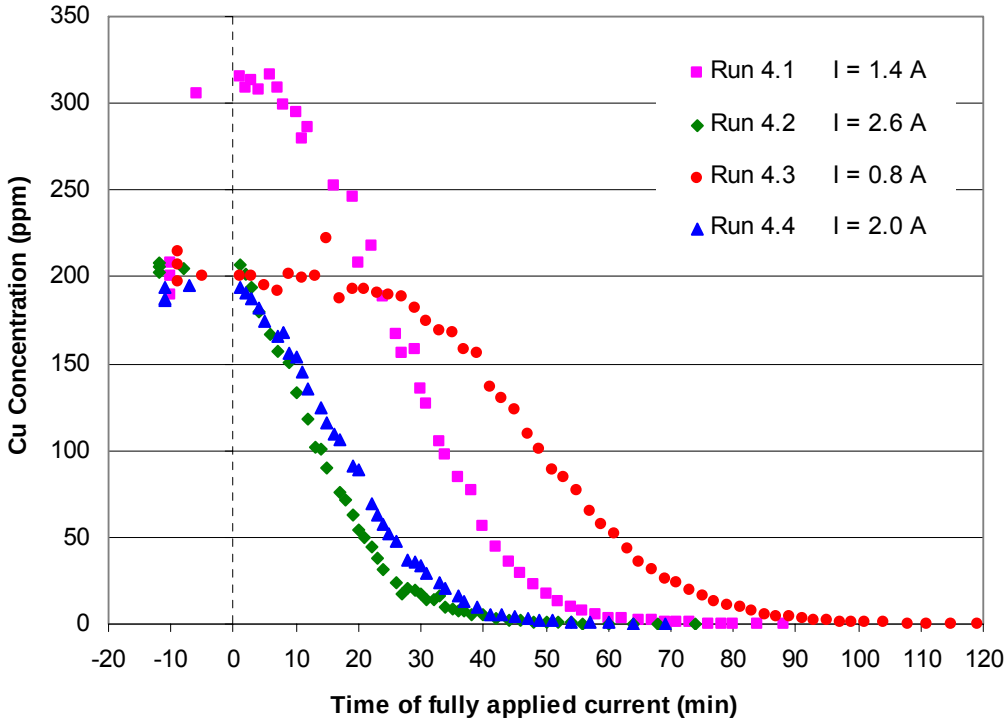


Figure 6.15 Concentration profile for Cu removal from Cu / Pd SIE catholytes for various applied currents

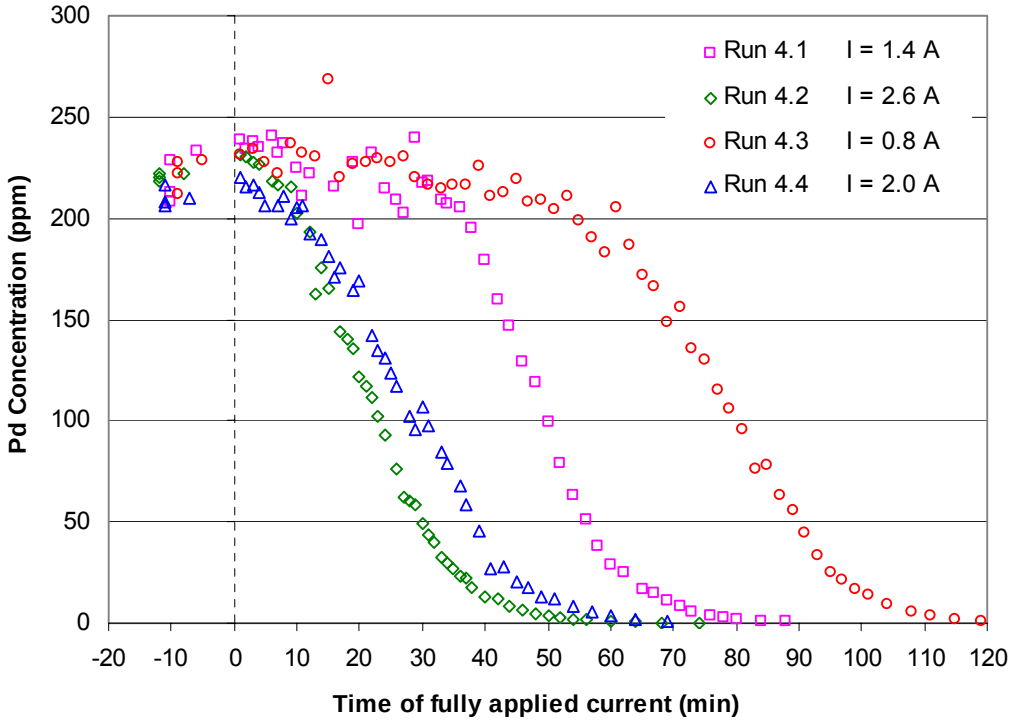


Figure 6.16 Concentration profile for Pd removal from Cu / Pd SIE catholytes for various applied currents

6.4.1 Degree of Separation

The main objective of the testwork with the Cu / Pd SIE catholytes was to demonstrate the effects of the applied current on the degree of separation of the copper from the palladium. The times at which palladium begins to deposit at a notable rate and the corresponding concentrations of copper are given in Table 6.9.

Table 6.9 Concentration of copper when palladium deposition commences for various applied currents

Test	Applied Current (A)	Time when Pd deposition begin, t_{Pd} (min)	Cu concentration at t_{Pd} (ppm)
Run 4.3	0.8	63	44
Run 4.1	1.4	38	57
Run 4.4	2.0	12	136
Run 4.2	2.6	9	151

Comparing these values it can be seen that for lower applied currents the precious metal deposition only commences when the concentration of copper in the reservoir solution is low. Thus the majority of the copper is removed prior to the codeposition of palladium. A perfect separation of the metal ions during the deposition process is unobtainable however, it is possible to decrease the contamination of Cu in the Pd product. This can be achieved by passing a low current through a reactor and reducing the copper concentration in the stream to a low value with minimal loss of palladium and then redirecting the catholyte outlet to a secondary bed where only the small amount of copper remaining in solution will codeposit with the Pd. Therefore when the metals are recovered from the respective beds two products streams are obtained, one with a high copper purity and the other with a lower copper to palladium ratio than the initial effluent. This ratio can be manipulated and controlled by the current applied to the first bed. A trade-off is made with respect to the time taken for the recovery process, with far greater times required for an enhanced degree of separation. The use of two beds can be avoided if the copper is removed from the first bed, that could then be reused for the Pd deposition, however this further increases the process time, which is a critical factor in PGM refining.

6.4.2 Reaction Kinetics

The mechanisms for the individual reactions that occur were determined from the testwork reported in Sections 6.2 and 6.3, where only either copper or palladium ions were present in solution, and from this the concentration profiles in Figures 6.15 and 6.16 above can be interpreted.

Only Run 4.1 exhibits an increase in copper concentration during the 10 minutes of circulation without applying a current. This is because of the copper deposit that remained on the electrode surface after previous experiments (Run 3) which were performed on the same bed. Following Run 4.1 the copper deposits were removed from the electrode surface by circulating the electrolyte without applying a current and hence no copper concentration increase is noted for Run 4.2 to 4.4. For an applied current of 0.8 A (Run 4.3) initially all the current is used for the reduction of Cu^{2+} to Cu^{+} and hence no change in the concentration is noted with time. As the concentration of Cu^{2+} decreases this reaction becomes mass transport controlled and the simultaneous reduction of Cu^{+} to Cu^{0} occurs and a decrease in the copper

concentration is observed. With time the codeposition of palladium commences and the rate of this reaction slowly increases as the rate of copper reduction decreases. For the higher applied currents both copper reactions occur simultaneously from the start of the experiment followed by palladium deposition shortly afterward. For Run 4.1 the starting solution contains only a small amount of Cu^{2+} ions and hence copper deposition occurs early on in the experiment as Cu^{2+} is rapidly depleted.

The mass transport controlled reaction rates are independent of the side reactions occurring and thus it is possible to determine the values for the mass transport coefficients in the multicomponent system. The plots of the natural logarithm of the concentrations of Cu and Pd as functions of time are shown in Figures 6.17 and 6.18 respectively with the calculated parameters given in Tables 6.10 and 6.11 below.

Table 6.10 Parameter estimation for the copper metal deposition reaction under mass transport controlled conditions for Cu / Pd SIE catholytes

Test	***Slope*** **(1/min)**	$\dot{Q}$ **(ml/min)**	V_{res} **(l)**	X_{SP}	k_m **(10^{-5} m/s)**
Run 4.1	-0.130	515	3.84	0.97	6.1
Run 4.2	-0.128	510	3.87	0.97	6.1
Run 4.3	-0.128	510	3.82	0.96	5.5
Run 4.4	-0.130	510	3.81	0.97	6.2

Table 6.11 Parameter estimation for the palladium metal deposition reaction under mass transport controlled conditions for Cu / Pd SIE catholytes

Test	***Slope*** **(1/min)**	$\dot{Q}$ **(ml/min)**	V_{res} **(l)**	X_{SP}	k_m **(10^{-5} m/s)**
Run 4.1	-0.127	515	3.83	0.94	5.0
Run 4.2	-0.127	510	3.84	0.96	5.4
Run 4.3	-0.128	510	3.76	0.95	5.0
Run 4.4	-0.121	510	3.81	0.91	4.0

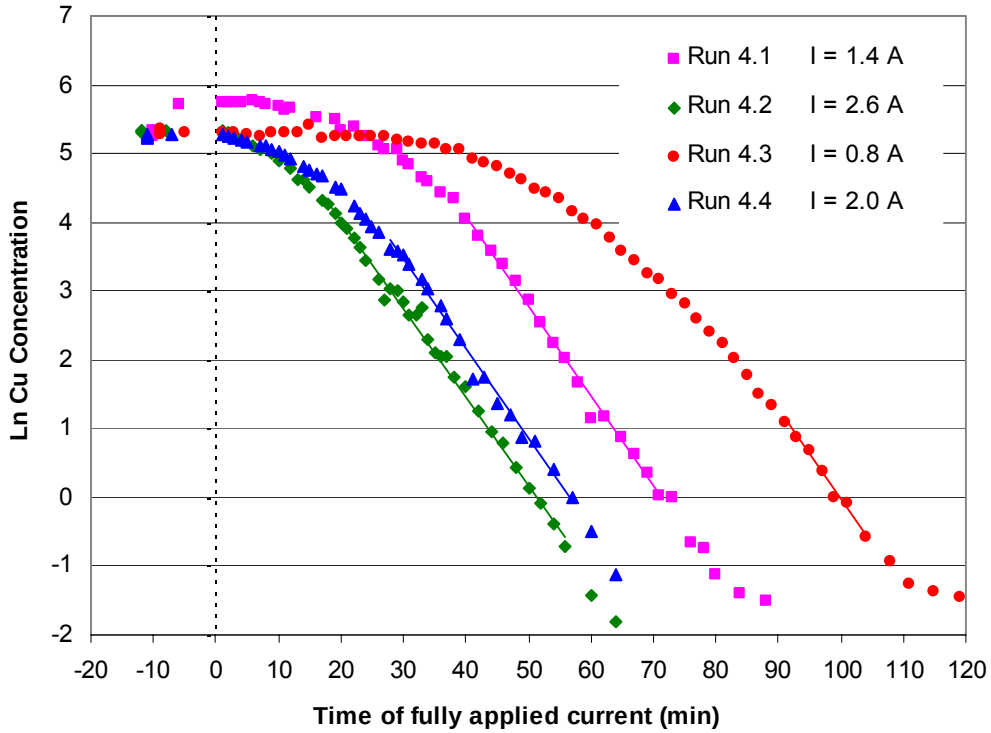


Figure 6.17 Plot of the natural logarithm of the Cu concentration as a function of time for Cu / Pd SIE catholytes

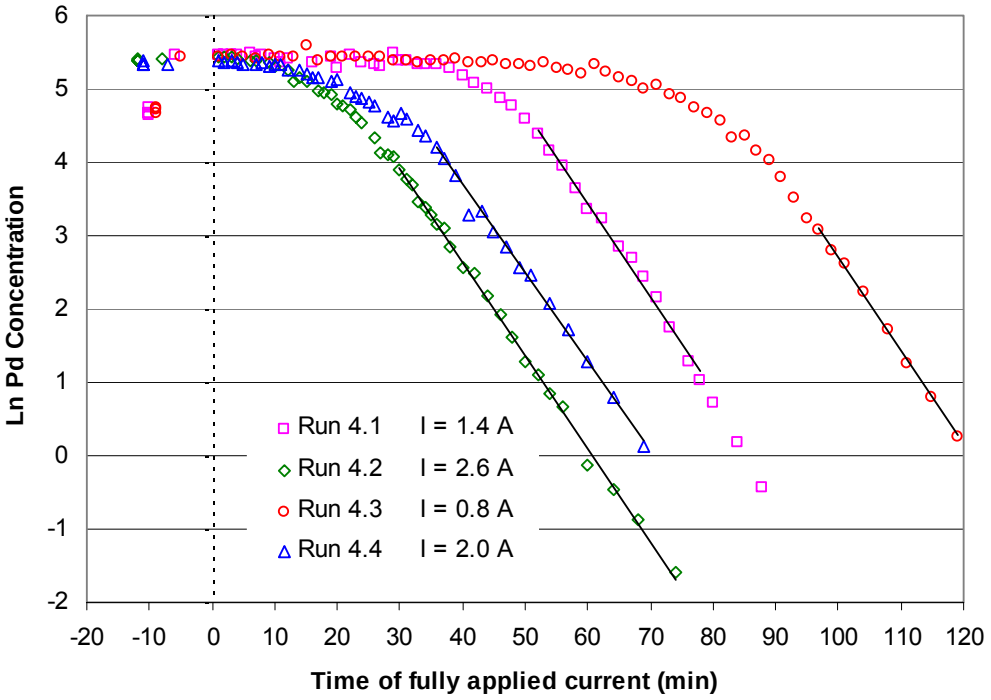


Figure 6.18 Plot of the natural logarithm of the Pd concentration as a function of time for Cu / Pd SIE catholytes

The current controlled reactions were not modelled for the testwork on the Cu / Pd SIE catholytes as multiple reactions occur simultaneously and at varying rates with time making it difficult to fit linear trends to the data.

6.4.3 Potential profile

The potential profiles measured for Run 4 are shown in Figure 6.19. As explained in Section 6.3.1, when the solution containing Cu^{2+} is exposed to a bed containing a copper deposit a redox reaction occurs whereby electrons are transferred and Cu^{+} forms. This reaction occurs at potentials more negative than 0.2 V. The open circuit potentials measured for $t < 0$ are more positive than 0.2 V for Runs 4.2 to 4.4 as these experiments were conducted on copper-free beds and that recorded for Run 4.1 is more negative as copper was present from previous experiments. As the reactions occurring at the start of the experiments are for Cu^{2+} to Cu^{+} and only require a small overpotential, no abrupt changes in potential are evident and charging effects of the double layer at the interface are negligible.

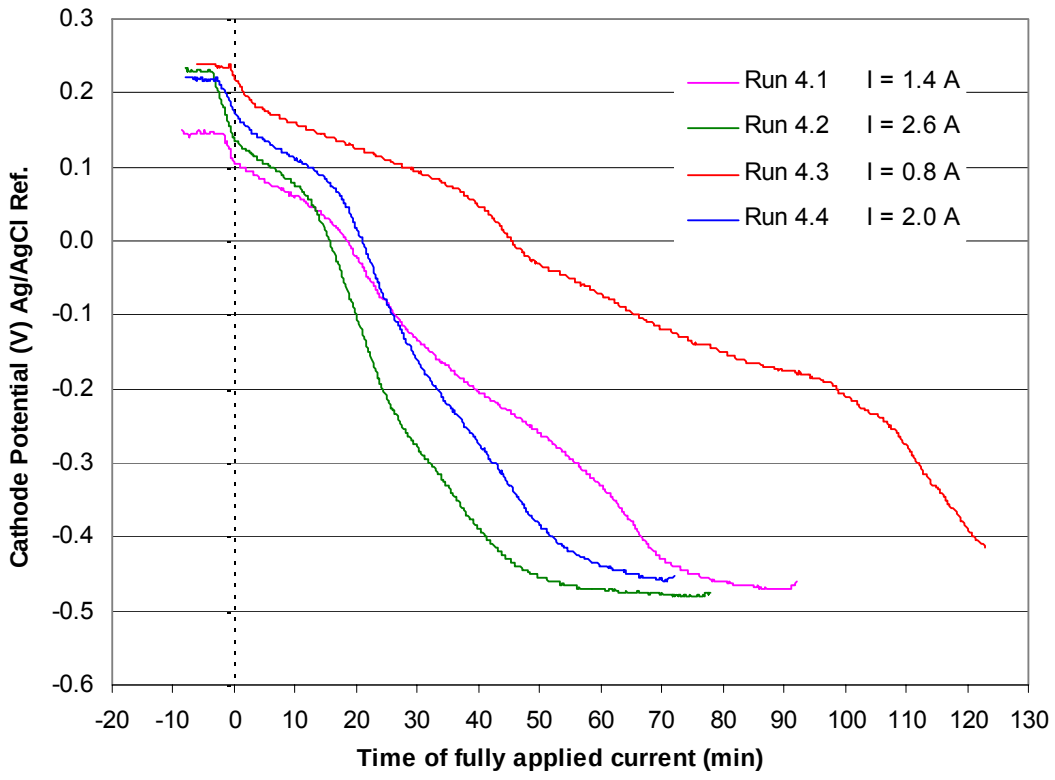


Figure 6.19 Cathode potential profiles for Cu / Pd SIE catholytes

6.5 GENERAL RESULTS

6.5.1 Membrane Permeability

The changes in the volumes of the reservoirs for each test were recorded and are listed in the appendices. The decrease in the volume of the catholyte was due to both the solution flow through the membrane as well as the numerous samples taken during the run. For Run 2 to Run 4 only 8 ml of solution were removed from the anolyte for sample analysis and thus the increase in the volume due to the flow across the membrane could be determined from the difference in the volumes at the start and end of the experiment less the 8 ml removed. From these values, the average flowrate of solution through the membrane could be calculated and was found to be approximately 20 ml/hr. The flow per unit area is thus given roughly as 2000 ml/hr/m^2. The membrane permeability was stated by the manufacturers (see Appendix A) to be less than 30 ml/hr/ft^2, which converts to less than 325 ml/hr/m^2. The calculated permeability is an order of magnitude greater than that specified but this is attributed to the pressure within cathode chamber.

Even with the fairly high permeability of the electrolyte, the flowrate of 20 ml/hr through the membrane was still deemed tolerable as the experiments were conducted for minimal periods of time, approximately one hour, and thus the change in volume due to flow through the membrane was only 0.5 %. For extended operation this may need to be minimised. This could be achieved by increasing the pressure of the anolyte chamber. It would be beneficial for the pressure in the anolyte chamber to be equal or marginally greater than that in the cathode chamber such that the flow is reversed as discussed in Section 2.3.4

6.5.2 Hydrogen Evolution

As the concentration of the metal ions decrease the reaction becomes mass transport controlled and for galvanostatic operation the side reaction namely, hydrogen evolution, commences. The onset of this reaction was shown in the previous sections by the exponential decay in the concentration profile of the depositing metal as well as the rapid shift in the cathode potential to more negative values. Furthermore, the gas bubbles were seen rising from the bed through the

transparent hood. A plot of the cell voltage with time may also provide an indication of the start of the hydrogen reaction due to the activation overpotential required for the reaction as well as the effect of the gas bubbles on the conductivity of the catholyte solution, both causing an increase in the voltage. The measured voltage between the anode and the current collector are shown in Figure 6.20 for Run 3 and the sudden rise in the trend is clearly observed for the lower applied currents. For an applied current of 1.4 A the recorded voltages are seen to increase just after 50 minutes. This is in good agreement with the estimated time for the start of mass transport control shown in Figure 6.12. Similarly the increase in voltage for an applied current of 2.0 A at approximately 30 minutes compares fairly well.

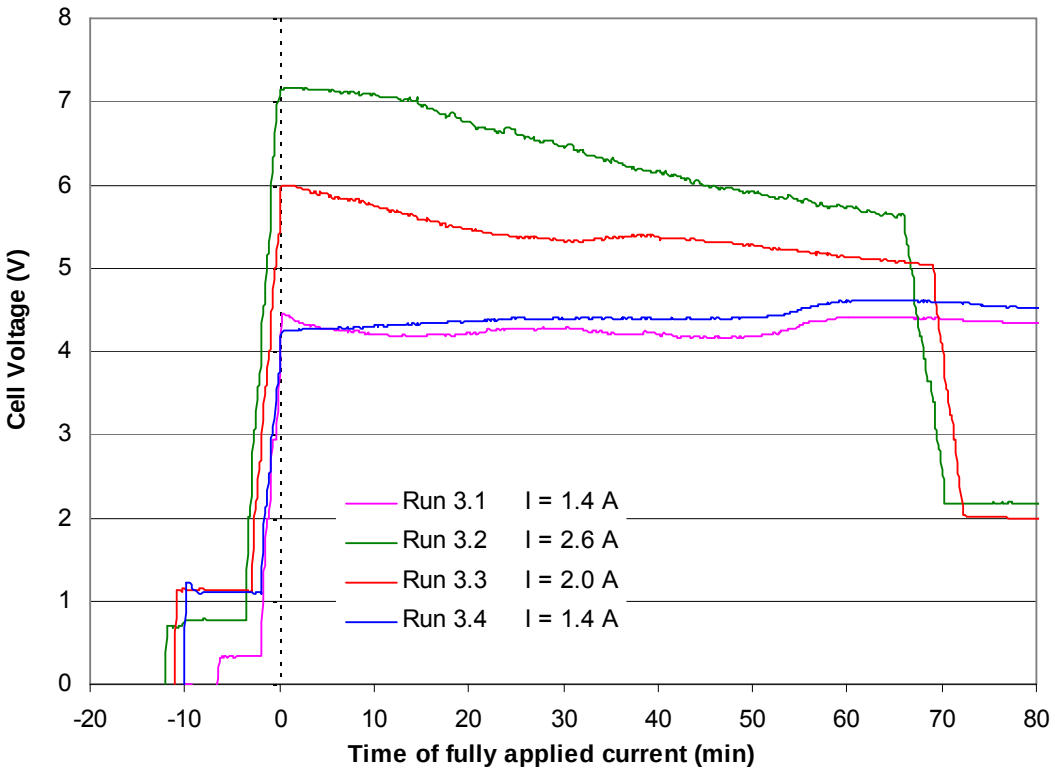


Figure 6.20 Cell voltages measured for Cu SMISIE catholytes

The exact time at which hydrogen evolution commences cannot be determined as a three-dimensional electrode has a complex potential distribution and a variety of reaction rates occur throughout the bed. The concentration decreases as the solution passes through the bed and the reaction rate will become mass transport controlled at the top of the bed before the inlet concentration is such that these conditions are obtained at the base. For higher applied currents the concentration

change across the bed during current controlled conditions is greater and hence bubbles are seen to form prior to the sudden drop in the cathode potential which was measured at the base.

In addition to the change in catholyte conductivity, the electrochemically generated gas bubbles act as turbulence promoters and hence may increase the mass transport coefficient as the rate of hydrogen reaction increases. The bubbles may also adhere to the particles and decrease the surface area available for reaction. Incorporating these effects into a model would be extremely difficult.

6.5.3 Temperatures

The temperature profiles for the catholyte and anolyte solutions are shown in the graphs of the appendices for the individual runs. For the first few experiments an increase in the catholyte temperature was noted and initially attributed to the heat generated when passing the current. During the following tests the temperatures were found to remain constant with time and in several tests even decrease. It was later established that no significant amount of heat is generated during the deposition process but that the change in temperature of the solutions was due to the difference in temperatures between the rooms in which the electrolytes were made up and the experimental testwork conducted. The temperatures recorded all range between 18 and 26 ^{o}C.

When making up catholyte solutions containing palladium, for which the kinetics of complex formation is sluggish, the mixtures were heated to reduce the time for the solution to reach equilibrium and then subsequently cooled. The solubility of the Pd complexes formed is strongly dependent on the temperature and precipitation was noted for solutions that were refrigerated or left out in winter months. The precipitate redissolved when heated.

6.5.4 Cathodic Protection and Corrosion

Copper is a relatively noble metal and is not corroded by non-complexing solutions free from oxidising agents, and carefully de-aerated water does not corrode copper at all[181a]. It was shown by ring-disc testwork[182b] that in a 1 M sodium chloride medium

corrosion of the copper ring occurred in oxygenated solutions. The oxidation reaction recorded at the ring confirmed that the corrosion mechanism in the chloride media was that indicated by Reaction 6.1 and as the corrosion ceased when the solution was purged with nitrogen the oxidising agent for the reaction was the dissolved oxygen. Therefore de-oxygenating the electrolyte would prevent corrosion in chloride solutions but the SMISIE also comprises ammonium ions which form very stable complexes with Cu^{+} ions. This complexing substance is able to produce vigorous corrosion of copper even in the absence of oxidising agents[181a]. Cathodic protection was therefore necessary and employed for all tests following Run 1.

The solution was continuously pumped through the reactor to discharge the hydrogen bubbles formed during cathodic protection. However, this recirculation of the electrolyte transported more oxygen into the reactor chamber and increased turbulence, both of which enhance the corrosion rate. A low current (0.05A) was applied after Run 3.1 which was insufficient to maintain the electrode at a potential below that recommended of 0.1 V SHE[181a] (-0.1V vs. Ag/AgCl). Applying a current of 0.1 A after Run 3.2 to Run 3.4 the required potential was sustained and the concentration of copper measured in the electrolyte was at most 2.5 ppm.

Palladium is a very noble metal and is thermodynamically stable in the presence of aqueous solutions of all pHs free from vigorous oxidising agents, reducing agents and complexing substances. Solutions of non-oxidising acids such as acetic and sulphuric acid do not affect it at all at room temperature. Palladium is dissolved only by solutions which are both very acidic and powerfully oxidising. Hydrochloric acid will attack palladium only slightly if oxygen is present and more rapidly if the acid contains chlorine[181b].

The nobility of palladium was seen from the results of the samples taken after the experiments of Run 4. Copper rapidly redissolved into solution with concentrations reaching over 1 g/l while the maximum measured concentration for palladium dissolution was less than 12 ppm. The slight dissolution was attributed to the complexing ammine species in solution.

The differences in the nobilities of the metals may possibly be manipulated to bring about a greater degree of separation than that gained by a deposition process. If

both metals were deposited onto the cathode the copper could be removed prior to the removal of the palladium using a solution that is insufficiently oxidising for palladium. The palladium can then be removed using more powerful oxidising agents such as HCl containing chlorine or via an electrochemically oxidative process.

6.5.5 Accuracy and Reproducibility

The values reported for the mass transport coefficients are extremely rough estimates. The potential distribution in a packed bed, dispersion, surface effects and the formation of turbulence generating gas bubbles result in a variety of reaction rates throughout the electrode making it impossible to calculate accurate values. However, it was not the intention of the testwork to determine exact kinetic parameters but rather to gain qualitative understanding of the processes occurring. More correct values are determined from RDE tests[178].

Furthermore, the volume of solution in the reservoir, the active surface area of the electrode and the flowrate of solution are all required for calculating the mass transport coefficient using the model derived. The volume of the catholyte was continuously decreasing with time, measuring in the range of 2 to 5 % depending on the number of samples taken. The active surface area of the particles was assumed to be equal to the total surface area calculated from the average diameter of the particles and no allowances for the porosity were made. The flowrates were calibrated before each run (for Run 3 and Run 4 only) using a beaker and stopwatch. These values were only approximate values owing to the inaccuracies of the measurements.

The tests were surprisingly reproducible considering the dynamics of the process. In Figures 6.1, 6.6 and 6.10 the concentration profiles are practically identical with the exception of the initial concentrations for Cu in Figures 6.1 and 6.10 where the Cu^{+} to Cu^{2+} ratios differed.

7 CONCLUSIONS AND RECOMMENDATIONS

7.1 METAL DEPOSITION

The results confirm that an electrochemical process is a potential alternative for PGM recovery. High surface area cathodes are required for treating dilute streams where mass transport limitations are significant owing to the low concentrations of the reacting species. Utilising a packed bed cathode, metal recoveries greater than 99.9% were achieved for synthetic solutions as well as for the industrial effluent tested. Palladium was reduced to well below the targeted concentration of 10 ppm with measured values reaching the limit of the analytical method namely, 0.1 ppm. No pre-treatment was necessary and the metal ions were rapidly removed.

Copper was also successfully removed from solution with concentrations as low as 0.1 ppm obtained without difficulty. The mechanism for copper reduction in the complexing solution containing ammonium and chloride ions was shown to be two consecutive reactions each involving a one electron transfer. Palladium reduction required a greater overpotential than either of the copper reactions and occurred via the transfer of two electrons.

The simplified model which was derived was used to estimate the mass transfer coefficients for the metal reductions. The calculated values for palladium deposition ranged between 3.4×10^{-5} and 5.5×10^{-5} m/s. For the reduction of the copper from Cu^{+} slightly higher estimates were obtained ranging between 4.8×10^{-5} and 6.2×10^{-5} m/s. These values are very rough approximations as parameters such as the surface area, flowrate and reservoir volume used in the determination thereof were not precisely measured. However, the calculated values do lie within the expected range of between 10^{-5} and 10^{-4} m/s.

As predicted by theory and shown in the results, the concentration at which mass transport begins to control, and the side reaction of hydrogen evolution commences, decreases for lower applied currents. Therefore the application of low currents results in high overall process efficiencies, whereas the application of higher currents increases the rate of removal and hence decreases the time required to obtain a

specified concentration. The maximum rate of removal is achieved by applying a current equal to the limiting current for the initial concentration of the solution. Further increase in current only produces more hydrogen and offers no additional advantages. When using galvanostatic operation a trade-off between process efficiency and processing time must therefore be made. The optimum condition can only be identified from an economical analysis, but considering the high value of the PGMs and the relatively low cost of electricity, the employment of higher currents would seem more beneficial.

7.2 DEGREE OF SEPARATION

It is not possible to achieve a perfect separation of the copper and palladium during cathodic deposition because as the concentration of copper ions decrease the potential shifts to more negative values and the co-deposition of palladium commences. Even with potentiostatic operation, copper reduction may primarily occur but due to the potential distribution in a three-dimensional electrode the co-deposition of palladium may still take place. The metals can however be separated to some degree by employing low current densities. The majority of the copper is removed from solution and, prior to the onset of palladium reduction, the solution is passed to another reactor where the palladium is deposited with the remaining copper. Lower levels of copper contamination in the palladium product are obtained for lower applied current densities. However, as the size of the bed would be limited for such a process due to potential distributions only low currents could be utilised and thus the method would require long processing times. Control of such a process could also prove problematic.

Although the viability of separating the metals during deposition cannot be assessed at this stage, other techniques were identified during the testwork and are discussed in the following section.

7.3 METAL RECOVERY

Among other reasons, graphite was selected for the cathode material as the deposited metals could easily be recovered by a smelting process without contamination. Employing this method would require that the particulate bed be

replaced on a regular basis. This could prove economically viable as the cost of the graphite is fairly low however, consideration of other costs such as transportation and increased smelting capacity may show otherwise. Other methods need to be considered and financial comparisons made.

A possible alternative could be an electrochemical technique such as anodic stripping. The stripping peaks for copper and palladium deposits were identified from CV experiments and the large difference in potentials (-0.1 V and 0.5 V for the copper and palladium respectively) suggest adequate separation may be possible provided the metals do not form an alloy during deposition. The analysis of such a process falls beyond the scope of this work but it is recommended that testwork be conducted to determine the stripping efficiency and selectivity. The formation of a passivating oxide layer under anodic conditions could prove problematic for this procedure.

A further possibility for metal recovery is that of chemical dissolution. The testwork showed that the deposited copper is rapidly redissolved in complexing solutions. This could also prove to be a useful method for separation, as palladium requires strongly acidic and highly oxidising conditions for dissolution to occur. Thus copper may be removed chemically and the palladium then removed either by anodic stripping, chlorine treatment or combustion of the graphite.

7.4 RECOMMENDATIONS FOR FUTURE WORK

The applicability of an electrochemical process has been verified for treatment of the palladium containing effluent tested. It is recommended that other waste streams be examined to determine the extent of removal of the other PGMs and the effects of the composition and pH of the solution.

The model derived showed that a reaction rate under complete mass transport control would produce a concentration profile that decreased exponentially with time and that, if completely controlled by the applied current, it would decrease linearly. For high conversions per pass, the changes in the concentration across the reactor are significant and for a certain period of time the concentrations at the top of the bed are such that mass transport controls, while at the entrance to the bed the reaction is still controlled by the applied current. This results in a region of transition between

the controlling mechanisms with the fraction of the bed under mass transport control increasing with time for a batch re-circulating process. Although marginal, this effect was seen in the results and on scale-up of the reactor this transition region would become considerable, making the simplified model derived here inept for analysis. Also, the influence of the bed height and diameter on the potential and current distributions, due to resistances in the solution and solid phases, would have to be established for optimisation of the reactor dimensions. It is therefore recommended that multiple probes be placed in the bed and the potential distribution throughout the reactor be recorded. This would assist in more detailed modelling of the reactions occurring at various positions in the bed and allow for multiple reactions to be modelled simultaneously. Numerous parameters would be required for such an analysis, some of which should be determined from rotating disc electrode studies.

8 REFERENCES

1. **Kramer J, Driessen WL, Koch KR, Reedijk J,** *Highly selective extraction of platinum group metals with silica-based (poly)amine ion exchangers applied to industrial metal refinery effluents,* Hydrometallurgy, vol 64, 2002, pp 59-68.
2. **Ricci LJ,** *Heavy-metals recovery promises to pare water-cleanup bills,* Chem. Eng., December 22, 1975, pp 29-31.
3. **Jones L, Nel I, Koch KR,** *Polyurethane foams as selective sorbents for noble metals. Quantitative extraction and separation of rhodium from iridium in hydrochloric acid containing tin(II)chloride.,* Analytica Chimica Acta, vol 182, 1986, pp 61-70.
4. **Brackenberry KFG, Jones L, Koch KR,** *Polyurethane foams as selective sorbents for noble metals. Selective preconcentration of small amounts of platinum from hydrochloric acid containing tin(II)chloride followed by flame atomic absorption analysis,* Analyst, vol 112, 1987, pp 459-462.
5. **DeNora V, Penny RD, Frank LL, Vaccaro AJ, Stewart JJ,** Eltech Systems Corporation U.S.A, *Electrolytic Precious Metal Recovery System,* EP0309389, Mar, 1989.
6. **Fukuda K, Kurauchi Y, Mori T, Suematsu T,** Toyo Soda MFG CO LTD, *Method for Recovering a Metal,* EP0249316, Dec, 1987.
7. **Dalrymple IM, Sunderland JG,** EA Tech LTD, *Cell and Method for the Recovery of Metals from Dilute Solutions,* US5690806, Nov, 1997.
8. **MacGregor JJ,** Matthey Rustenburg Refines, *Recovering Metal from Metal Complex Containing Liquors,* GB2036083, Jun, 1980.
9. **Grehl M, Meyer H,** *Electrochemical versus chemical reactions in precious metal refining,* Precious Metals, International Precious Metals Institute, 1997, pp. 13-28.
10. **Dalrymple IM, Northcote SA, Sunderland JG,** *Electrochemical techniques for the removal and recovery of heavy and precious metals from waste sources,* Int. Congr. Electr. Appl., 13th, 1996, pp. 1-8.
11. **Danilova FI, Antokolskaya II,** Exmet, *Method for Extraction of Noble Metals from Materials Comprising Thereof,* ZA9205992, Sep, 1993.
12. **Mounina V, Bogaditsa S, McNight C, Wintle RH,** Chemomet Projects Ltd, *An Electrochemical Sorption Process,* ZA9303503, Feb, 1994.

13. **Kammel R, Lieber H-W,** *Electrolytic recovery of precious metals from dilute solutions,* J. Metals, vol 33, no. 10, 1981, pp. 45-48.
14. **Le Penven R, Levason W, Pletcher D,** *Studies of platinum electroplating baths Part I: The chemistry of a platinum tetrammine bath,* J. Appl. Electrochem., vol 22, 1992, pp 415-420.
15. **Gregory AJ, Levason W, Noftle RE, Le Penven R, Pletcher D,** *Studies of platinum electroplating baths Part III: The electrochemistry of* $Pt(NH_3)_{4-x}(H_2O)_x^{2+}$ *and* $PtCl_{4-x}(H_2O)_x^{(2-x)-}$, J. Electroanal. Chem., vol 399, 1995, pp 105-113.
16. **Gloaguen F, Leger J-M, Lamy C,** *Electrocatalytic oxidation of methanol on platinum nanoparticles electrodeposited onto porous carbon substrates,* J. Appl. Electrochem., vol 27, 1997, pp 1052-1060.
17. **Tsventarnyi EG, Kravtsov VI,** *Kinetics and mechanism pertaining to electroreduction of ammonia complexes of palladium(II) at the palladium electrode,* Russian J. Electrochem., vol 35, no. 5, 1999, pp 545-551.
18. **Munichandraiah N, Shivananjaiah HN, Iyengar RR,** *Voltammetric studies of Pd(II) ammonia complex: Solvent effects,* Indian J. Chem., vol 28A, July, 1989, pp 561-564.
19. **Gimeno Y, Hernandez Creus A, Carro P, Gonzalez S, Salvarezza RC, Arvia AJ,** *Electrochemical formation of Pd islands on HOPG,* J. Phys. Chem. B, vol 106, no. 16, 2002, pp 4232-4244.
20. **Lubert K-H, Guttmann M, Beyer L,** *Electrode reactions of palladium(II) in chloride solution at carbon paste electrodes modified with derivatives of N-benzoylthiourea,* J. Solid State Electrochem, vol 6, 2002, pp 545-552.
21. **Elding LI,** Inorg. Chim. Acta, vol 6, 1972, pp. 647, referred to by 20.
22. **Lubert K-H, Guttmann M, Beyer L,** *Formation of palladium complex at carbon paste surface in chloride solutions as studied by cyclic voltammetry,* Collect. Czech. Chem. Commun., vol 66, no. 10, 2001, pp 1457-1472.
23. **Lubert K-H, Guttmann M, Beyer L, Kalcher K,** *Experimental indications for the existence of different states of palladium(0) at the surface of the carbon paste electrodes,* Electrochem. Commun., vol 3, 2001, pp 102-106.
24. **Kibler LA, Kleinert M, Randler R, Kolb DM,** *Initial stages of Pd deposition on Au (hkl) Part I: Pd on Au(III) ,* Surf. Sci, vol 443, 1999, pp 19-30.
25. **Al-Akl A, Attard GA,** *Anion effects in the UPD of copper on Pd/Pt(111) bimetallic electrodes,* J. Phys. Chem. B, vol 101, no. 23, 1997, pp 4597-4606.

26. **Styrkas AD, Styrkas D,** *Electrochemical dissolution of metals of the platinum group by alternating current,* J. Appl. Electrochem., vol 25, 1995, pp 490-494.
27. **Tilak BV, Conway BE, Angerstein-Kozlowska H,** *The real condition of oxidized Pt electrodes. Part III Kinetic theory of formation and reduction of surface oxides,* J. Electroanal. Chem., vol 48, 1973, pp 1-23.
28. **Folquer ME, Zerbino JO, de Tacconi NR, Arvia AJ,** *Kinetics of aging of the oxygen monolayer on platinum under a complex potentiodynamic perturbation program,* J. Electrochem. Soc., vol 126, no. 4, 1979, pp 592-598.
29. **Chialvo AC, Triaca WE, Arvia AJ,** *Changes in the electrochemical response of noble metals produced by square-wave potential perturbations. A new technique for the preparation of reproducible electrode surfaces of interest in electrocatalysis,* J. Electroanal. Chem., vol 146, 1983, pp 93-108.
30. **Rand DAJ, Woods R,** *A study of the dissolution of platinum, palladium, rhodium and gold electrodes in 1 M sulphuric acid by cyclic voltammetry,* J. Electroanal. Chem., vol 35, 1972, pp 209-218.
31. **Kim KS, Gossmann AF, Winograd N,** *X-ray Photoelectron Spectroscopic studies of palladium oxides and the palladium-oxygen electrode,* Anal. Chem., vol 46, no. 2, 1974, pp 197-200.
32. **Gossner K, Mizera E,** *The anodic behaviour of Pd electrodes in 1M H_2SO_4,* J. Electroanal. Chem., vol 125, 1981, pp 347-358.
33. **Bolzan AE, Martins ME, Arvia AJ,** *The complex processes involved at Pd electrodes in 1 M H_2SO_4 in the potential range of oxygen electroadsorption - electrodesorption reactions,* J. Electroanal. Chem., vol 157, 1983, pp 339-358.
34. **Bolzan AE, Martins ME, Arvia AJ,** *The electrodissolution of base palladium in relation to the oxygen electroadsorption and electrodesorption in sulphuric acid solution,* J. Electroanal. Chem., vol 172, 1984, pp 221-233.
35. **Burke LD, Roche MBC,** *An electrochemical investigation of monolayer and multilayer oxide films on palladium in aqueous media,* J. Electroanal. Chem., vol 186, 1985, pp 139-154.
36. **Pallotta C, de Tacconi NR, Arvia,** *Potentiodynamic behaviour of the rhodium / H_2SO_4 (aq) interface in the potential range of the hydrogen and oxygen electrosorption,* Electrochimica Acta, vol 26, 1981, pp 261-273.
37. **Finkelstein NP, Hawkins FA, Nicol MJ,** *An electrochemical investigation of the dissolution and passivation of platinum in acid solutions,* NIM, Report No. 1800, April 12, 1976.

38. **Lubert K-H, Guttmann M, Beyer L,** *Electrode reactions and accumulation of hydrogen at carbon paste electrodes in presence of tetrachloropalladate,* J. Electroanal. Chem., vol 462, 1999, pp 174-180.
39. **Dunsch L, Inzelt G, Horanyi G, Lubert K-H,** *Radiotracer evidence proving the embedding of Cl^- ions into glassy carbon electrodes,* J. Electroanal. Chem., vol 260, 1989, pp 495-499.
40. **Dunsch L, Inzelt G, Horanyi G, Lubert K-H,** *Electrochemical studies of polymeric carbons. II Surface layer formation on glassy carbon electrodes in chloride solutions as studied by radiotracer techniques,* Isotopenpraxis, vol 26, no. 7, 1990, pp 343-346.
41. **Naohara H, Ye S, Uosaki K,** *Electrochemical layer-by-layer growth of palladium on an Au(111) electrode surface: Evidence for important role of adsorbed Pd complex,* J. Phys. Chem. B, vol 102, 1998, pp 4366-4373.
42. **Chierchie T, Mayer C, Lorenz WJ,** *Structural changes of surface oxide layers on palladium,* J. Electroanal. Chem., vol 135, 1982, pp 211-220.
43. **Zou S, Chan HYH, Williams CT, Weaver MJ,** *Formation and stability of oxide films on platinum-group metals in electrochemical and related environments as probed by surface-enhanced Raman Spectroscopy: Dependence on the chemical oxidant,* Langmuir, vol 16, no. 2, 2000, pp 754-763.
44. **Bolzan AE,** *Phenomenological aspects related to the electrochemical behaviour of smooth palladium electrodes in alkaline solutions,* J. Electroanal. Chem., vol 380, 1995, pp 127-138.
45. **Li F, Zhang B, Dong S, Wang E,** *A novel method of electrodepositing highly dispersed nano palladium particles on glassy carbon electrode,* Electrochimica Acta, vol 42, no. 16, 1997, pp 2563-2568.
46. **Lubert K-H, Guttmann M, Beyer L,** *Voltammetric study of the immobilization of palladium at the surface of carbon paste electrodes,* Electroanal., vol 8, no. 4, 1996, pp 320-325.
47. **Tarasevich MR, Khrushcheva EI,** *Electrocatalytic properties of carbon materials,* Modern Aspects of Electrochemistry, vol 19, 1989, pp 295-358.
48. **Han JN, Pyun SI, Yang TH,** J. Electrochem. Soc., vol 144, 1997, pp. 4266, referred to by 20.
49. **Zou S, Weaver MJ,** *Surface-enhanced Raman scattering on uniform transition-metal films: Toward a versatile adsorbate vibrational strategy for solid-nonvacuum interfaces?,* Anal. Chem., vol 70, 1998, pp 2387-2395.

50. **Newman J, Teidemann W,** *Porous-electrode theory with battery applications,* AIChE Journal, vol 21, no. 1, 1975, pp 25-41.
51. **Khalifa H, Ateya BG, Arafat EAS,** *Electrochemical reduction of oxygen at a porous flow-through electrode,* J. Electroanal. Chem., vol 81, 1977, pp 301-307.
52. **Goodridge F, Plimley RE, Backhurst JR, Fleischmann M,** Nat Res Dev (GB), *Electrochemical process using a fluidized electrode,* US4236991, Jun, 1980.
53. **Oloman C, Watkinson AP,** *The electroreduction of oxygen to hydrogen peroxide on fluidized cathodes,* Can. J. Chem. Eng., vol 53, 1975, pp 268-273.
54. **Alkire RC, Gould RM,** *An engineering model for electro-organic synthesis in continuous flow-through porous electrodes,* J. Electrochem. Soc., vol 127, no. 3, 1980, pp 605-612.
55. **Robertson PM, Schwager F, Ibl N,** *A new cell for electrochemical processes,* J. Electroanal. Chem., vol 65, 1975, pp 883-900.
56. **Le Bolay N, Guilland JF, Ricard A,** *Mass transfer study in a pulsed bed electrode - Application to the electrodeposition of a poly(dibenzo-18-crown-6) film,* Can. J. Chem. Eng., vol 72, 1994, pp 153-159.
57. **Oloman C, Radcliffe,** *An experimental study of a fixed bed chlor-alkali reactor,* J. Appl. Electrochem., vol 16, 1986, pp 457-462.
58. **Walsh FC,** *The performance of electrochemical reactors for removal of silver from photographic process liquors,* IChe Symp. Ser., vol 98, 1986, pp 137-157.
59. **Van Zee J, Newman J,** *Electrochemical removal of silver ions from photographic fixing solutions using a porous flow-through electrode,* J. Electrochem. Soc., vol 124, no. 5, 1977, pp 706-103.
60. **Hu X, Bautista RG,** *Mass transfer model of chromium reduction in a fluidized bed electrochemical reactor,* Sep. Sci. Tech., vol 32, no. 10, 1997, pp 1769-1785.
61. **Chin D-T,** *Electrochemical extraction of copper from scrap steel,* AIChE Journal, vol 23, no. 4, 1977, pp 434-440.
62. **Bennion DN, Newman J,** *Electrochemical removal of copper ions from very dilute solutions,* J. Appl. Electrochem., vol 2, 1972, pp 113-122.
63. **Jiricny V, Evans JW,** *Fluidized-bed electrodeposition of zinc,* Metall. Mater. Trans. B, vol 15, 1984, pp 623-631.

64. **Savage PR,** *Electrolytic technique makes initial CPI thrust,* Chem. Eng., August 14, 1978, pp 74D-74F.

65. **Fleischmann M, Kelsall GH,** *A feasibility study of mercury deposition in a lead fluidized bed electrode,* J. Appl. Electrochem., vol 14, 1984, pp 277-284.

66. **Houghton RW, Kuhn AT,** *Mass-transport problems and some design concepts of electrochemical reactors,* J. Appl. Electrochem., vol 4, 1974, pp 173-190.

67. **Coeuret F,** *The fluidized bed electrode for the continuous recovery of metals,* J. Appl. Electrochem., vol 10, 1980, pp 687-696.

68. **Weininger JL,** *Electrochemical recovery of metals from wastewater,* AIChE Symp. Ser., vol 79, no. 229, 1983, pp 179-186.

69. **Newman JS, Tobias CW,** *Theoretical analysis of current distribution in porous electrodes,* J. Electrochem. Soc, vol 109, 1962, pp 1183-1191.

70. **Grens EA, Tobias CW,** *Analysis of the dynamic behaviour of flooded porous electrodes,* Berichte der Bunsengesellschaft, vol 68, no. 3, 1964, pp 236-249.

71. **Grens EA, Tobias CW,** *The influence of electrode reaction kinetics on the polarisation of flooded porous electrodes,* Electrochimica Acta, vol 10, 1965, pp 761-772.

72. **Oloman C, Matte M, Lum C,** *Electronic conductivity of graphite fiber fixed-bed electrodes,* J. Electrochem. Soc., vol 138, no. 8, 1991, pp 2330-2334.

73. **Soltan EA, Nosier SA, Salem AY, Monsour IAS, Sedahmed GH,** *Mass transfer behaviour of a flow-by fixed bed electrochemical reactor under different hydrodynamic conditions,* Chem. Eng., vol 4041, 2002, pp 1-12.

74. **Mobarak AA, Abdo MSE, Hassan MSM, Sedahmed GH,** *Mass transfer behaviour of a flow-by fixed bed electrochemical reactor composed of a vertical stack of screens under single and upward two phase flow,* J. Appl. Electrochem., vol 30, 2000, pp 1269-1276.

75. **Leroux F, Coeuret F,** *Mass transfer and potential distribution within axial flow-through electrodes of expanded metal,* Electrochimica Acta, vol 28, no. 12, 1983, pp 1857-1863.

76. **Letord-Quemere MM, Legrand J, Coeuret F,** *Improvement of mass transfer in electrochemical cells by means of expanded materials,* IChe Symp. Ser., vol 98, 1986, pp 71-81.

77. **Zaki MM, El-Taweel YA, Zatout AA, El-Abd MZ, Sadahmed GH,** *Mass transfer at oscillating grids,* J. Electrochem. Soc., vol 138, no. 2, 1991, pp 430-434.

78. **Storck A, Robertson PM, Ibl N,** *Mass transfer study of three-dimensional electrodes composed of stacks of nets,* Electrochimica Acta, vol 24, 1979, pp 373-380.

79. **Alkire R, Ng PK,** *Studies on flow-by porous electrodes having perpendicular directions of current and electrolyte flow,* J. Electrochem. Soc., vol 124, no. 8, 1977, pp 1220-1227.

80. **Alkire R, Gracon B,** *Flow-through porous electrodes,* J. Electrochem. Soc., vol 122, no. 12, 1975, pp 1594-1601.

81. **Gould RM, Alkire RC,** *Effect of multiple reactions on metal deposition in flow-through porous electrodes,* J. Electrochem. Soc., vol 126, no. 12, 1979, pp 2125-2133.

82. **Leroux F, Coeuret F,** *Flow-by electrodes of ordered sheets of expanded metal - II. Potential distribution for the diffusional regime,* Electrochimica Acta, vol 30, no. 2, 1985, pp 167-172.

83. **Van der Heiden G, Raats CMS, Boon HF,** *Fluidised bed electrolysis for removal or recovery of metals from dilute solutions,* Chem. Ind., vol 13, 1978, pp 465-468.

84. **Yen S, Yao C,** *Enhanced metal recovery in fluidized bed electrodes with a fin-type current feeder,* J. Electrochem. Soc., vol 138, no. 8, 1991, pp 2344-2348.

85. **Fleischmann M, Kelsall GH,** *A parametric study of copper deposition in a fluidised bed electrode,* J. Appl. Electrochem., vol 14, 1984, pp 269-275.

86. **Goodridge F, Holden DI, Murray HD, Plimley RF,** *Fluidised-bed electrodes Part I A mathematical model of the fluidised bed electrode,* Trans. Instn. Chem. Engrs., vol 49, 1971, pp 128-136.

87. **Goodridge F, Holden DI, Murray HD, Plimley RF,** *Fluidised-bed electrodes Part II: Non-uniform behaviour of the hydrodynamic entrance region,* Trans. Instn. Chem. Engrs., vol 49, 1971, pp 137-141.

88. **Fleischmann M, Oldfield JW,** J. Electroanal. Chem., vol 29, 1971, pp 231, referred to by 89.

89. **Beenackers AACM, van Swaaij WPM, Welmers A,** *Mechanism of charge transfer in the discontinuous metal phase of a fluidized bed electrode,* Electrochimica Acta, vol 22, 1977, pp 1277-1281.

90. **Sabacky BJ, Evans JW,** *The electrical conductivity of fluidized bed electrodes - its significance and some experimental measurements,* Metallurgical Transactions B, 1977, pp 5-13.
91. **Sabacky BJ, Evans JW,** *Electrodeposition of metals in fluidized bed electrodes Part I. Mathematical Model,* J. Electrochem. Soc., vol 126, no. 7, 1979, pp 1176-1180.
92. **Kusakabe K, Morooka S, Kato Y,** *Charge transfer rate in liquid-solid and gas-solid fluidized bed electrodes,* J. Chem. Eng. Jpn., vol 14, no. 3, 1981, pp 208-214.
93. **Plimley RE, Wright AR,** *A bipolar mechanism for charge transfer in a fluidised bed electrode,* Chem. Eng. Sci., vol 39, no. 3, 1984, pp 395-405.
94. **Lee JK, Shemilt LW, Chun HS,** *Studies of bipolarity in fluidized bed electrodes,* J. Appl. Electrochem., vol 19, 1989, pp 877-881.
95. **Lee JK, Chun HS, Shemilt LW,** *Overpotential distribution for nominally monopolar fluidized bed electrodes,* J. Chem. Eng. Jpn., vol 28, no. 1, 1995, pp 25-30.
96. **Masterson IF, Evans JW,** *Fluidized bed electrowinning of copper; experiments using 150 ampere and 1000 ampere cells and some mathematical modeling,* Metall. Mater. Trans. B, vol 13, 1982, pp 3-13.
97. **Hutin D, Coeuret F,** *Experimental study of copper deposition in a fluidized bed electrode,* J. Appl. Electrochem., vol 7, 1977, pp 463-471.
98. **Bareau JY, Coeuret F,** *The anodic dissolution of copper in a fluidised bed electrode,* J. Appl. Electrochem., vol 9, 1979, pp 737-743.
99. **Kreysa G, Juttner K, Bisang JM,** *Cylindrical three-dimensional electrodes under limiting current conditions,* J. Appl. Electrochem., vol 23, 1993, pp 707-714.
100. **Kazdobin K, Shvab N, Tsapakh S,** *Scaling-up of fluidised-bed electrochemical reactors,* Chem. Eng. J., vol 79, 2000, pp 203-209.
101. **Wilkinson JAE, Leslie RSE, Glindon DM, Haines KP, Baker K,** CJB Developments Ltd, *Electrolytic cells,* US3956086, May, 1976.
102. **Wilkinson JAE, Leslie RSE, Glindon DM, Haines KP, Baker K,** CJB Developments Ltd, *Electrolytic cells time synchronisation particularly for seismic work,* GB1440072, Jun, 1976.
103. **Wilkinson JAE, Leslie RSE, Glindon DM, Haines KP, Baker K,** CJB Developments Ltd, *Electrolytic cells,* US4035278, Jul, 1977.

104. **Kreysa G, Pionteck S, Heitz E,** *Comparative investigations of packed and fluidized bed electrodes with non-conducting and conducting particles,* J. Appl. Electrochem., vol 5, 1975, pp 305-312.
105. **Wragg AA,** *An ultrasonically stimulated particulate electrode for metal extraction processes,* Chem. Ind, 1975, pp 333-335.
106. **Coeuret F, Paulin M,** *Experiments on copper recovery in a pulsed granular fixed bed electrodes,* J. Appl. Electrochem., vol 18, 1988, pp 162-165.
107. **Chu AKP, Fleischmann M, Hills GJ,** *Packed bed electrodes. I. The electrochemical extraction of copper ions from dilute solutions ,* J. Appl. Electrochem., vol 4, 1974, pp 323-330.
108. **Chu AKP, Hills GJ,** *Packed bed electrodes. II. Anodic stripping and the recovery of copper from dilute solutions ,* J. Appl. Electrochem., vol 4, 1974, pp 331-336.
109. **Scott K,** *A consideration of circulating bed electrodes for the recovery of metal from dilute solutions,* J. Appl. Electrochem., vol 18, 1988, pp 504-510.
110. **Scott K, Lui WK,** *The performance of a moving bed electrode during the electrowinning of cobalt,* IChe Symp. Ser., vol 98, 1986, pp 161-172.
111. **Salas-Morales JC, Evans JW, Newman OMG, Adcock PA,** *Spouted bed electrowinning of zinc: Part I. Laboratory-scale electrowinning experiments,* Metall. Mater. Trans. B, vol 28, 1997, pp 59-68.
112. **Verma A, Salas-Morales JC, Evans JW,** *Spouted bed electrowinning of zinc: Part II. Investigations of the dynamics of particles in large thin spouted beds,* Metall. Mater. Trans. B, vol 28, 1997, pp 69-79.
113. **Sedahmed GH, Farag HA, Zatout AA, Katkout FA,** *Mass transfer characteristics of gas-sparged fixed-bed electrodes composed of stacks of vertical screens,* J. Appl. Electrochem., vol 16, 1986, pp 374-378.
114. **Sedahmed GH,** *Mass transfer enhancement by the counter-electrode gases in a new cell design involving a three dimensional gauze electrode,* J. Appl. Electrochem., vol 8, 1978, pp 399-404.
115. **Sedahmed GH,** *Electrochemical mass transfer at a fixed bed of spheres under forced convection induced by counterelectrode gas bubbles,* Can. J. Chem. Eng., vol 64, 1986, pp 75-79.
116. **Sedahmed GH,** *Mass transfer behaviour of a fixed bed electrochemical reactor with a gas evolving upstream counter electrode,* Can. J. Chem. Eng., vol 74, 1996, pp 487-492.

117. **Oloman C,** *Trickle bed electrochemical reactors,* J. Electrochem. Soc., vol 126, no. 11, 1979, pp 1885-1892.
118. **Stankovic VD, Grujic R, Wragg AA,** *Water electrolysis and pressure drop behaviour in a three-dimensional electrode ,* J. Appl. Electrochem., vol 28, 1998, pp 321-327.
119. **Mowla D, Olive H, Lacoste G,** *Application of volumetric electrodes to the recuperation of metals in industrial effluents - III. Potential distributions and design of radial field electrodes,* Electrochimica Acta, vol 28, no. 6, 1983, pp 839-846.
120. **Kreysa G, Heitz E,** *The similarity law of effective bed height of packed bed electrodes,* Electrochimica Acta, vol 20, 1975, pp 919-921.
121. **Alkire R, Ng PK,** *Two-dimensional current distribution within a packed-bed electrochemical flow reactor,* J. Electrochem. Soc., vol 121, no. 1, 1974, pp 95-103.
122. **Coeuret F,** *L'Electrode foreuse percolante (EPP) - III. Difference de potentiel metal-solution au sein de l'electrode en regime diffusionnel,* Electrochimica Acta, vol 21, 1976, pp 203-213.
123. **Coeuret F, Hutin D, Gaunand A,** *Study of the effectiveness of fixed flow-through electrodes,* J. Appl. Electrochem., vol 6, 1976, pp 417-423.
124. **Ateya BG, Austin LG,** *Steady-state polarization at porous, flow-through electrodes with small pore diameter: I. Reversible kinetics,* J. Electrochem. Soc., vol 124, no. 1, 1977, pp 83-89.
125. **Ateya BG, Austin LG,** *Steady-state polarization at porous, flow-through electrodes with small pore diameter: II. Irreversible kinetics for one-electron and consecutive two electron transfer reactions,* J. Electrochem. Soc., vol 124, no. 10, 1977, pp 1540-1548.
126. **Ateya BG, Arafat EAS, Kafafi SA,** *Hydrodynamic effects on the efficiency of porous flow-through electrodes,* J. Appl. Electrochem., vol 7, 1977, pp 107-112.
127. **Gaunand A, Hutin D, Coeuret F,** *Potential distribution in flow-through porous electrodes under limiting current conditions,* Electrochimica Acta, vol 22, 1977, pp 93-97.
128. **Trainham JA, Newman J,** *A flow-through porous electrode model: Application to metal-ion recovery from dilute streams,* J. Electrochem. Soc., vol 124, no. 10, 1977, pp 1528-1540.

129. **Paulin M, Hutin D, Coeuret F,** *Theoretical and experimental study of flow-through porous electrodes,* J. Electrochem. Soc., vol 124, no. 2, 1977, pp 180-188.
130. **Olive H, Lacoste G,** *Application of volumetric electrodes to the recuperation of metals in industrial effluents - I. Mass transfer in fixed beds of spherical conductive particles,* Electrochimica Acta, vol 24, 1979, pp 1109-1114.
131. **Olive H, Lacoste G,** *Application of volumetric electrodes to the recuperation of metals in industrial effluents - II. Design of an axial field flow through porous electrodes,* Electrochimica Acta, vol 25, 1980, pp 1303-1308.
132. **Sioda RE, Piotrowska H,** *Flow-through electrode for the retention of copper,* Electrochimica Acta, vol 25, 1980, pp 331-334.
133. **Trainham JA, Newman J,** *The effect of electrode placement and finite matrix conductivity on the performance of flow-through porous electrodes,* J. Electrochem. Soc., vol 125, no. 1, 1978, pp 58-68.
134. **Sioda RE,** Electrochimica Acta, vol 19, 1974, pp 57, referred to by 105.
135. **Edson GI,** *Electrochemical recovery of metal values,* Precious Metals, 1984, pp 163-188.
136. **Stauffer JE,** *Electrochemical process for removing ions from solution,* US6391186, May, 2002.
137. **Goodridge F,** *Some recent developments of monopolar and bipolar fluidized bed electrodes,* Electrochimica Acta, vol 22, 1977, pp 929-933.
138. **Fleischmann M, Goodridge F, King CJH,** Nat Res Dev (GB), *Electrochemical cells,* GB1496660, Dec, 1977.
139. **Goodridge F, King CJH, Wright AR,** *Performance studies on a bipolar fluidised bed electrode,* Electrochimica Acta, vol 22, 1977, pp 1087-1091.
140. **Moskalyk RR, Alfantazi A, Tombalakiam AS, Valic D,** *Anode effects in electrowinning,* Min. Eng., vol 12, no. 1, 1999, pp 65-73.
141. **Gupta CK, Mukherjee TK,** *Hydrometallurgy in Extraction Processes Volume II,* CRC Press, 1990, pp 232.
142. **Wilkinson JAE, Haines KP,** *Feasibility study on the electrowinning of copper with fluidised-bed electrodes,* Trans. Instn. Min. Metall., vol 81, 1972, pp C157-C162.
143. **Dubrovsky M, Evans JW,** *An investigation of fluidized bed electrowinning of cobalt using 50 and 1000 amp cells,* Metall. Mater. Trans. B, vol 13, 1982, pp 293-301.

144. **Sabacky BJ, Evans JW,** *Electrodeposition of metals in fluidized bed electrodes Part II. An experimental investigation of copper electrodeposition at high current density,* J. Electrochem. Soc., vol 126, no. 7, 1979, pp 1180-1187.
145. **Ziegler DP, Dubrovksy M, Evans JW,** *A preliminary investigation of some anodes for use in fluidized-bed electrodeposition of metals,* J. Appl. Electrochem., vol 11, 1981, pp 625-637.
146. **Huh T, Evans JW, Carey CD,** *The fluidized bed electrowinning of silver,* Metall. Mater. Trans. B, vol 14, 1983, pp 353-357.
147. **Urbaniczky C, Lundstrom K,** *Voltammetric studies on carbon paste electrodes. The influence of paste composition on electrode capacity and kinetics.,* J. Electroanal. Chem., vol 176, 1984, pp 169-182.
148. **Handley D, Eardley DC,** *Bipolar electrolysis with intraphase conduction in fluidised beds,* Chem. Ind, 1975, pp 330-332.
149. **Huh T, Evans JW,** *Electrical and electrochemical behavior of fluidized bed electrodes II. Effective bed resistivities,* J. Electrochem. Soc., vol 134, no. 2, 1987, pp 317-321.
150. **Vatistas N, Bartolozzi M,** *A three-dimensional current feeder for fluidized bed electrodes,* J. Appl. Electrochem., vol 20, 1990, pp 951-954.
151. **Goodridge F, Lister K, Scott K,** *Metal deposition in diaphragmless fluidized-bed electrolytic cells,* J. Appl. Electrochem., vol 11, 1981, pp 723-725.
152. **Ricci LJ,** *Antipollution processes top Boston AIChE meeting,* Chem. Eng., October 13, 1975, pp 73-75.
153. **Carlos L-C,** Electricity Council, London, *Electrolytic cells and process for treating dilute waste solutions,* GB1423369, Aug, 1976.
154. **Walsh F,** *A first course in electrochemical engineering,* The Electrochemical Consultancy, 1993, pp 283 (a), pp 77 (b), pp 89 (c), pp 81 (d), pp 100 (e), pp 109 (f), pp 34 (g).
155. **Cook GM, Portal C,** Kennott Copper Corp (US), *Stationary particulate bed dual electrode,* US4197181, Apr, 1980.
156. **Bushell TG,** CJB Developments Ltd, *Electrochemical processes,* GB1331251, Sept, 1973.
157. **Goodridge F, Vance CJ,** *Copper deposition in a pilot-plant-scale fluidized bed cell,* Electrochimica Acta, vol 24, 1979, pp 1237-1242.
158. **Min. Mag.,** *Fluidised bed electrolysis for metal recovery at low concentrations,* vol 139, no. 3, 1978, pp 313-317.

159. **Yasuda M, Ohkawa A, Yasukawa S, Sekine T,** *Electrochemical activity of fluidized bed electrodes (FBEs) inserted electroconductive partition plates,* J. Chem. Eng. Jpn., vol 21, no. 3, 1988, pp 306-310.
160. **Zaromb S,** *Fluidized-bed electrodes and related apparatus and methods,* WO7900332, Jun, 1979.
161. **Kinneberg DJ, Nadkarni RM,** Metalor USA Refining Corp (US), *Fluidised bed electrowinning of copper,* US5695629, Dec, 1997.
162. **Malpas RE, Spijkerman JB, Honders A, Jansen GJC,** Shell Int Research (NL), *Fluid bed electrolysis cell,* EP0261747, Mar, 1988.
163. **Goto N, Ezawa N,** Chlorine Eng Corp Ltd (JP), Tanaka Precious Metal Ind (JP), *Electrolyzing method and electrolytic cell employing fluidised bed,* US4569729, Feb, 1986.
164. **Sherwood WG, Hodges DR, Nikolic C,** Amax Inc, *Nickel electrowinning using reduced nickel oxide as a fluidised cathode,* US4243498, Jan, 1981.
165. **Hodges DR, Nikolic C, Sherwood WG,** Amax Inc, *Cell with multiple anode-cathode chambers for fluid bed electrolysis,* US4202752, May, 1980.
166. **Avedsian MM, Holko AP,** Noranda Mines Ltd, *Process for electrowinning metal from metal bearing solutions,* US4141804, Feb, 1979.
167. **Backhurst JR, Fleischmann M, Goodridge F, Plimley RE,** Nat Res Dev (GB), *Improvements relating to electrode arrangements for electrochemical cells,* GB1194181, Jun, 1970.
168. **Prober R, Haycock EW,** Shell Oil Co, *Method of carrying out electrochemical processes in a fluidized-bed electrolytic cell,* US3703446, Nov, 1972.
169. **Stankovic VD, Janes D,** *Three-dimensional electrode cells - economic considerations,* IChe Symp. Ser., vol 98, 1986, pp 269-279.
170. **Oloman C, Reilly P,** *Modeling and parameter estimation for a fixed-bed electrochemical reactor,* J. Electrochem. Soc., vol 134, no. 4, 1987, pp 859-866.
171. **Matic D,** *Packed-bed reactor with continuous recirculation of electrolyte,* J. Appl. Electrochem., vol 9, 1979, pp 15-20.
172. **Walker ATS, Wragg AA,** *The modelling of concentration-time relationships in recirculating electrochemical reactor systems,* Electrochimica Acta, vol 22, 1977, pp 1129-1134.
173. **Walker ATS, Wragg AA,** *Mass transfer in fluidised bed electrochemical reactors,* Electrochimica Acta, vol 25, 1980, pp 323-330.

174. **Walker ATS, Wragg AA,** *Behaviour of a fluidised bed electrochemical reactor during batch recirculation copper extraction,* Chem. Eng. Sci., vol 35, 1980, pp 405-412.
175. **Welse L, Giron M, Valentin G, Storck A,** *A chemical engineering approach to selectivity analysis in electrochemical reactors,* IChe Symp. Ser., vol 98, 1986, pp 47-57.
176. **Stankovic VD, Wragg AA,** *Modelling of time-dependent performance criteria in a three-dimensional cell system during batch recirculation copper recovery,* J. Appl. Electrochem., vol 25, 1995, pp 563-573.
177. **Schlain D, McCawley FX, Smith GR,** *Electrodeposition of platinum-group metals,* BuMines. RI 8249 , , 1977, 22 pp.
178. **van Aswegen A,** *The electrochemistry of metal ions in industrial streams,* Dissertation, University of the Witwatersrand, to be published.
179. **Trainham JA, Newman J,** *A thermodynamic estimation of the minimum concentration attainable in a flow-through porous electrode reactor,* J. Appl. Electrochem., vol 7, 1977, pp 287-297.
180. **Mustoe LH, Wragg AA,** *Concentration-time behaviour in a recirculating electrochemical reactor system using a dispersed plug-flow model,* J. Appl. Electrochem., vol 8, 1978, pp 467-472.
181. **Pourbaix M,** *Atlas of electrochemical equilibria in aqueous solutions,* Pergamon Press Ltd, 1966, pp 390 (a), pp 361 (b).
182. **Pletcher D,** *A first course in electrode processes,* The Electrochemical Consultancy, 1991, pp 240 (a), pp 261 (b).

APPENDIX A

Reactor Components

Table A1 Cation exchange membrane specifications

Supplier	Membranes International Inc.	
Type	CMI-7000 Continuous Roll (Cation Exchange)	
Ion Form	Sodium	
Electrical Resistance	Ω/cm^2 0.1 N NaCl at 25 ^oC 1.0 N NaCl at 25 ^oC	 18 ± 2 8 ± 1
Water Permeability	$ml/hr/ft^2$ @ 5 psi	 less than 30
Permselectivity	% 0.5 N NaCl / 1.0 N NaCl	 95
Standard Thickness	mils	20 ± 1
Mullen Burst Test strength	psi	150
Total Exchange Capacity	meq/g	1.3±1
Thermal Stability	^oC	90
Chemical Stability Range	pH	1 - 12
Preconditioning Procedure	Membranes should be preconditioned by emersion in a salt solution or a solution similar to that of the intended application for several hours to allow for membrane expansion	
Characteristics	• High permselectivity with low permeability • Wide range of chemical and temperature stability • Exceptional mechanical strength	
Typical Applications	• Electrocoating for Cationic systems • Electrodialysis for desalination and demineralisation • Electroplating for metal recovery	

Table A2 Graphite particles specifications

Supplier	Electrographite Carbon Co. (PTY) LTD	
Grade	Isostatically pressed graphite ET10	
Density	g/cm^3	1.75
Shore Hardness		50
Specific Resistance	$\mu\Omega/cm$	1400
Flexural Strength	kg/cm^2	600
Compressive Strength	kg/cm^2	1000
Young's Modulus	kg/mm^2	1100
Thermal Expansion Rate	$x\ 10^{-6}\ ^oC$	3.80
Thermal Conductivity	W/mK	104.4
Porosity Rate	%	15
Ash Content	ppm	100
Typical Applications	Industrial applications such as high purity graphite for semiconductor production and analytical applications. Continuous casting, EDM and pressure sintering parts. Graphite for cemented carbides, industry and powder metallurgy, chemical industry and electrolytic technology, steel and aluminium industry and granules. • Continuous casting dies for the precious metal industry • Casting moulds and furnace parts for hot metals • Boats and trays for pressure sintering applications • Crucibles for melting and alloying • Electrical Discharge Machining (EDM)	



Figure A1 Photograph of the benchscale electrochemical reactor



Figure A2 Corroded copper current collector shown after Run 1

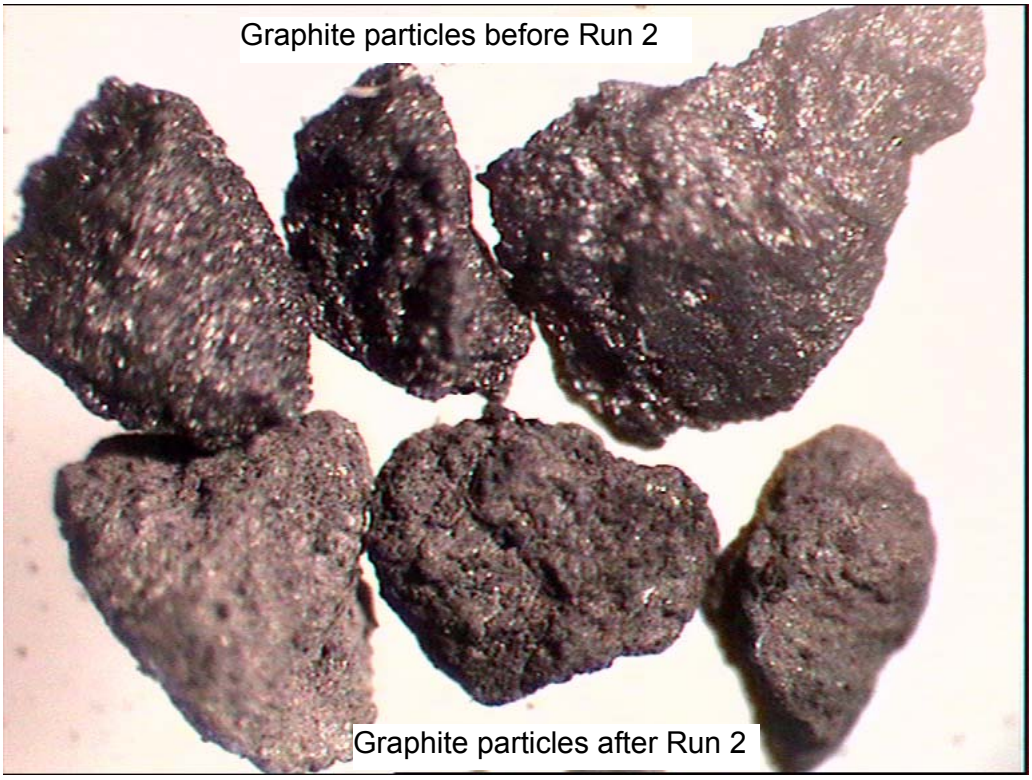


Figure A3 Graphite particles showing powdery deposition after Run 2

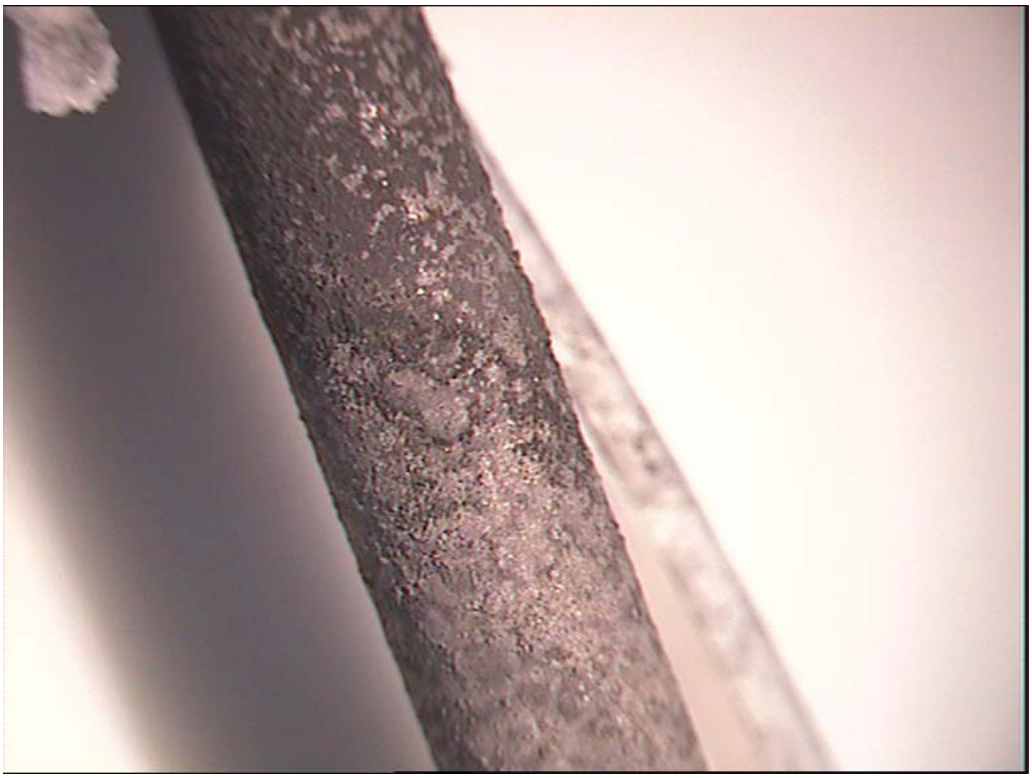


Figure A4 Current collector showing powdery deposition after Run 2

APPENDIX B

Results for Run 1

Plant Solution Testwork

RUN 1.1

Date of experiment:	26/05/03
Catholyte solution:	Plant Solution
Constant applied current:	1.4 A
Flowrate of catholyte:	620 ml/min

Table B1 pH values of electrolytes for Run 1.1

	Catholyte	**Anolyte**
pH at start of experiment	4.255	2.085
pH at end of experiment	4.271	1.933

Table B2 Volumes of electrolytes in reservoirs for Run 1.1

	Catholyte	**Anolyte**
Volume at the start of experiment (ml)	3820	3870
Volume at the end of experiment (ml)	3690	3830

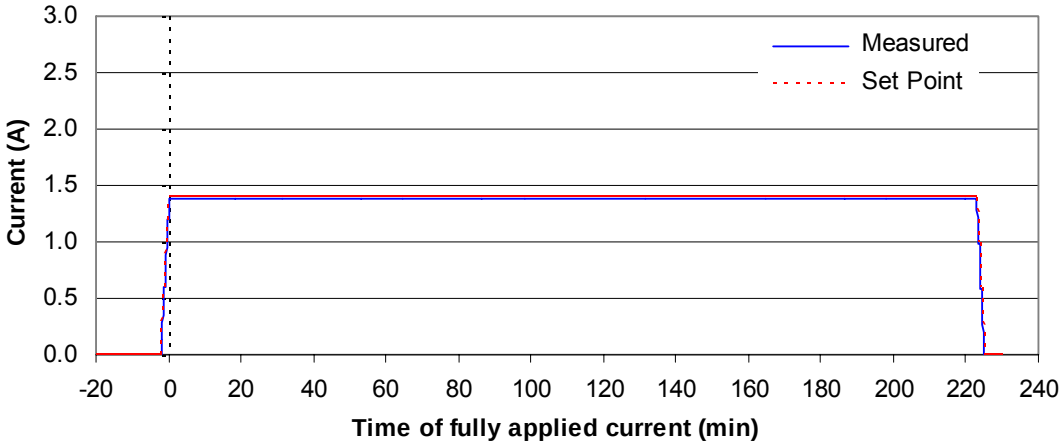


Figure B1 Current applied during Run 1.1

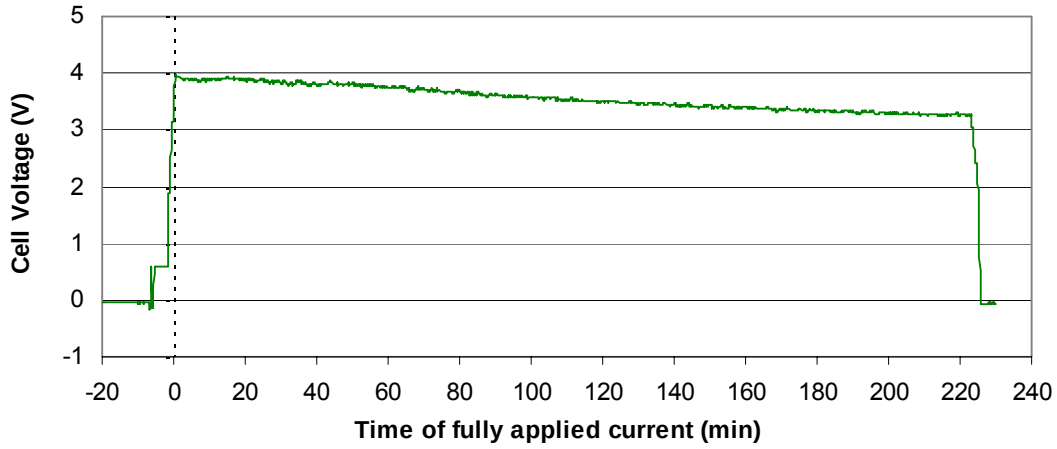


Figure B2 Cell voltage measured during Run 1.1

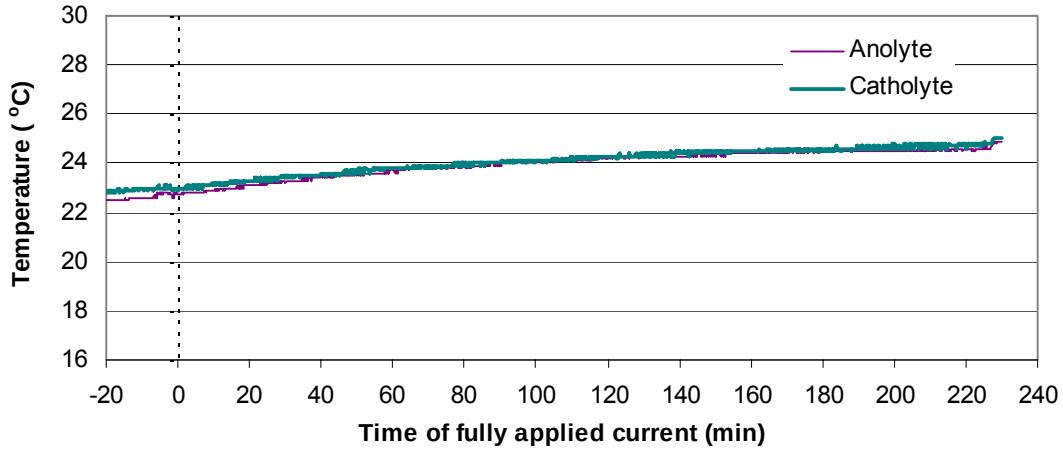


Figure B3 Temperatures of electrolytes measured during Run 1.1

Table B3 ICP results for copper - Run 1.1

Sample ID	Dilution	x	s	sr	Time (min)	Conc (ppm)	Ln Conc
C1	500	0.3913	0.0028	0.721	-51	195.7	5.28
C2	500	0.5080	0.0033	0.659	-30	254.0	5.54
C3	500	0.5490	0.0047	0.865	-17	274.5	5.61
C4	500	0.6680	0.0027	0.405	-4	334.0	5.81
C5	500	0.6730	0.0065	0.968	1	336.5	5.82
C6	500	0.6190	0.0038	0.619	5	309.5	5.73
C7	500	0.5910	0.0044	0.751	9	295.5	5.69
C8	500	0.5560	0.0054	0.971	13	278.0	5.63
C9	500	0.4714	0.0040	0.849	18	235.7	5.46
C10	500	0.3528	0.0012	0.349	24	176.4	5.17
C11	200	0.7070	0.0040	0.567	28	141.4	4.95
C12	100	1.0100	0.0013	0.132	33	101.0	4.62
C13	100	0.6240	0.0053	0.847	38	62.4	4.13
C14	100	0.4063	0.0033	0.803	43	40.6	3.70
C15	100	0.1758	0.0049	2.759	49	17.6	2.87
C16	10	0.6300	0.0113	1.791	55	6.3	1.84
C17	10	0.2665	0.0011	0.431	60	2.7	0.98
C18	10	0.0702	0.0022	3.158	68	0.7	-0.35
C19	10	0.0188	0.0008	4.225	78	0.2	-1.67
C20	10	0.0069	0.0005	7.184	98	0.1	-2.67
C21	10	0.0107	0.0007	6.969	118	0.1	-2.23
C22	10	0.0091	0.0001	1.584	156	0.1	-2.40
C23	10	0.0054	0.0002	3.888	193	0.1	-2.92
C24	10	0.0041	0.0001	1.527	218	0.0	-3.19

Table B4 ICP results for palladium - Run 1.1

Sample ID	Dilution	x	s	sr	Time (min)	Conc (ppm)	Ln Conc
C1	500	0.2477	0.0046	1.859	-51	123.9	4.82
C2	500	0.2555	0.0024	0.931	-30	127.8	4.85
C3	500	0.2578	0.0016	0.612	-17	128.9	4.86
C4	500	0.2658	0.0053	1.998	-4	132.9	4.89
C5	500	0.2571	0.0032	1.236	1	128.6	4.86
C6	500	0.2422	0.0030	1.249	5	121.1	4.80
C7	500	0.2379	0.0058	2.443	9	119.0	4.78
C8	500	0.2364	0.0023	0.968	13	118.2	4.77
C9	200	0.5740	0.0030	0.530	18	114.8	4.74
C10	200	0.5900	0.0035	0.597	24	118.0	4.77
C11	200	0.5460	0.0090	1.641	28	109.2	4.69
C12	100	0.9510	0.0014	0.152	33	95.1	4.55
C13	100	0.7140	0.0050	0.705	38	71.4	4.27
C14	100	0.5690	0.0052	0.915	43	56.9	4.04
C15	100	0.2760	0.0045	1.631	49	27.6	3.32
C16	10	1.1780	0.0118	1.003	55	11.8	2.47
C17	10	0.4955	0.0029	0.588	60	5.0	1.60
C18	10	0.1182	0.0029	2.477	68	1.2	0.17
C19	10	0.0213	0.0015	7.000	78	0.2	-1.55
C20	10	0.0039	0.0049	125.420	98	0.0	-3.24
C21	10	0.0060	0.0016	26.702	118	0.1	-2.81
C22	10	0.0039	0.0030	75.401	156	0.0	-3.24
C23	10	0.0053	0.0020	37.938	193	0.1	-2.94
C24	10	0.0039	0.0009	24.111	218	0.0	-3.24

xxx out of range

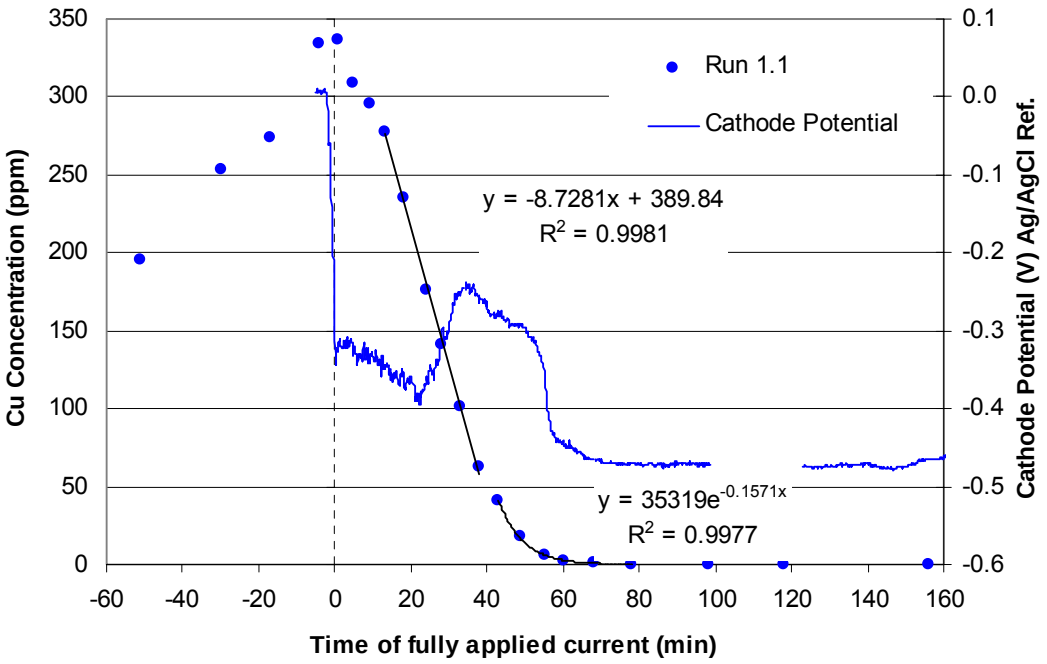


Figure B4 Cu concentration profile for Run 1.1 with the measured cathode potential shown on the secondary axis

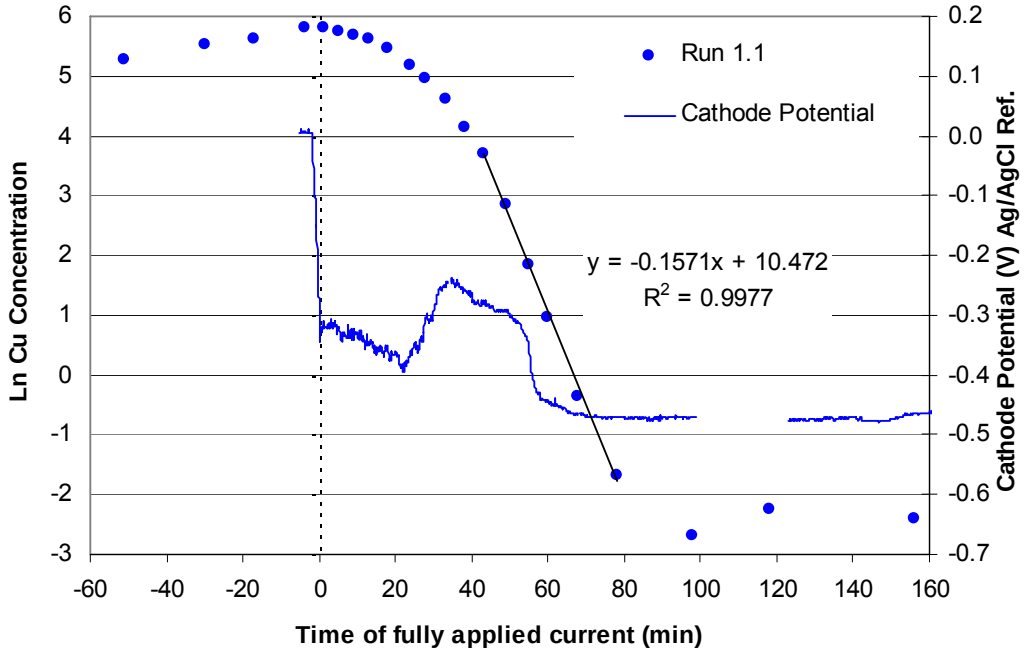


Figure B5 Cu concentration profile for Run 1.1 indicating the mass transport controlled region with the measured cathode potential shown on the secondary axis

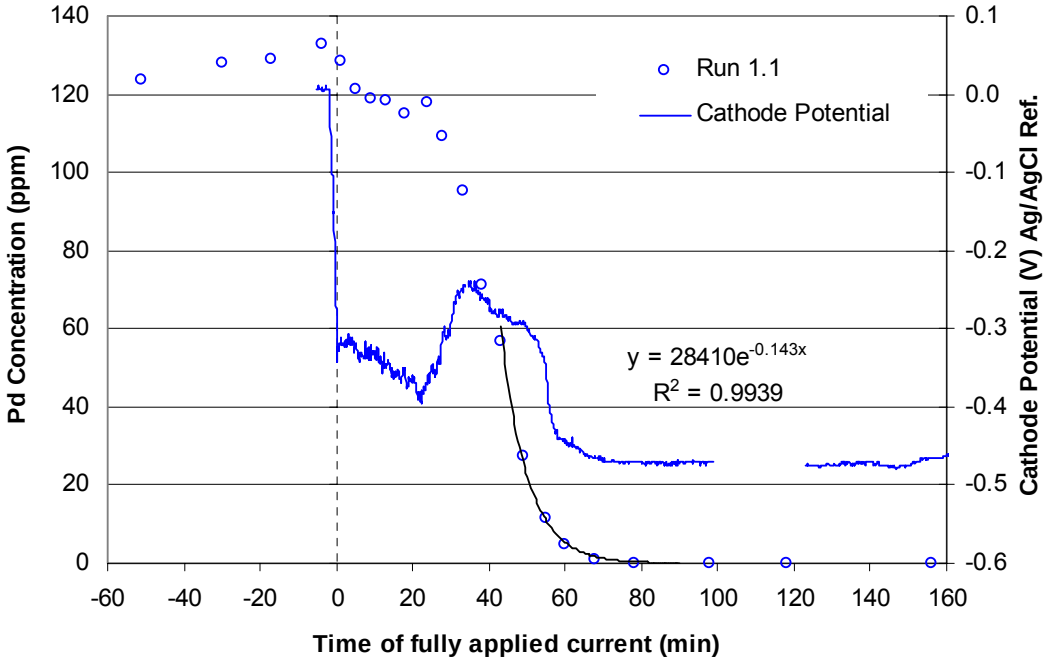


Figure B6 Pd concentration profile for Run 1.1 with the measured cathode potential shown on the secondary axis

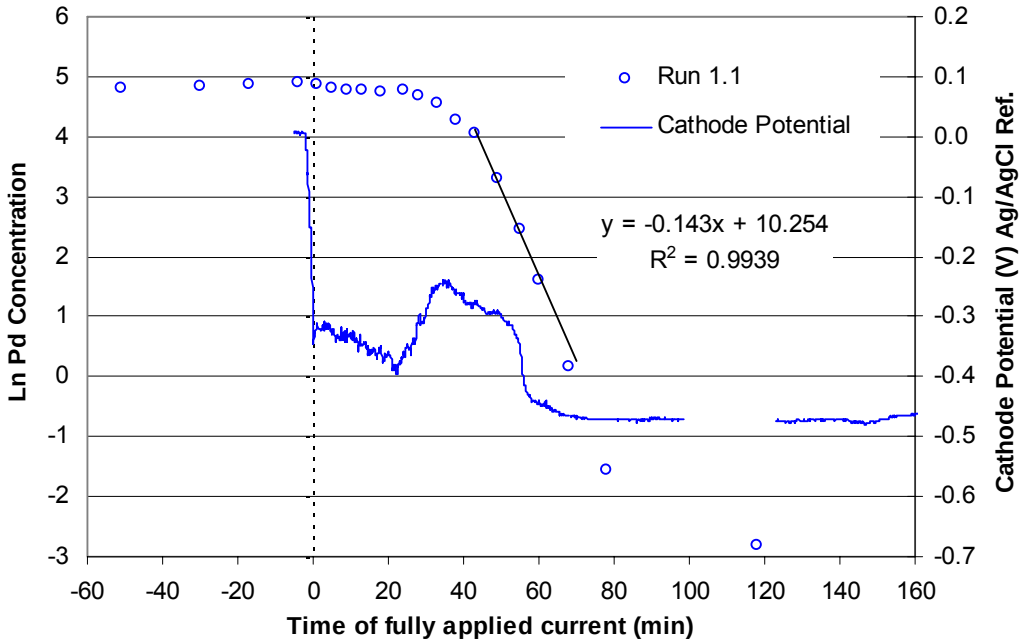


Figure B7 Pd concentration profile for Run 1.1 indicating the mass transport controlled region with the measured cathode potential shown on the secondary axis

RUN 1.2

Date of experiment:	28/05/03
Catholyte solution:	Plant Solution
Constant applied current:	1.4 A
Flowrate of catholyte:	620 ml/min

Table B5 pH values of electrolytes for Run 1.2

	Catholyte	**Anolyte**
pH at start of experiment	4.319	Not measured
pH at end of experiment	4.351	Not measured

Table B6 Volumes of electrolytes in reservoirs for Run 1.2

	Catholyte	**Anolyte**
Volume at the start of experiment (ml)	3700	3810
Volume at the end of experiment (ml)	3580	3780

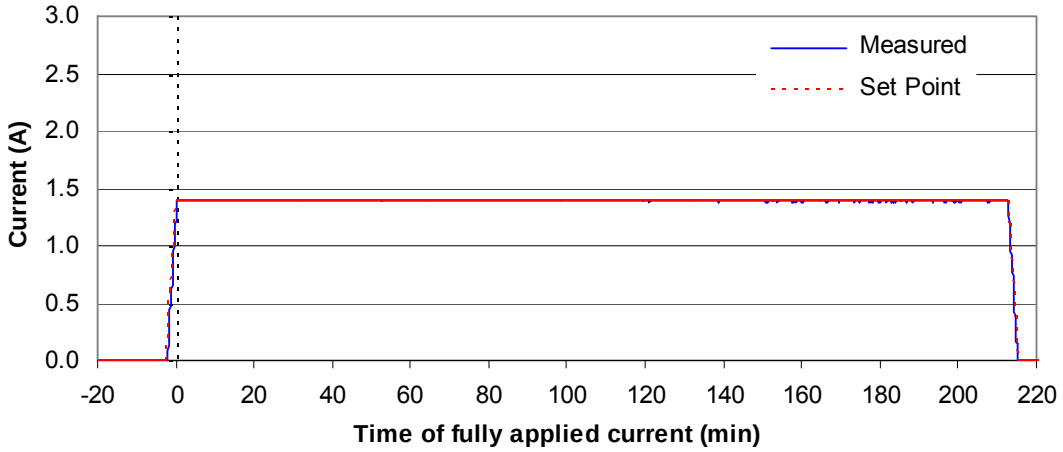


Figure B8 Current applied during Run 1.2

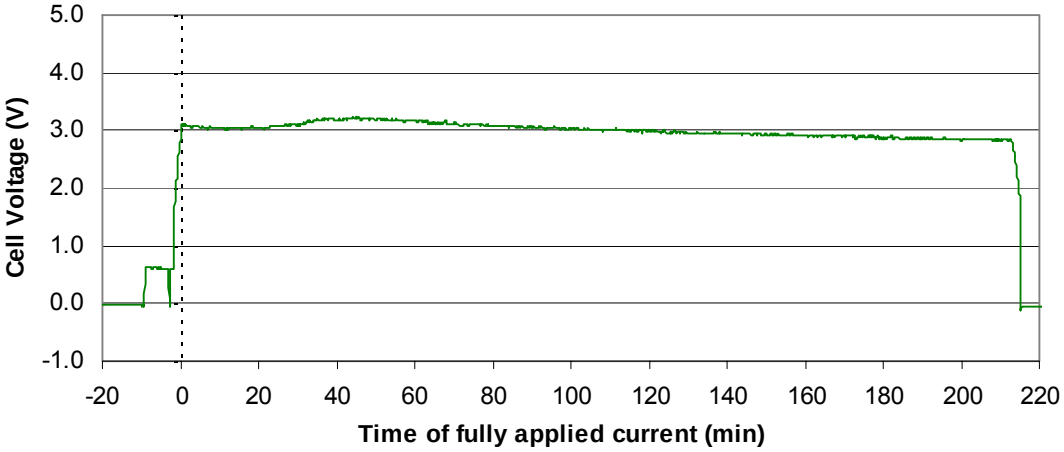


Figure B9 Cell voltage measured during Run 1.2

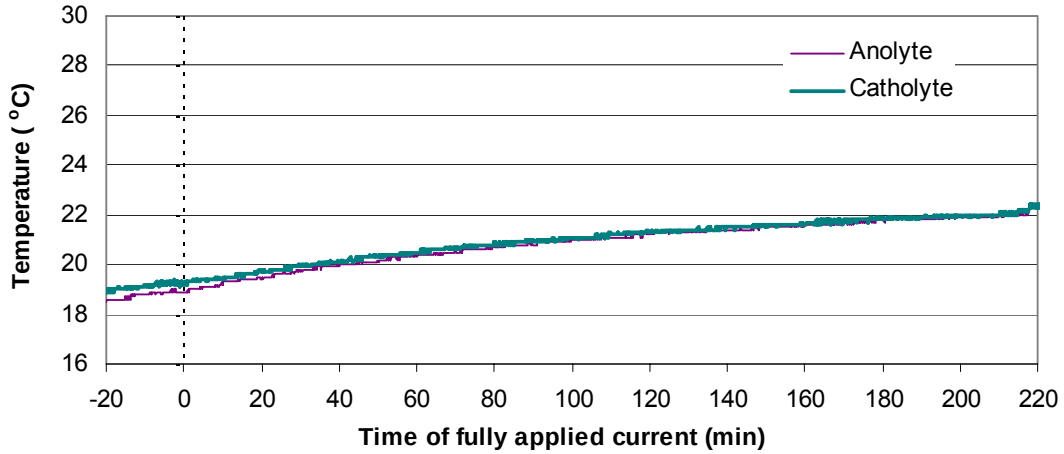


Figure B10 Temperatures of electrolytes measured during Run 1.2

Table B7 ICP results for copper - Run 1.2

Sample ID	Dilution	x	s	sr
C1	500	0.6950	0.0066	0.946
C2	500	0.8350	0.0021	0.254
C3	500	0.9030	0.0078	0.862
C4	500	0.9650	0.0040	0.412
C5	500	0.9640	0.0085	0.884
C6	500	0.9190	0.0054	0.586
C7	500	0.9050	0.0044	0.491
C8	500	0.7810	0.0051	0.659
C9	500	0.7300	0.0063	0.868
C10	500	0.6340	0.0031	0.486
C11	200	1.2160	0.0065	0.535
C12	200	1.0620	0.0031	0.295
C13	200	1.0000	0.0159	1.592
C14	200	0.7150	0.0022	0.304
C15	100	1.0500	0.0140	1.336
C16	100	0.8270	0.0111	1.337
C17	100	0.6500	0.0137	2.109
C18	100	0.3718	0.0029	0.789
C19	20	0.8670	0.0089	0.011
C20	10	0.7900	1.0280	1.347
C21	10	0.3017	0.0043	1.437
C22	10	0.1339	0.0041	3.084
C23	10	0.0526	0.0012	2.368
C24	10	0.0171	0.0004	2.285
C25	10	0.0062	0.0002	3.559
C26	10	0.0053	0.0019	35.403
C27	10	0.0191	0.0025	12.995

Time (min)	Conc (ppm)	Ln Conc
-62	347.5	5.85
-47	417.5	6.03
-27	451.5	6.11
-8	482.5	6.18
1	482.0	6.18
4	459.5	6.13
6	452.5	6.11
8	390.5	5.97
11	365.0	5.90
16	317.0	5.76
21	243.2	5.49
24	212.4	5.36
26	200.0	5.30
28	143.0	4.96
32	105.0	4.65
36	82.7	4.42
43	65.0	4.17
48	37.2	3.62
53	17.3	2.85
58	7.9	2.07
64	3.0	1.10
69	1.3	0.29
75	0.5	-0.64
83	0.2	-1.77
113	0.1	-2.78
144	0.1	-2.94
203	0.2	-1.66

Table B8 ICP results for palladium - Run 1.2

Sample ID	Dilution	x	s	sr
C1	500	0.2395	0.0034	1.438
C2	500	0.2351	0.0016	0.678
C3	500	0.2228	0.0050	2.241
C4	500	0.2493	0.0012	0.493
C5	500	0.2516	0.0088	3.505
C6	500	0.2573	0.0113	4.406
C7	500	0.2673	0.0027	0.991
C8	500	0.2333	0.0075	3.194
C9	500	0.2274	0.0082	3.620
C10	500	0.2125	0.0051	2.423
C11	200	0.5270	0.0063	1.201
C12	200	0.4996	0.0055	1.109
C13	200	0.4980	0.0088	1.758
C14	200	0.4153	0.0105	2.527
C15	100	0.7340	0.0178	2.431
C16	100	0.6520	0.0137	2.108
C17	100	0.5770	0.0072	1.255
C18	100	0.3968	0.0113	2.839
C19	20	1.1200	0.0053	0.475
C20	10	1.0720	0.0079	0.739
C21	10	0.4317	0.0053	1.238
C22	10	0.1922	0.0066	3.439
C23	10	0.0797	0.0027	3.438
C24	10	0.0206	0.0031	14.813
C25	10	0.0039	0.0028	71.782
C26	10	0.0053	0.0011	21.307
C27	10	0.0315	0.0089	28.259

Time (min)	Conc (ppm)	Ln Conc
-62	119.8	4.79
-47	117.6	4.77
-27	111.4	4.71
-8	124.7	4.83
1	125.8	4.83
4	128.7	4.86
6	133.7	4.90
8	116.7	4.76
11	113.7	4.73
16	106.3	4.67
21	105.4	4.66
24	99.9	4.60
26	99.6	4.60
28	83.1	4.42
32	73.4	4.30
36	65.2	4.18
43	57.7	4.06
48	39.7	3.68
53	22.4	3.11
58	10.7	2.37
64	4.3	1.46
69	1.9	0.65
75	0.8	-0.23
83	0.2	-1.58
113	0.0	-3.24
144	0.1	-2.94
203	0.3	-1.16

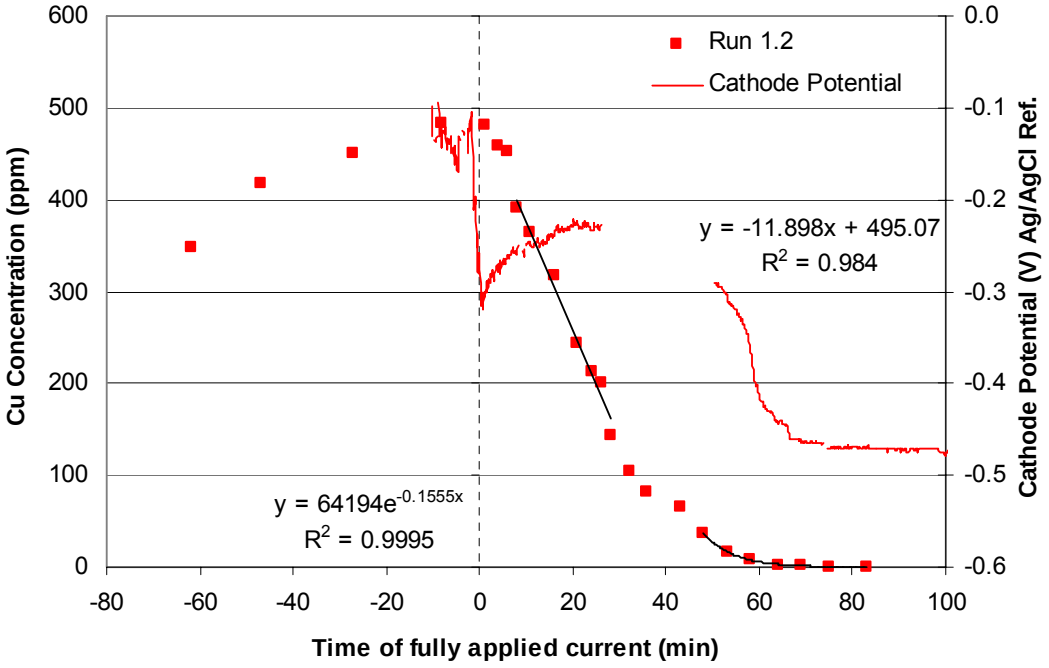


Figure B11 Cu concentration profile for Run 1.2 with the measured cathode potential shown on the secondary axis

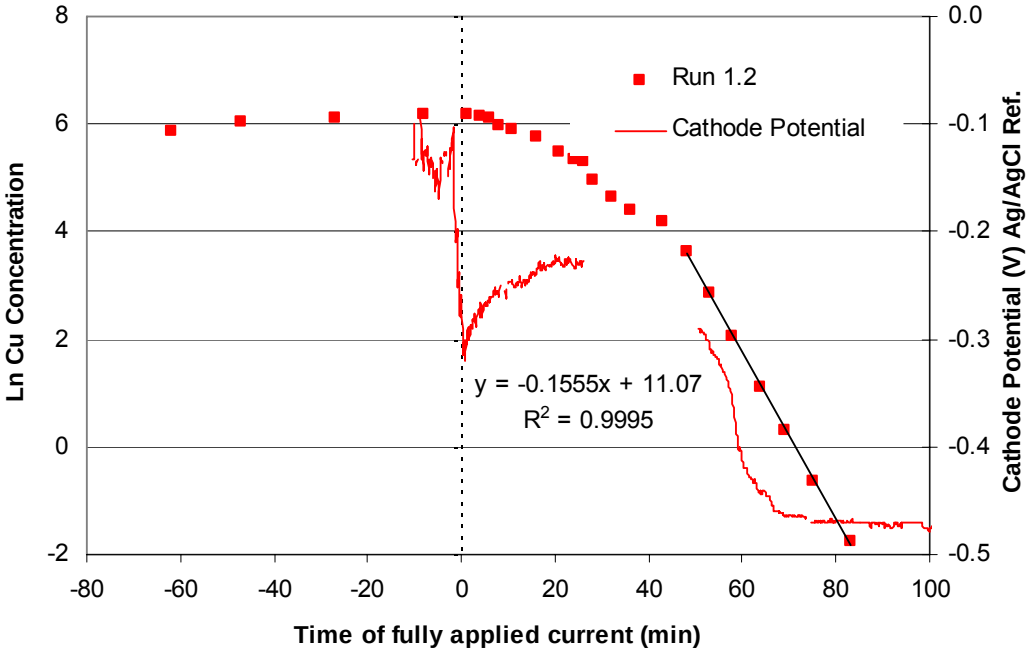


Figure B12 Cu concentration profile for Run 1.2 indicating the mass transport controlled region with the measured cathode potential shown on the secondary axis

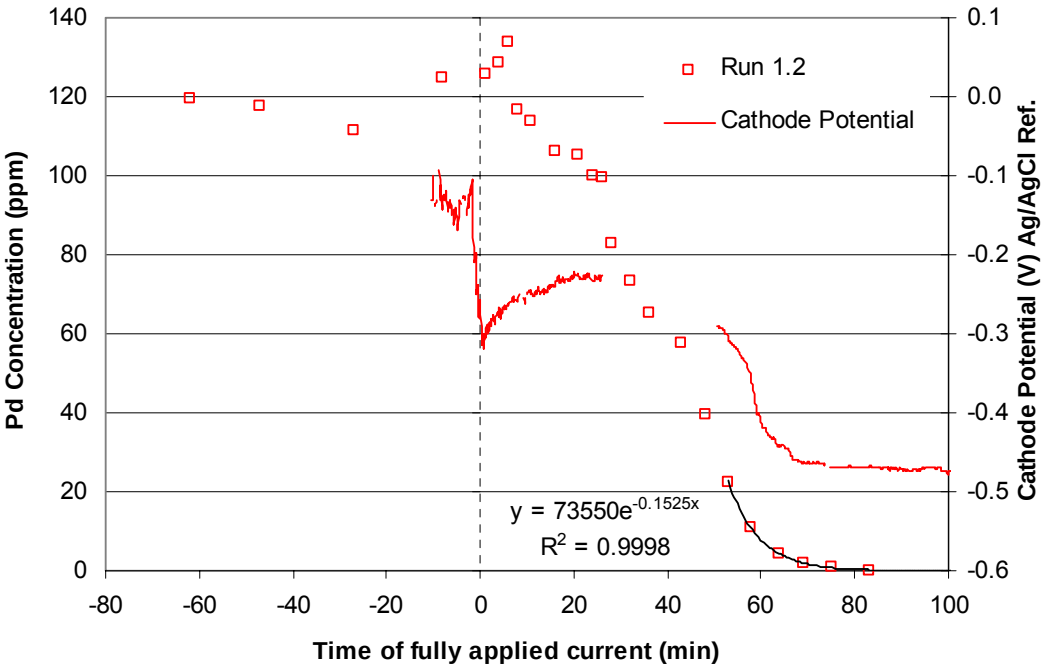


Figure B13 Pd concentration profile for Run 1.2 with the measured cathode potential shown on the secondary axis

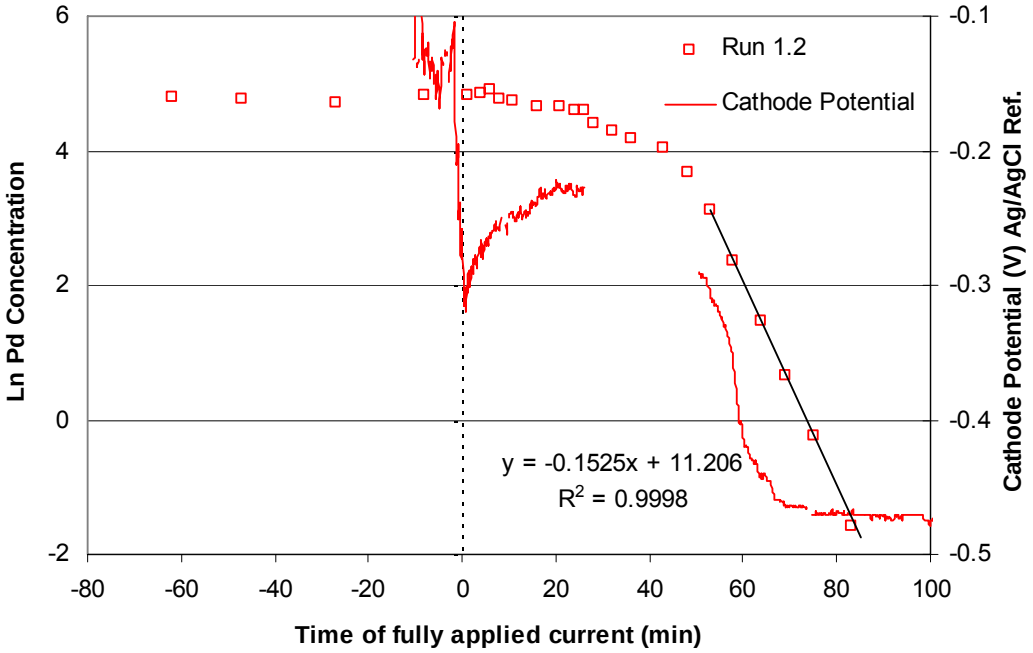


Figure B14 Pd concentration profile for Run 1.2 indicating the mass transport controlled region with the measured cathode potential shown on the secondary axis

RUN 1.3

Date of experiment:	02/06/03
Catholyte solution:	Plant Solution
Constant applied current:	2.0 A
Flowrate of catholyte:	620 ml/min

Table B9 pH values of electrolytes for Run 1.3

	Catholyte	**Anolyte**
pH at start of experiment	4.318	Not measured
pH at end of experiment	4.333	Not measured

Table B10 Volumes of electrolytes in reservoirs for Run 1.3

	Catholyte	**Anolyte**
Volume at the start of experiment (ml)	3800	3810
Volume at the end of experiment (ml)	3710	3790

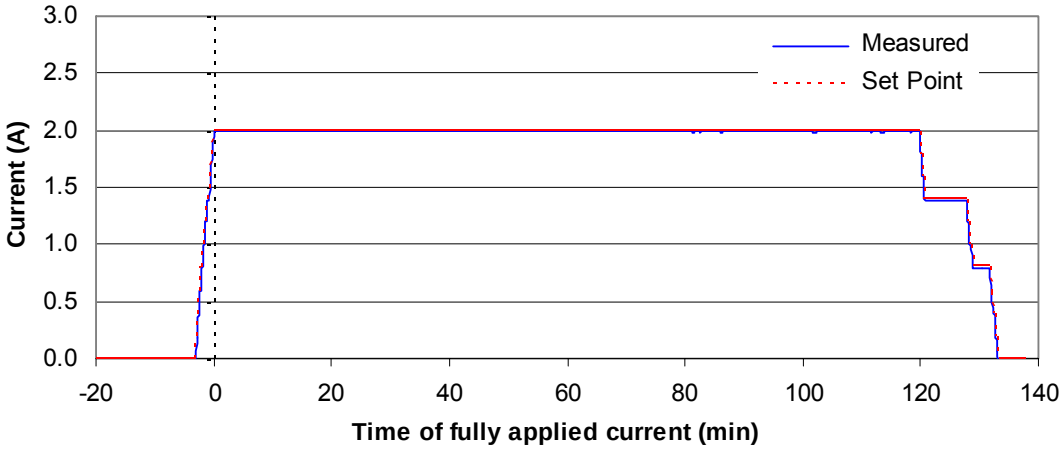


Figure B15 Current applied during Run 1.3

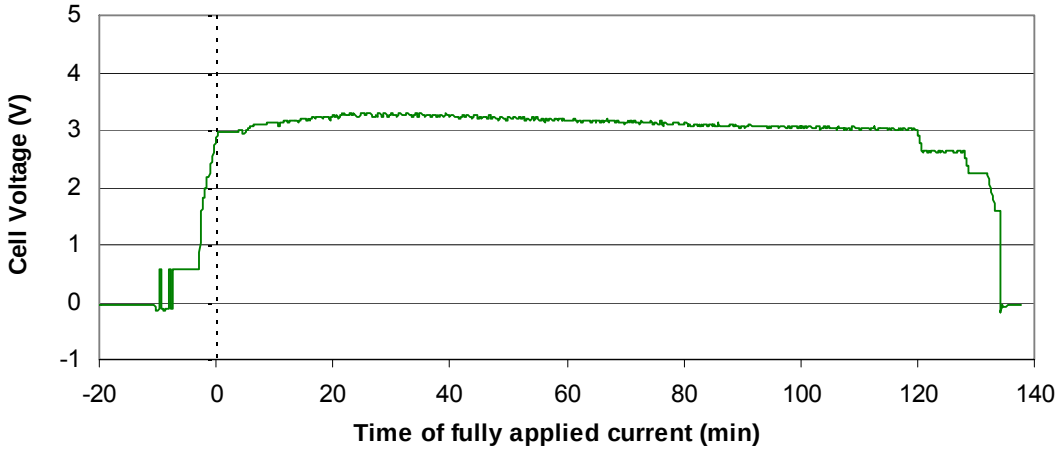


Figure B16 Cell voltage measured during Run 1.3

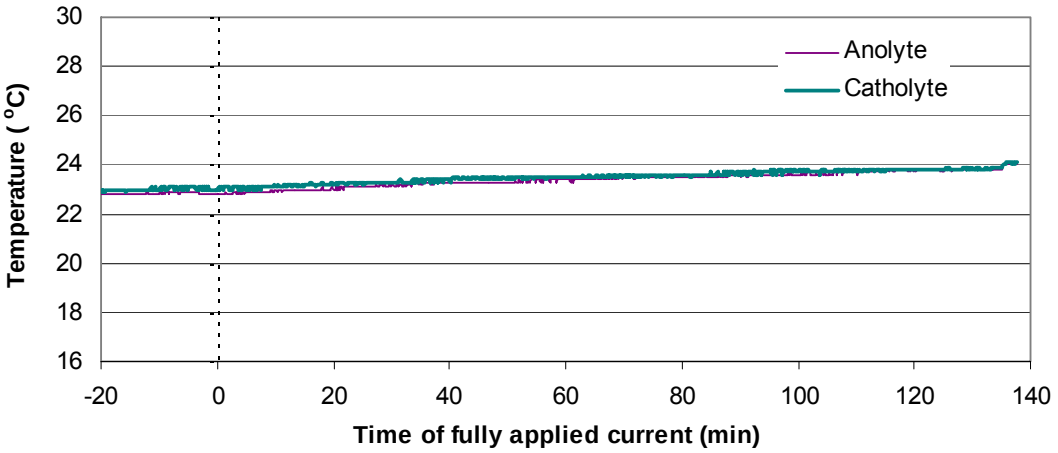


Figure B17 Temperatures of electrolytes measured during Run 1.3

Table B11 ICP results for copper - Run 1.3

Sample ID	Dilution	x	s	sr	Time (min)	Conc (ppm)	Ln Conc
C1	500	0.6890	0.0052	0.754	-61	344.5	5.84
C2	500	0.7740	0.0027	0.355	-46	387.0	5.96
C3	500	0.9670	0.0029	0.303	-26	483.5	6.18
C4	500	1.1380	0.0082	0.718	-5	569.0	6.34
C5	500	0.9970	0.0049	0.496	1	498.5	6.21
C6	500	0.8500	0.0054	0.637	4	425.0	6.05
C7	500	0.7610	0.0052	0.684	7	380.5	5.94
C8	500	0.6990	0.0023	0.327	10	349.5	5.86
C9	500	0.5950	0.0051	0.855	13	297.5	5.70
C10	500	0.5110	0.0039	0.761	16	255.5	5.54
C11	200	0.9580	0.0020	0.212	19	191.6	5.26
C12	200	0.8570	0.0043	0.498	22	171.4	5.14
C13	100	1.4360	0.0165	1.149	25	143.6	4.97
C14	100	0.9200	0.0066	0.716	31	92.0	4.52
C15	100	0.6910	0.0104	1.499	34	69.1	4.24
C16	100	0.4920	0.0062	1.256	37	49.2	3.90
C17	20	1.6330	0.0117	0.714	40	33.2	3.50
C18	10	1.2170	0.0040	0.331	46	12.2	2.50
C19	10	0.6700	0.0120	1.787	50	6.7	1.90
C20	10	0.2090	0.0038	1.800	57	2.1	0.74
C21	10	0.0694	0.0035	5.042	64	0.7	-0.37
C22	10	0.0102	0.0005	5.039	79	0.1	-2.28
C23	10	0.0056	0.0003	4.904	102	0.1	-2.88
C24	10	0.0064	0.0003	5.394	117	0.1	-2.75

Table B12 ICP results for palladium - Run 1.3

Sample ID	Dilution	x	s	sr	Time (min)	Conc (ppm)	Ln Conc
C1	500	0.2193	0.0059	2.685	-61	109.7	4.70
C2	500	0.2107	0.0006	0.271	-46	105.4	4.66
C3	500	0.2060	0.0052	2.506	-26	103.0	4.63
C4	500	0.2881	0.0066	2.305	-5	144.1	4.97
C5	500	0.2636	0.0020	0.769	1	131.8	4.88
C6	500	0.2416	0.0053	2.186	4	120.8	4.79
C7	500	0.2368	0.0061	2.585	7	118.4	4.77
C8	500	0.2386	0.0077	3.223	10	119.3	4.78
C9	500	0.2186	0.0039	1.789	13	109.3	4.69
C10	500	0.1992	0.0051	2.551	16	99.6	4.60
C11	200	0.3974	0.0072	1.810	19	79.5	4.38
C12	200	0.3746	0.0176	4.697	22	74.9	4.32
C13	100	0.7340	0.0072	0.987	25	73.4	4.30
C14	100	0.5740	0.0022	0.388	31	57.4	4.05
C15	100	0.4781	0.0052	1.089	34	47.8	3.87
C16	100	0.3812	0.0062	1.618	37	38.1	3.64
C17	100	0.2753	0.0048	1.731	40	27.5	3.32
C18	10	1.1900	0.0031	0.258	46	11.9	2.48
C19	10	0.6920	0.0055	0.790	50	6.9	1.93
C20	10	0.2284	0.0037	1.613	57	2.3	0.83
C21	10	0.0840	0.0058	6.847	64	0.8	-0.17
C22	10	0.0135	0.0007	5.224	79	0.1	-2.00
C23	10	0.0062	0.0022	36.317	102	0.1	-2.78
C24	10	0.0040	0.0022	55.480	117	0.0	-3.22

xxx out of range

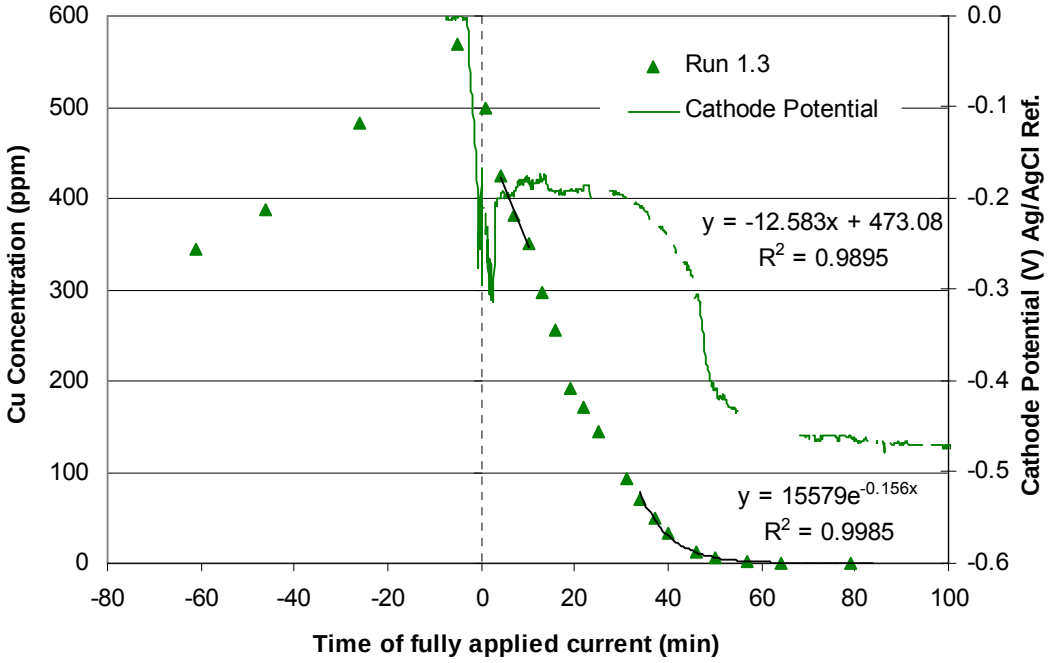


Figure B18 Cu concentration profile for Run 1.3 with the measured cathode potential shown on the secondary axis

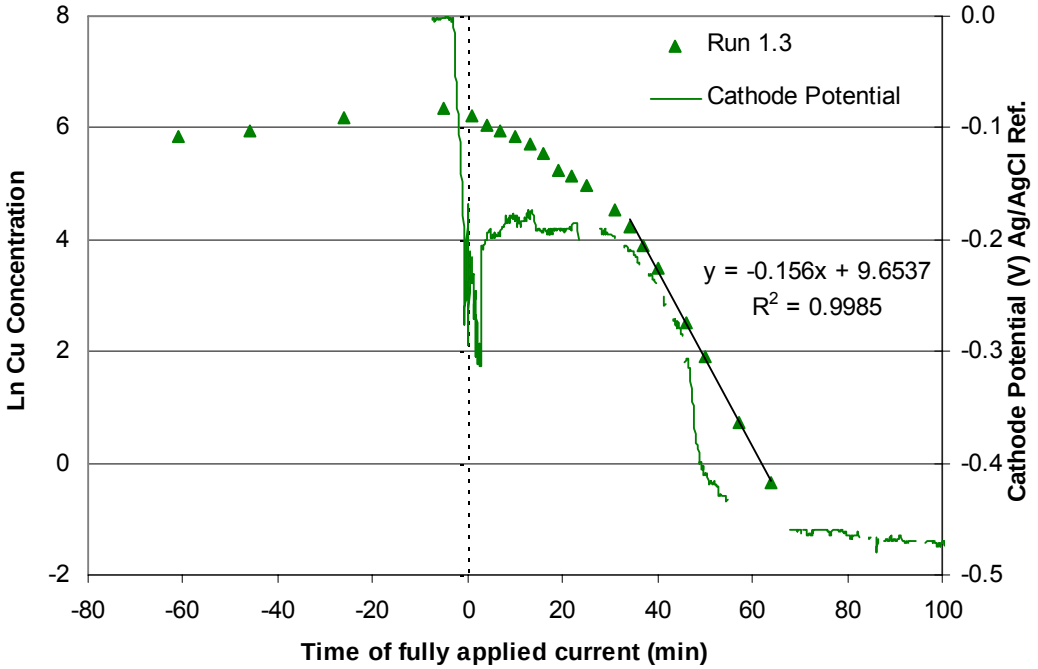


Figure B19 Cu concentration profile for Run 1.3 indicating the mass transport controlled region with the measured cathode potential shown on the secondary axis

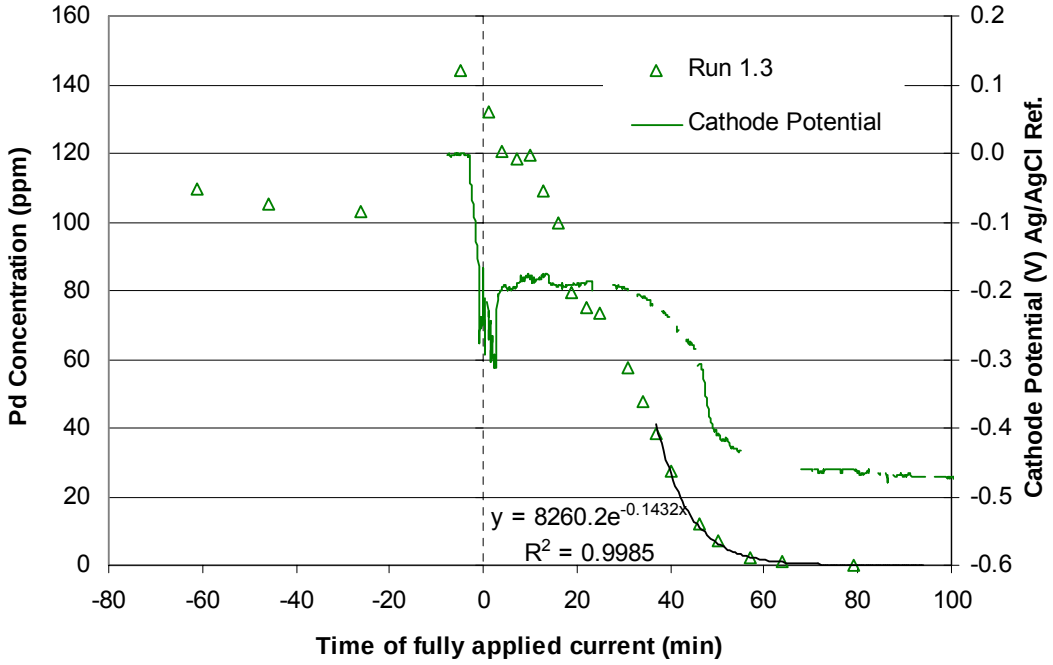


Figure B20 Pd concentration profile for Run 1.3 with the measured cathode potential shown on the secondary axis

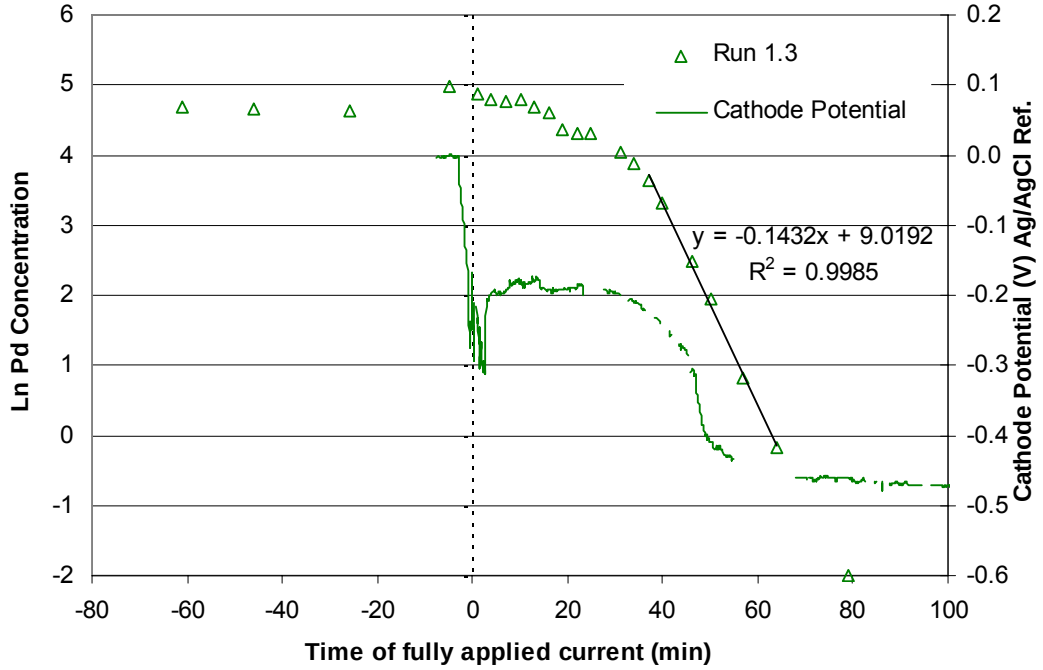


Figure B21 Pd concentration profile for Run 1.3 indicating the mass transport controlled region with the measured cathode potential shown on the secondary axis

APPENDIX C

Results for Run 2

Pd SMISIE Testwork

RUN 2.1

Date of experiment:	16/07/03
Catholyte solution:	Pd SMISIE
Constant applied current:	1.4 A
Flowrate of catholyte:	620 ml/min

Table C1 Catholyte make-up for Run 2.1

NaCl (g)	233.76
$CuCl_2.2H_2O$ (g)	0
Pd Stock Solution (10 g/l Pd in 20% HCl) (ml)	80
NH_4Ac (g)	308.37
CH_3COOH (ml)	230

Table C2 pH values of electrolytes for Run 2.1

	Catholyte	**Anolyte**
pH at start of experiment	4.494	2.123
pH at end of experiment	4.491	2.047

Table C3 Volumes of electrolytes in reservoirs for Run 2.1

	Catholyte	**Anolyte**
Volume at the start of experiment (ml)	3990	4070
Volume at the end of experiment (ml)	3840	4120

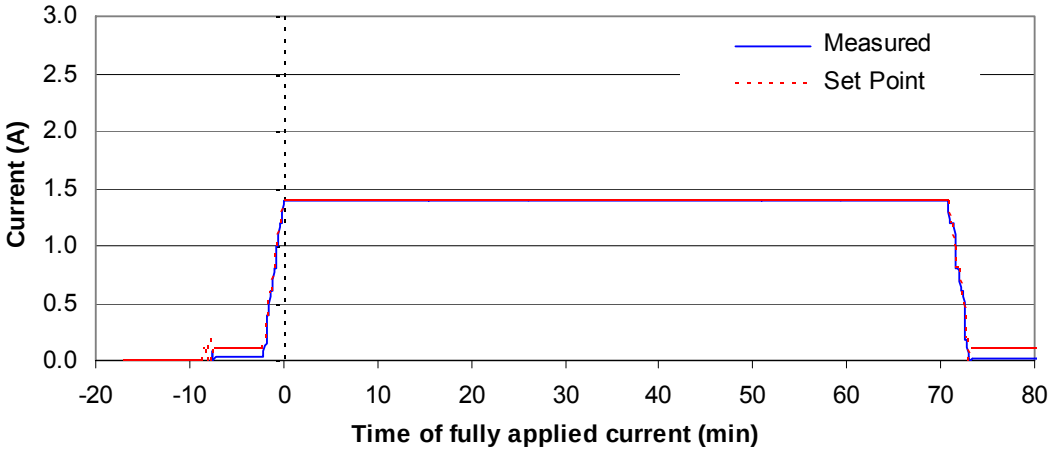


Figure C1 Current applied during Run 2.1

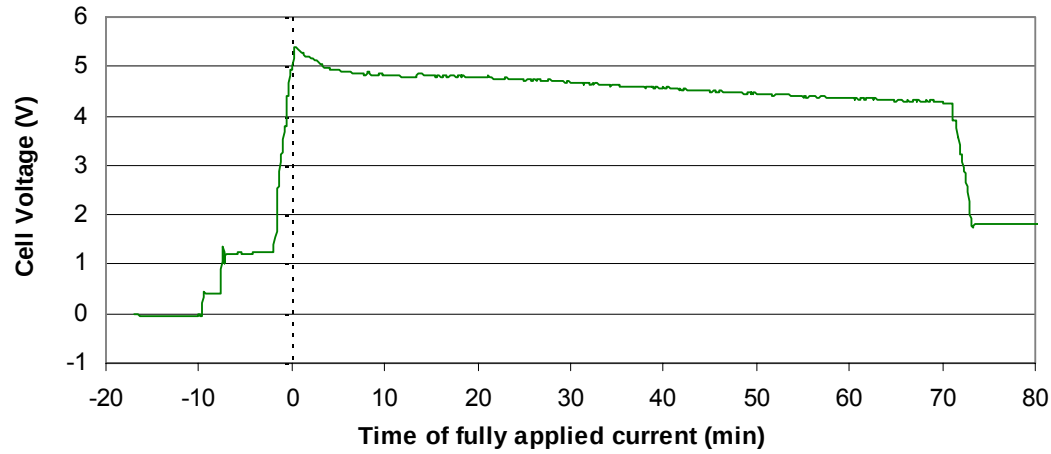


Figure C2 Cell voltage measured during Run 2.1

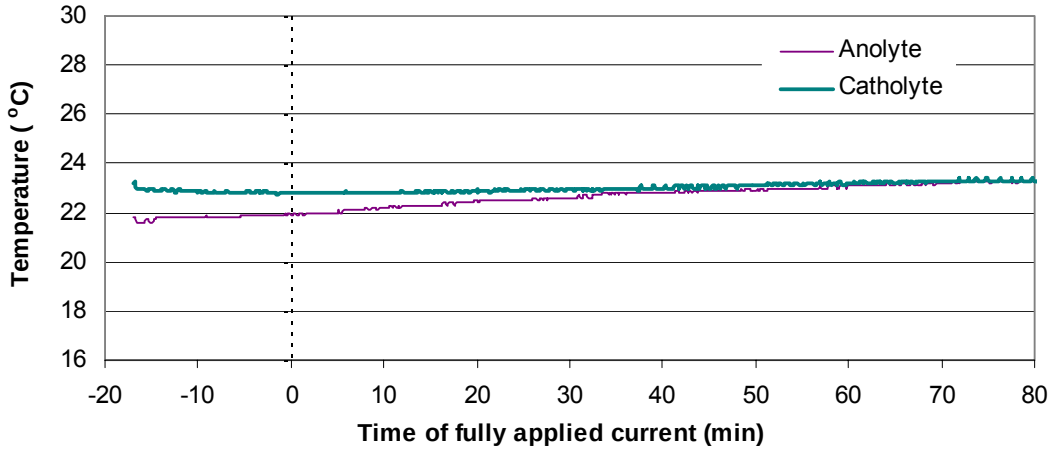


Figure C3 Temperatures of electrolytes measured during Run 2.1

Table C4 ICP results for Run 2.1

Sample ID	Dilution	x	s	sr	Time (min)	Conc (ppm)	Ln Conc
C10a (head)	400	0.588	0.005	0.859	-17	235.2	5.46
C20a (head)	400	0.573	0.0031	0.544	-17	229.2	5.43
C30a (head)	400	0.542	0.0053	0.970	-17	216.8	5.38
C1	400	0.5440	0.0014	0.251	-14	217.6	5.38
C2	400	0.5390	0.0030	0.561	-5	215.6	5.37
C3	200	1.0540	0.0102	0.972	1	210.8	5.35
C4	200	0.9790	0.0032	0.322	3	195.8	5.28
C5	200	0.8980	0.0084	0.933	4	179.6	5.19
C6	200	0.8510	0.0062	0.734	5	170.2	5.14
C7	200	0.8230	0.0022	0.269	6	164.6	5.10
C8	200	0.7470	0.0055	0.732	7	149.4	5.01
C9	200	0.7080	0.0054	0.762	8	141.6	4.95
C10	200	0.5850	0.0018	0.312	10	117.0	4.76
C11	200	0.5480	0.0046	0.836	11	109.6	4.70
C12	200	0.4897	0.0018	0.370	12	97.9	4.58
C13	200	0.4253	0.0033	0.775	13	85.1	4.44
C14	200	0.3434	0.0029	0.836	15	68.7	4.23
C15	200	0.2672	0.0023	0.846	17	53.4	3.98
C16	200	0.2263	0.0016	0.711	18	45.3	3.81
C17	200	0.1993	0.0016	0.819	19	39.9	3.69
C18	200	0.1454	0.0034	2.306	21	29.1	3.37
C19	200	0.1295	0.0026	1.973	22	25.9	3.25
C20	200	0.1118	0.0031	2.749	23	22.4	3.11
C21	20	1.0860	0.0084	0.775	24	21.7	3.08
C22	20	0.9150	0.0012	0.131	25	18.3	2.91
C23	20	0.7870	0.0032	0.412	26	15.7	2.76
C24	20	0.5730	0.0026	0.449	28	11.5	2.44
C25	20	0.4702	0.0035	0.751	29	9.4	2.24
C26	20	0.3200	0.0019	0.580	31	6.4	1.86
C27	20	0.2376	0.0011	0.454	32	4.8	1.56
C28	20	0.2311	0.0010	0.417	33	4.6	1.53
C29	20	0.1660	0.0010	0.669	35	3.3	1.20
C30	20	0.1358	0.0013	0.944	36	2.7	1.00
C31	20	0.0989	0.0017	1.728	37	2.0	0.68
C32	20	0.0877	0.0004	0.407	38	1.8	0.56
C33	20	0.0609	0.0003	0.510	40	1.2	0.20
C34	20	0.0374	0.0008	2.166	43	0.7	-0.29
C35	20	0.0243	0.0004	1.518	46	0.5	-0.72
C36	20	0.0183	0.0001	0.338	49	0.4	-1.01
C37	20	0.0083	0.0002	2.937	53	0.2	-1.80
C38	20	0.0075	0.0003	4.388	58	0.2	-1.90
C39	20	0.0055	0.0003	6.063	68	0.1	-2.21

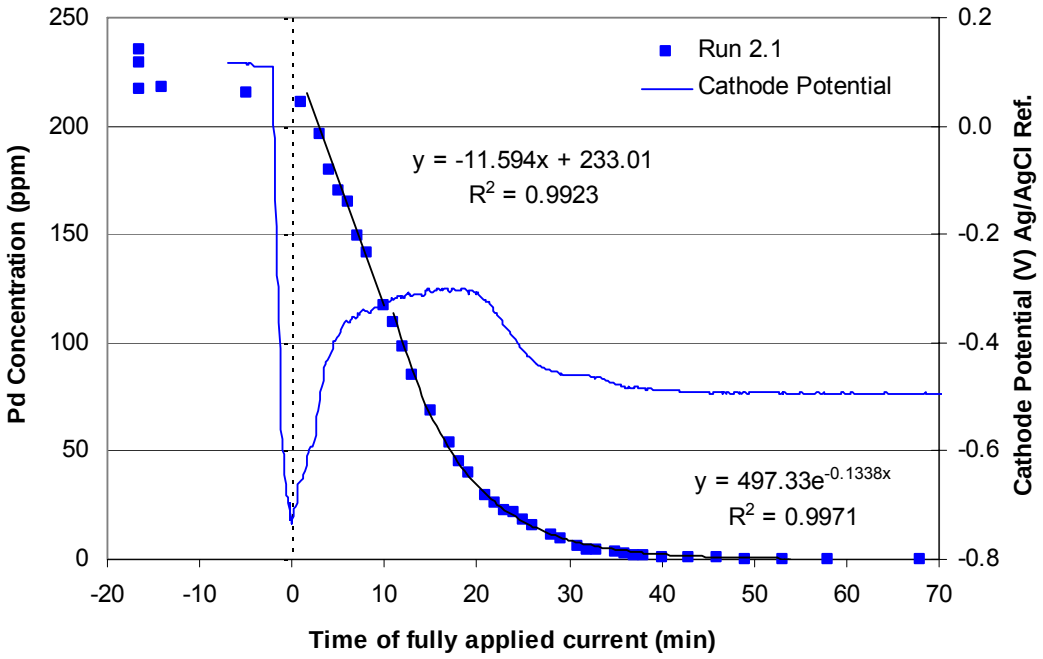


Figure C4 Concentration profile for Run 2.1 with the measured cathode potential shown on the secondary axis

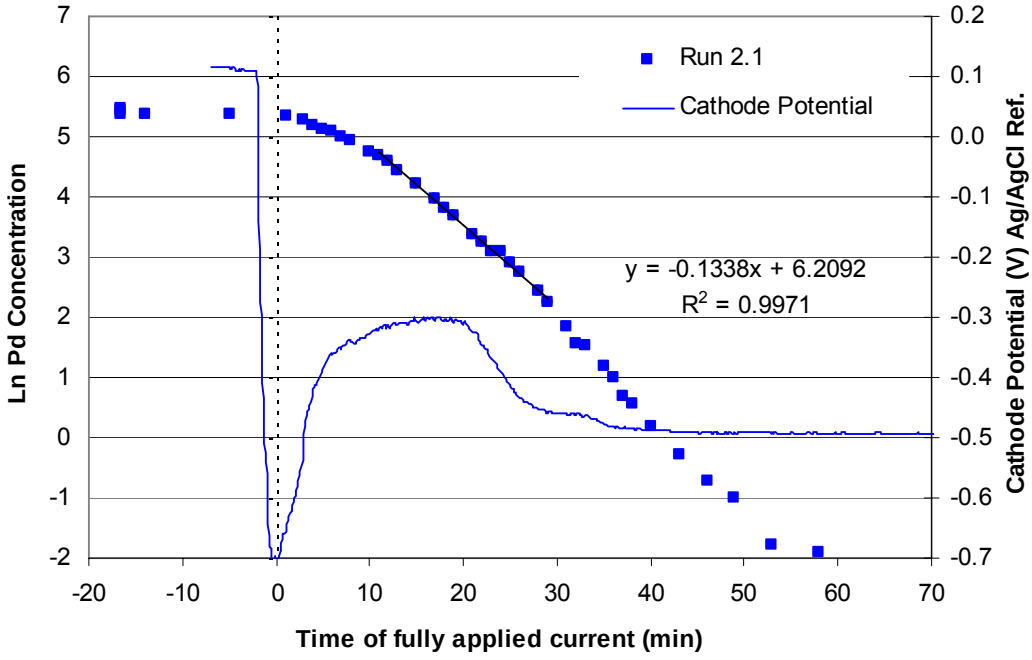


Figure C5 Concentration profile for Run 2.1 indicating the mass transport controlled region with the measured cathode potential shown on the secondary axis

RUN 2.2

Date of experiment:	17/07/03
Catholyte solution:	Pd SMISIE
Constant applied current:	2.0 A
Flowrate of catholyte:	620 ml/min

Table C5 Catholyte make-up for Run 2.2

NaCl (g)	233.77
$CuCl_2.2H_2O$ (g)	0
Pd Stock Solution (10 g/l Pd in 20% HCl) (ml)	80
NH_4Ac (g)	308.36
CH_3COOH (ml)	230

Table C6 pH values of electrolytes for Run 2.2

	Catholyte	**Anolyte**
pH at start of experiment	4.506	2.112
pH at end of experiment	4.517	2.070

Table C7 Volumes of electrolytes in reservoirs for Run 2.2

	Catholyte	**Anolyte**
Volume at the start of experiment (ml)	3920	4070
Volume at the end of experiment (ml)	3770	4090

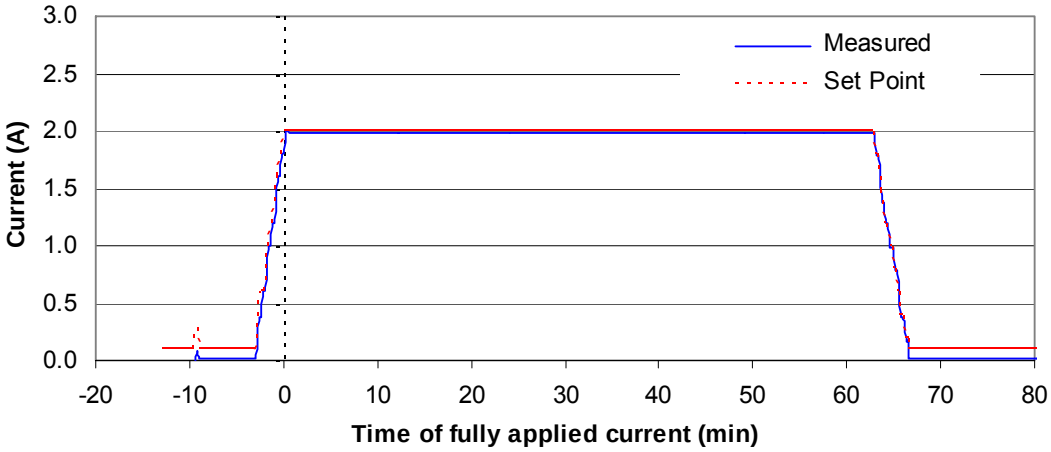


Figure C6 Current applied during Run 2.2

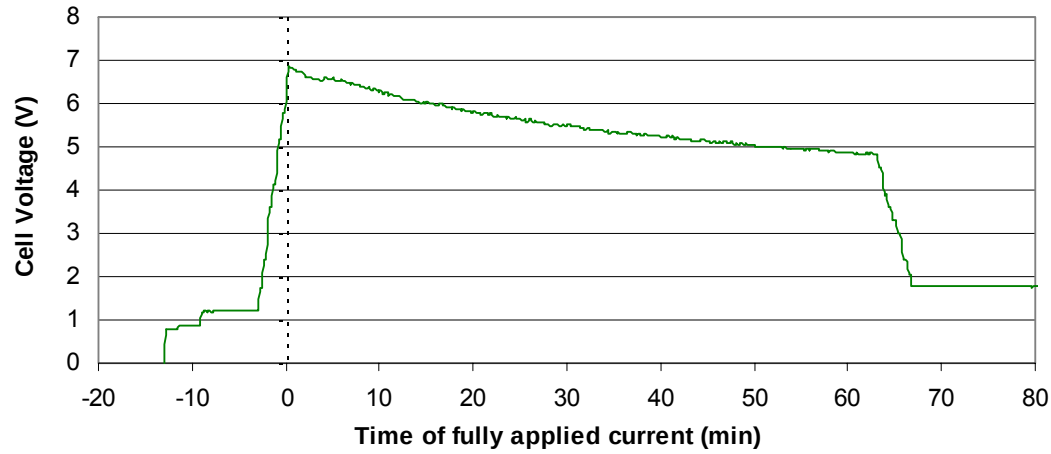


Figure C7 Cell voltage measured during Run 2.2

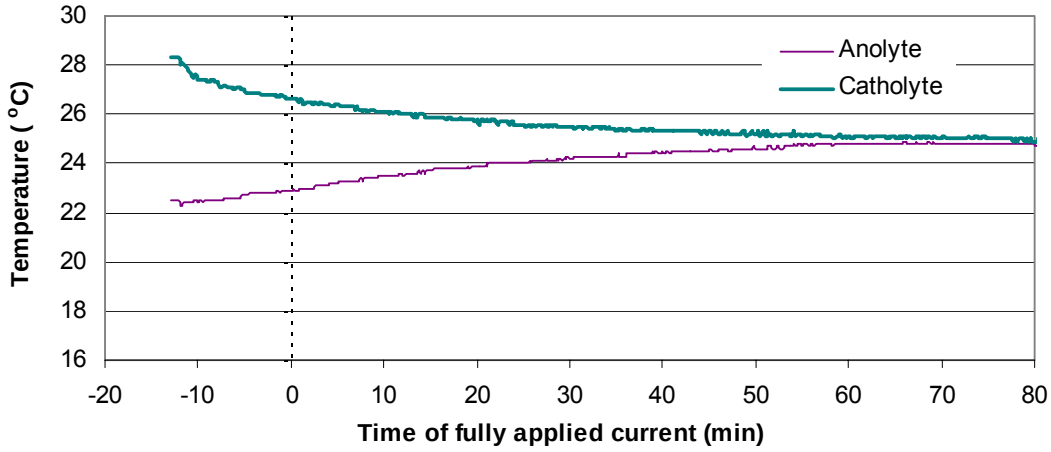


Figure C8 Temperatures of electrolytes measured during Run 2.2

Table C8 ICP results for Run 2.2

Sample ID	Dilution	x	s	sr	Time (min)	Conc (ppm)	Ln Conc
C10 (head)	400	0.649	0.006	0.925	-13	259.6	5.56
C20 (head)	400	0.619	0.0003	0.054	-13	247.6	5.51
C30 (head)	400	0.664	0.0005	0.082	-13	265.6	5.58
C1	400	0.615	0.005	0.816	-7	246.0	5.51
C2	200	1.0680	0.0016	0.149	1	213.6	5.36
C3	200	0.9740	0.0084	0.863	2	194.8	5.27
C4	200	0.8690	0.0070	0.801	3	173.8	5.16
C5	200	0.7670	0.0038	0.496	4	153.4	5.03
C6	200	0.6860	0.0061	0.895	5	137.2	4.92
C7	200	0.5920	0.0043	0.731	6	118.4	4.77
C8	200	0.5410	0.0041	0.764	7	108.2	4.68
C9	200	0.4820	0.0048	1.001	8	96.4	4.57
C11	200	0.3476	0.0023	0.676	10	69.5	4.24
C12	200	0.2998	0.0014	0.462	11	60.0	4.09
C13	200	0.2553	0.0017	0.647	12	51.1	3.93
C14	200	0.2161	0.0016	0.744	13	43.2	3.77
C15	200	0.1826	0.0011	0.590	14	36.5	3.60
C16	200	0.1475	0.0020	1.360	15	29.5	3.38
C17	20	1.3410	0.0094	0.704	16	26.8	3.29
C18	20	0.8760	0.0046	0.529	18	17.5	2.86
C19	20	0.7000	0.0074	1.053	19	14.0	2.64
C21	20	0.4729	0.0032	0.678	20	9.5	2.25
C22	20	0.2622	0.0004	0.161	21	5.2	1.66
C23	20	0.1440	0.0009	0.604	23	2.9	1.06
C24	20	0.1146	0.0006	0.530	25	2.3	0.83
C25	20	0.1042	0.0010	1.012	26	2.1	0.73
C26	20	0.1034	0.0005	0.461	27	2.1	0.73
C27	20	0.0929	0.0007	0.800	28	1.9	0.62
C28	20	0.0770	0.0008	0.981	30	1.5	0.43
C29	20	0.0850	0.0005	0.560	31	1.7	0.53
C31	20	0.0363	0.0006	1.524	32	0.7	-0.32
C32	20	0.0194	0.0004	1.825	34	0.4	-0.95
C33	20	0.0334	0.0010	3.098	36	0.7	-0.40
C34	20	0.0219	0.0016	7.163	38	0.4	-0.83
C35	20	0.0290	0.0009	3.053	40	0.6	-0.54
C36	20	0.0222	0.0005	2.224	41	0.4	-0.81
C37	20	0.0287	0.0001	0.460	43	0.6	-0.56
C38	20	0.0326	0.0005	1.456	45	0.7	-0.43
C39	20	0.0136	0.0002	1.794	47	0.3	-1.30
C40	20	0.0084	0.0010	11.692	52	0.2	-1.78
C41	20	0.0077	0.0003	3.711	60	0.2	-1.87

xxx out of range

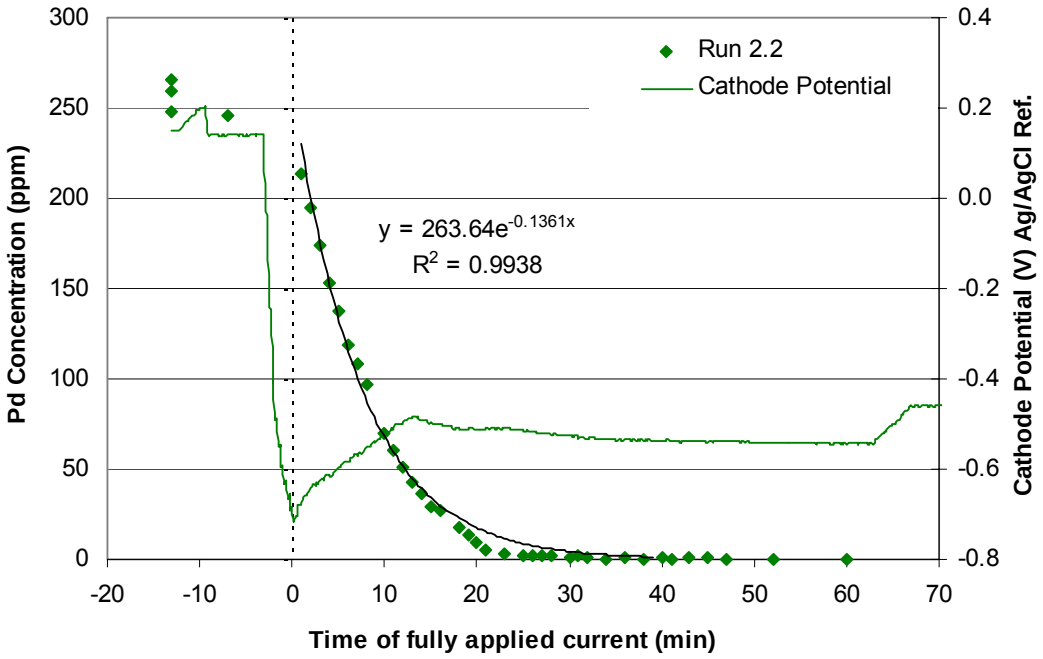


Figure C9 Concentration profile for Run 2.2 with the measured cathode potential shown on the secondary axis

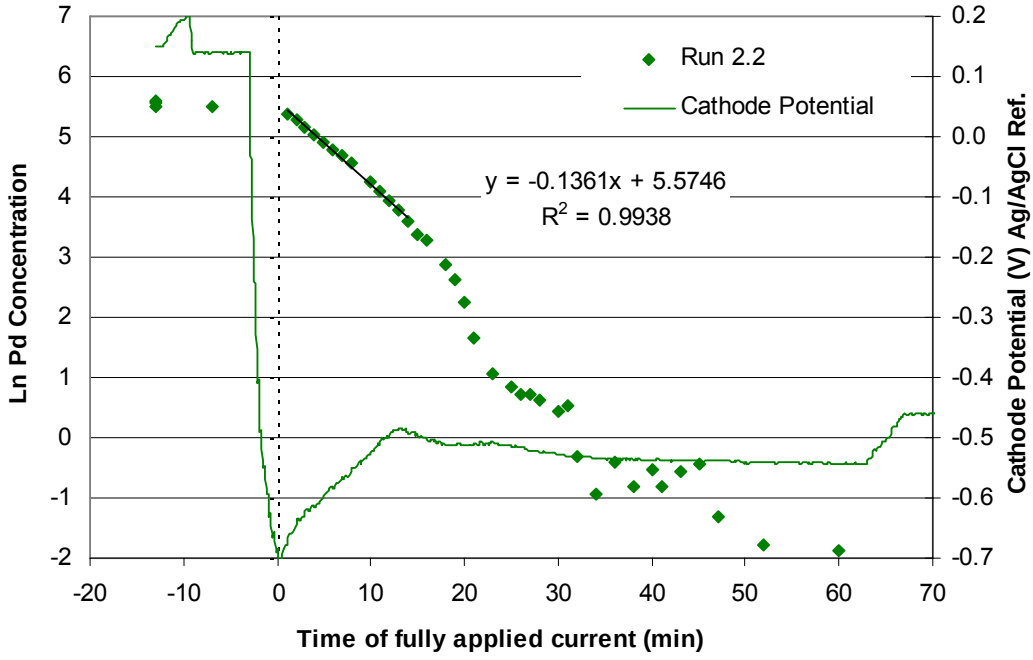


Figure C10 Concentration profile for Run 2.2 indicating the mass transport controlled region with the measured cathode potential shown on the secondary axis

RUN 2.3

Date of experiment:	18/07/03
Catholyte solution:	Pd SMISIE
Constant applied current:	0.8 A
Flowrate of catholyte:	620 ml/min

Table C9 Catholyte make-up for Run 2.3

NaCl (g)	233.78
$CuCl_2.2H_2O$ (g)	0
Pd Stock Solution (10 g/l Pd in 20% HCl) (ml)	80
NH_4Ac (g)	308.41
CH_3COOH (ml)	230

Table C10 pH values of electrolytes for Run 2.3

	Catholyte	**Anolyte**
pH at start of experiment	4.466	2.403
pH at end of experiment	4.510	2.182

Table C11 Volumes of electrolytes in reservoirs for Run 2.3

	Catholyte	**Anolyte**
Volume at the start of experiment (ml)	4010	4060
Volume at the end of experiment (ml)	3820	4090

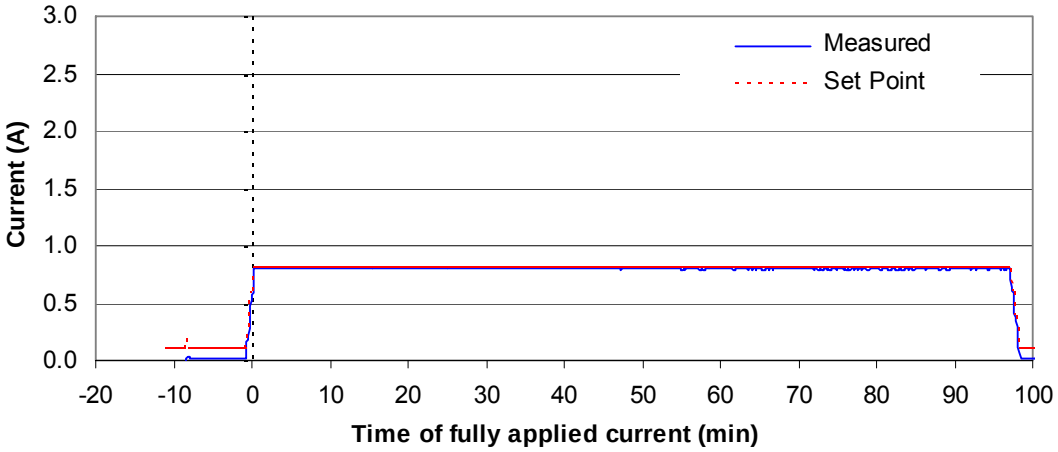


Figure C11 Current applied during Run 2.3

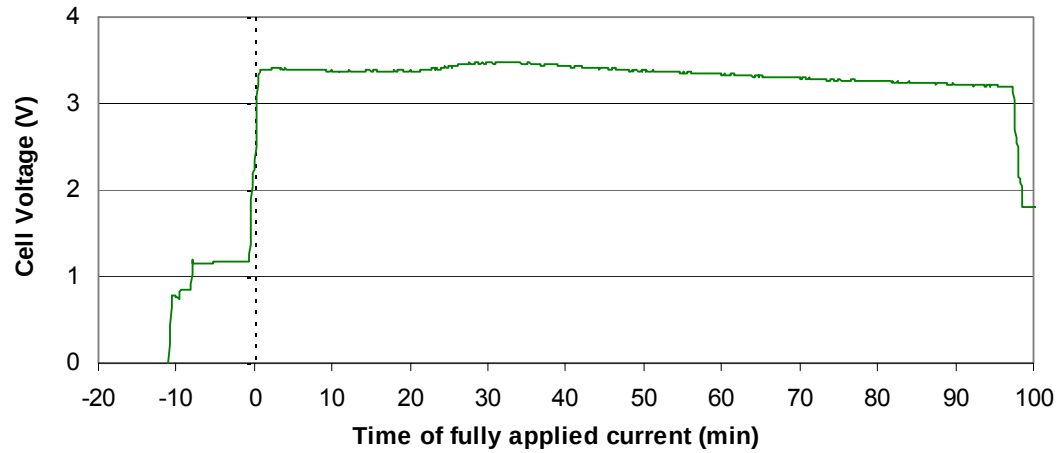


Figure C12 Cell voltage measured during Run 2.3

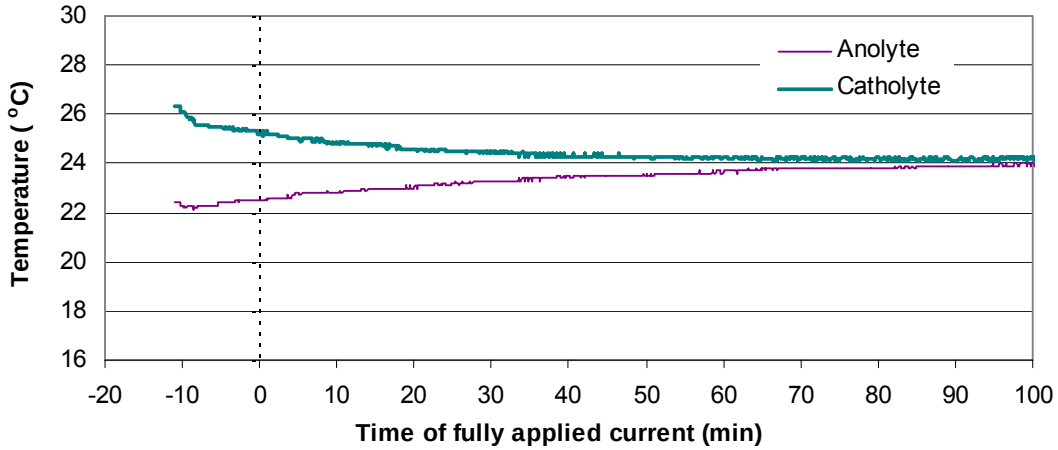


Figure C13 Temperatures of electrolytes measured during Run 2.3

Table C12 ICP results for Run 2.3

Sample ID	Dilution	x	s	sr	Time (min)	Conc (ppm)	Ln Conc
C10 (head)	400	0.663	0.0026	0.390	-11	232.2	5.45
C20 (head)	200	1.214	0.01	0.826	-11	242.8	5.49
C30 (head)	200	1.226	0.019	1.549	-11	245.2	5.50
C1	400	0.6300	0.0036	0.566	-6	220.7	5.40
C2	400	0.6240	0.0059	0.940	1	218.6	5.39
C3	400	0.5920	0.0041	0.688	2	207.4	5.33
C4	400	0.5850	0.0013	0.227	3	204.9	5.32
C5	400	0.5460	0.0016	0.291	4	191.2	5.25
C6	400	0.5590	0.0053	0.943	5	195.8	5.28
C7	400	0.5310	0.0025	0.464	6	186.0	5.23
C8	200	1.0520	0.0063	0.600	7	184.2	5.22
C9	400	0.5050	0.0012	0.229	8	176.9	5.18
C11	400	0.4795	0.0021	0.432	9	168.0	5.12
C12	200	0.9640	0.0027	0.277	10	168.8	5.13
C13	200	0.9420	0.0026	0.272	11	165.0	5.11
C14	200	0.8590	0.0006	0.068	13	150.4	5.01
C15	200	0.8050	0.0028	0.347	14	141.0	4.95
C16	200	0.7800	0.0064	0.816	15	136.6	4.92
C17	200	0.7200	0.0089	1.235	16	126.1	4.84
C18	200	0.5700	0.0025	0.444	18	114.0	4.74
C19	200	0.5410	0.0011	0.204	19	108.2	4.68
C21	200	0.5170	0.0013	0.250	20	103.4	4.64
C22	200	0.4234	0.0022	0.521	22	84.7	4.44
C23	200	0.3830	0.0015	0.398	23	76.6	4.34
C24	200	0.3574	0.0029	0.799	24	71.5	4.27
C25	200	0.3122	0.0000	0.010	25	62.4	4.13
C26	200	0.2804	0.0005	0.182	26	56.1	4.03
C27	200	0.2482	0.0006	0.243	27	49.6	3.90
C28	200	0.2113	0.0005	0.248	29	42.3	3.74
C29	200	0.1902	0.0054	2.834	30	38.0	3.64
C31	200	0.1524	0.0009	0.578	31	30.5	3.42
C32	200	0.1344	0.0018	1.338	32	26.9	3.29
C33	20	1.2780	0.0047	0.368	33	25.6	3.24
C35	20	1.1400	0.0031	0.270	34	22.8	3.13
C36	20	0.7580	0.0069	0.916	37	15.2	2.72
C37	20	0.6650	0.0058	0.871	38	13.3	2.59
C38	20	0.5080	0.0016	0.313	40	10.2	2.32
C39	20	0.4385	0.0031	0.718	41	8.8	2.17
C40	20	0.3888	0.0033	0.837	42	7.8	2.05
C41	20	0.2965	0.0020	0.678	44	5.9	1.78
C42	20	0.2539	0.0024	0.927	45	5.1	1.62
C43	20	0.2286	0.0012	0.547	46	4.6	1.52
C44	20	0.1688	0.0016	0.928	48	3.4	1.22
C45	20	0.1450	0.0009	0.598	49	2.9	1.06
C46	20	0.1097	0.0016	1.413	51	2.2	0.79
C34	20	0.0894	0.0008	0.933	53	1.8	0.58
C47	20	0.0686	0.0006	0.815	54	1.4	0.32
C48	20	0.0557	0.0001	0.248	56	1.1	0.11
C49	20	0.0363	0.0006	1.517	58	0.7	-0.32
C50	20	0.0333	0.0008	2.286	60	0.7	-0.41
C51	20	0.0261	0.0002	0.702	62	0.5	-0.65
C52	20	0.0164	0.0003	1.974	65	0.3	-1.11
C53	20	0.0149	0.0002	1.288	67	0.3	-1.21
C54	20	0.0131	0.0001	0.725	69	0.3	-1.34
C55	20	0.0098	0.0004	4.427	71	0.2	-1.63
C56	20	0.0093	0.0000	0.395	73	0.2	-1.68
C57	20	0.0128	0.0006	4.691	78	0.3	-1.36
C58	20	0.0081	0.0002	2.151	83	0.2	-1.82
C59	20	0.0084	0.0002	2.368	89	0.2	-1.78
C60	20	0.0073	0.0004	5.281	94	0.1	-1.92

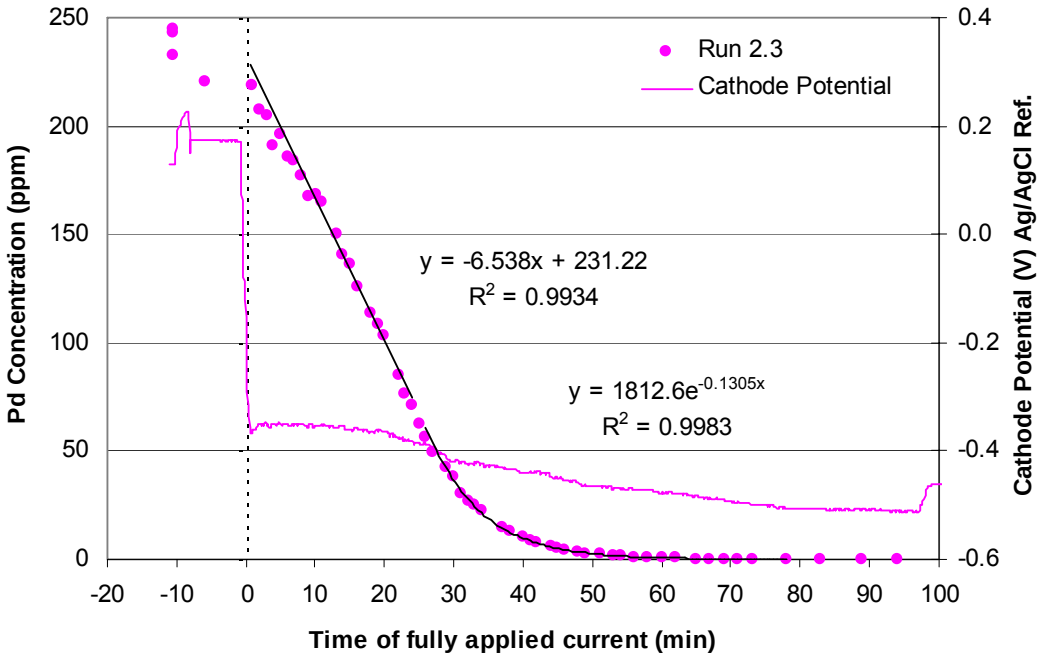


Figure C14 Concentration profile for Run 2.3 with the measured cathode potential shown on the secondary axis

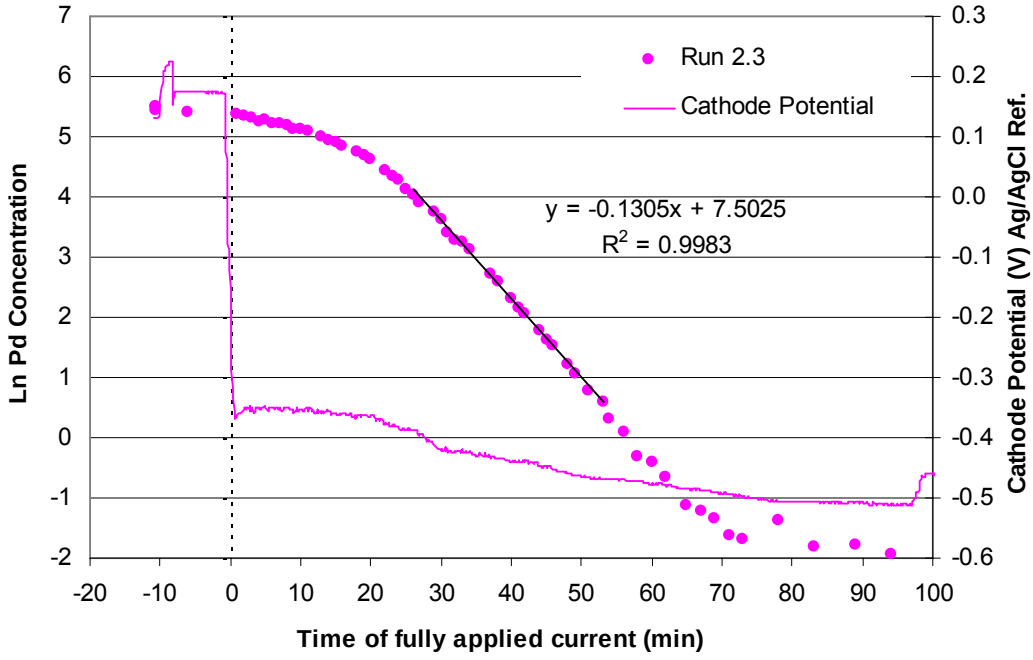


Figure C15 Concentration profile for Run 2.3 indicating the mass transport controlled region with the measured cathode potential shown on the secondary axis

RUN 2.4

Date of experiment:	21/07/03
Catholyte solution:	Pd SMISIE
Constant applied current:	2.6 A
Flowrate of catholyte:	620 ml/min

Table C13 Catholyte make-up for Run 2.4

NaCl (g)	233.74
$CuCl_2.2H_2O$ (g)	0
Pd Stock Solution (10 g/l Pd in 20% HCl) (ml)	80
NH_4Ac (g)	308.32
CH_3COOH (ml)	230

Table C14 pH values of electrolytes for Run 2.4

	Catholyte	**Anolyte**
pH at start of experiment	4.451	2.950
pH at end of experiment	4.486	1.973

Table C15 Volumes of electrolytes in reservoirs for Run 2.4

	Catholyte	**Anolyte**
Volume at the start of experiment (ml)	3990	4090
Volume at the end of experiment (ml)	3870	4120

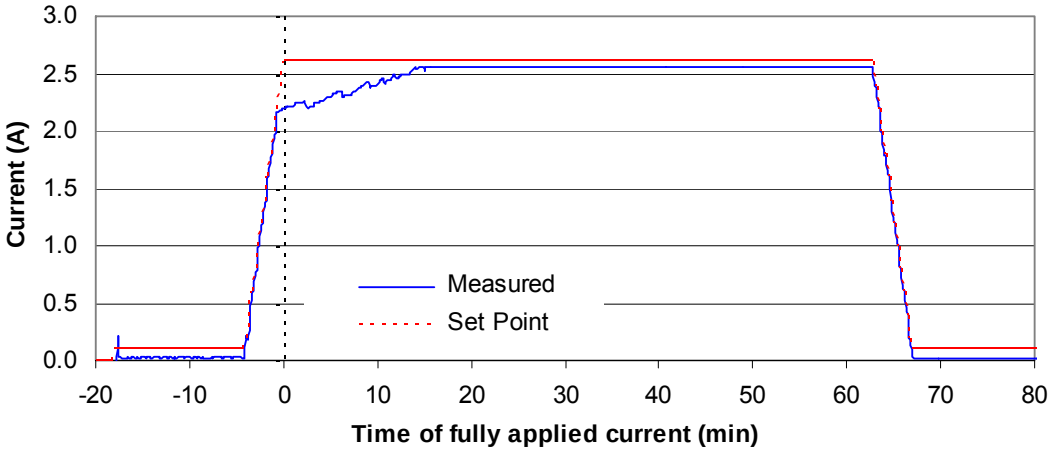


Figure C16 Current applied during Run 2.4

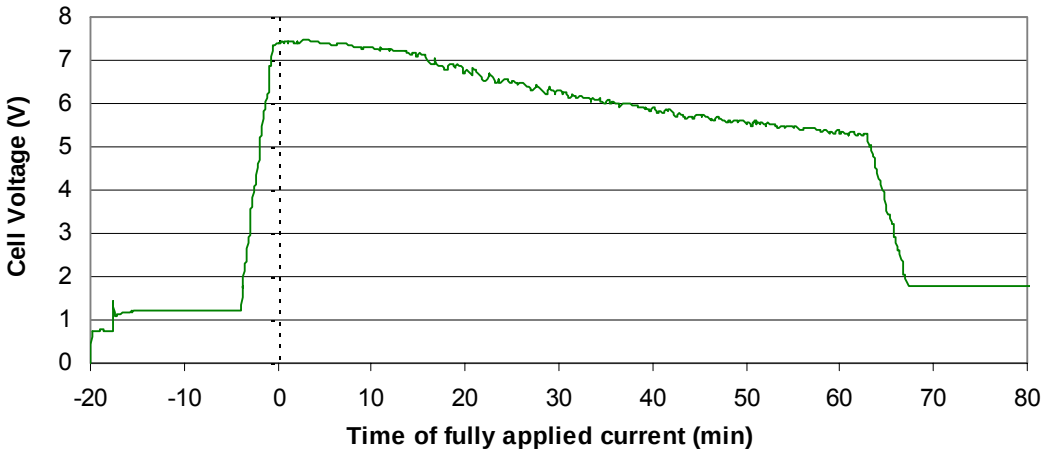


Figure C17 Cell voltage measured during Run 2.4

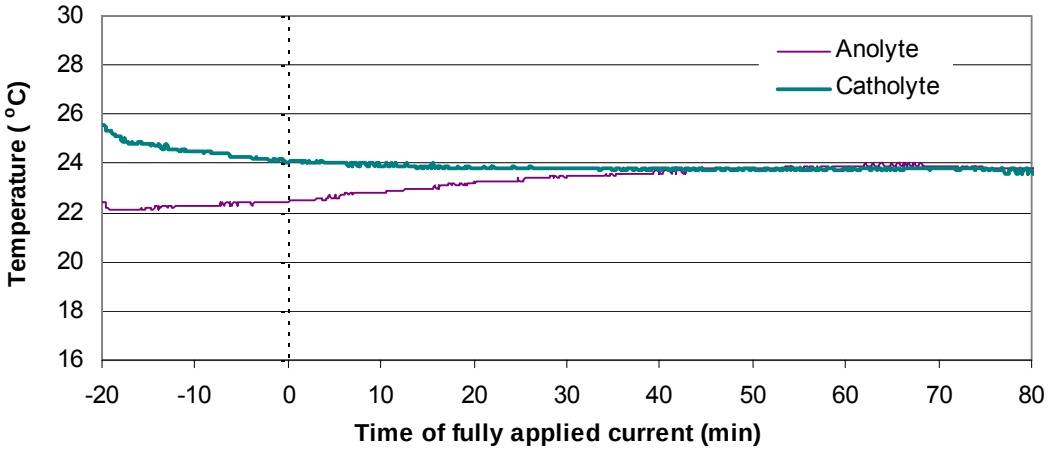


Figure C18 Temperatures of electrolytes measured during Run 2.4

Table C16 ICP results for Run 2.4

Sample ID	Dilution	x	s	sr	Time (min)	Conc (ppm)	Ln Conc
C3 (head)	400	0.632	0.0042	0.670	-18	252.8	5.53
C5 (head)	400	0.622	0.0035	0.566	-18	248.8	5.52
C9 (head)	400	0.633	0.0056	0.882	-18	253.2	5.53
C1	400	0.6030	0.0032	0.531	-12	241.2	5.49
C2	400	0.4763	0.0031	0.645	1	190.5	5.25
C4	200	0.8730	0.0020	0.231	2	174.6	5.16
C6	200	0.7850	0.0019	0.237	3	157.0	5.06
C7	200	0.7040	0.0042	0.593	4	140.8	4.95
C8	200	0.6500	0.0026	0.407	5	130.0	4.87
C10	200	0.5690	0.0044	0.769	6	113.8	4.73
C11	200	0.4356	0.0024	0.557	8	87.1	4.47
C12	200	0.3944	0.0017	0.421	9	78.9	4.37
C13	200	0.3523	0.0006	0.176	10	70.5	4.26
C14	200	0.3153	0.0030	0.951	11	63.1	4.14
C15	200	0.2743	0.0014	0.519	12	54.9	4.00
C16	200	0.2437	0.0017	0.696	13	48.7	3.89
C17	200	0.2143	0.0021	0.960	14	42.9	3.76
C18	200	0.1866	0.0005	0.274	15	37.3	3.62
C19	200	0.1635	0.0008	0.491	16	32.7	3.49
C20	200	0.1346	0.0010	0.774	17	26.9	3.29
C21	200	0.1079	0.0008	0.765	18	21.6	3.07
C22	20	1.0490	0.0022	0.208	19	21.0	3.04
C23	20	0.8390	0.0004	0.053	20	16.8	2.82
C24	20	0.6540	0.0017	0.266	21	13.1	2.57
C25	20	0.4448	0.0023	0.514	22	8.9	2.19
C26	20	0.1320	0.0010	0.732	24	2.6	0.97
C27	20	0.1065	0.0006	0.571	26	2.1	0.76
C28	20	0.0764	0.0004	0.573	28	1.5	0.42
C29	20	0.0554	0.0004	0.768	32	1.1	0.10
C30	20	0.0297	0.0006	1.869	33	0.6	-0.52
C31	20	0.0281	0.0003	1.157	34	0.6	-0.58
C37	20	0.0068	0.0006	9.477	43	0.1	-2.00
C38	20	0.0114	0.0003	3.075	47	0.2	-1.48
C40	20	0.0070	0.0013	18.199	57	0.1	-1.97
C41	20	0.0075	0.0006	7.970	60	0.2	-1.90

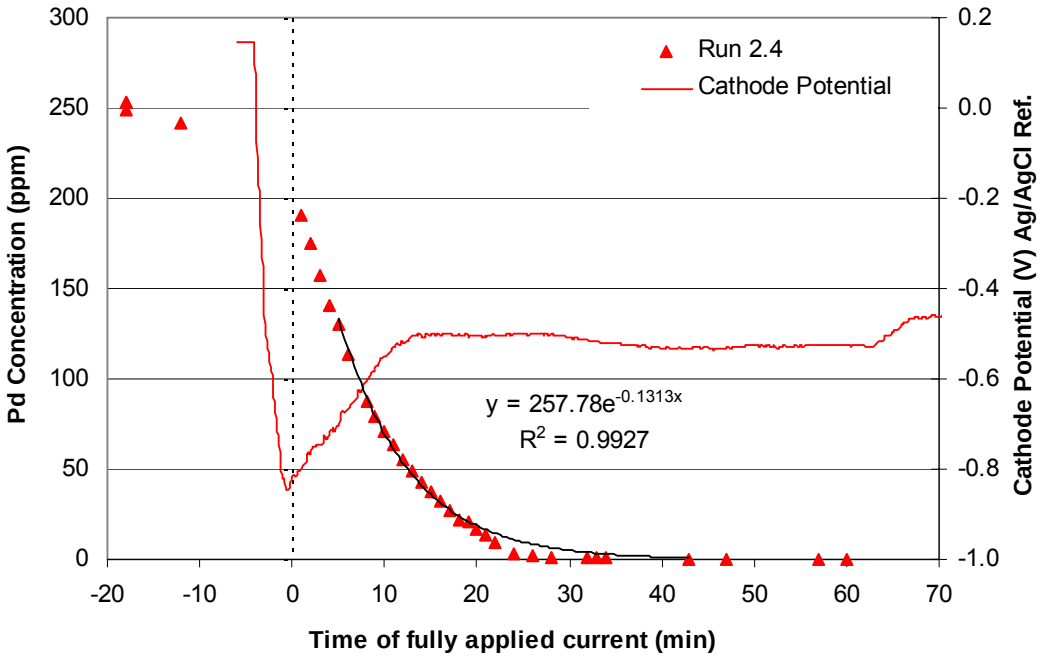


Figure C19 Concentration profile for Run 2.4 with the measured cathode potential shown on the secondary axis

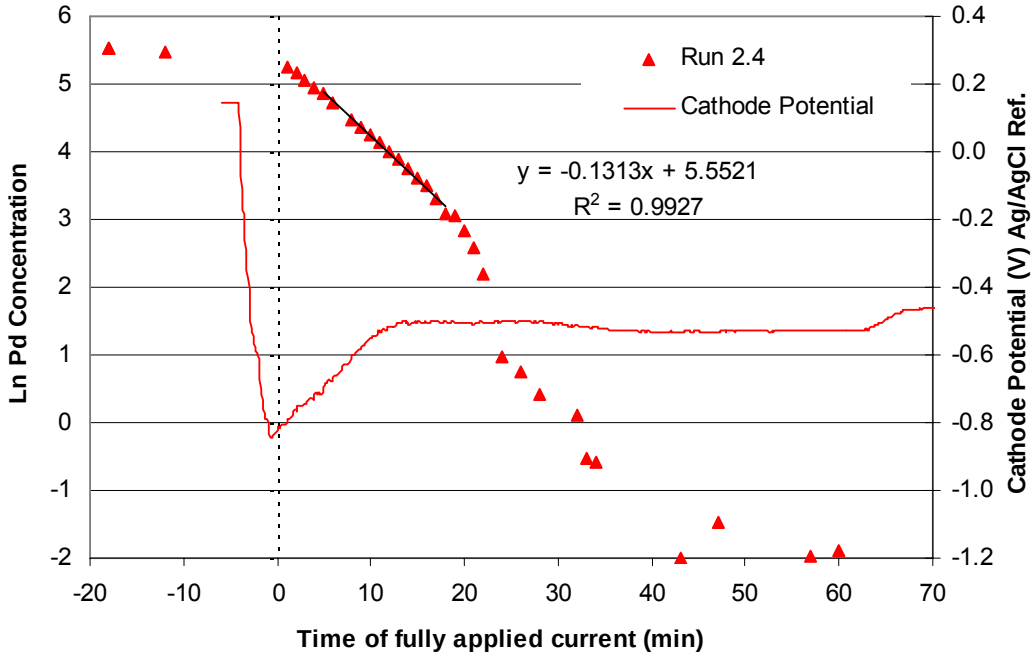


Figure C20 Concentration profile for Run 2.4 indicating the mass transport controlled region with the measured cathode potential shown on the secondary axis

RUN 2.5

Date of experiment:	21/10/03
Catholyte solution:	Pd SMISIE
Constant applied current:	1.4 A
Flowrate of catholyte:	550 ml/min

Table C17 Catholyte make-up for Run 2.5

NaCl (g)	233.76
$CuCl_2.2H_2O$ (g)	0
Pd Stock Solution (10 g/l Pd in 20% HCl) (ml)	80
NH_4Ac (g)	308.35
CH_3COOH (ml)	230

Table C18 pH values of electrolytes for Run 2.5

	Catholyte	**Anolyte**
pH at start of experiment	4.517	3.170
pH at end of experiment	4.532	2.304

Table C19 Volumes of electrolytes in reservoirs for Run 2.5

	Catholyte	**Anolyte**
Volume at the start of experiment (ml)	3980	4090
Volume at the end of experiment (ml)	3890	4130

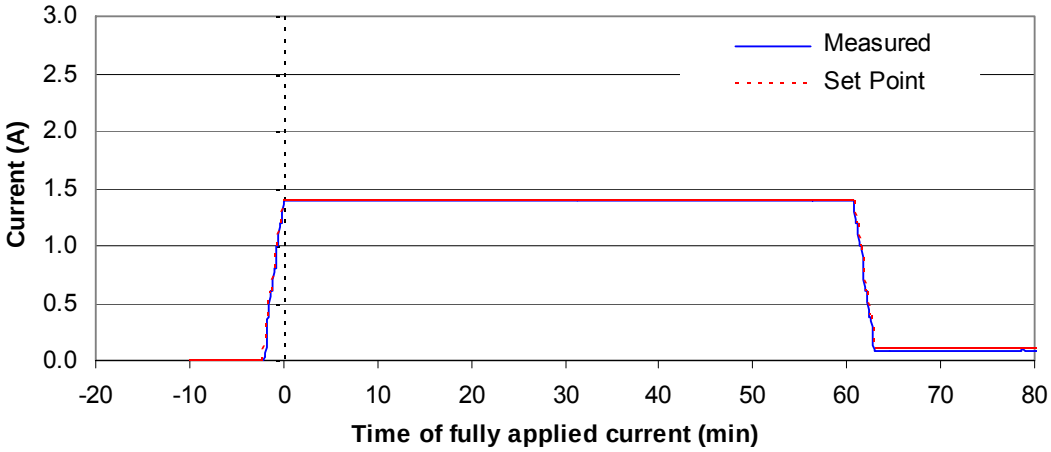


Figure C21 Current applied during Run 2.5

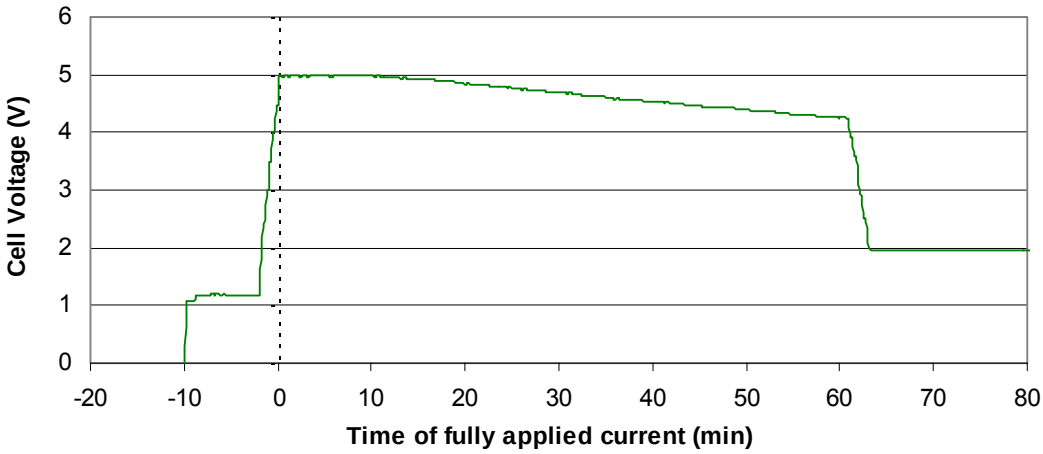


Figure C22 Cell voltage measured during Run 2.5

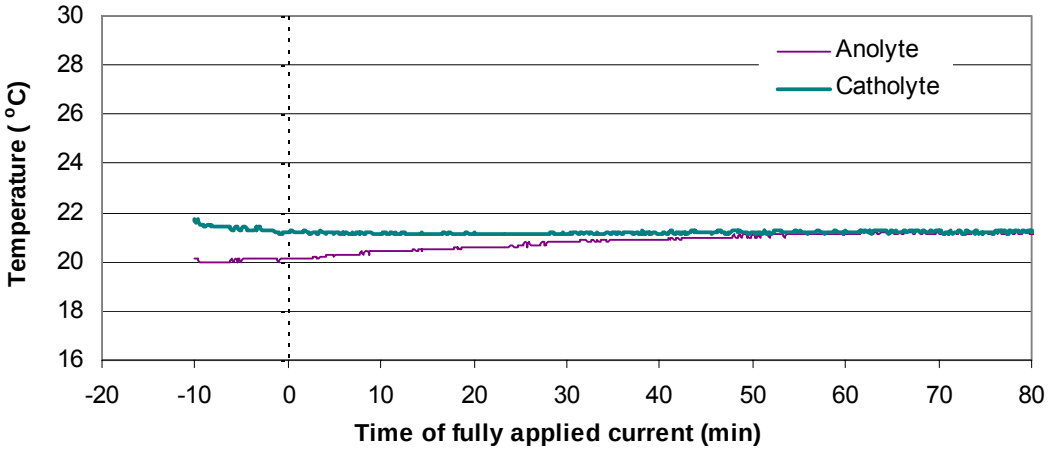


Figure C23 Temperatures of electrolytes measured during Run 2.5

Table C20 ICP results for Run 2.5

Sample ID	Dilution	x	s	sr	Time (min)	Conc (ppm)	Ln Conc
C12 (head)	2 x 200	0.59	0.0043	0.736	-10	236.0	5.46
C17 (head)	2 x 100	1.18	0.0221	1.873	-10	236.0	5.46
C21 (head)	2 x 200	0.585	0.0028	0.487	-10	234.0	5.46
C1	200	0.9870	0.0071	0.719	-6	197.4	5.29
C2	200	0.9590	0.0083	0.867	1	191.8	5.26
C3	200	1.0000	0.0023	0.234	2	200.0	5.30
C4	200	0.8890	0.0063	0.706	4	177.8	5.18
C5	200	0.8330	0.0010	0.121	5	166.6	5.12
C6	200	0.6910	0.0015	0.210	8	138.2	4.93
C7	200	0.6110	0.0081	1.321	10	122.2	4.81
C8	200	0.5130	0.0031	0.605	12	102.6	4.63
C9	200	0.4677	0.0035	0.758	13	93.5	4.54
C10	200	0.4118	0.0055	1.338	15	82.4	4.41
C11	100	0.7430	0.0066	0.885	16	74.3	4.31
C13	100	0.5460	0.0035	0.640	18	54.6	4.00
C14	100	0.4310	0.0040	0.927	20	43.1	3.76
C15	100	0.3675	0.0016	0.430	21	36.8	3.60
C16	100	0.3000	0.0036	1.215	23	30.0	3.40
C18	100	0.2186	0.0043	1.977	24	21.9	3.08
C19	100	0.2034	0.0017	0.854	25	20.3	3.01
C20	100	0.1745	0.0022	1.245	27	17.5	2.86
C22	100	0.1192	0.0028	2.315	29	11.9	2.48
C23	10	1.0450	0.0013	0.126	31	10.5	2.35
C24	10	0.7530	0.0028	0.378	33	7.5	2.02
C25	10	0.5430	0.0050	0.912	35	5.4	1.69
C26	10	0.4230	0.0021	0.494	37	4.2	1.44
C27	10	0.3070	0.0011	0.348	39	3.1	1.12
C28	10	0.2189	0.0011	0.520	41	2.2	0.78
C29	10	0.1681	0.0009	0.552	43	1.7	0.52
C30	10	0.1317	0.0001	0.092	45	1.3	0.28
C31	10	0.0700	0.0004	0.521	49	0.7	-0.36
C32	10	0.0394	0.0002	0.616	53	0.4	-0.93
C33	10	0.0197	0.0005	2.501	58	0.2	-1.62

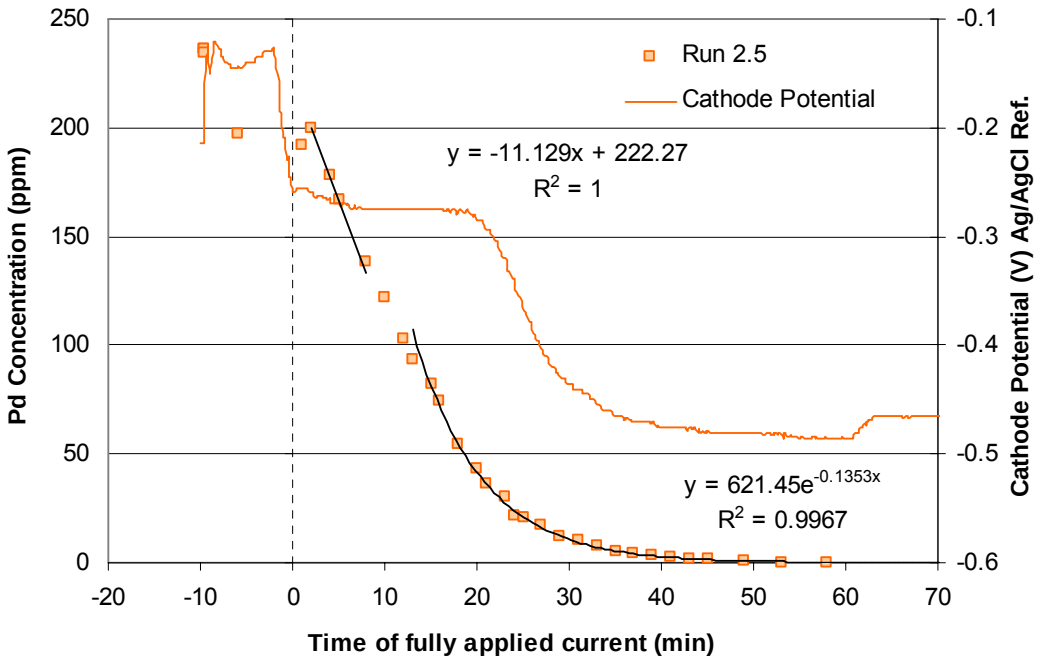


Figure C24 Concentration profile for Run 2.5 with the measured cathode potential shown on the secondary axis

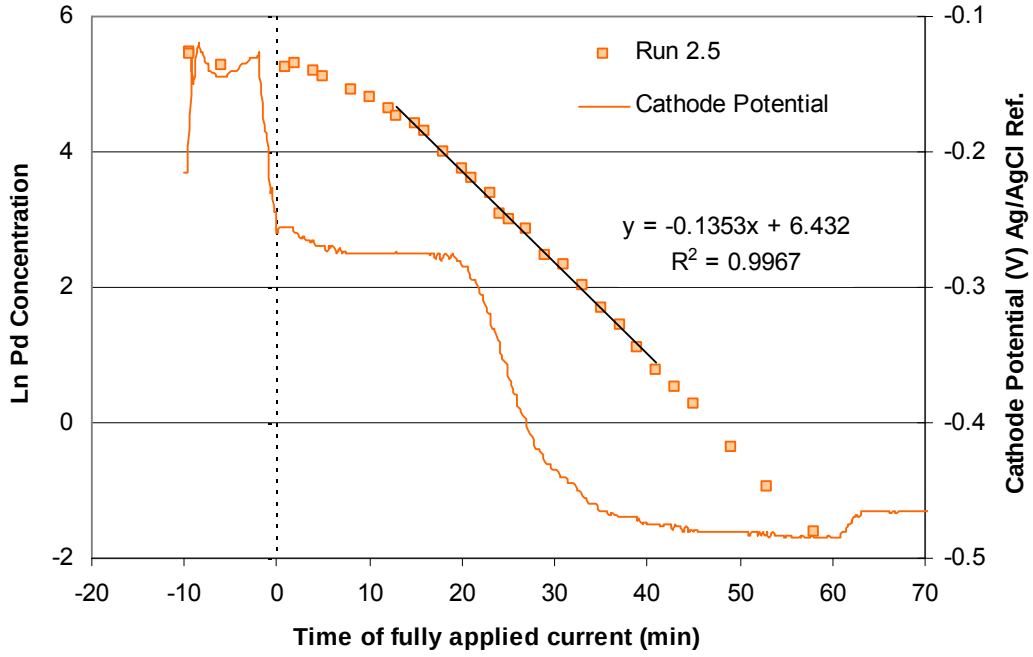


Figure C25 Concentration profile for Run 2.5 indicating the mass transport controlled region with the measured cathode potential shown on the secondary axis

APPENDIX D

Results for Run 3

Cu SMISIE Testwork

RUN 3.1

Date of experiment:	15/10/03
Catholyte solution:	Cu SMISIE
Constant applied current:	1.4 A
Flowrate of catholyte:	530 ml/min

Table D1 Catholyte make-up for Run 3.1

NaCl (g)	233.76
$CuCl_2.2H_2O$ (g)	4.31
Pd Stock Solution (10 g/l Pd in 20% HCl) (ml)	0
NH_4Ac (g)	308.37
CH_3COOH (ml)	230

Table D2 pH values of electrolytes for Run 3.1

	Catholyte	**Anolyte**
pH at start of experiment	4.542	2.120
pH at end of experiment	4.541	1.981

Table D3 Volumes of electrolytes in reservoirs for Run 3.1

	Catholyte	**Anolyte**
Volume at the start of experiment (ml)	4000	4070
Volume at the end of experiment (ml)	3820	4090

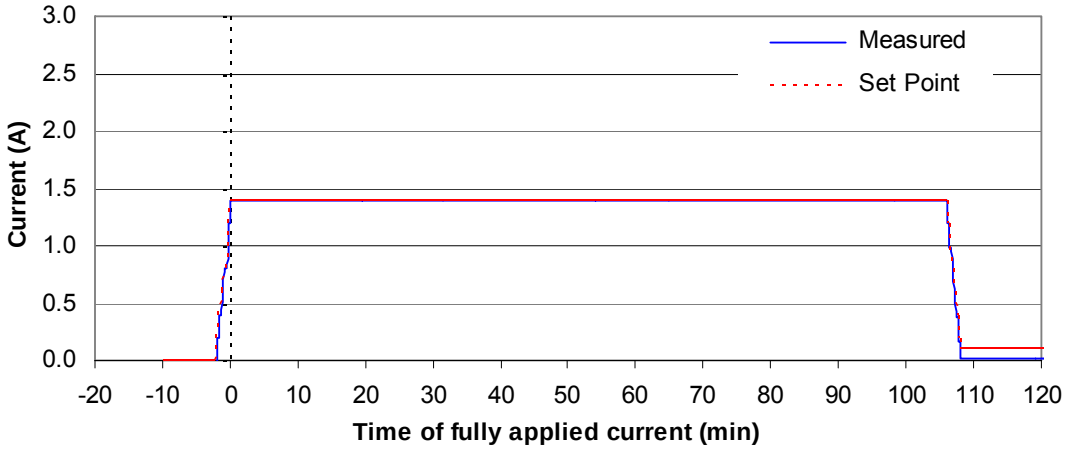


Figure D1 Current applied during Run 3.1

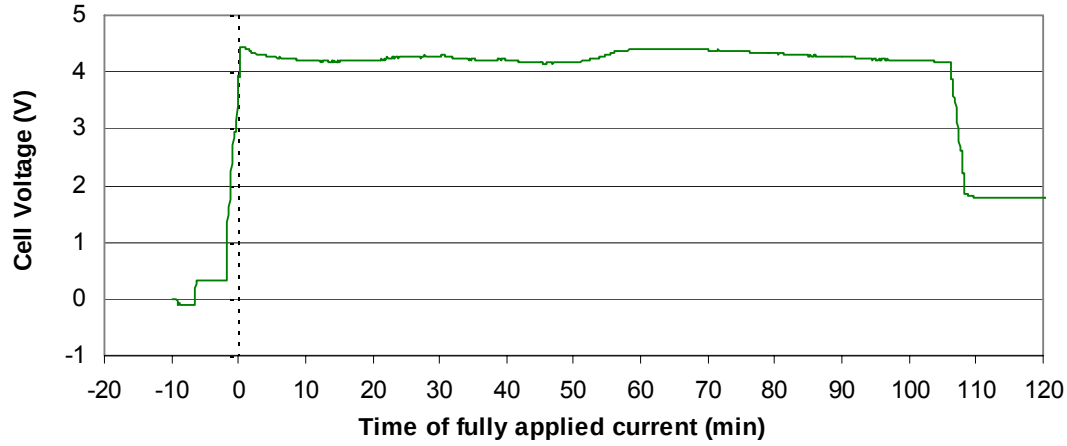


Figure D2 Cell voltage measured during Run 3.1

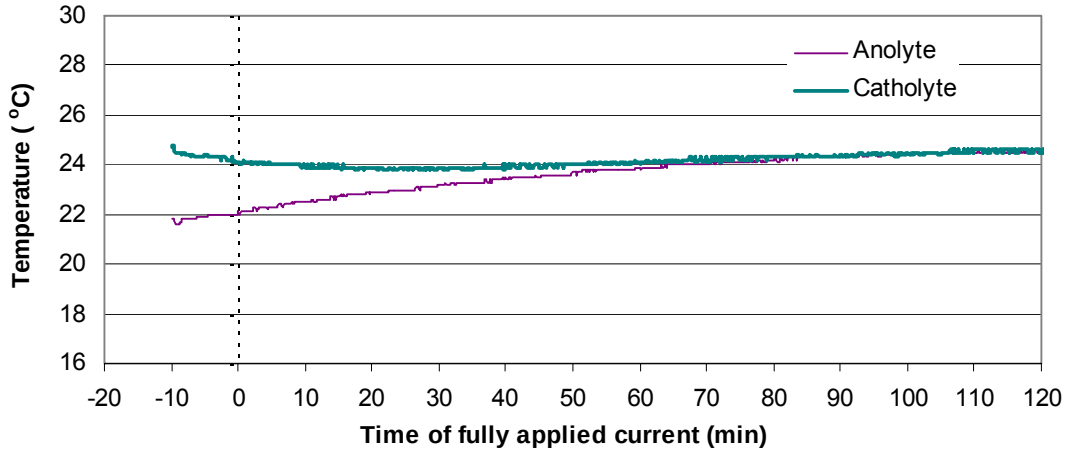


Figure D3 Temperatures of electrolytes measured during Run 3.1

Table D4 ICP results for Run 3.1

Sample ID	Dilution	x	s	sr	Time (min)	Conc (ppm)	Ln Conc
C10 (head)	2 x 400	0.5370	0.0006	0.144	-12	429.6	6.06
C15 (head)	2 x 400	0.5680	0.0007	0.123	-12	454.4	6.12
C20 (head)	2 x 400	0.5380	0.0005	0.090	-12	430.4	6.06
C1	400	1.1000	0.0022	0.202	-6	440.0	6.09
C2	400	1.0940	0.0023	0.214	1	437.6	6.08
C3	400	1.0880	0.0005	0.044	2	435.2	6.08
C4	400	1.0880	0.0086	0.787	3	435.2	6.08
C5	400	1.0830	0.0017	0.160	5	433.2	6.07
C6	400	1.0880	0.0015	0.140	6	435.2	6.08
C7	400	1.0730	0.0099	0.919	7	429.2	6.06
C8	400	1.0050	0.0013	0.130	9	402.0	6.00
C9	400	1.0020	0.0010	0.100	10	400.8	5.99
C11	400	0.9570	0.0026	0.262	12	382.8	5.95
C12	400	1.0240	0.0019	0.183	15	409.6	6.02
C13	400	1.0050	0.0051	0.509	18	402.0	6.00
C14	400	1.0100	0.0012	0.122	19	404.0	6.00
C16	400	1.0040	0.0068	0.681	20	401.6	6.00
C17	400	1.0120	0.0014	0.140	22	404.8	6.00
C18	400	0.9950	0.0008	0.076	23	398.0	5.99
C19	400	1.0080	0.0010	0.097	24	403.2	6.00
C21	400	1.0010	0.0010	0.104	25	400.4	5.99
C22	400	0.9870	0.0080	0.814	27	394.8	5.98
C23	400	0.9760	0.0061	0.626	29	390.4	5.97
C24	400	0.9450	0.0017	0.178	30	378.0	5.93
C25	400	0.8980	0.0060	0.670	31	359.2	5.88
C26	400	0.8460	0.0139	1.642	33	338.4	5.82
C27	200	1.6300	0.0020	0.123	34	326.0	5.79
C28	200	1.6090	0.0025	0.158	36	321.8	5.77
C29	200	1.5000	0.0010	0.069	37	300.0	5.70
C30	200	1.4430	0.0027	0.185	39	288.6	5.67
C31	200	1.3140	0.0062	0.474	41	262.8	5.57
C32	200	1.2400	0.0019	0.152	42	248.0	5.51
C33	200	1.1510	0.0071	0.619	43	230.2	5.44
C34	200	1.0610	0.0014	0.131	45	212.2	5.36
C35	200	1.0270	0.0006	0.061	46	205.4	5.32
C36	200	0.9430	0.0019	0.205	47	188.6	5.24
C37	200	0.8180	0.0051	0.621	49	163.6	5.10
C38	200	0.6840	0.0033	0.480	51	136.8	4.92
C39	100	1.1230	0.0020	0.174	53	112.3	4.72
C40	100	0.8530	0.0034	0.401	55	85.3	4.45
C41	100	0.6250	0.0043	0.691	57	62.5	4.14
C42	20	2.5320	0.0086	0.339	59	50.6	3.92
C43	20	2.2740	0.0155	0.683	60	45.5	3.82
C44	20	1.9490	0.0051	0.264	61	39.0	3.66
C45	20	1.3290	0.0009	0.067	64	26.6	3.28
C46	10	2.3340	0.0054	0.231	65	23.3	3.15
C47	10	2.0030	0.0049	0.247	66	20.0	3.00
C48	10	1.5780	0.0086	0.543	68	15.8	2.76
C49	10	1.3450	0.0073	0.541	69	13.5	2.60
C50	10	1.0880	0.0036	0.335	71	10.9	2.39
C51	10	0.8080	0.0039	0.482	73	8.1	2.09
C52	10	0.6570	0.0032	0.495	75	6.6	1.88
C53	10	0.4840	0.0025	0.519	77	4.8	1.58
C54	10	0.3719	0.0050	1.357	79	3.7	1.31
C55	10	0.2760	0.0011	0.392	82	2.8	1.02
C56	10	0.1684	0.0012	0.728	86	1.7	0.52
C57	10	0.0958	0.0003	0.283	92	1.0	-0.04
C58	10	0.0607	0.0006	0.995	98	0.6	-0.50
C59	10	0.0434	0.0003	0.620	103	0.4	-0.83

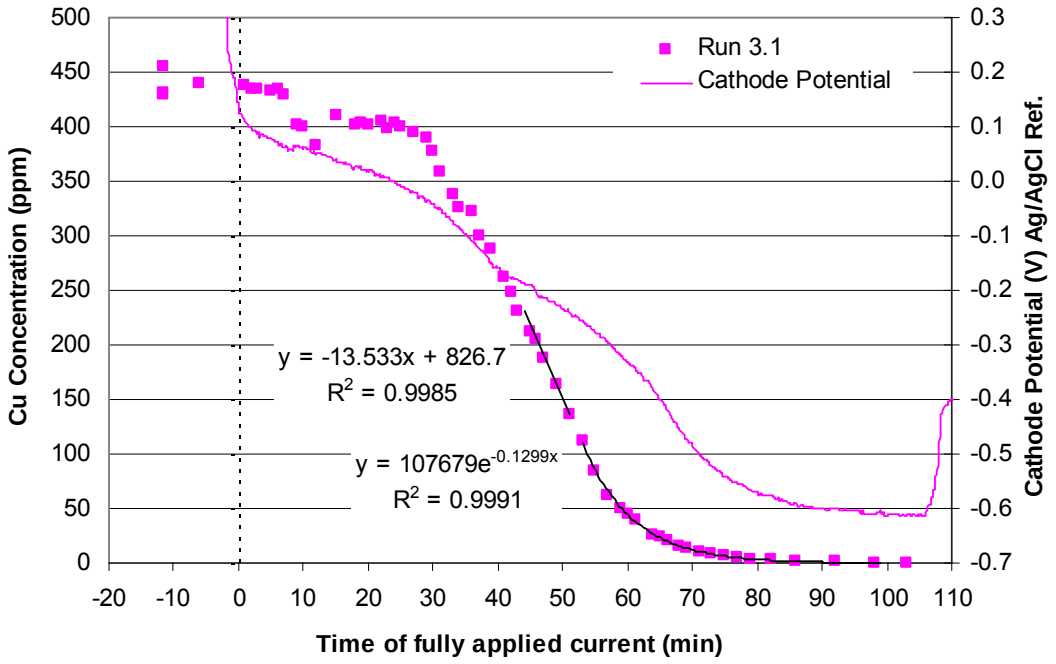


Figure D4 Concentration profile for Run 3.1 with the measured cathode potential shown on the secondary axis

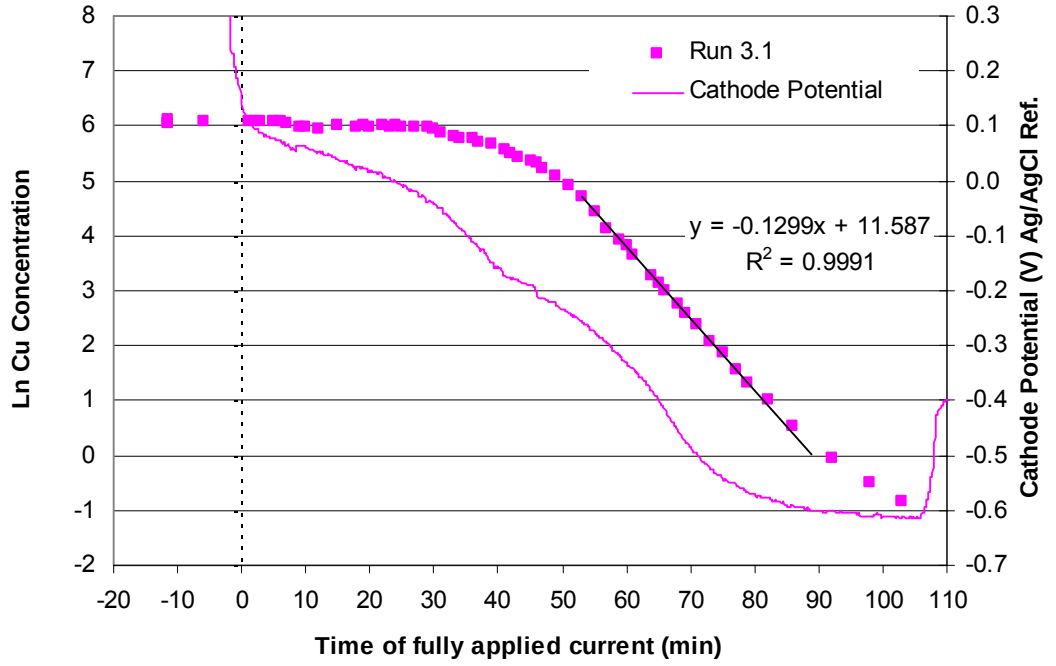


Figure D5 Concentration profile for Run 3.1 indicating the mass transport controlled region with the measured cathode potential shown on the secondary axis

RUN 3.2

Date of experiment:	16/10/03
Catholyte solution:	Cu SMISIE
Constant applied current:	2.6 A
Flowrate of catholyte:	515 ml/min

Table D5 Catholyte make-up for Run 3.2

NaCl (g)	233.76
$CuCl_2.2H_2O$ (g)	4.30
Pd Stock Solution (10 g/l Pd in 20% HCl) (ml)	0
NH_4Ac (g)	308.37
CH_3COOH (ml)	230

Table D6 pH values of electrolytes for Run 3.2

	Catholyte	**Anolyte**
pH at start of experiment	4.538	2.557
pH at end of experiment	4.563	2.011

Table D7 Volumes of electrolytes in reservoirs for Run 3.2

	Catholyte	**Anolyte**
Volume at the start of experiment (ml)	4000	4070
Volume at the end of experiment (ml)	3840	4090

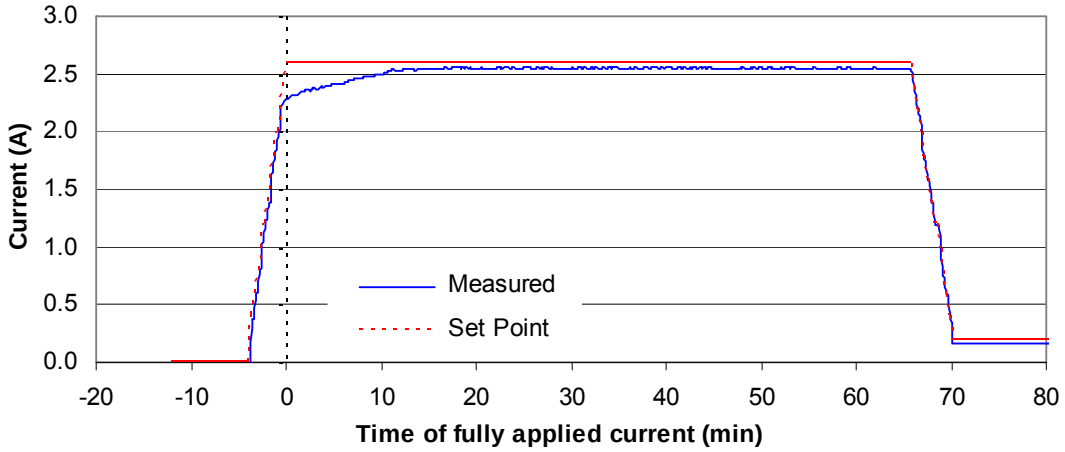


Figure D6 Current applied during Run 3.2

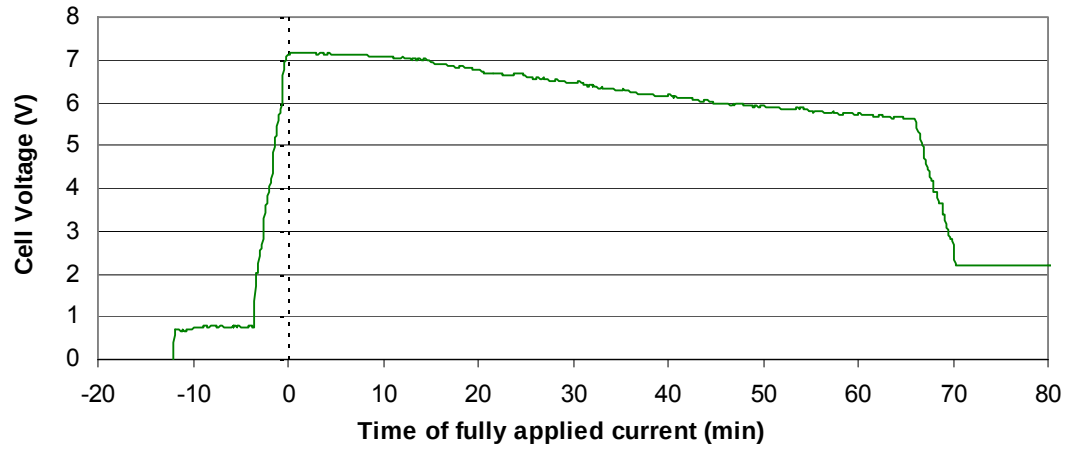


Figure D7 Cell voltage measured during Run 3.2

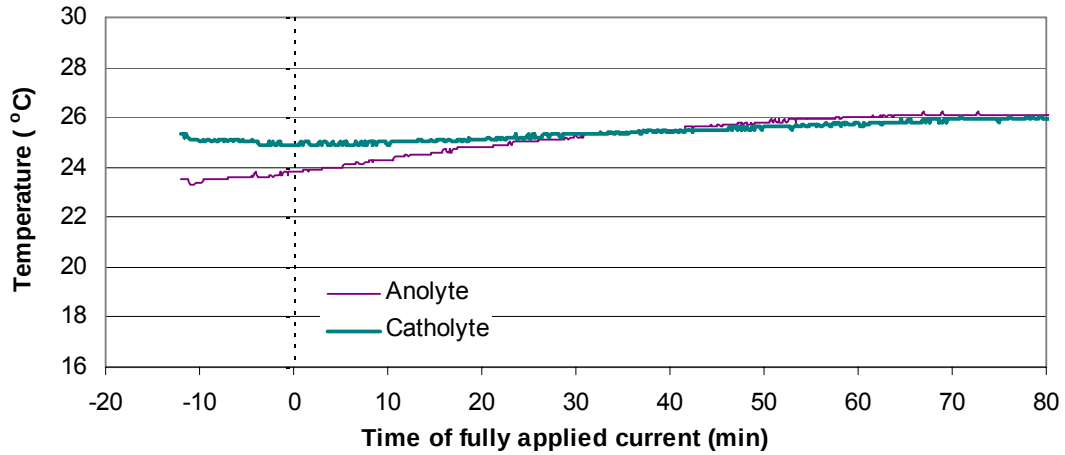


Figure D8 Temperatures of electrolytes measured during Run 3.2

Table D8 ICP results for Run 3.2

Sample ID	Dilution	x	s	sr	Time (min)	Conc (ppm)	Ln Conc
C12 (head)	2 x 400	0.5620	0.0007	0.124	-12	449.6	6.11
C18 (head)	2 x 400	0.5490	0.0016	0.286	-12	439.2	6.08
C24 (head)	2 x 400	0.5460	0.0037	0.676	-12	436.8	6.08
C1	400	1.1100	0.0033	0.301	-8	444.0	6.10
C2	400	1.1030	0.0046	0.419	1	441.2	6.09
C3	400	1.1100	0.0031	0.282	2	444.0	6.10
C4	400	1.1460	0.0057	0.496	4	458.4	6.13
C5	400	1.0920	0.0073	0.669	6	436.8	6.08
C6	400	1.1000	0.0064	0.578	7	440.0	6.09
C7	400	1.0530	0.0069	0.658	8	421.2	6.04
C8	400	1.0770	0.0009	0.087	9	430.8	6.07
C9	400	1.1010	0.0095	0.866	10	440.4	6.09
C10	400	1.0360	0.0025	0.239	12	414.4	6.03
C11	400	1.0360	0.0032	0.312	13	414.4	6.03
C13	400	0.9800	0.0056	0.577	14	392.0	5.97
C14	400	0.9890	0.0076	0.769	15	395.6	5.98
C15	400	1.0040	0.0097	0.965	16	401.6	6.00
C16	400	0.8490	0.0061	0.724	18	339.6	5.83
C17	400	0.7940	0.0032	0.408	19	317.6	5.76
C19	400	0.7380	0.0050	0.672	20	295.2	5.69
C20	400	0.6810	0.0068	0.996	21	272.4	5.61
C21	400	0.6550	0.0011	0.166	22	262.0	5.57
C22	400	0.5590	0.0010	0.179	24	223.6	5.41
C23	400	0.5050	0.0010	0.198	25	202.0	5.31
C25	400	0.4340	0.0060	1.372	26	173.6	5.16
C26	400	0.3752	0.0043	1.142	27	150.1	5.01
C27	200	0.6150	0.0012	0.193	29	123.0	4.81
C28	200	0.5270	0.0013	0.250	30	105.4	4.66
C29	200	0.4749	0.0025	0.520	31	95.0	4.55
C30	200	0.4147	0.0021	0.511	32	82.9	4.42
C31	200	0.3229	0.0006	0.196	34	64.6	4.17
C32	200	0.2853	0.0015	0.541	35	57.1	4.04
C33	200	0.2542	0.0012	0.470	36	50.8	3.93
C34	200	0.2203	0.0004	0.166	37	44.1	3.79
C35	200	0.1982	0.0009	0.452	38	39.6	3.68
C36	200	0.1715	0.0001	0.071	39	34.3	3.54
C37	200	0.1286	0.0006	0.496	41	25.7	3.25
C38	200	0.1033	0.0011	1.102	42	20.7	3.03
C39	10	1.8520	0.0040	0.217	43	18.5	2.92
C40	10	1.7140	0.0044	0.255	44	17.1	2.84
C41	10	1.5080	0.0036	0.241	45	15.1	2.71
C42	10	1.1620	0.0044	0.378	47	11.6	2.45
C43	10	0.9000	0.0028	0.315	49	9.0	2.20
C44	10	0.7560	0.0015	0.204	50	7.6	2.02
C45	10	0.6290	0.0005	0.084	52	6.3	1.84
C46	10	0.4840	0.0007	0.153	54	4.8	1.58
C47	10	0.3845	0.0023	0.611	56	3.8	1.35
C48	10	0.2997	0.0003	0.102	58	3.0	1.10
C49	10	0.2127	0.0020	0.960	61	2.1	0.75
C50	10	0.1644	0.0019	1.160	63	1.6	0.50

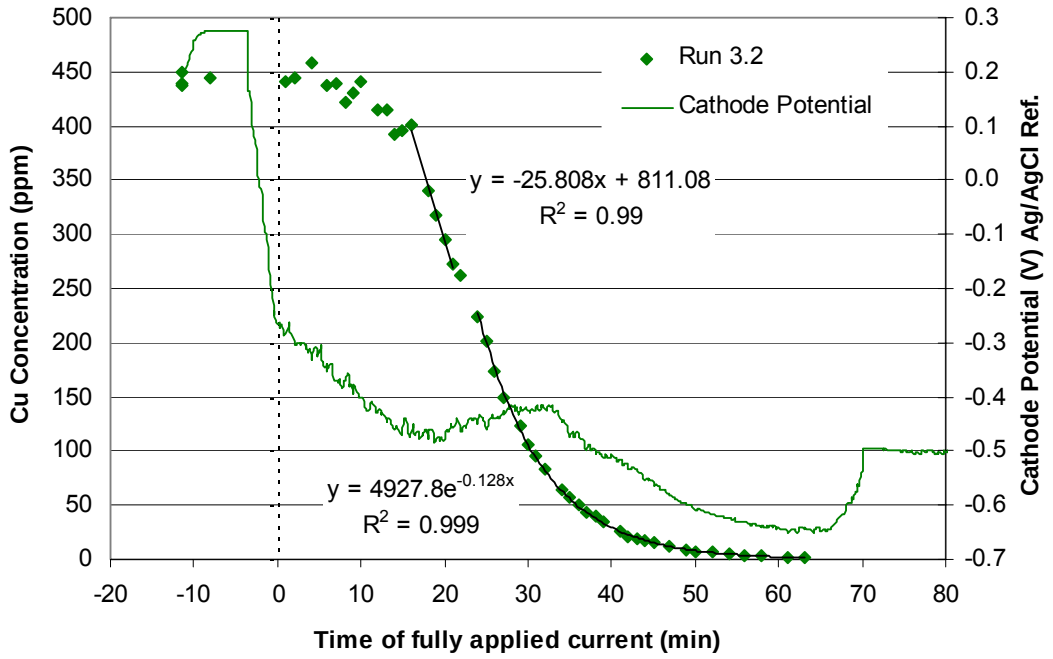


Figure D9 Concentration profile for Run 3.2 with the measured cathode potential shown on the secondary axis

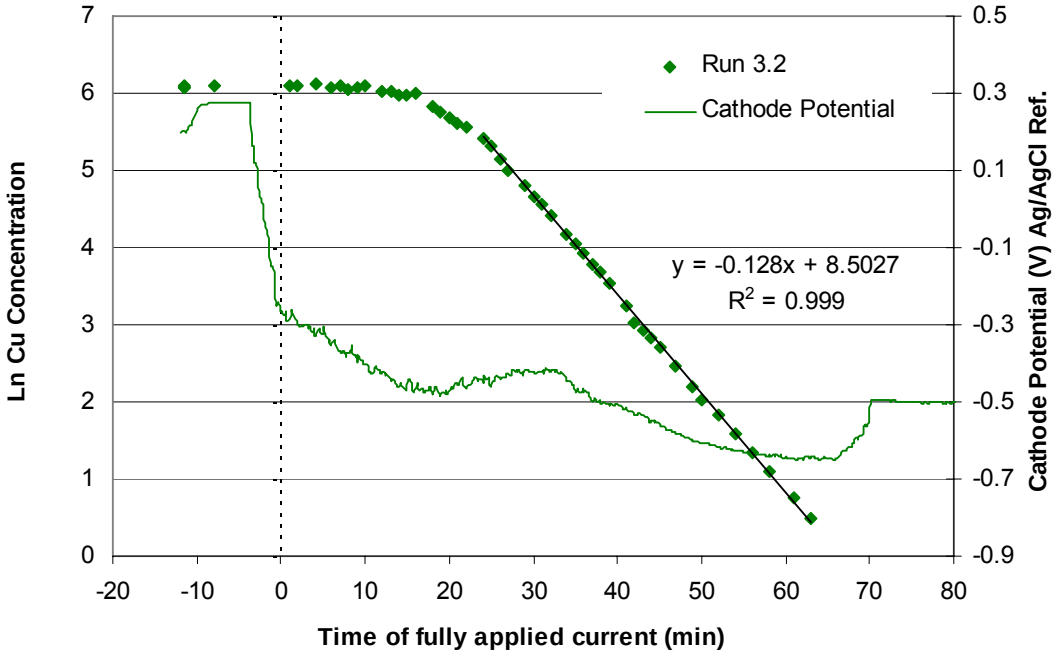


Figure D10 Concentration profile for Run 3.2 indicating the mass transport controlled region with the measured cathode potential shown on the secondary axis

RUN 3.3

Date of experiment:	17/10/03
Catholyte solution:	Cu SMISIE
Constant applied current:	2.0 A
Flowrate of catholyte:	495 ml/min

Table D9 Catholyte make-up for Run 3.3

NaCl (g)	233.76
$CuCl_2.2H_2O$ (g)	4.31
Pd Stock Solution (10 g/l Pd in 20% HCl) (ml)	0
NH_4Ac (g)	308.37
CH_3COOH (ml)	230

Table D10 pH values of electrolytes for Run 3.3

	Catholyte	**Anolyte**
pH at start of experiment	4.532	2.583
pH at end of experiment	4.550	2.061

Table D11 Volumes of electrolytes in reservoirs for Run 3.3

	Catholyte	**Anolyte**
Volume at the start of experiment (ml)	4010	4070
Volume at the end of experiment (ml)	3870	4100

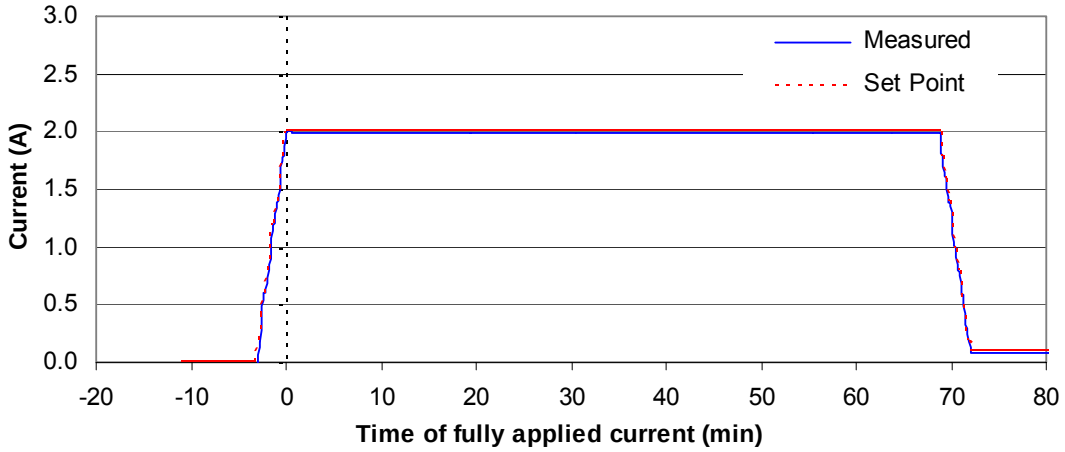


Figure D11 Current applied during Run 3.3

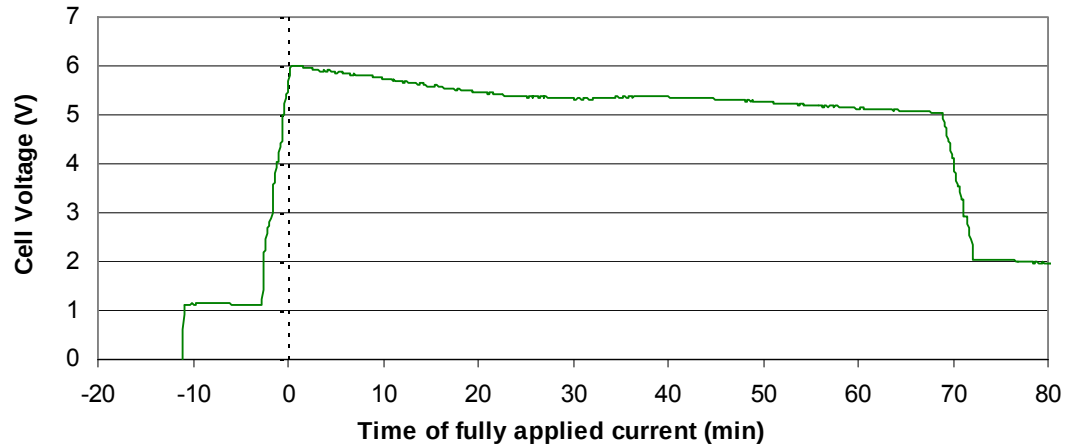


Figure D12 Cell voltage measured during Run 3.3

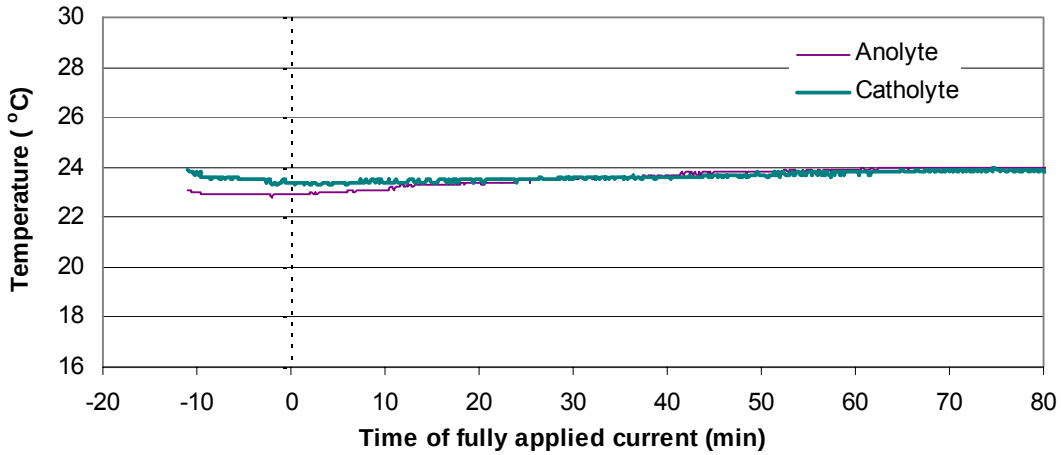


Figure D13 Temperatures of electrolytes measured during Run 3.3

Table D12 ICP results for Run 3.3

Sample ID	Dilution	x	s	sr	Time (min)	Conc (ppm)	Ln Conc
C9 (head)	2 x 400	0.5430	0.0006	0.113	-12	434.4	6.07
C12 (head)	2 x 400	0.6170	0.0011	0.179	-12	493.6	6.20
C16 (head)	2 x 400	0.4981	0.0045	0.909	-12	398.5	5.99
C1	400	1.2880	0.0050	0.387	-7	515.2	6.24
C2	400	1.6020	0.0053	0.328	1	640.8	6.46
C3	400	1.6140	0.0081	0.499	2	645.6	6.47
C4	400	1.6240	0.0047	0.290	3	649.6	6.48
C5	400	1.5560	0.0079	0.509	4	622.4	6.43
C6	400	1.6470	0.0136	0.825	6	658.8	6.49
C7	400	1.4100	0.0082	0.585	8	564.0	6.34
C8	400	1.3830	0.0063	0.453	10	553.2	6.32
C10	400	1.2900	0.0050	0.388	12	516.0	6.25
C11	400	1.2130	0.0038	0.310	14	485.2	6.18
C13	400	1.1260	0.0087	0.770	16	450.4	6.11
C14	400	1.0460	0.0078	0.749	18	418.4	6.04
C15	400	0.9820	0.0076	0.778	19	392.8	5.97
C17	400	0.9500	0.0085	0.893	20	380.0	5.94
C18	400	0.8920	0.0050	0.565	22	356.8	5.88
C19	400	0.8660	0.0038	0.441	23	346.4	5.85
C20	400	0.8150	0.0043	0.523	24	326.0	5.79
C21	400	0.7510	0.0044	0.580	26	300.4	5.71
C22	400	0.6350	0.0048	0.757	28	254.0	5.54
C23	400	0.5660	0.0050	0.888	29	226.4	5.42
C24	400	0.5460	0.0008	0.145	30	218.4	5.39
C25	400	0.5240	0.0024	0.457	31	209.6	5.35
C26	400	0.4599	0.0042	0.917	32	184.0	5.21
C27	400	0.4124	0.0035	0.840	33	165.0	5.11
C28	200	0.7170	0.0044	0.616	35	143.4	4.97
C29	200	0.6350	0.0005	0.080	36	127.0	4.84
C30	200	0.5780	0.0062	1.074	37	115.6	4.75
C31	200	0.5050	0.0049	0.963	38	101.0	4.62
C32	200	0.3666	0.0006	0.155	40	73.3	4.29
C33	200	0.3407	0.0017	0.493	41	68.1	4.22
C34	200	0.2985	0.0010	0.349	42	59.7	4.09
C35	200	0.2627	0.0025	0.936	43	52.5	3.96
C36	200	0.2234	0.0020	0.912	44	44.7	3.80
C37	200	0.1919	0.0014	0.735	46	38.4	3.65
C38	200	0.1396	0.0012	0.867	48	27.9	3.33
C39	200	0.1161	0.0011	0.930	49	23.2	3.15
C40	10	2.2950	0.0118	0.514	50	23.0	3.13
C41	10	1.8790	0.0088	0.468	51	18.8	2.93
C42	10	1.6620	0.0046	0.277	52	16.6	2.81
C43	10	1.6660	0.0023	0.140	54	16.7	2.81
C44	10	0.9200	0.0018	0.196	57	9.2	2.22
C45	10	0.6100	0.0027	0.447	60	6.1	1.81
C46	10	0.4834	0.0005	0.107	63	4.8	1.58
C47	10	0.2915	0.0054	1.867	67	2.9	1.07

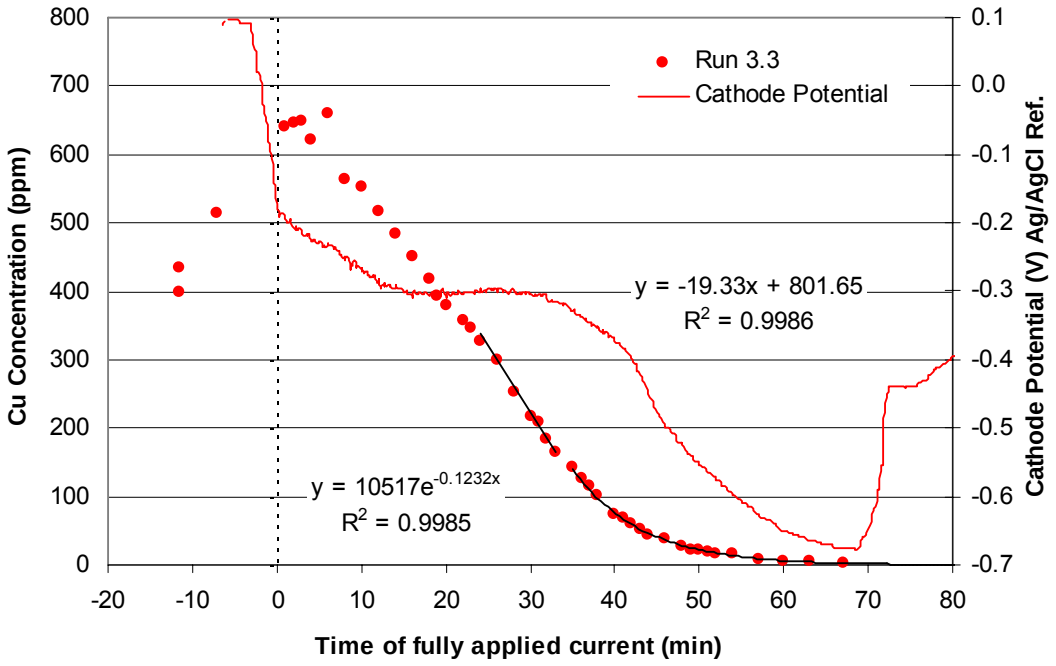


Figure D14 Concentration profile for Run 3.3 with the measured cathode potential shown on the secondary axis

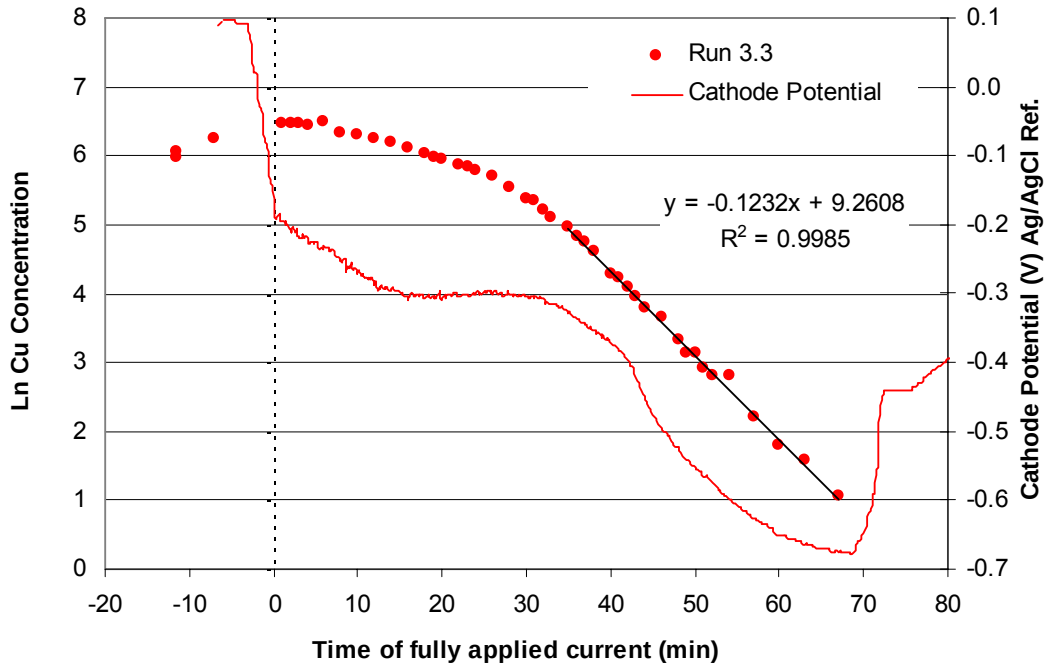


Figure D15 Concentration profile for Run 3.3 indicating the mass transport controlled region with the measured cathode potential shown on the secondary axis

RUN 3.4

Date of experiment:	20/10/03
Catholyte solution:	Cu SMISIE
Constant applied current:	1.4 A
Flowrate of catholyte:	475 ml/min

Table D13 Catholyte make-up for Run 3.4

NaCl (g)	233.77
$CuCl_2.2H_2O$ (g)	4.31
Pd Stock Solution (10 g/l Pd in 20% HCl) (ml)	0
NH_4Ac (g)	308.37
CH_3COOH (ml)	230

Table D14 pH values of electrolytes for Run 3.4

	Catholyte	**Anolyte**
pH at start of experiment	4.550	3.836
pH at end of experiment	4.552	2.345

Table D15 Volumes of electrolytes in reservoirs for Run 3.4

	Catholyte	**Anolyte**
Volume at the start of experiment (ml)	4010	4070
Volume at the end of experiment (ml)	3860	4120

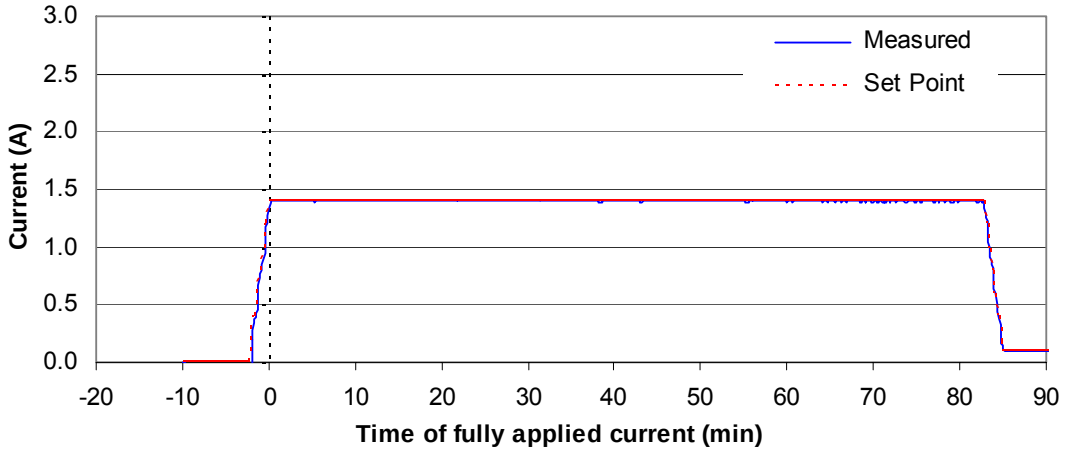


Figure D16 Current applied during Run 3.4

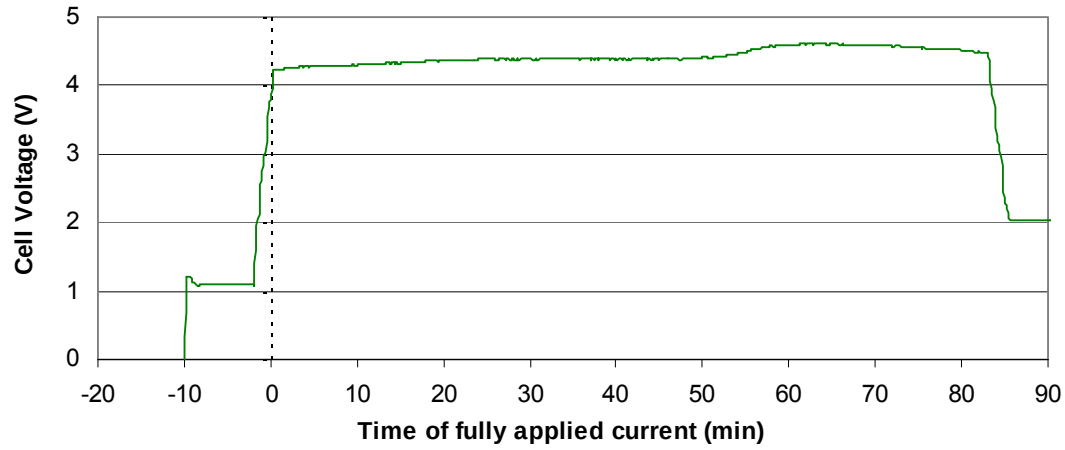


Figure D17 Cell voltage measured during Run 3.4

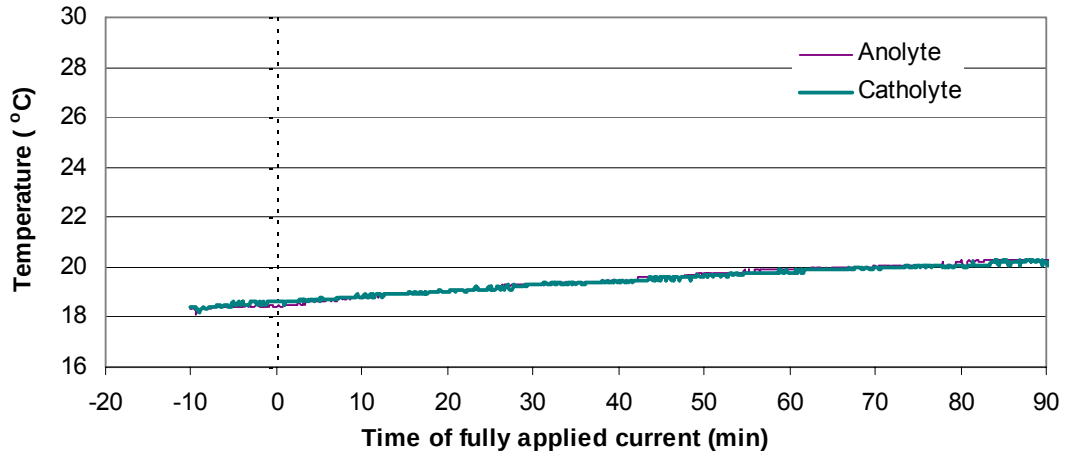


Figure D18 Temperatures of electrolytes measured during Run 3.4

Table D16 ICP results for Run 3.4

Sample ID	Dilution	x	s	sr	Time (min)	Conc (ppm)	Ln Conc
C10 (head)	2 x 500	0.4079	0.0036	0.875	-12	407.9	6.01
C15 (head)	2 x 500	0.2642	0.0010	0.395	-12	264.2	5.58
C20 (head)	2 x 400	0.4896	0.0028	0.564	-12	391.7	5.97
C1	500	0.9830	0.0030	0.304	-6	491.5	6.20
C2	500	1.3520	0.0135	1.002	1	676.0	6.52
C3	500	1.2370	0.0039	0.316	2	618.5	6.43
C4	500	1.2260	0.0126	1.030	3	613.0	6.42
C5	500	1.2440	0.0051	0.412	5	622.0	6.43
C6	500	1.1980	0.0090	0.749	6	599.0	6.40
C7	500	1.2410	0.0067	0.540	8	620.5	6.43
C8	500	1.1520	0.0037	0.318	10	576.0	6.36
C9	500	1.1210	0.0080	0.714	11	560.5	6.33
C11	500	1.1760	0.0082	0.698	12	588.0	6.38
C12	500	1.0790	0.0137	1.268	14	539.5	6.29
C13	500	1.1310	0.0066	0.585	15	565.5	6.34
C14	500	1.1240	0.0035	0.313	16	562.0	6.33
C16	500	1.0250	0.0038	0.374	18	512.5	6.24
C17	500	0.9850	0.0082	0.834	20	492.5	6.20
C18	500	1.0310	0.0115	1.118	22	515.5	6.25
C19	400	1.1850	0.0031	0.259	24	474.0	6.16
C21	400	1.1030	0.0070	0.637	25	441.2	6.09
C22	400	1.0730	0.0080	0.744	26	429.2	6.06
C23	400	1.0160	0.0059	0.585	28	406.4	6.01
C24	400	1.0000	0.0129	1.287	30	400.0	5.99
C25	400	0.8630	0.0043	0.492	32	345.2	5.84
C26	400	0.8670	0.0026	0.301	34	346.8	5.85
C27	400	0.8170	0.0049	0.596	36	326.8	5.79
C28	400	0.7300	0.0038	0.525	38	292.0	5.68
C29	400	0.6740	0.0061	0.900	40	269.6	5.60
C30	400	0.6200	0.0050	0.806	42	248.0	5.51
C31	200	1.1870	0.0117	0.985	44	237.4	5.47
C32	200	0.9940	0.0120	1.208	46	198.8	5.29
C33	200	0.9330	0.0055	0.594	48	186.6	5.23
C34	200	0.7730	0.0011	0.143	50	154.6	5.04
C35	200	0.6780	0.0006	0.084	52	135.6	4.91
C36	200	0.5640	0.0010	0.171	54	112.8	4.73
C37	200	0.4888	0.0012	0.255	55	97.8	4.58
C38	200	0.3776	0.0037	0.978	57	75.5	4.32
C39	200	0.2984	0.0013	0.428	59	59.7	4.09
C40	200	0.2577	0.0025	0.979	60	51.5	3.94
C41	200	0.2284	0.0027	1.194	61	45.7	3.82
C42	200	0.2121	0.0005	0.218	62	42.4	3.75
C43	200	0.1851	0.0029	1.556	63	37.0	3.61
C44	200	0.1420	0.0012	0.864	65	28.4	3.35
C45	200	0.1134	0.0007	0.610	67	22.7	3.12
C46	200	0.0982	0.0006	0.575	68	19.6	2.98
C47	200	0.0802	0.0005	0.665	70	16.0	2.78
C48	200	0.0619	0.0005	0.783	72	12.4	2.52
C49	10	0.8680	0.0011	0.132	75	8.7	2.16
C50	10	0.6050	0.0038	0.620	78	6.1	1.80
C51	10	0.4856	0.0010	0.200	80	4.9	1.58

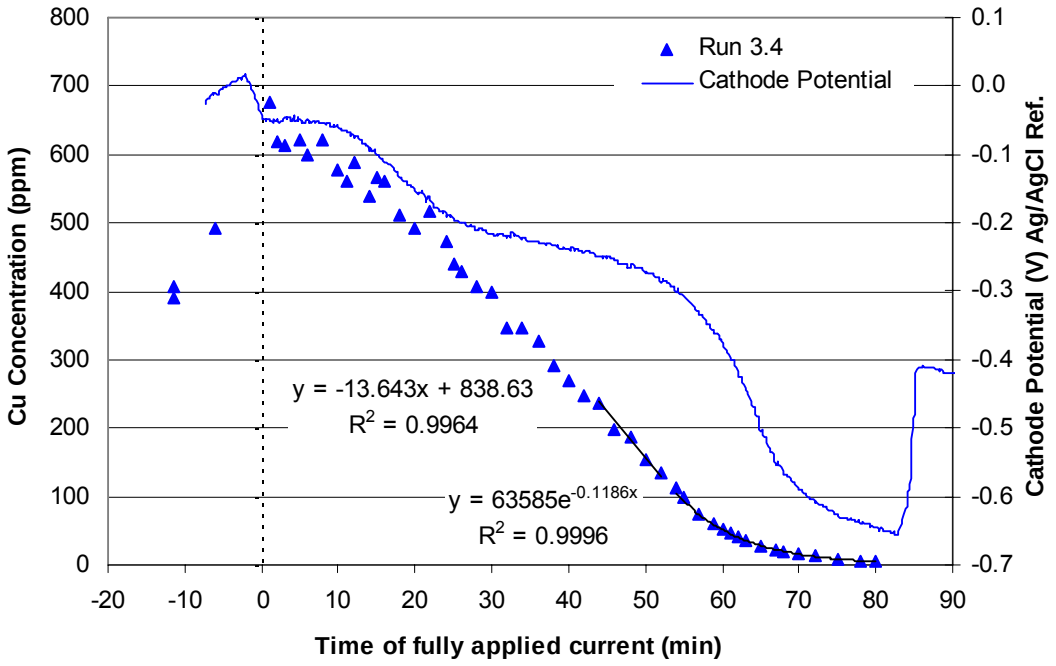


Figure D19 Concentration profile for Run 3.4 with the measured cathode potential shown on the secondary axis

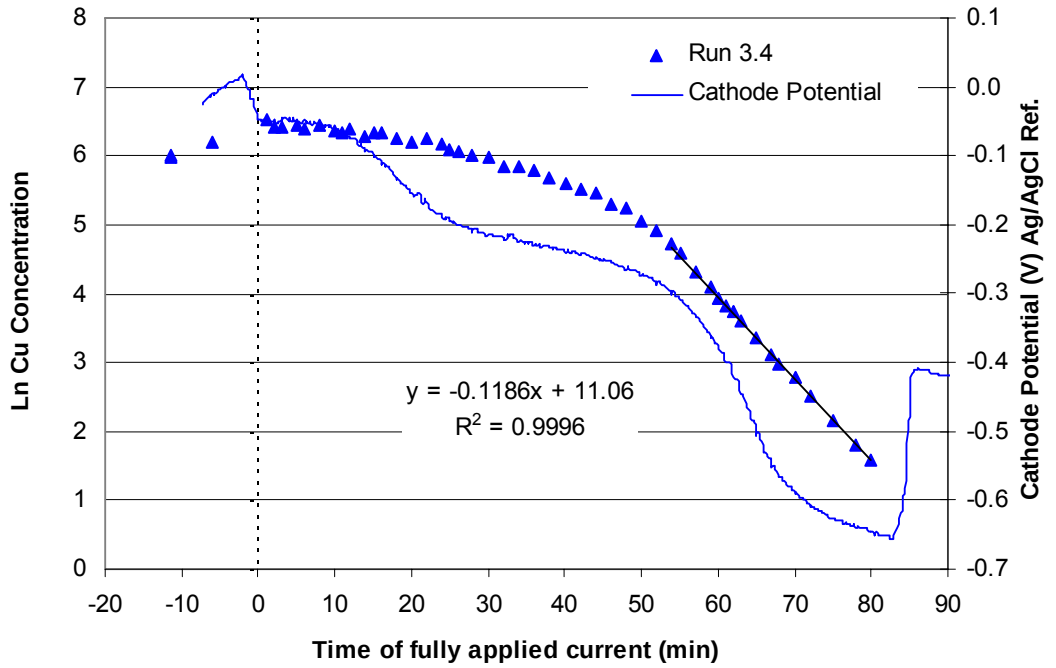


Figure D20 Concentration profile for Run 3.4 indicating the mass transport controlled region with the measured cathode potential shown on the secondary axis

APPENDIX E

Results for Run 4

Cu / Pd SIE Testwork

RUN 4.1

Date of experiment:	22/10/03
Catholyte solution:	Cu / Pd SIE
Constant applied current:	1.4 A
Flowrate of catholyte:	515 ml/min

Table E1 Catholyte make-up for Run 4.1

NaCl (g)	233.76
$CuCl_2.2H_2O$ (g)	2.15
Pd Stock Solution (10 g/l Pd in 20% HCl) (ml)	80
NH_4Ac (g)	308.39
CH_3COOH (ml)	230

Table E2 pH values of electrolytes for Run 4.1

	Catholyte	**Anolyte**
pH at start of experiment	4.497	3.162
pH at end of experiment	4.472	2.069

Table E3 Volumes of electrolytes in reservoirs for Run 4.1

	Catholyte	**Anolyte**
Volume at the start of experiment (ml)	4010	4080
Volume at the end of experiment (ml)	3820	4140

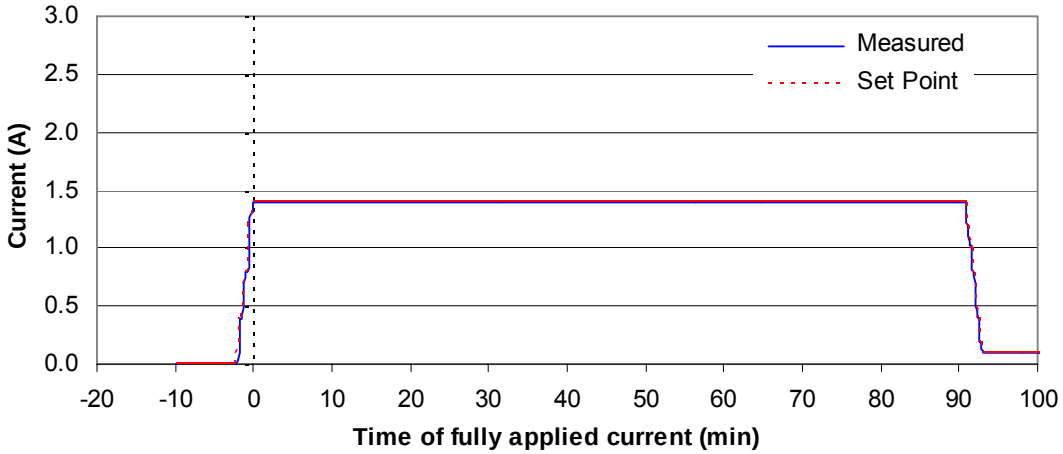


Figure E1 Current applied during Run 4.1

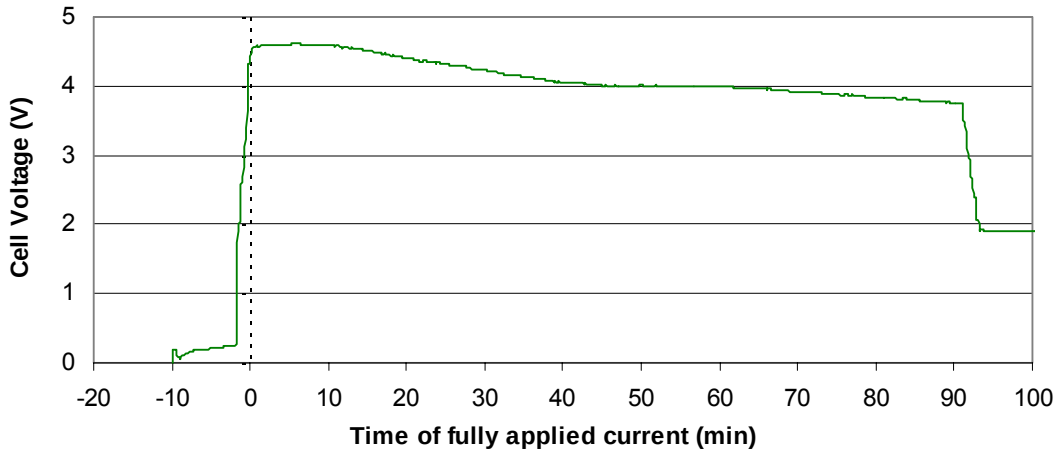


Figure E2 Cell voltage measured during Run 4.1

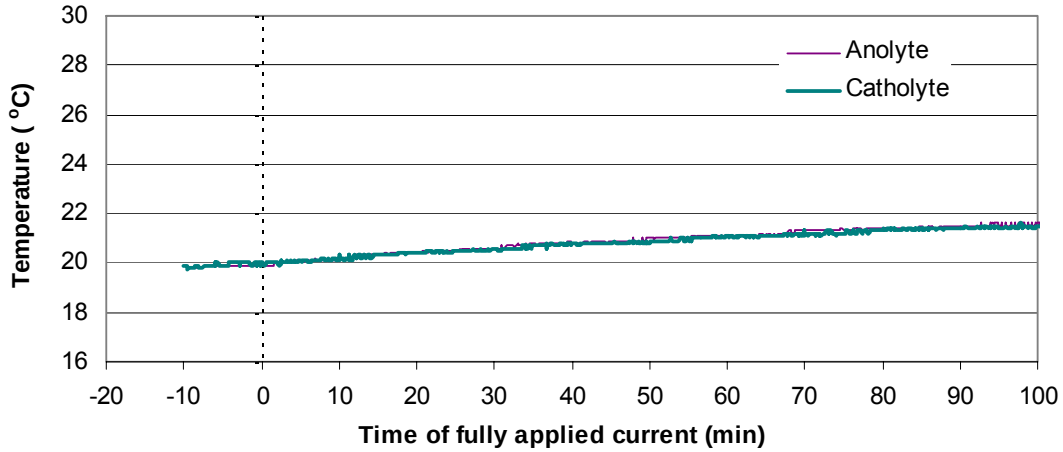


Figure E3 Temperatures of electrolytes measured during Run 4.1

Table E4 ICP results for copper - Run 4.1

Sample ID	Dilution	x	s	sr	Time (min)	Conc (ppm)	Ln Conc
C9 (head)	2 x 400	0.2606	0.0076	2.921	-10	208.5	5.34
C14 (head)	2 x 400	0.2364	0.0006	0.263	-10	189.1	5.24
C19 (head)	2 x 400	0.2500	0.0003	0.130	-10	200.0	5.30
C1	400	0.7630	0.0012	0.160	-6	305.2	5.72
C2	400	0.7880	0.0043	0.552	1	315.2	5.75
C3	400	0.7730	0.0064	0.829	2	309.2	5.73
C4	400	0.7820	59.0000	0.752	3	312.8	5.75
C5	400	0.7700	0.0078	1.008	4	308.0	5.73
C6	400	0.7900	0.0035	0.443	6	316.0	5.76
C7	400	0.7720	0.0033	0.431	7	308.8	5.73
C8	400	0.7480	0.0113	1.509	8	299.2	5.70
C10	400	0.7370	0.0064	0.867	10	294.8	5.69
C11	400	0.6990	0.0082	1.171	11	279.6	5.63
C12	400	0.7150	0.0121	1.700	12	286.0	5.66
C13	400	0.1969	0.0034	1.707	14	78.8	4.37
C15	400	0.3804	0.0004	0.117	15	152.2	5.02
C16	400	0.6320	0.0090	1.423	16	252.8	5.53
C17	400	0.1315	0.0010	0.765	17	52.6	3.96
C18	400	0.6160	0.0069	1.118	19	246.4	5.51
C20	400	0.5200	0.0031	0.597	20	208.0	5.34
C31	200	1.0890	0.0142	1.301	22	217.8	5.38
C21	400	0.4716	0.0050	1.061	24	188.6	5.24
C22	400	0.4181	0.0023	0.558	26	167.2	5.12
C23	400	0.3910	0.0016	0.410	27	156.4	5.05
C24	200	0.7900	0.0043	0.540	29	158.0	5.06
C25	200	0.6760	0.0025	0.375	30	135.2	4.91
C26	200	0.6320	0.0054	0.854	31	126.4	4.84
C27	200	0.5230	0.0025	0.482	33	104.6	4.65
C28	200	0.4886	0.0050	1.022	34	97.7	4.58
C29	200	0.4233	0.0021	0.487	36	84.7	4.44
C30	200	0.3851	0.0071	1.854	38	77.0	4.34
C32	200	0.2826	0.0045	1.577	40	56.5	4.03
C33	200	0.2228	0.0034	1.515	42	44.6	3.80
C34	200	0.1807	0.0050	2.785	44	36.1	3.59
C35	200	0.1478	0.0060	4.046	46	29.6	3.39
C36	200	0.1147	0.0015	1.301	48	22.9	3.13
C37	200	0.0878	0.0010	1.117	50	17.6	2.87
C38	200	0.0634	0.0023	3.569	52	12.7	2.54
C39	200	0.0470	0.0014	2.937	54	9.4	2.24
C40	200	0.0375	0.0011	2.812	56	7.5	2.01
C41	200	0.0264	0.0007	2.613	58	5.3	1.66
C42	200	0.0157	0.0012	7.352	60	3.1	1.14
C43	20	0.1610	0.0015	0.959	62	3.2	1.17
C44	20	0.1198	0.0002	0.194	65	2.4	0.87
C45	20	0.0929	0.0011	1.169	67	1.9	0.62
C46	20	0.0709	0.0009	1.273	69	1.4	0.35
C47	20	0.0519	0.0006	1.186	71	1.0	0.04
C48	10	0.1006	0.0011	1.068	73	1.0	0.01
C49	10	0.0522	0.0005	0.917	76	0.5	-0.65
C50	10	0.0473	0.0014	3.031	78	0.5	-0.75
C51	10	0.0327	0.0007	2.090	80	0.3	-1.12
C52	10	0.0247	0.0011	4.436	84	0.2	-1.40
C53	10	0.0223	0.0010	4.493	88	0.2	-1.50

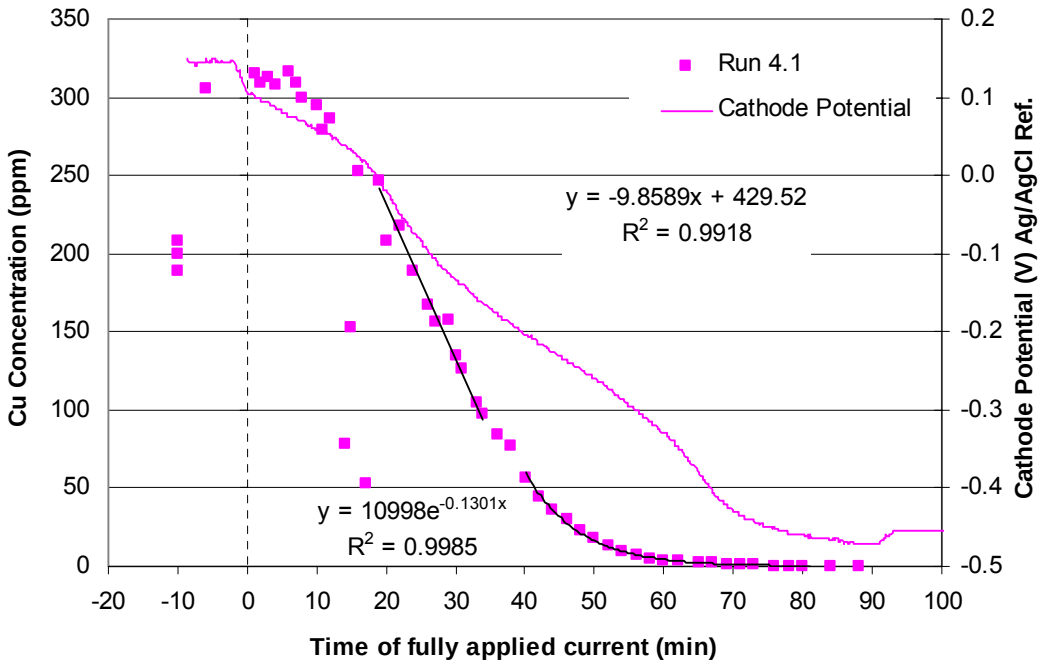


Figure E4 Cu concentration profile for Run 4.1 with the measured cathode potential shown on the secondary axis

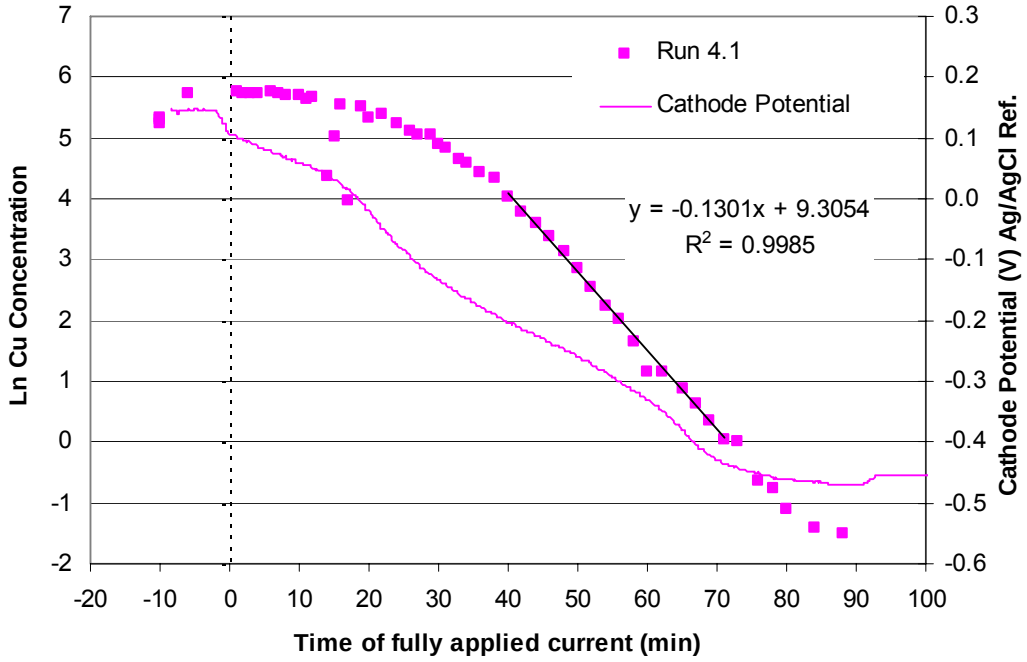


Figure E5 Cu concentration profile for Run 4.1 indicating the mass transport controlled region with the measured cathode potential shown on the secondary axis

Table E5 ICP results for palladium - Run 4.1

Sample ID	Dilution	x	s	sr	Time (min)	Conc (ppm)	Ln Conc
C9 (head)	2 x 400	0.2602	0.0071	2.714	-10	208.2	4.65
C14 (head)	2 x 400	0.2662	0.0026	0.991	-10	213.0	4.67
C19 (head)	2 x 400	0.2856	0.0077	2.684	-10	228.5	4.74
C1	400	0.5830	0.0026	0.446	-6	233.2	5.45
C2	400	0.5960	0.0057	0.964	1	238.4	5.47
C3	400	0.5860	0.0068	1.162	2	234.4	5.46
C4	400	0.5940	0.0029	0.482	3	237.6	5.47
C5	400	0.5880	0.0033	0.567	4	235.2	5.46
C6	400	0.6020	0.0034	0.558	6	240.8	5.48
C7	400	0.5810	0.0014	0.235	7	232.4	5.45
C8	400	0.5910	0.0049	0.835	8	236.4	5.47
C10	400	0.5620	0.0089	1.591	10	224.8	5.42
C11	400	0.5260	0.0149	2.828	11	210.4	5.35
C12	400	0.5560	0.0044	0.791	12	222.4	5.40
C13	400	0.1268	0.0022	1.763	14	50.7	3.93
C15	400	0.2988	0.0018	0.613	15	119.5	4.78
C16	400	0.5380	0.0110	2.048	16	215.2	5.37
C17	400	0.0862	0.0027	3.109	17	34.5	3.54
C18	400	0.5700	0.0104	1.831	19	228.0	5.43
C20	400	0.4921	0.0049	1.006	20	196.8	5.28
C31	200	1.1630	0.0086	0.738	22	232.6	5.45
C21	400	0.5370	0.0070	1.298	24	214.8	5.37
C22	400	0.5220	0.0044	0.840	26	208.8	5.34
C23	400	0.5070	0.0101	1.998	27	202.8	5.31
C24	200	1.2000	0.0047	0.390	29	240.0	5.48
C25	200	1.0870	0.0090	0.831	30	217.4	5.38
C26	200	1.0920	0.0014	0.125	31	218.4	5.39
C27	200	1.0450	0.0031	0.297	33	209.0	5.34
C28	200	1.0360	0.0127	1.228	34	207.2	5.33
C29	200	1.0260	0.0047	0.460	36	205.2	5.32
C30	200	0.9760	0.0054	0.556	38	195.2	5.27
C32	200	0.8960	0.0076	0.850	40	179.2	5.19
C33	200	0.8010	0.0033	0.416	42	160.2	5.08
C34	200	0.7340	0.0108	1.467	44	146.8	4.99
C35	200	0.6460	0.0189	2.931	46	129.2	4.86
C36	200	0.5940	0.0037	0.631	48	118.8	4.78
C37	200	0.4961	0.0079	1.587	50	99.2	4.60
C38	200	0.3966	0.0054	1.365	52	79.3	4.37
C39	200	0.3156	0.0027	0.870	54	63.1	4.15
C40	200	0.2572	0.0066	2.581	56	51.4	3.94
C41	200	0.1926	0.0030	1.562	58	38.5	3.65
C42	200	0.1452	0.0111	7.661	60	29.0	3.37
C43	20	1.2500	0.0046	0.370	62	25.0	3.22
C44	20	0.8510	0.0031	0.360	65	17.0	2.83
C45	20	0.7300	0.0081	1.108	67	14.6	2.68
C46	20	0.5740	0.0064	1.117	69	11.5	2.44
C47	20	0.4292	0.0030	0.696	71	8.6	2.15
C48	10	0.5670	0.0052	0.921	73	5.7	1.74
C49	10	0.3571	0.0014	0.400	76	3.6	1.27
C50	10	0.2761	0.0049	1.786	78	2.8	1.02
C51	10	0.2076	0.0018	0.873	80	2.1	0.73
C52	10	0.1205	0.0009	0.727	84	1.2	0.19
C53	10	0.0651	0.0008	1.259	88	0.7	-0.43

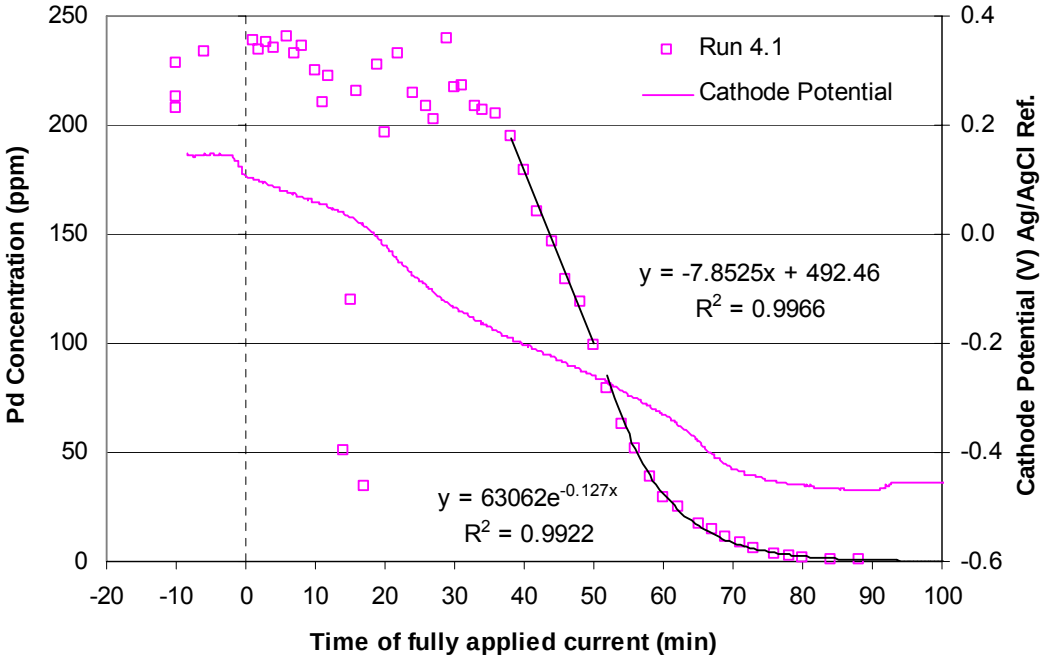


Figure E6 Pd concentration profile for Run 4.1 with the measured cathode potential shown on the secondary axis

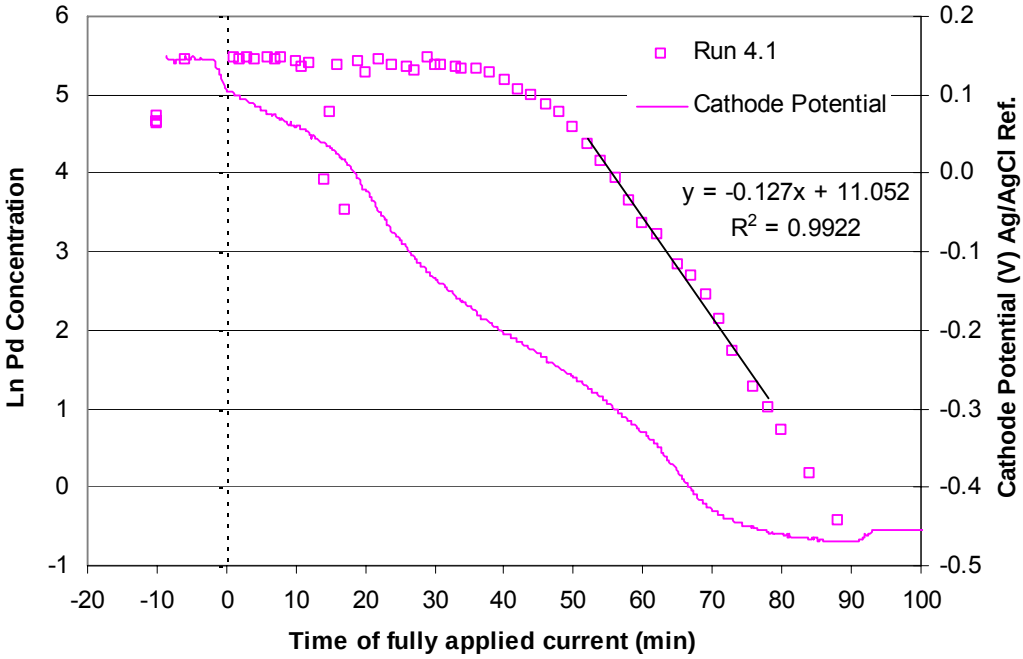


Figure E7 Pd concentration profile for Run 4.1 indicating the mass transport controlled region with the measured cathode potential shown on the secondary axis

RUN 4.2

Date of experiment:	24/10/03
Catholyte solution:	Cu / Pd SIE
Constant applied current:	2.6 A
Flowrate of catholyte:	510 ml/min

Table E6 Catholyte make-up for Run 4.2

NaCl (g)	233.76
$CuCl_2.2H_2O$ (g)	2.16
Pd Stock Solution (10 g/l Pd in 20% HCl) (ml)	79
NH_4Ac (g)	308.36
CH_3COOH (ml)	230

Table E7 pH values of electrolytes for Run 4.2

	Catholyte	**Anolyte**
pH at start of experiment	4.501	3.170
pH at end of experiment	4.518	1.935

Table E8 Volumes of electrolytes in reservoirs for Run 4.2

	Catholyte	**Anolyte**
Volume at the start of experiment (ml)	3960	4090
Volume at the end of experiment (ml)	3820	4140

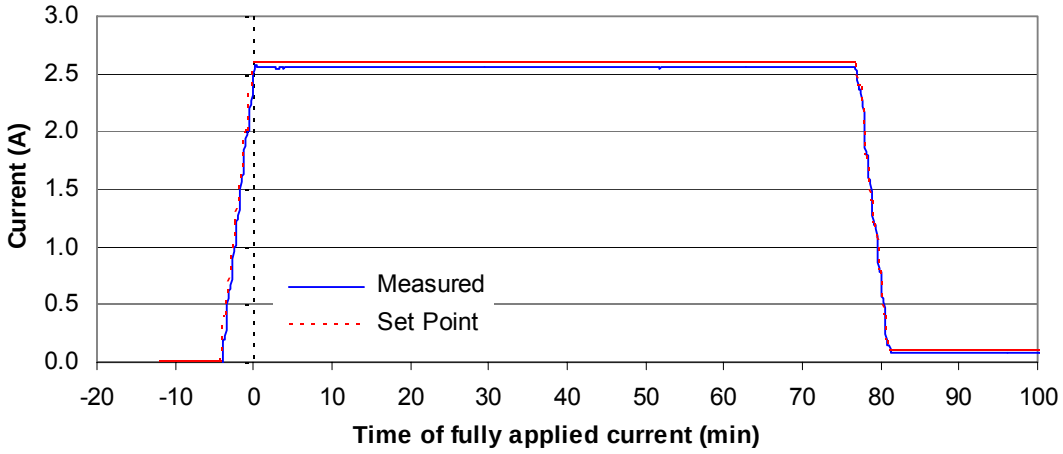


Figure E8 Current applied during Run 4.2

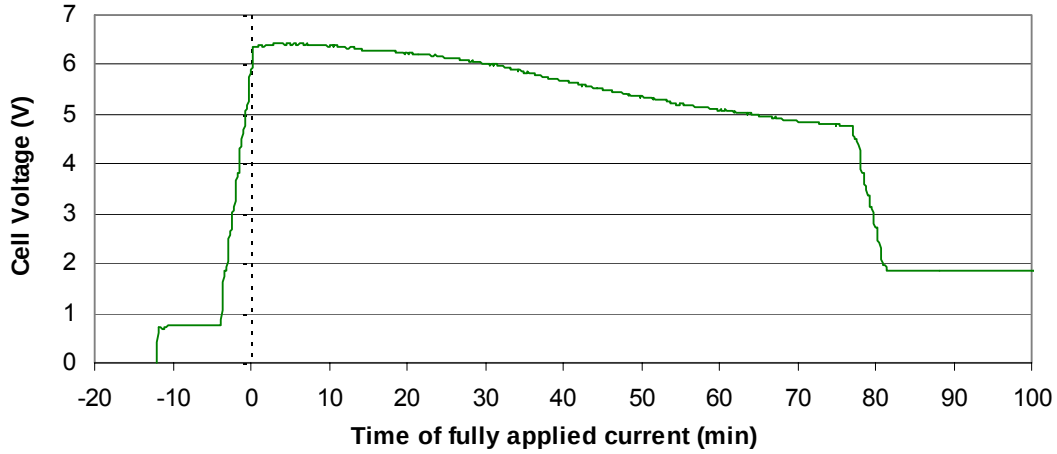


Figure E9 Cell voltage measured during Run 4.2

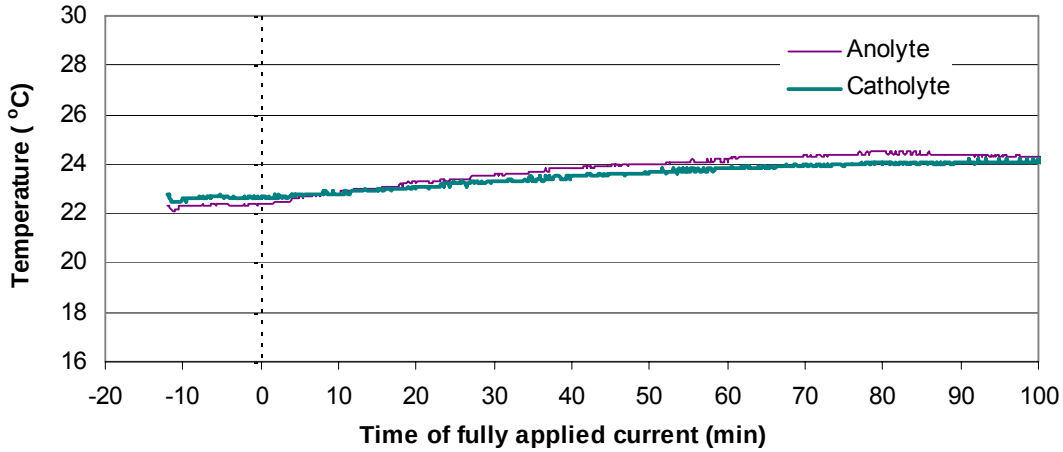


Figure E10 Temperatures of electrolytes measured during Run 4.2

Table E9 ICP results for copper - Run 4.2

Sample ID	Dilution	x	s	sr	Time (min)	Conc (ppm)	Ln Conc
C6 (head)	2 x 400	0.2602	0.0017	0.658	-12	208.2	5.34
C9 (head)	2 x 400	0.2580	0.0007	0.280	-12	206.4	5.33
C13 (head)	2 x 400	0.2531	0.0042	1.671	-12	202.5	5.31
C1	400	0.5130	0.0031	0.602	-8	205.2	5.32
C2	400	0.5180	0.0052	1.002	1	207.2	5.33
C3	400	0.5050	0.0010	0.206	2	202.0	5.31
C4	400	0.4852	0.0080	1.653	3	194.1	5.27
C5	400	0.4510	0.0056	1.232	4	180.4	5.20
C7	400	0.4184	0.0059	1.442	6	167.4	5.12
C8	400	0.3931	0.0022	0.550	7	157.2	5.06
C10	400	0.3771	0.0044	1.155	9	150.8	5.02
C11	400	0.3340	0.0032	0.967	10	133.6	4.89
C12	400	0.2957	0.0037	1.236	12	118.3	4.77
C14	400	0.2545	0.0024	0.938	13	101.8	4.62
C15	400	0.2524	0.0028	1.122	14	101.0	4.61
C16	400	0.2261	0.0028	1.251	15	90.4	4.50
C17	400	0.1883	0.0035	1.852	17	75.3	4.32
C18	400	0.1791	0.0009	0.527	18	71.6	4.27
C19	400	0.1560	0.0013	0.820	19	62.4	4.13
C20	400	0.1358	0.0020	1.501	20	54.3	3.99
C21	400	0.1253	0.0021	1.706	21	50.1	3.91
C22	400	0.1098	0.0014	1.252	22	43.9	3.78
C23	400	0.0939	0.0017	1.817	23	37.6	3.63
C24	400	0.0793	0.0009	1.098	24	31.7	3.46
C25	400	0.0603	0.0007	1.205	26	24.1	3.18
C26	400	0.0443	0.0010	2.348	27	17.7	2.87
C27	200	0.1037	0.0014	1.395	28	20.7	3.03
C28	200	0.1000	0.0002	0.157	29	20.0	3.00
C29	200	0.0851	0.0010	1.140	30	17.0	2.83
C30	200	0.0708	0.0009	1.324	31	14.2	2.65
C31	200	0.0703	0.0013	1.871	32	14.1	2.64
C32	200	0.0796	0.0030	0.433	33	15.9	2.77
C33	200	0.0491	0.0060	1.307	34	9.8	2.28
C34	200	0.0414	0.0005	1.118	35	8.3	2.11
C35	200	0.0384	0.0004	0.931	36	7.7	2.04
C36	200	0.0386	0.0002	0.646	37	7.7	2.04
C37	200	0.0287	0.0015	5.254	38	5.7	1.75
C38	200	0.0248	0.0013	5.159	40	5.0	1.60
C39	20	0.1750	0.0021	1.220	42	3.5	1.25
C40	20	0.1298	0.0008	0.594	44	2.6	0.95
C41	20	0.1095	0.0002	0.146	46	2.2	0.78
C42	20	0.0767	0.0008	1.096	48	1.5	0.43
C43	20	0.0569	0.0003	0.487	50	1.1	0.13
C44	20	0.0459	0.0003	0.743	52	0.9	-0.09
C45	10	0.0676	0.0011	1.684	54	0.7	-0.39
C46	10	0.0491	0.0006	1.320	56	0.5	-0.71
C47	10	0.0239	0.0002	0.890	60	0.2	-1.43
C48	10	0.0166	0.0009	5.267	64	0.2	-1.80
C49	10	0.0113	0.0004	3.843	68	0.1	-2.18
C50	10	0.0074	0.0004	5.912	74	0.1	-2.60

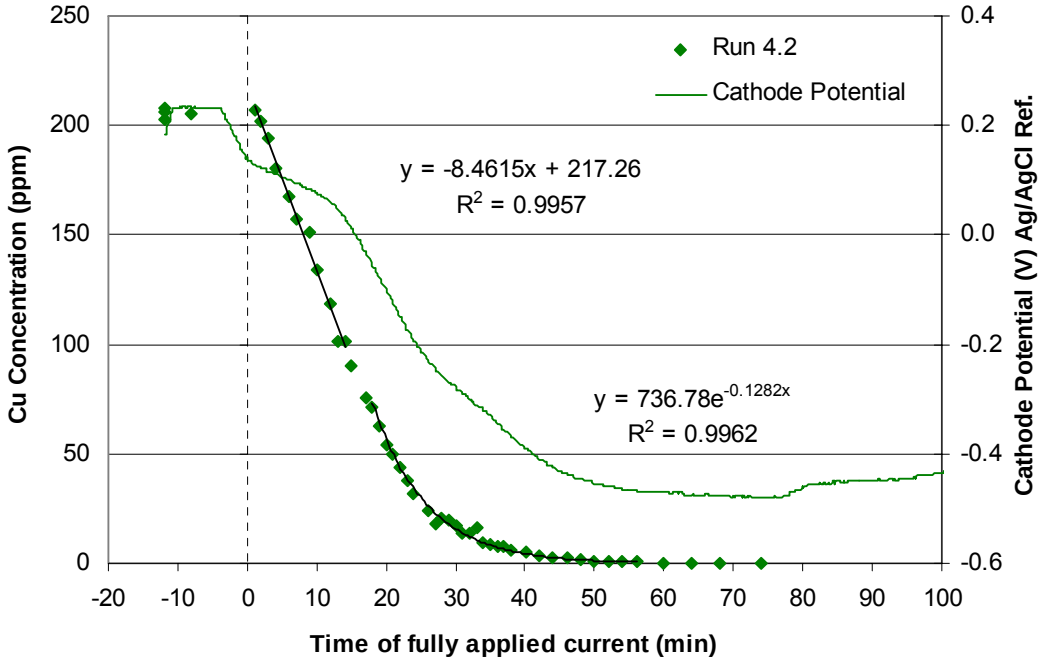


Figure E11 Cu concentration profile for Run 4.2 with the measured cathode potential shown on the secondary axis

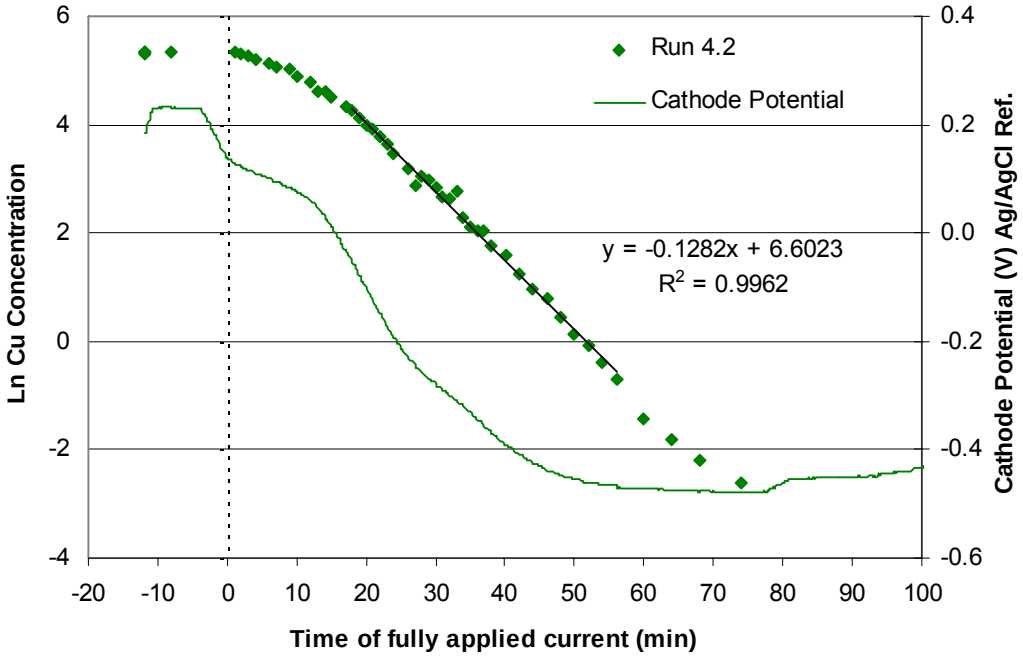


Figure E12 Cu concentration profile for Run 4.2 indicating the mass transport controlled region with the measured cathode potential shown on the secondary axis

Table E10 ICP results for palladium - Run 4.2

Sample ID	Dilution	x	s	sr	Time (min)	Conc (ppm)	Ln Conc
C6 (head)	2 x 400	0.2772	0.0017	0.596	-12	221.8	5.40
C9 (head)	2 x 400	0.2752	0.0022	0.797	-12	220.2	5.39
C13 (head)	2 x 400	0.2725	0.0018	0.674	-12	218.0	5.38
C1	400	0.5540	0.0031	0.567	-8	221.6	5.40
C2	400	0.5780	0.0039	0.683	1	231.2	5.44
C3	400	0.5750	0.0020	0.349	2	230.0	5.44
C4	400	0.5700	0.0076	1.333	3	228.0	5.43
C5	400	0.5660	0.0042	0.740	4	226.4	5.42
C7	400	0.5450	0.0041	0.756	6	218.0	5.38
C8	400	0.5410	0.0085	1.568	7	216.4	5.38
C10	400	0.5380	0.0034	0.631	9	215.2	5.37
C11	400	0.5070	0.0057	1.134	10	202.8	5.31
C12	400	0.4841	0.0011	0.226	12	193.6	5.27
C14	400	0.4074	0.0063	1.539	13	163.0	5.09
C15	400	0.4381	0.0075	1.723	14	175.2	5.17
C16	400	0.4131	0.0031	0.740	15	165.2	5.11
C17	400	0.3598	0.0067	1.875	17	143.9	4.97
C18	400	0.3516	0.0059	1.684	18	140.6	4.95
C19	400	0.3394	0.0052	1.526	19	135.8	4.91
C20	400	0.3048	0.0022	0.729	20	121.9	4.80
C21	400	0.2925	0.0050	1.696	21	117.0	4.76
C22	400	0.2796	0.0027	0.982	22	111.8	4.72
C23	400	0.2547	0.0057	2.253	23	101.9	4.62
C24	400	0.2331	0.0019	0.835	24	93.2	4.54
C25	400	0.1904	0.0014	0.718	26	76.2	4.33
C26	400	0.1563	0.0029	1.866	27	62.5	4.14
C27	200	0.3037	0.0027	0.883	28	60.7	4.11
C28	200	0.2934	0.0025	0.855	29	58.7	4.07
C29	200	0.2460	0.0015	0.605	30	49.2	3.90
C30	200	0.2194	0.0033	1.518	31	43.9	3.78
C31	200	0.2020	0.0040	1.965	32	40.4	3.70
C32	200	0.1605	0.0042	2.637	33	32.1	3.47
C33	200	0.1479	0.0007	0.458	34	29.6	3.39
C34	200	0.1334	0.0028	2.076	35	26.7	3.28
C35	200	0.1159	0.0019	1.645	36	23.2	3.14
C36	200	0.1121	0.0010	0.914	37	22.4	3.11
C37	200	0.0865	0.0013	1.557	38	17.3	2.85
C38	200	0.0655	0.0072	11.019	40	13.1	2.57
C39	20	0.6060	0.0058	0.948	42	12.1	2.49
C40	20	0.4393	0.0014	0.319	44	8.8	2.17
C41	20	0.3399	0.0021	0.626	46	6.8	1.92
C42	20	0.2532	0.0014	0.538	48	5.1	1.62
C43	20	0.1824	0.0027	1.463	50	3.6	1.29
C44	20	0.1502	0.0010	0.659	52	3.0	1.10
C45	10	0.2318	0.0026	1.131	54	2.3	0.84
C46	10	0.1923	0.0050	2.615	56	1.9	0.65
C47	10	0.0883	0.0017	1.971	60	0.9	-0.12
C48	10	0.0624	0.0011	1.739	64	0.6	-0.47
C49	10	0.0418	0.0013	3.157	68	0.4	-0.87
C50	10	0.0203	0.0006	2.712	74	0.2	-1.59

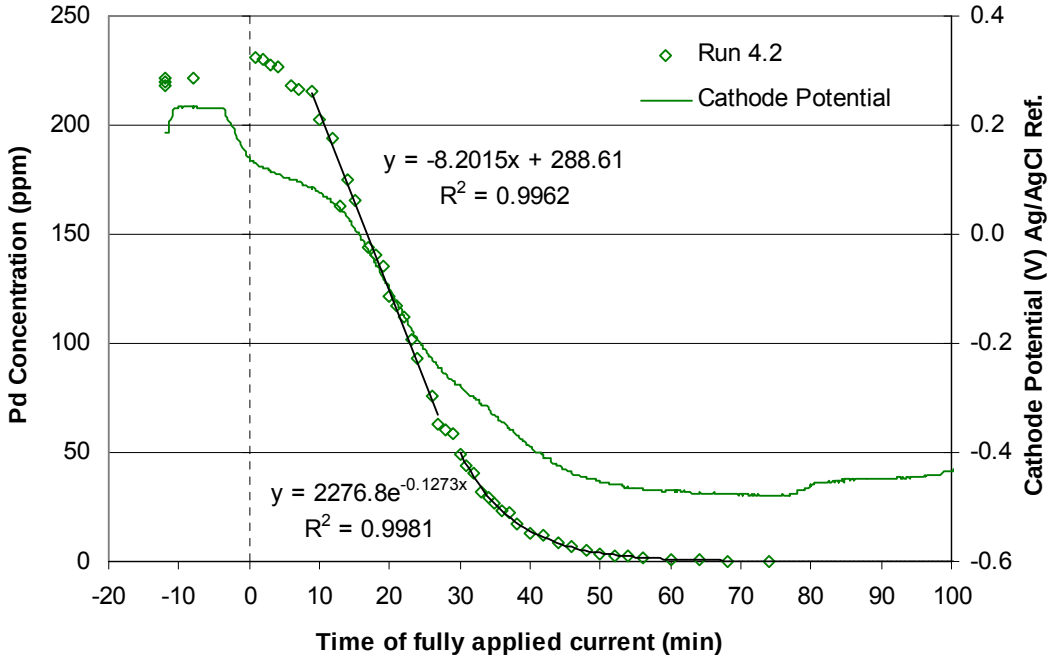


Figure E13 Pd concentration profile for Run 4.2 with the measured cathode potential shown on the secondary axis

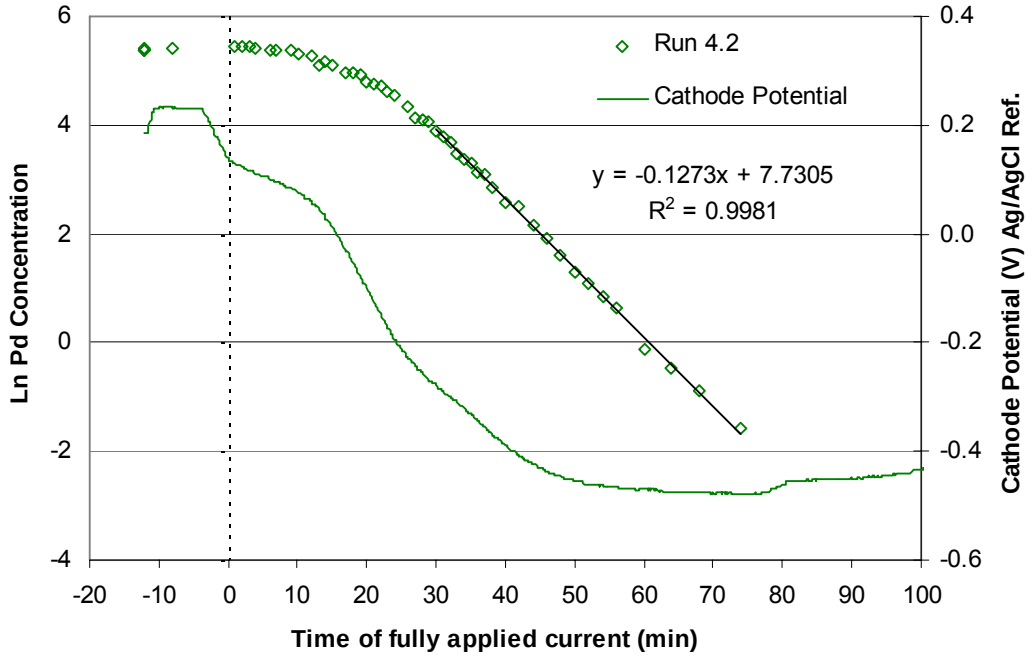


Figure E14 Pd concentration profile for Run 4.2 indicating the mass transport controlled region with the measured cathode potential shown on the secondary axis

RUN 4.3

Date of experiment:	27/10/03
Catholyte solution:	Cu / Pd SIE
Constant applied current:	0.8 A
Flowrate of catholyte:	515 ml/min

Table E11 Catholyte make-up for Run 4.3

NaCl (g)	233.76
$CuCl_2.2H_2O$ (g)	2.15
Pd Stock Solution (10 g/l Pd in 20% HCl) (ml)	79
NH_4Ac (g)	308.37
CH_3COOH (ml)	230

Table E12 pH values of electrolytes for Run 4.3

	Catholyte	**Anolyte**
pH at start of experiment	4.510	2.286
pH at end of experiment	4.527	2.387

Table E13 Volumes of electrolytes in reservoirs for Run 4.3

	Catholyte	**Anolyte**
Volume at the start of experiment (ml)	3990	3880
Volume at the end of experiment (ml)	3760	3960

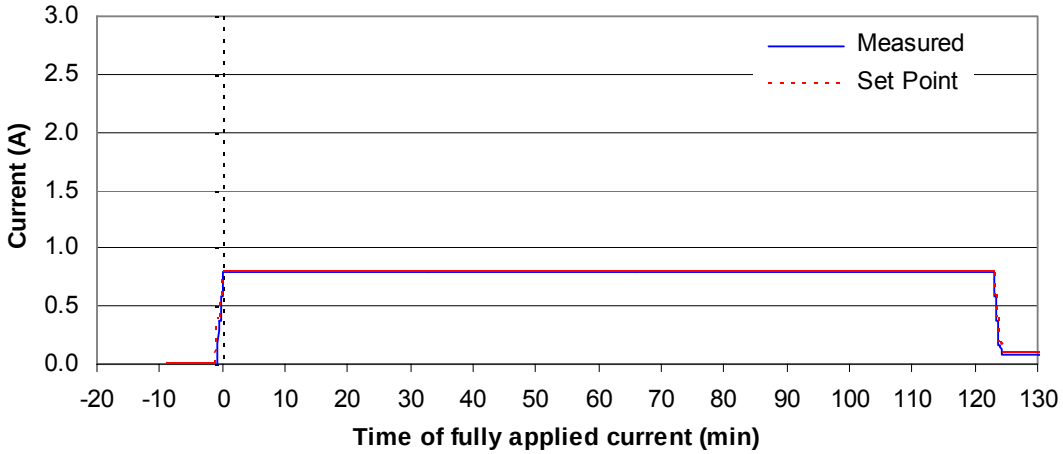


Figure E15 Current applied during Run 4.3

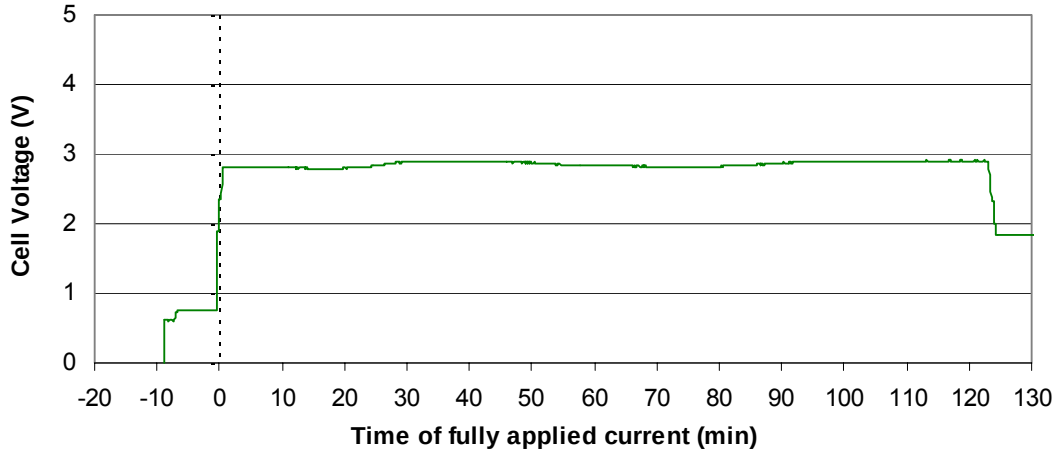


Figure E16 Cell voltage measured during Run 4.3

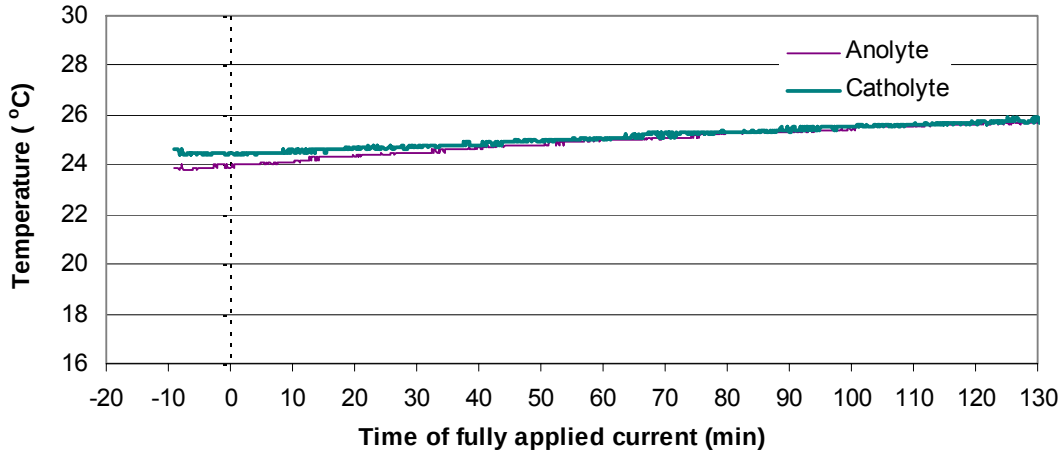


Figure E17 Temperatures of electrolytes measured during Run 4.3

Table E14 ICP results for copper - Run 4.3

Sample ID	Dilution	x	s	sr
C10 (head)	2 x 400	0.2676	0.0047	1.774
C15 (head)	2 x 400	0.2585	0.0002	0.068
C18 (head)	2 x 400	0.2471	0.0036	1.443
C1	400	0.5010	0.0015	0.293
C2	400	0.5010	0.0050	0.988
C3	400	0.5010	0.0052	1.030
C4	400	0.4876	0.0030	0.612
C5	400	0.4793	0.0019	0.390
C6	400	0.5050	0.0023	0.460
C7	400	0.4984	0.0046	0.917
C8	400	0.5000	0.0017	0.331
C9	400	0.5540	0.0011	0.201
C11	400	0.4682	0.0043	0.910
C12	400	0.4823	0.0041	0.849
C13	400	0.4819	0.0043	0.901
C14	400	0.4764	0.0049	1.019
C16	400	0.4753	0.0043	0.902
C17	400	0.4706	0.0010	0.215
C19	400	0.4552	0.0011	0.246
C20	400	0.4374	0.0033	0.749
C21	400	0.4239	0.0053	1.242
C22	400	0.4210	0.0044	1.044
C23	400	0.3950	0.0021	0.520
C24	400	0.3905	0.0004	0.093
C25	400	0.3404	0.0036	1.063
C26	400	0.3257	0.0014	0.420
C27	400	0.3096	0.0007	0.234
C28	400	0.2738	0.0035	1.271
C29	400	0.2523	0.0046	1.841
C30	400	0.2232	0.0007	0.327
C31	400	0.2109	0.0019	0.899
C32	400	0.1934	0.0049	2.530
C33	400	0.1613	0.0013	0.830
C34	400	0.1439	0.0003	0.236
C35	200	0.2613	0.0017	0.654
C36	200	0.2175	0.0026	1.186
C37	200	0.1811	0.0024	1.325
C38	200	0.1582	0.0012	0.733
C39	200	0.1279	0.0010	0.798
C40	200	0.1202	0.0009	0.763
C41	200	0.0951	0.0022	2.308
C42	200	0.0824	0.0007	0.877
C43	200	0.0669	0.0003	0.477
C44	200	0.0560	0.0014	2.554
C45	200	0.0474	0.0005	1.124
C46	200	0.0379	0.0002	0.414
C47	100	0.0594	0.0004	0.748
C48	100	0.0447	0.0003	0.710
C49	100	0.0383	0.0007	1.706
C50	100	0.0300	0.0009	3.001
C51	100	0.0239	0.0005	1.898
C52	100	0.0199	0.0005	2.441
C53	20	0.0729	0.0007	0.954
C54	20	0.0505	0.0017	3.389
C55	10	0.0923	0.0004	0.428
C56	10	0.0564	0.0008	1.337
C57	10	0.0389	0.0001	0.225
C58	10	0.0286	0.0002	0.660
C59	10	0.0252	0.0007	2.662
C60	10	0.0235	0.0008	3.489

Time (min)	Conc (ppm)	Ln Conc
-9	214.1	5.37
-9	206.8	5.33
-9	197.7	5.29
-5	200.4	5.30
1	200.4	5.30
3	200.4	5.30
5	195.0	5.27
7	191.7	5.26
9	202.0	5.31
11	199.4	5.30
13	200.0	5.30
15	221.6	5.40
17	187.3	5.23
19	192.9	5.26
21	192.8	5.26
23	190.6	5.25
25	190.1	5.25
27	188.2	5.24
29	182.1	5.20
31	175.0	5.16
33	169.6	5.13
35	168.4	5.13
37	158.0	5.06
39	156.2	5.05
41	136.2	4.91
43	130.3	4.87
45	123.8	4.82
47	109.5	4.70
49	100.9	4.61
51	89.3	4.49
53	84.4	4.44
55	77.4	4.35
57	64.5	4.17
59	57.6	4.05
61	52.3	3.96
63	43.5	3.77
65	36.2	3.59
67	31.6	3.45
69	25.6	3.24
71	24.0	3.18
73	19.0	2.95
75	16.5	2.80
77	13.4	2.59
79	11.2	2.42
81	9.5	2.25
83	7.6	2.03
85	5.9	1.78
87	4.5	1.50
89	3.8	1.34
91	3.0	1.10
93	2.4	0.87
95	2.0	0.69
97	1.5	0.38
99	1.0	0.01
101	0.9	-0.08
104	0.6	-0.57
108	0.4	-0.94
111	0.3	-1.25
115	0.3	-1.38
119	0.2	-1.45

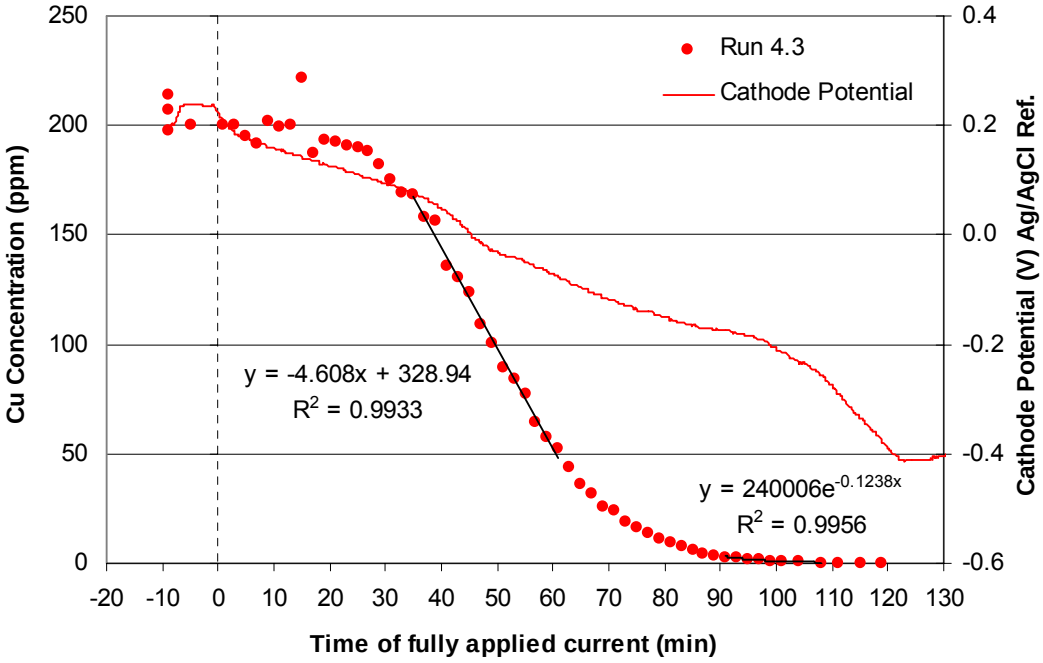


Figure E18 Cu concentration profile for Run 4.3 with the measured cathode potential shown on the secondary axis

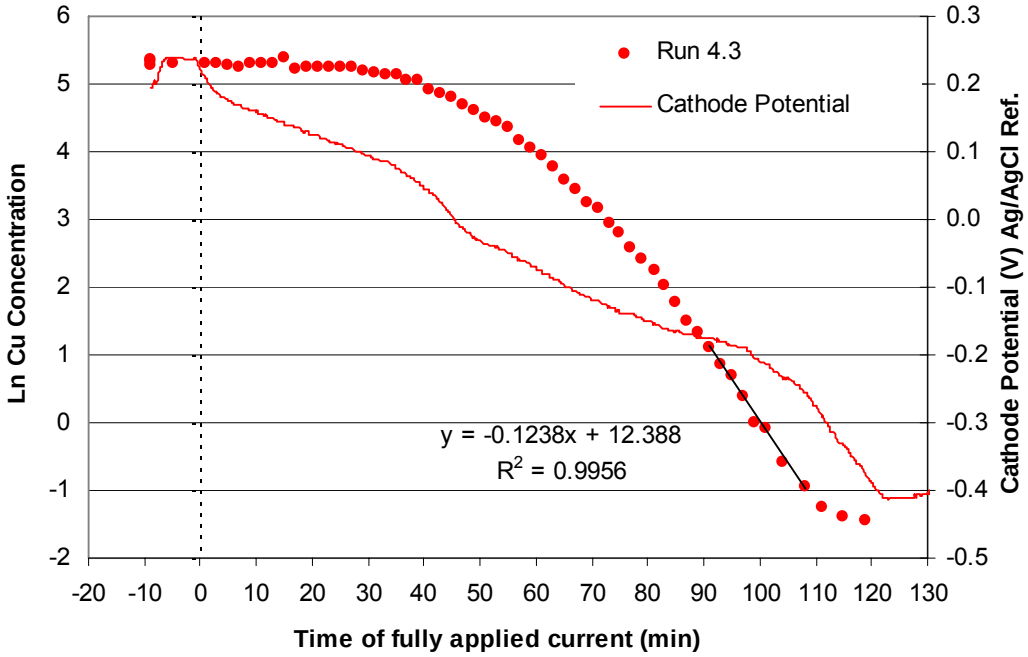


Figure E19 Cu concentration profile for Run 4.3 indicating the mass transport controlled region with the measured cathode potential shown on the secondary axis

Table E15 ICP results for palladium - Run 4.3

Sample ID	Dilution	x	s	sr	Time (min)	Conc (ppm)	Ln Conc
C10 (head)	2 x 400	0.2848	0.0004	0.129	-9	227.8	4.74
C15 (head)	2 x 400	0.2775	0.0043	1.549	-9	222.0	4.71
C18 (head)	2 x 400	0.2644	0.0043	1.645	-9	211.5	4.66
C1	400	0.5720	0.0028	0.489	-5	228.8	5.43
C2	400	0.5790	0.0033	0.572	1	231.6	5.45
C3	400	0.5840	0.0059	1.008	3	233.6	5.45
C4	400	0.5690	0.0072	1.264	5	227.6	5.43
C5	400	0.5540	0.0038	0.677	7	221.6	5.40
C6	400	0.5930	0.0048	0.807	9	237.2	5.47
C7	400	0.5800	0.0048	0.824	11	232.0	5.45
C8	400	0.5770	0.0032	0.557	13	230.8	5.44
C9	400	0.6720	0.0165	2.462	15	268.8	5.59
C11	400	0.5500	0.0025	0.451	17	220.0	5.39
C12	400	0.5670	0.0033	0.577	19	226.8	5.42
C13	400	0.5680	0.0037	0.654	21	227.2	5.43
C14	400	0.5740	0.0026	0.448	23	229.6	5.44
C16	400	0.5680	0.0015	0.257	25	227.2	5.43
C17	400	0.5750	0.0117	2.027	27	230.0	5.44
C19	400	0.5500	0.0046	0.838	29	220.0	5.39
C20	400	0.5400	0.0047	0.877	31	216.0	5.38
C21	400	0.5360	0.0011	0.205	33	214.4	5.37
C22	400	0.5420	0.0073	1.353	35	216.8	5.38
C23	400	0.5410	0.0066	1.218	37	216.4	5.38
C24	400	0.5640	0.0043	0.766	39	225.6	5.42
C25	400	0.5260	0.0036	0.693	41	210.4	5.35
C26	400	0.5310	0.0015	0.288	43	212.4	5.36
C27	400	0.5480	0.0034	0.615	45	219.2	5.39
C28	400	0.5190	0.0049	0.951	47	207.6	5.34
C29	400	0.5220	0.0054	1.044	49	208.8	5.34
C30	400	0.5110	0.0011	0.220	51	204.4	5.32
C31	400	0.5270	0.0054	1.033	53	210.8	5.35
C32	400	0.4974	0.0062	1.236	55	199.0	5.29
C33	400	0.4756	0.0041	0.870	57	190.2	5.25
C34	400	0.4584	0.0038	0.832	59	183.4	5.21
C35	200	1.0250	0.0020	0.192	61	205.0	5.32
C36	200	0.9320	0.0050	0.533	63	186.4	5.23
C37	200	0.8610	0.0034	0.400	65	172.2	5.15
C38	200	0.8300	0.0020	0.240	67	166.0	5.11
C39	200	0.7430	0.0030	0.409	69	148.6	5.00
C40	200	0.7780	0.0039	0.500	71	155.6	5.05
C41	200	0.6800	0.0032	0.464	73	136.0	4.91
C42	200	0.6480	0.0066	1.020	75	129.6	4.86
C43	200	0.5760	0.0047	0.819	77	115.2	4.75
C44	200	0.5290	0.0045	0.857	79	105.8	4.66
C45	200	0.4786	0.0051	1.066	81	95.7	4.56
C46	200	0.3820	0.0066	1.729	83	76.4	4.34
C47	100	0.7800	0.0056	0.715	85	78.0	4.36
C48	100	0.6300	0.0041	0.659	87	63.0	4.14
C49	100	0.5550	0.0025	0.445	89	55.5	4.02
C50	100	0.4469	0.0005	0.116	91	44.7	3.80
C51	100	0.3356	0.0060	1.792	93	33.6	3.51
C52	100	0.2528	0.0077	3.058	95	25.3	3.23
C53	20	1.0890	0.0074	0.676	97	21.8	3.08
C54	20	0.8190	0.0155	1.404	99	16.4	2.80
C55	10	1.3530	0.0051	0.378	101	13.5	2.60
C56	10	0.9220	0.0061	0.662	104	9.2	2.22
C57	10	0.5510	0.0020	0.360	108	5.5	1.71
C58	10	0.3545	0.0044	1.236	111	3.5	1.27
C59	10	0.2193	0.0043	1.949	115	2.2	0.79
C60	10	0.1305	0.0027	2.032	119	1.3	0.27

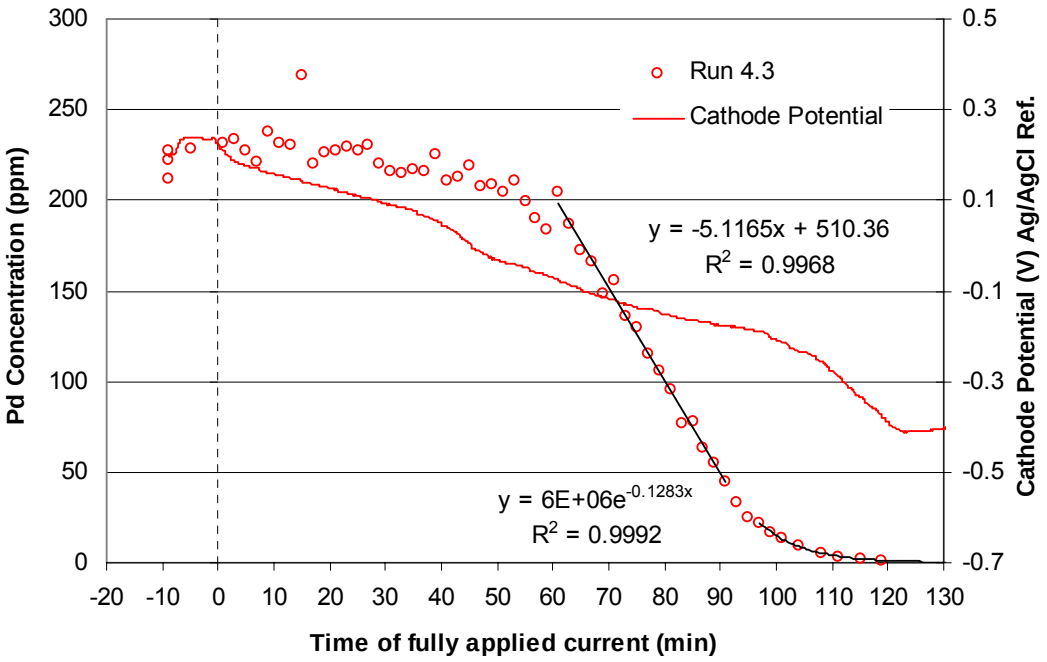


Figure E20 Pd concentration profile for Run 4.3 with the measured cathode potential shown on the secondary axis

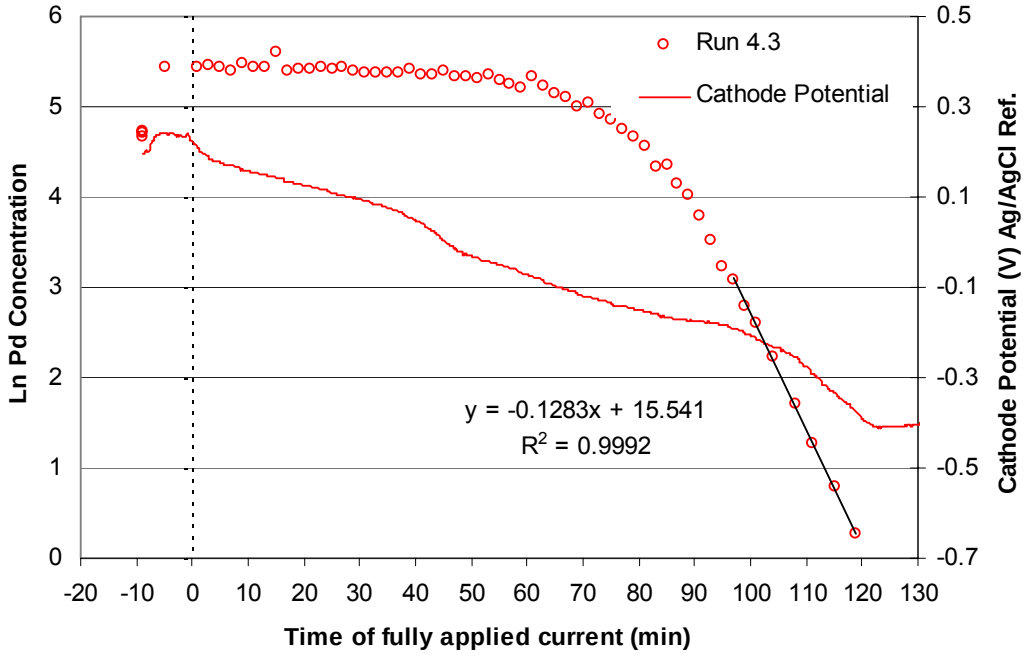


Figure E21 Pd concentration profile for Run 4.3 indicating the mass transport controlled region with the measured cathode potential shown on the secondary axis

RUN 4.4

Date of experiment:	28/10/03
Catholyte solution:	Cu / Pd SIE
Constant applied current:	2.0 A
Flowrate of catholyte:	500 ml/min

Table E16 Catholyte make-up for Run 4.4

NaCl (g)	233.76
$CuCl_2.2H_2O$ (g)	2.16
Pd Stock Solution (10 g/l Pd in 20% HCl) (ml)	80
NH_4Ac (g)	308.38
CH_3COOH (ml)	230

Table E17 pH values of electrolytes for Run 4.4

	Catholyte	**Anolyte**
pH at start of experiment	4.468	3.498
pH at end of experiment	4.494	2.112

Table E18 Volumes of electrolytes in reservoirs for Run 4.4

	Catholyte	**Anolyte**
Volume at the start of experiment (ml)	3990	4100
Volume at the end of experiment (ml)	3820	4140

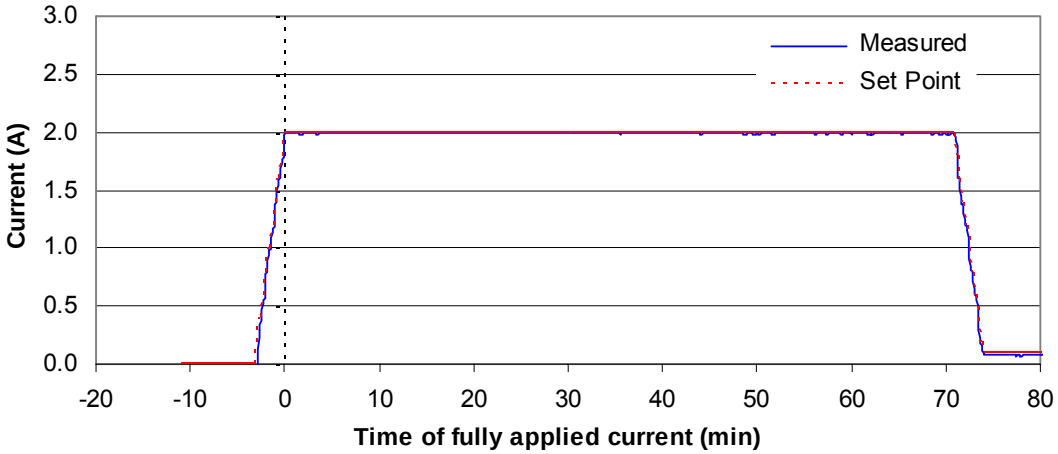


Figure E22 Current applied during Run 4.4

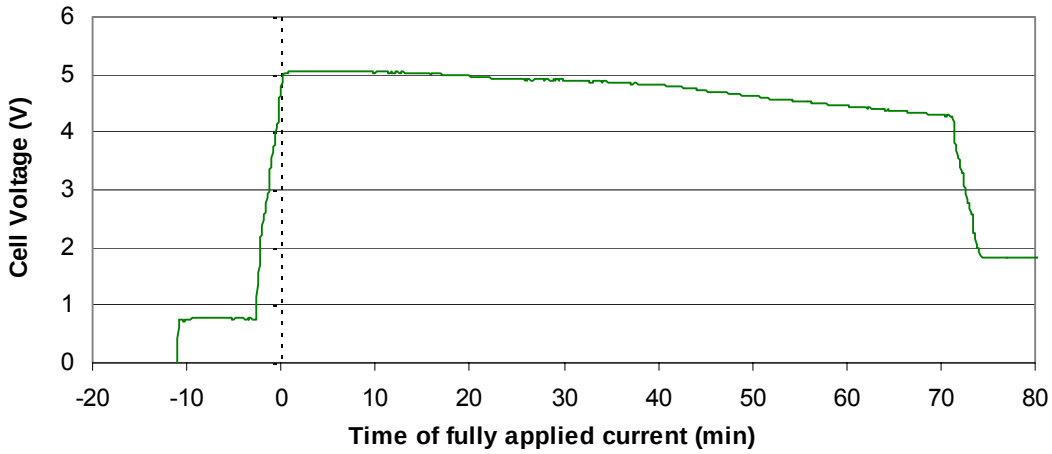


Figure E23 Cell voltage measured during Run 4.4

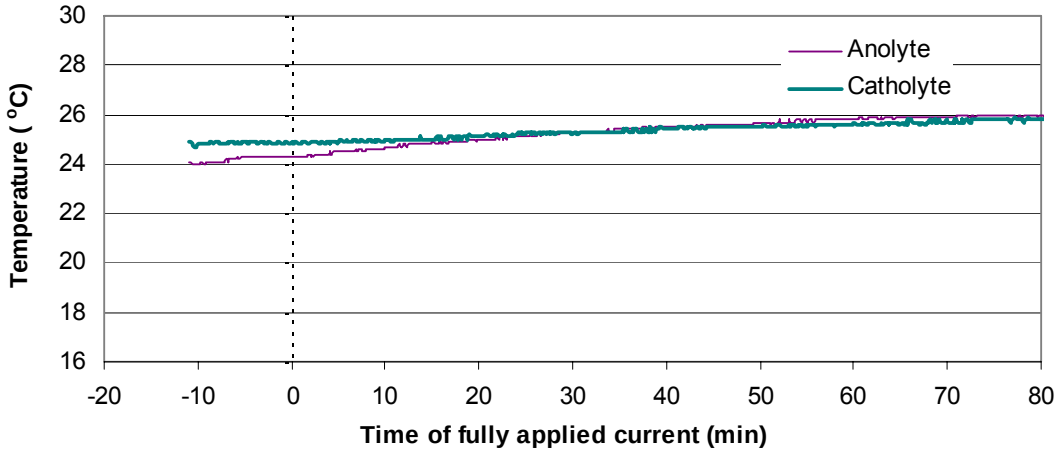


Figure E24 Temperatures of electrolytes measured during Run 4.4

Table E19 ICP results for copper - Run 4.4

Sample ID	Dilution	x	s	sr	Time (min)	Conc (ppm)	Ln Conc
C12 (head)	2 x 400	0.2421	0.0009	0.392	-11	193.7	5.27
C18 (head)	2 x 400	0.2336	0.0043	1.850	-11	186.9	5.23
C21 (head)	2 x 400	0.2349	0.0008	0.328	-11	187.9	5.24
C1	400	0.4863	0.0048	0.982	-7	194.5	5.27
C2	400	0.4860	0.0056	1.153	1	194.4	5.27
C3	400	0.4759	0.0035	0.730	2	190.4	5.25
C4	400	0.4675	0.0043	0.917	3	187.0	5.23
C5	400	0.4564	0.0019	0.406	4	182.6	5.21
C6	400	0.4355	0.0012	0.269	5	174.2	5.16
C7	400	0.4133	0.0024	0.592	7	165.3	5.11
C8	400	0.4195	0.0047	1.115	8	167.8	5.12
C9	400	0.3900	0.0050	1.286	9	156.0	5.05
C10	400	0.3855	0.0017	0.431	10	154.2	5.04
C11	400	0.3637	0.0031	0.854	11	145.5	4.98
C13	400	0.3395	0.0010	0.284	12	135.8	4.91
C14	400	0.3114	0.0029	0.928	14	124.6	4.82
C15	400	0.2887	0.0024	0.820	15	115.5	4.75
C16	400	0.2736	0.0007	0.255	16	109.4	4.70
C17	400	0.2648	0.0028	1.040	17	105.9	4.66
C19	400	0.2267	0.0029	1.275	19	90.7	4.51
C20	400	0.2233	0.0040	1.773	20	89.3	4.49
C22	400	0.1734	0.0026	1.520	22	69.4	4.24
C23	400	0.1559	0.0022	1.434	23	62.4	4.13
C24	400	0.1427	0.0019	1.307	24	57.1	4.04
C25	400	0.1293	0.0023	1.783	25	51.7	3.95
C26	400	0.1183	0.0018	1.493	26	47.3	3.86
C27	400	0.0926	0.0007	0.769	28	37.0	3.61
C28	400	0.0903	0.0011	1.258	29	36.1	3.59
C29	100	0.3356	0.0015	0.449	30	33.6	3.51
C30	100	0.2938	0.0024	0.825	31	29.4	3.38
C31	100	0.2386	0.0037	1.560	33	23.9	3.17
C32	100	0.2082	0.0025	1.181	34	20.8	3.04
C33	100	0.1628	0.0005	0.322	36	16.3	2.79
C34	100	0.1351	0.0017	1.284	37	13.5	2.60
C35	100	0.1004	0.0010	0.971	39	10.0	2.31
C36	100	0.0565	0.0010	1.701	41	5.7	1.73
C37	100	0.0574	0.0002	0.266	43	5.7	1.75
C38	100	0.0396	0.0006	1.409	45	4.0	1.38
C39	100	0.0328	0.0007	2.044	47	3.3	1.19
C40	100	0.0239	0.0009	3.738	49	2.4	0.87
C41	10	0.2261	0.0012	0.514	51	2.3	0.82
C42	10	0.1509	0.0010	0.652	54	1.5	0.41
C43	10	0.1001	0.0010	1.042	57	1.0	0.00
C44	10	0.0605	0.0007	1.181	60	0.6	-0.50
C45	10	0.0328	0.0004	1.110	64	0.3	-1.11
C46	10	0.0114	0.0003	2.619	69	0.1	-2.17

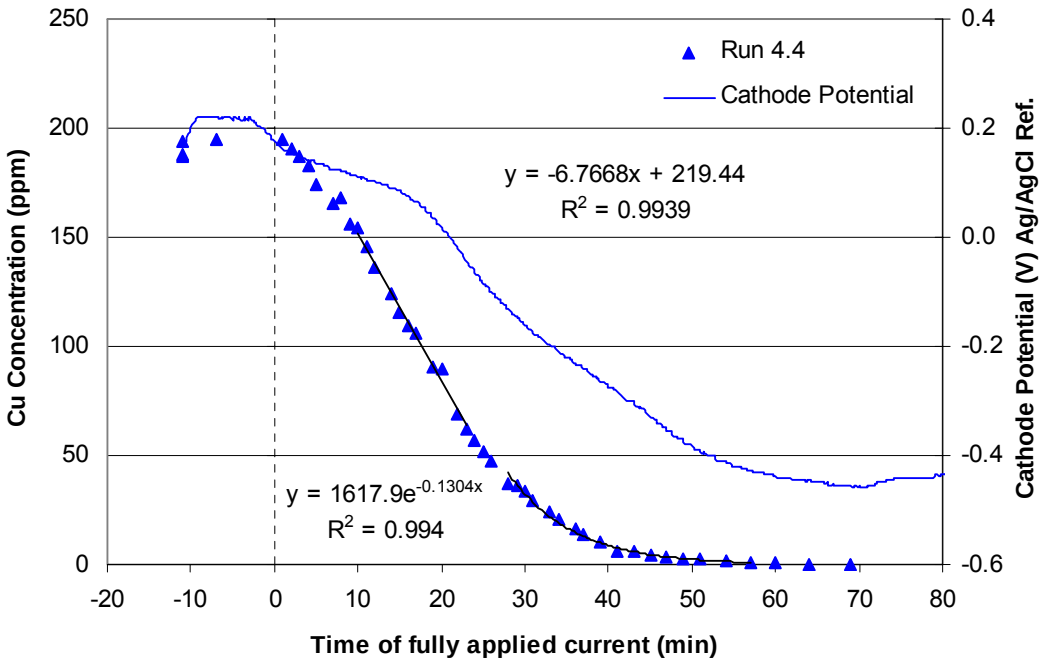


Figure E25 Cu concentration profile for Run 4.4 with the measured cathode potential shown on the secondary axis

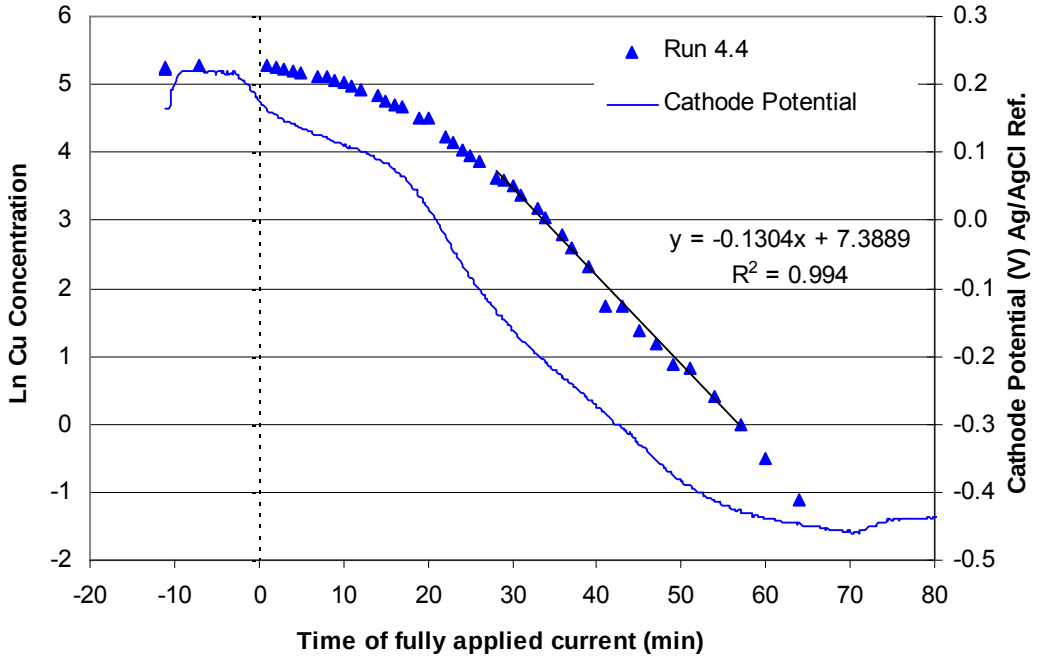


Figure E26 Cu concentration profile for Run 4.4 indicating the mass transport controlled region with the measured cathode potential shown on the secondary axis

Table E20 ICP results for palladium - Run 4.4

Sample ID	Dilution	x	s	sr	Time (min)	Conc (ppm)	Ln Conc
C12 (head)	2 x 400	0.2700	0.0019	0.704	-11	216.0	5.38
C18 (head)	2 x 400	0.2576	0.0023	0.883	-11	206.1	5.33
C21 (head)	2 x 400	0.2596	0.0005	0.200	-11	207.7	5.34
C1	400	0.5240	0.0051	0.967	-7	209.6	5.35
C2	400	0.5500	0.0010	0.178	1	220.0	5.39
C3	400	0.5380	0.0021	0.392	2	215.2	5.37
C4	400	0.5420	0.0077	1.424	3	216.8	5.38
C5	400	0.5310	0.0055	1.035	4	212.4	5.36
C6	400	0.5160	0.0028	0.540	5	206.4	5.33
C7	400	0.5150	0.0024	0.463	7	206.0	5.33
C8	400	0.5280	0.0084	1.598	8	211.2	5.35
C9	400	0.4999	0.0065	1.296	9	200.0	5.30
C10	400	0.5140	0.0014	0.266	10	205.6	5.33
C11	400	0.5160	0.0068	1.309	11	206.4	5.33
C13	400	0.4815	0.0029	0.598	12	192.6	5.26
C14	400	0.4745	0.0049	1.028	14	189.8	5.25
C15	400	0.4531	0.0053	1.170	15	181.2	5.20
C16	400	0.4276	0.0025	0.580	16	171.0	5.14
C17	400	0.4380	0.0022	0.492	17	175.2	5.17
C19	400	0.4114	0.0024	0.584	19	164.6	5.10
C20	400	0.4224	0.0069	1.640	20	169.0	5.13
C22	400	0.3551	0.0035	0.987	22	142.0	4.96
C23	400	0.3367	0.0024	0.726	23	134.7	4.90
C24	400	0.3285	0.0059	1.799	24	131.4	4.88
C25	400	0.3084	0.0046	1.481	25	123.4	4.82
C26	400	0.2931	0.0025	0.848	26	117.2	4.76
C27	400	0.2545	0.0007	0.259	28	101.8	4.62
C28	400	0.2388	0.0065	2.702	29	95.5	4.56
C29	100	1.0660	0.0081	0.762	30	106.6	4.67
C30	100	0.9760	0.0049	0.497	31	97.6	4.58
C31	100	0.8480	0.0077	0.902	33	84.8	4.44
C32	100	0.7900	0.0043	0.540	34	79.0	4.37
C33	100	0.6770	0.0031	0.461	36	67.7	4.22
C34	100	0.5820	0.0025	0.424	37	58.2	4.06
C35	100	0.4593	0.0076	1.660	39	45.9	3.83
C36	100	0.2672	0.0013	0.476	41	26.7	3.29
C37	100	0.2777	0.0024	0.860	43	27.8	3.32
C38	100	0.2088	0.0047	2.256	45	20.9	3.04
C39	100	0.1720	0.0036	2.095	47	17.2	2.84
C40	100	0.1313	0.0023	1.740	49	13.1	2.57
C41	10	1.1680	0.0079	0.674	51	11.7	2.46
C42	10	0.8030	0.0044	0.553	54	8.0	2.08
C43	10	0.5550	0.0072	1.299	57	5.6	1.71
C44	10	0.3640	0.0053	1.468	60	3.6	1.29
C45	10	0.2196	0.0013	0.587	64	2.2	0.79
C46	10	0.1145	0.0018	1.584	69	1.1	0.14

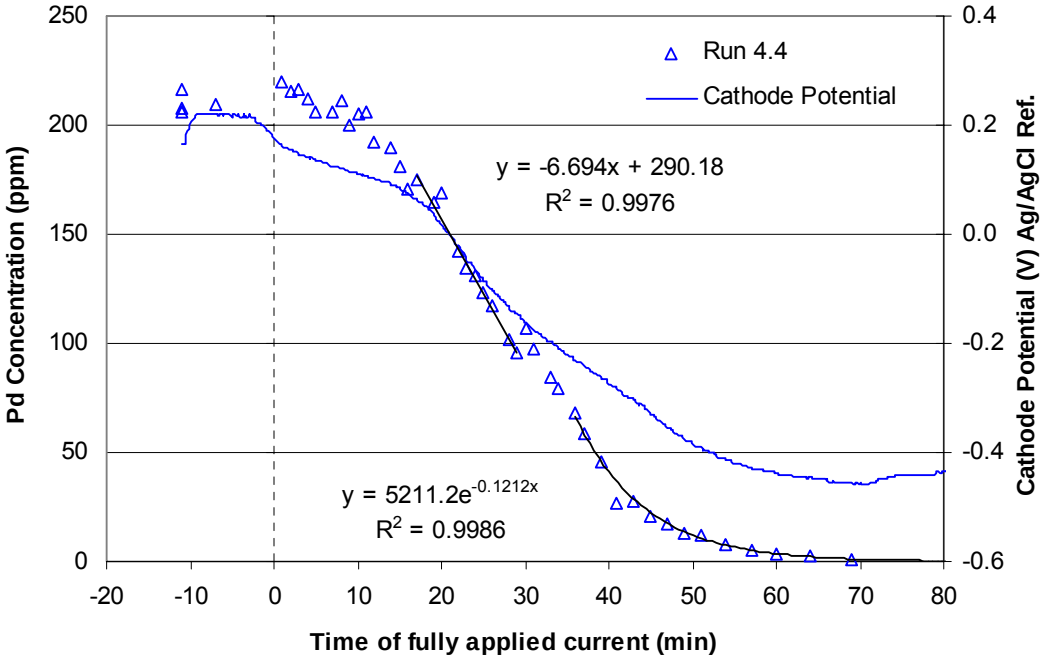


Figure E27 Pd concentration profile for Run 4.4 with the measured cathode potential shown on the secondary axis

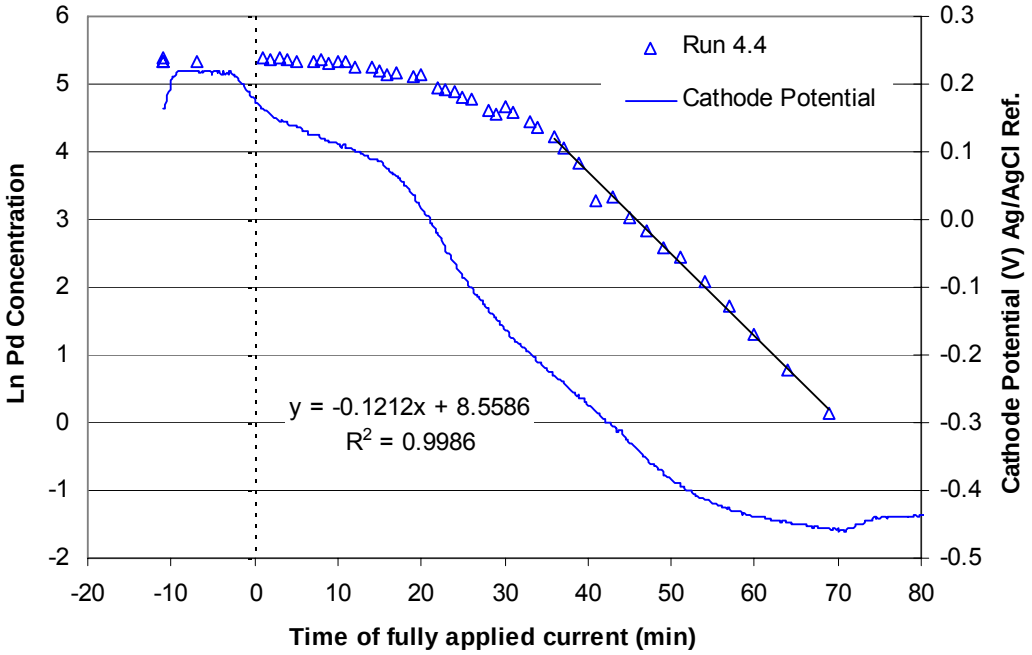


Figure E28 Pd concentration profile for Run 4.4 indicating the mass transport controlled region with the measured cathode potential shown on the secondary axis